PhD

PROGRAM IN TRANSLATIONAL

AND MOLECULAR MEDICINE

DIMET

Functional analysis of *m*-AAA homo- and heterocomplexes: the role of mitochondrial protein quality control system in spinocerebellar neurodegeneration

Coordinator: Prof. Andrea Biondi

Tutor: Dr. Valeria Tiranti

Cotutor: Dr. Franco Taroni

Dr. Stefania Magri

Matr. No. 725279

XXIV CYCLE

ACADEMIC YEAR

2010-2011

Table of Contents

Chapter 1

General introduction

Mitochondrial dysfunction and neurodegenerative diseases

Mitochondria are considered the cellular "powerhouse" because they supply the majority of the cellular energy by oxidative phosphorylation (OXPHOS). During this process the energy liberated by oxidation of metabolites is used to transport protons across the inner mitochondrial membrane generating an electron chemical gradient. This gradient is a source of potential energy used to generate ATP by ATP-synthase and to transport substrates and ions. In addition to this key role, mitochondria are an integral part of diverse aspects of cell biology, including regulation of intracellular calcium, signalling for cell-cycle progression and apoptosis (McBride et al., 2006). Impairment of mitochondrial essential functions, as defects in energy production, dynamics, communication with other organelles and turnover is likely to be an important common theme in numerous disease. Moreover mutations and deletions accumulated within the mitochondrial genome (mtDNA) and damaging effects of reactive oxygen species (ROS) generated by the electron transport chain predominantly contribute to aging. Additionally many mitochondria-related proteins are implicated in genetic forms of neurodegenerative disease (reviewed in Schon et al., 2011; Lin et al., 2006) (Fig.1).

To preserve organelle functions cells have elaborated several processes of monitoring and defence mitochondria at different level (recently reviewed

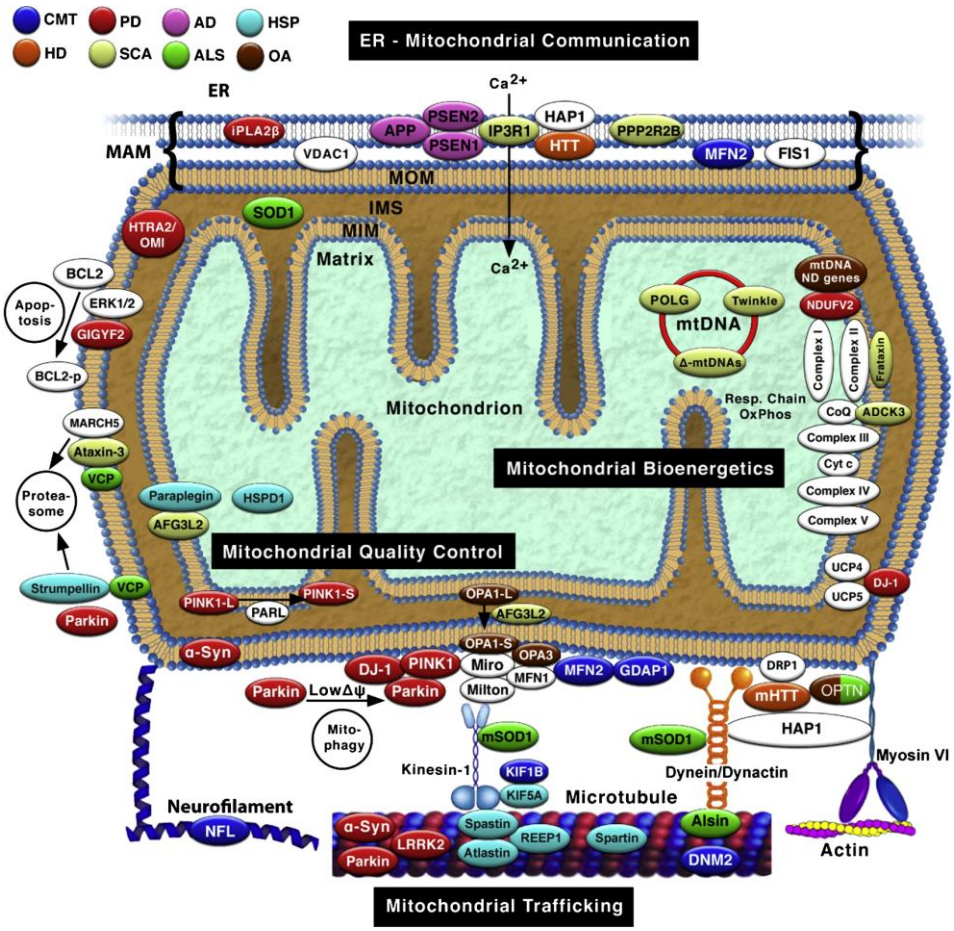

Figure1 Mitochondrial-related protein involved in neurodegenerative disease.

Proteins associated with mutations causing neurodegenerative disorders are in colour (Schon, 2011)

in Rugarli and Langer, 2012). The mechanism of surveillance that act at an intraorganellar level is the quality control system composed of chaperones and proteases that monitor the folding of mitochondrial proteins and removes non-assembled and misfolded proteins selectively. Moreover this surveillance can be increased under stress condition by the mitochondrial unfolded protein response, mtUPR, a transcriptional

programme that induces the nuclear expression of mitochondrial chaperone proteins and proteases (Benedetti et al., 2006). The second mechanism of control of mitochondrial turnover and bioenergetic efficiency involved an integration of fusion-fission events and autophagy (Chen and Chan, 2010). Fusion events facilitate the exchange of organelle contents such as solutes, metabolites, proteins, and mtDNA. While fission allow segregation of damaged components in a fragmented mitochondria and their elimination by an autophagic breakdown termed mitophagy (reviewed in Twig, 2008;). If mitophagy is not sufficient to prevent the release of pro-apoptotic protein, damaged mitochondria trigger the cascades that lead to apoptosis pathway.

In this scenario essential roles are played by mitochondrial proteases. They not only remove unfold and damaged proteins but also perform housekeeping roles during biogenesis of mitochondrial proteins and regulatory functions in mitochondrial dynamics. Therefore, each mitochondrial compartment exhibit specific processing peptidases (Table1).

Name	Compartment	Yeast	Function in yeast	Mammals homologues
Processing peptidases				
MPP	matrix	Mas1, Mas2	Presequence cleavage	α-MPP, β-MPP
MIP	matrix	Oct1	Removal of octapeptides	MIPEP (HMIP)
IMP	Inner membrane	Imp1, Imp2	Presequence cleavage	IMMP1L, IMMP2L
Rhomboid	Inner membrane	Pcp1	Ccp1 and Mgm1 processing	PARL
ATP-dependent proteases				
i -AAA	Inner membrane	Yme1	Quality control	YMEL1
***m*-AAA**	Inner membrane	Yta10, Yta12	Quality control, protein processing, membrane dislocation	paraplegin, AFG3L1∗,AFG3L2
Lon	matrix	Pim1	Quality control, mtDNA maintenance and gene expression	LON
ClpXP	Matrix	-		ClpP, ClpX
Oligopeptidases				
	Inner membrane space	Mop112	Degradation o f peptides and presequences	PreP
	Inner membrane space	Prd1	Degradation of peptides and presequences	Neurolysin
	Matrix	Lap3	Aminopeptidase, protection against homocysteine	Bleomycin hydrolase
Other proteases				
	Inner membrane	Oma1	Quality control	OMA1
	Inner membrane space	-		HtrA2 (omi)

Table 1: Mitochondrial protease associated to each compartments

(Modified from Koppen and Langer, 2007)

Mitochondrial proteases and protein processing

Mitochondrial proteome is composed of 13 mitochondrial DNA-encoded proteins which are core subunits of respiratory chain complexes. Whereas the majority of mitochondrial proteins is encoded by nuclear genome, synthesized in the cytosol and subsequently imported into mitochondria. Nucleus-encoded mitochondrial precursor proteins possess targeting signals that are recognized by receptors on the mitochondrial surface. The mitochondrial targeting signal can be a N-terminal presequence that can be proteolitically removed or an internal sequence that remain part of the

mature protein (reviewed in Mossmann et al., 2011). Most of the precursors entries by the translocase of the outer membrane (TOM) complex, then they use different pathways to reach the appropriate subcompartments (reviewd in detail in Schmidt et al., 2010). Upon import in the matrix space, most presequences are proteolytically removed by the mitochondrial processing peptidase (MPP), a conserved hetero-dimeric metallopeptidase. MPP cleaves both fully translocated preproteins and proteins in transit that are relocated in the IM or released into the IMS proteins upon sequential cleavage by an additional protease. In these cases the cleavage by MPP converts precursors into intermediate proteins that subsequently undergo to a second processing. Proteins direct to the intermembrane space (IMS) and into the inner membrane (IM), are relocated in the IM thanks to an hydrophobic sorting signal that is cleaved off by the inner membrane peptidase (IMP) allowing the correct insertion in the membrane or the release in the IMS (Nunnari et al., 1993). The IMP is a hetero-oligomeric complex constituted of two catalytic subunits that differs in substrates specificity, Imp1 and Imp2, and the auxiliary protein Som1 (Esser et al., 1996). IMP can also process mitochondrial encoded precursor proteins like Cox2, cytochrome c oxidase subunit 2, which is co-translationally inserted into the inner membrane by Oxa1. In the matrix the second cleavage step is mediated by the mitochondrial intermediate peptidase (MIP) a monomeric metallopeptidase that removes an octapeptide after MPP processing (Isaya et al., 1991). Recently the intermediate cleaving peptidase Icp55 was identified in yeast, it removes a single amino acid residue after processing by MPP (Naamati et al., 2009).

Besides the classical presequence peptidases, a subset of precursors is processed by proteases with specialized functions located in the inner membrane and interme*m*-brane space of mitochondria. One of these is the rhomboid protease, an intramembrane serine protease that acts within the lipid bilayer cleaving the transmembrane domains of integral membrane proteins. The yeast rhomboid Pcp1 is primarily involved in the processing of the dynamin-related GTPase Mgm1 and the ROS scavenger cytochrome c peroxidase Ccp1 (Herlan et al. , 2003; Esser et al.,2002).

Similarly, the mammalian homologue, PARL (presenilin-associated rhomboid like protease) (McQuibban et al., 2003) is implicated in controlling apoptosis through the processing of OPA1, the homologue of Mgm1 (Cipolat et al., 2006). At least another protease have a role in the processing of protein located in the inner membrane: the *m*-AAA active at the matrix side (see below). Finally, the Atp23 is a conserved metalloprotease localized in the IMS that performs Atp6 processing and assembly. This Atp23 function is not conserved through-out evolution as the mammalian homologues of Atp6 are synthesized without cleavable presequences (Tatsuta and Langer, 2008).

Mitochondrial proteases and quality control

Non-assembled and damaged proteins in mitochondria are selectively recognized and degraded by a quality control system (reviewed in Koppen and Langer, 2007; Tatsuta and Langer, 2008; Baker et al., 2011; Rugarli and Langer, 2012). This proteolytic system is constituted by several ATP-dependent proteases with chaperone-like functions located in each mitochondrial subcompartments (Fig.2).

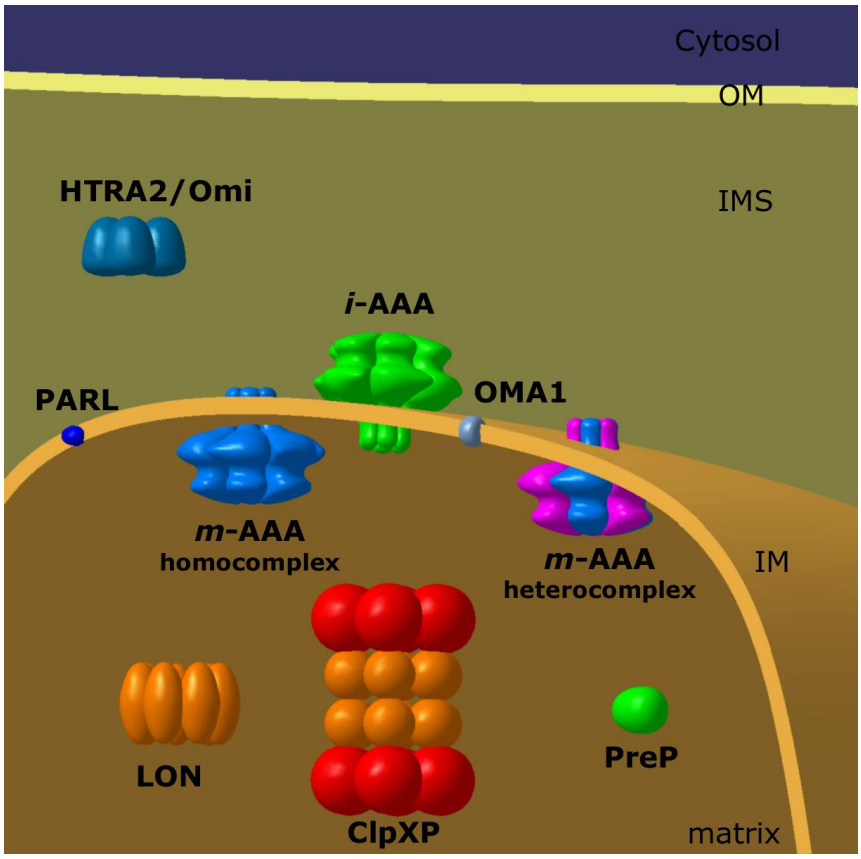

Figure 2 : Quality Control proteases.

QC proteases monitor and protect all four mitochondrial compartments against deleterious accumulation of misfolded, misassembled or unfolded proteins. The matrix is controlled by the soluble AAA proteases ClpXP and Lon, whereas the intermembrane space (IMS) is monitored by HtrA2. The Inner membrane (IM) contains two AAA proteases, with opposite orientation of the active site. The *i*-AAA is a homo-oligomeric complex composed of YME1L1, and the *m*-AAA is present as a homo-oligomeric complex constituted by AFG3L2 and a hetero-oligomeric complex composed of paraplegin and AFG3L2. The rhomboid protease PARL resides in the IM where it is involved in intramembrane proteolysis of substrates, while its role in QC is not clear. Ubiquitin–proteasome system is probably involved in QC of the mitochondrial outer memebrane (OM).

Matrix

In the mitochondrial matrix the protein folding if facilitated by two ATP-dependent chaperone systems, mtHSP70 and HSP60, whereas quality control is performed by two ATP-dependent proteases: the Lon and the ClpXP proteases (Suzuki et al., 1994; Van Dyck et al., 1994; Wang et al., 1994;). The Lon protease, named PIM1 in yeast, is a serine protease constituted of a ring-shaped homo-heptamer. It performed its own maturation by autocatalytic cleavage after MPP processing. The Lon/PIM1 protease mediates complete proteolysis of misfolded and damaged proteins preventing their accumulation and deleterious effects on mitochondrial activities (Bota et al., 2005). Moreover PIM1 deletion in yeast suggest a role of this protease in DNA maintenance (Van Dyck et al., 1994). Consistently, also the human Lon protease is found to be associated with mtDNA under physiological conditions, even if its exact molecular function in mtDNA quality control is still to be elucidated (Lu et al., 2007). ClpXP protease is present in the matrix of mammalian, but not yeast, mitochondria (De Sagarra et al., 1999). It is a hetero-oligomeric protease composed of proteolytic ClpP subunits with serine peptidase activity and of ClpX subunits with ATPase activity. ClpXP is involved in the unfolded protein response, but its role is not clear yet (Zhao et al., 2002; Haynes et al., 2007).

Inner membrane

The protein-rich inner membrane (IM) contains many complexes involved in mitochondrial metabolism among which the respiratory chain complexes, metabolite carriers and the polypeptide import machinery. In this compartment the quality control surveillance is primarily performed by two membrane-integrated ATP-dependent proteolytic complexes: the *i*-AAA and *m*-AAA proteases. They exert overlapping substrate specificities in yeast and it is apparently solely the membrane topology of substrates that determines which protease is involved in degradation. In fact *i*-AAA protease exposes its catalytic side to the intermembrane space, whereas the *m*-AAA protease is active on the matrix side (Leonhard et al., 1996).

These protease proteases recognize and degrade solvent-exposed domains of misfolded substrates, loops of multispanning membrane proteins or short terminal tails protruding from the lipid bilayer (Leonhard et al, 2000).

Intermembrane space

The only soluble quality control protease in the intermembrane space is the high temperature requirement A2 (HtrA2) also called Omi (Savopoulos et al., 2000; Gray et al., 2000; VandeWalle et al., 2008; Johnson et al., 2009) HtrA2/Omi is a homo-trimeric serine protease that shares homology with bacterial QC proteases DegS and DegP, but do not appear to be present in yeast or worms. In mammals, HtrA2/Omi is upregulated in response to several stress stimuli (Faccio et al., 2000; Suzuki et al.,2001; Dadga et al., 2009). Moreover it activates proapoptotic proteins upon its release to the cytosol from damaged mitochondria. (Hegde et al. 2002 ; van Loo et al. 2002). However, mice lacking HtrA2/Omi function exhibit a Parkinson-like neurodegenerative disorder which is caused by neuronal cell death indicating an essential and protective role of HtrA2/Omi in vivo (Jones et al., 2003; Martins et al., 2004). Moreover, loss-of-function mutations in the gene encoding HtrA2/Omi were recently identified in patients with Parkinson's disease (Strauss et al., 2005). Intriguingly, in humans PINK1, a serine/threonine kinase mutated in Parkinson disease patients, is required for phosphorylation of HtrA2, which increases its proteolytic activity in vitro (Plun-Favreau et al,2007; Li et al. 2010).

Outer membrane

Mechanisms that regulate quality control of mitochondrial protein import or outer membrane (OM) proteins are largely unknown. Several reports indicate a role of cytosolic chaperones and the ubiquitin proteasome In fact, several ubiquitin ligases localize to the cytosolic side of the OM, including mitochondrial ubiquitin ligase MITOL/MARCH-V, mitochondrial E3 ubiquitin protein ligase 1 (MULAN), and mitochondrial distribution and morphology protein 30 (Mdm30) (Nakamura et al., 2006; Yonashiro et al., 2006; Karbowski et al., 2007). Recently, a role in the degradation of ubiquitylated OM proteins was shown for p97 (Cdc48 in yeast) (Tanaka et

al., 2010). Its recruitment is mediated by Vms1 (VCP/Cdc48 associated mitochondrial stress responsive 1), who traffics from the cytoplasm to mitochondria upon mitochondrial stress (Heo et al., 2010).

Mitochondrial proteases and dynamics

Mitochondria are very dynamic organelle: they exist in networks that are continuously remodelled through fusion and fission events (Westermann et al., 2002; Karbowski et al., 2003). When fusion is reduced, mitochondria fragment due to ongoing fission. The control of mitochondrial shape is required for correct segregation and distribution of mitochondria and for maintaining of the bioenergetic functionality (Chan, 2006). In fact, fragmentation is a common stress response that permits the segregation of dysfunctional mitochondria that are subsequently eliminated by autophagic pathway. Mitochondrial fusion not only compensate for metabolic depletions by transferring soluble and membranous components, but also constitute a mechanism of selection. Depolarized mitochondria that are not able to regenerate their membrane potential are excluded from the fusion-population and undergo to elimination. Thus, combination of fusion, fission and autophagy acts as a quality control mechanism (Twig et al., 2008) (Fig.3). Mitochondrial proteases and proteolytic events on both the inner and outer mitochondrial membrane regulate these surveillance mechanisms.

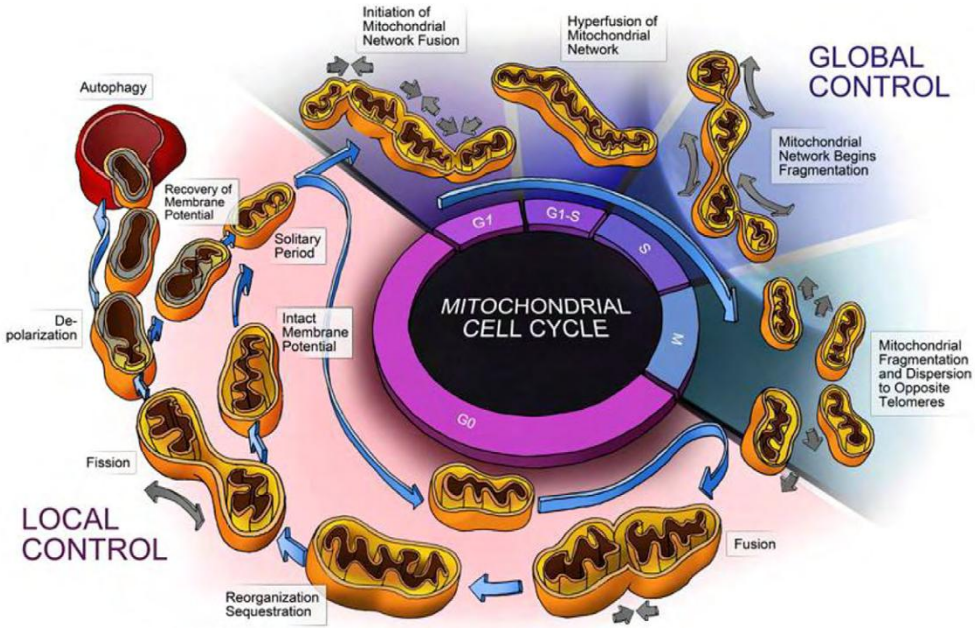

Figure 3: Mitochondrial dynamics

The mitochondrion undergoes fusion, fission, depolarization, and degradation by autophagy. This process is largely controlled by the local energetic status and associated local signals. During the cell cycle global signals cause concerted changes in the mitochondrial population, as noted by hyperfusion in G1-S and fragmentation during M phase. These global population effects are governed by the cells demand for energy required by cell division and the need for homogenization and sequestration of cellular components during met-phase (Hyde et al., 2010).

OPA1

OPA1 is a dynamin-like GTPase involved in the fusion of the inner mitochondrial membrane, cristae morphogenesis and mtDNA maintenance (Landes et al., 2010). In humans, OPA1 gene is formed by 30 exons, 3 of which (4, 4b and 5b) are alternatively spliced leading to 8 mRNA (Delettre et al., 2001). OPA1 precursors are targeted to mitochondria and processed by MPP upon import to give rise to long isoforms (L-OPA1) (Olichon et al., 2002). Proteolytic processing at two sites, s1 and s2, converts L-OPA1 isoforms in short isoforms (S-OPA1) (Song et al., 2007). Both short and long isoforms of OPA1 may be associated to mitochondrial

membrane: L-OPA1 is proposed to be anchor to the IM while S-OPA1, lacking the transmembrane TM1, is peripherally attached to the IM, but can also diffuse in the IMS and to associate to OM (Cipolat et al., 2006). As mitochondrial fusion depends on the presence of both long and short forms, constitutive cleavage is necessary in physiologic conditions. Moreover under stress condition L-OPA1 is completely converted into S-OPA1 (stress-induced cleavage). Thus proteolytic processing represents a central regulatory step determining mitochondrial morphology (Duvezin-Caubet et al, 2006; Ishihara et al, 2006). Numerous and discordant studies have identified several mitochondrial proteases implicated in the generation of S-OPA1 (Fig.4). The *i*-AAA protease YME1L mediates constitutive processing at the s2 site, whereas a debate still exist about the protease responsible for OPA1 cleavage at s1 (Griparic et al, 2007; Song et al, 2007; Ehses et al, 2009; Head et al, 2009). Both the metallopeptidase OMA1 and the *m*-AAA complex seem to be involved in OPA1 physiological processing at the s1 site. At decreased mitochondrial ATP levels, after dissipation of membrane potential, or in the absence of mtDNA, OMA1 promotes stress-induced OPA1 processing, resulting in the complete conversion of long OPA1 forms to short variants (Ehses et al, 2009). Although not essential, also PARL seems to be involved in the release of short OPA1 isoforms from mitochondria during apoptosis (Cipolat et al, 2006). Furthermore the stability of L-OPA1 depends on prohibitin complexes that regulate the activity of some mitochondrial proteases among which the *m*-AAA protease (Steglich et al, 1999; Merkwirth et al, 2008; Ehses et al, 2009).

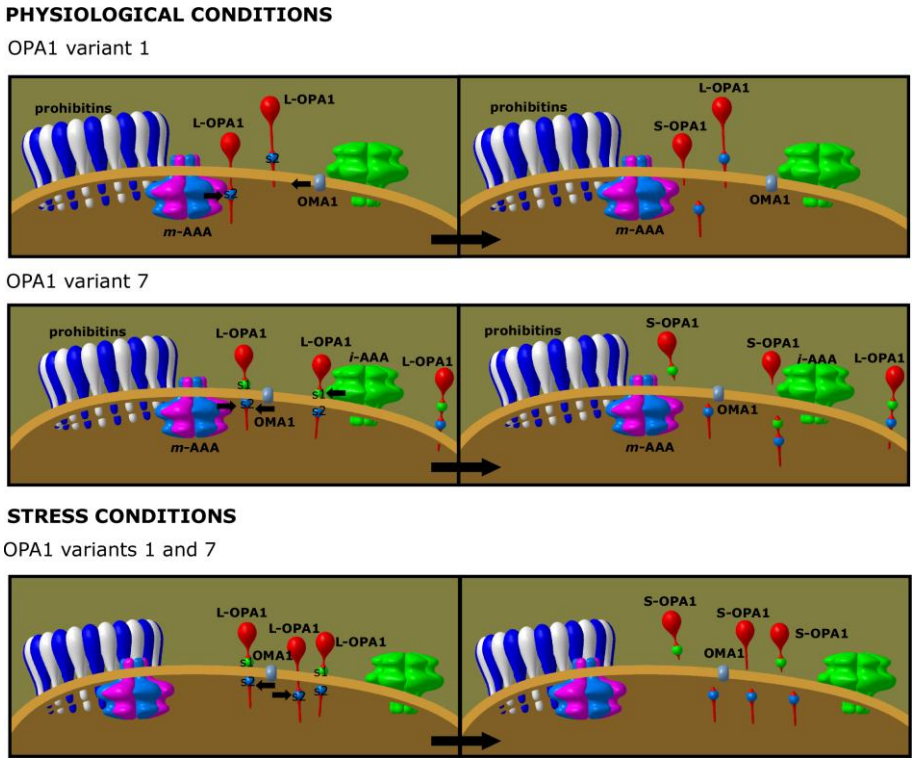

Figure 4: OPA1 proteolytic cleveage under physiological and stress conditions.

In physiological conditions, most tissues express two OPA1 splicing variants (variant 1 and 7). They differ for the absence or presence of exon 5b, which coding for the processing site s1. OPA1 variants are first processed by the mitochondrial processing peptidase (MPP) that removes the mitochondrial targeting signal (MTS) generating OPA1 long isoforms (L-OPA1). Subsequently, L-OPA1 are partially processed at s1 and s2 sites leading to the formation short OPA1 forms. The *m*-AAA protease and OMA1 seem to be involved in the cleavage of OPA1 at site s1, located in exon 5. The *i*-AAA protease instead cleaves OPA1 at s2 within exon 5b. Under stress conditions, OMA1 cleaves all OPA1 proteins at s1 causing the loss of long OPA1 forms (Martinelli et al., 2010).

PINK

Dysfunctional mitochondria are selectively removed by mitophagy. This process requires the accumulation of specific receptor proteins at the mitochondrial surface recruiting the autophagic machinery to mitochondria (Youle and Narendra, 2011). Accumulation of PINK1 at mitochondrial surface and the subsequently recruitment of parkin is necessary for mitophagy. PINK1 precursor proteins are imported into mitochondria and the mitochondrial target sequences is cleaved off by MPP. Newly imported PINK1 is degraded in the inner membrane by PARL and an MG132-sensitive peptidase, yet to be identified. Mitochondria depolarization impairs import but not mitochondrial targeting of PINK1 resulting in its accumulation at the mitochondrial surface (Narendra et al., 2010).

AAA proteases

AAA$^+$ superfamily

The AAA$^+$ (ATPases Associated with various cellular Activity) superfamily is a lineage of the larger class of P-loop NTPase characterized by the presence of a conserved nucleotide phosphate-binding motif (named P-loop or Walker A) and a second, more variable region, called Walker B motif (Snider et al., 2008). The activity of AAA+ proteins relies on their ability to use ATP hydrolysis-driven conformational changes to generate a mechanical force, leading to the remodelling of bound substrate. They are involved in DNA replication, recombination, transcriptional regulation, membrane fusion, organelle biogenesis and the assembly and disassembly of complexes (Neuwald et al., 1999). The AAA+ proteins can be divided into two distinct classes, on the basis of the number of AAA domains present in the protein. Class I proteins contain two AAA domains, while class II proteins contain only one AAA domain. Functional diversity of AAA+ proteins is caused by the presence of additional domains (Mogk et al., 2008).

AAA metalloprotease

The AAA proteases are membrane-embedded metallopeptidases belonging to the AAA+ superfamily (Langer et al., 2001; Sauer et al., 2004). They are ubiquitously present in eubacteria as well as in chloroplasts and

mitochondria of eukaryotic cells (Juhola et al., 2000). They form large complexes which are composed of either closely related or identical subunits of 70-80 kDa (Atorino et al., 2003; Urantowka et al., 2005; Koppen et al., 2007). They are highly conserved: with sequence identities of >40% between the bacterial, yeast and human members (Langer, 2000). Most bacteria have only one AAA protease, called FtsH in Escherichia coli, which forms a homo-oligomeric complex in the plasma membrane. Eukaryotes have rather different orthologs that appear to be localized exclusively in mitochondria and chloroplasts. Two AAA protease complexes are integrated into the mitochondrial inner membrane exposing their catalytic sites to opposite membrane surfaces : the *i*-AAA protease exposing its catalytic side to the intermembrane space and the *m*-AAA protease which is active on the matrix side (Arlt et al., 1996; Leonhard et al., 1996; Weber et al., 1996; Arlt et al., 1998).

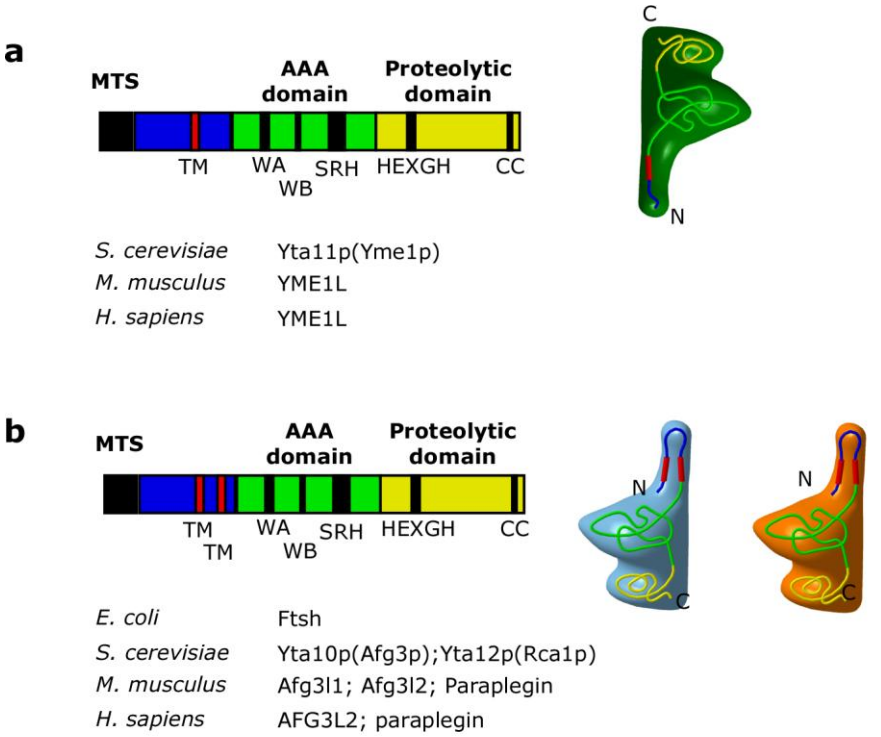

Figure 5: AAA metalloproteases topology and domains.

The AAA proteases in mitochondria face either the matrix (*m*-AAA) or intermembrane space (*i*-AAA). (a) domains of *i*-AAA proteases; (b) domains of *m*-AAA proteases. (c) mitochondrial localization of *i*-AAA and *m*-AAA. MTS, mitochondrial target sequencing; TM, transmembrane motif; WA, walker A; WB,

Walker B; CC, coiled-coil motif; SRH, second region of homology; HEXGH= conserved proteolytic site IM, inner membrane; OM, outer membrane.

AAA metalloprotease domains

AAA proteases are constituted of homo- or hetero-oligomers, usually hexamers, organized in ring-shaped complexes and they share a conserved domain structure. Mitochondrial localisation of AAA protease subunits is ensured by mitochondrial targeting sequences in the N-terminal region. After that they contain one or two transmembrane segments that allow membrane spanning (Fig.5). In particular, the *m*-AAA proteases have two transmembrane regions and expose their catalytic domain into the matrix, whereas the *i*-AAA subunits have only one transmembrane domain and expose the catalytic sites in the intermembrane space (Fig.5) (Arlt et al., 1996; Weber et al., 1996). The resolution of the crystal structure of the whole cytosolic region of Ftsh, the homologue AAA protease of *E. coli,* and mutational analysis shed light on domain structure and crucial role of highly conserved residues.

AAA proteases contain a conserved Walker-type ATPase domain (AAA domain) of approximately 230 amino acid residues, which characterized the AAA superfamily (recently reviewed in Wendler et al., 2012). The AAA domain consists of two discrete structural domains: a domain α/β nucleotide-binding domain and an α-helical bundle (Fig.6a). The nucleotide-binding domain is composed by WalkerA (or P-loop) and WalkerB, necessary for ATP binding and hydrolysis, and SRH (Fig.6b). The WalkerA motif contains the consensus sequence GXXXXGKT located between β2 and α2 (Krzywda 2000). The conserved lysine (K201 in FtsH) forms hydrogen bonds with the oxygens of both β- and γ-phosphate of ATP. Whereas the hydroxyl of the adjacent treonine (T202 in Ftsh) coordinates the Mg^{2+} (Karata et al., 2001) (Fig.6c). The Walker B motif, instead, is characterized by the sequence ψψψψDE (ψ represents a hydrophobic amino acid) and it is associated with the β4 strand (Krzywda 2000). The carboxylate of the conserved glutamic acid (E255 in Ftsh) coordinates the Mg2+, together with the carboxylate of the adjacent aspartic acid (D256), and interacts with a possible catalytic water molecule (Karata et al., 2001) (Fig.6c). The second region of homology

(SRH), that characterize the AAA-family, it consists of 19 highly conserved amino acids that are essential for the activity of the complex and the interaction between different subunits. In particular, the asparagine N301 forms a hydrogen bond with K201 of Walker A and E255 of Walker B. Whereas, the lateral side of the arginine 315 protrudes in the ATP binding pocket of the neighbouring subunit where interacts with the γ-phosphate of the bound ATP. This residue, termed "arginine finger", is suggested to coordinate intermolecular conformational changes during ATPase cycles, thereby stimulating ATP hydrolysis (Ogura et al 2004; Hanson and Whiteheart, 2005). Mutagenesis experiments revealed that two other invariant residues, D307 and R312 are essential in ATP hydrolysis. They seem to form a salt bridge that stabilizes the conformation of the SRH and contributes to positioning and orientation of R315 (Karata et al. 1999; Karata et al., 2001).

At the c-terminus of the nucleotide-binding domain there is a less conserved domain constituting of a bundle of four α-helices organized as two helical hairpins arranged in a left-handed superhelical structure (Fig. 6a). The functional role of this domain is already unknown (Snider et al., 2008).

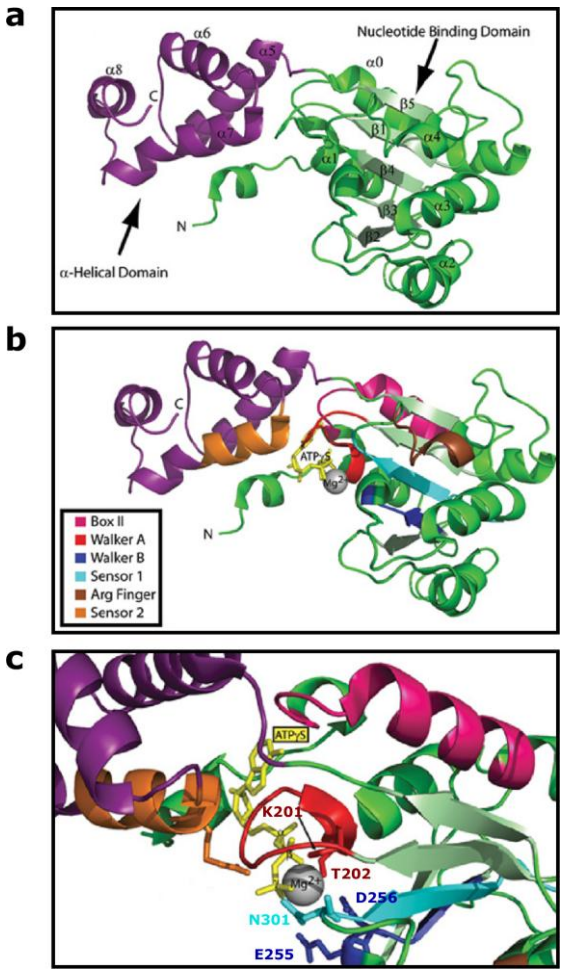

Figure 6: AAA domain

(Modified from Snider et al., 2008)

The AAA domain is followed by a highly-conserved proteolytic domain. Analysis of the primary structure of the protease domain has revealed the presence of a consensus sequence motif HEXXH for binding to zinc (X represents a variable amino acid residue) which is conserved in the M41 family of metallopeptidases (Rawlings and Barrett, 1995; Hooper, 1994). The catalytic site of the protease domain lies at a rather peripheral position of the hexamer plate and is located in the cleft composed of the

three helices α 13, α 15, and α 16, as well as b6 and it is covered by a "lid helix" constituted of the helix α14 (Fig.7)(Suno et al., 2006). The catalytic metal ion in FtsH is coordinated with the imidazole rings of H417 and H421 in the HEXXH motif in α 13. The third amino acid involved in Zn2+ coordination is still uncertain: it is proposed to be the carboxyl group of D495 in α16 or the glutamic acid E479 in helix α15 (Suno et al., 2006). At the C-terminal region, there is another highly-conserved helical region of unknown function presumably forming leucine zipper-like coiled-coil structure (Langer, 2000).

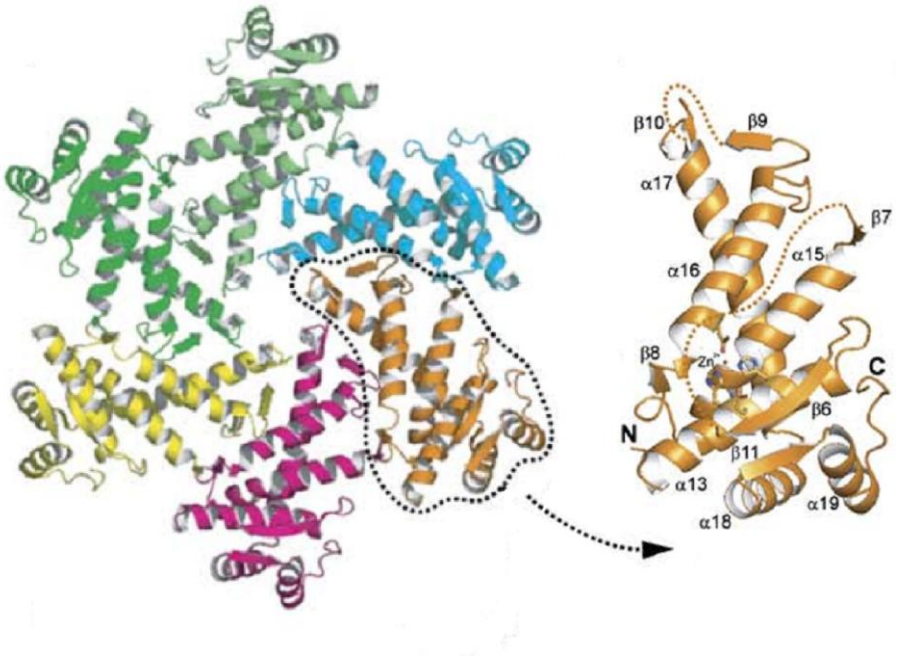

Figure 7: Proteolytic domain.

(Modiefied from Suno et al., 2006)

Structure-function relationship (operational model)

Based on crystal structures of the FtsH protease, the AAA protease is proposed to adopts an hexameric ring shape composed of two structurally separated disk: a lower disk, constituted by the proteolytic domains of the six subunits, and a upper one, composed of six AAA domain (Bieniossek et

al., 2006; Suno et al., 2006). The AAA domains facing the membrane form a narrow central pore which allows substrates to enter the proteolytic chamber inside the complex. Translocation of substrates into the proteolytic chamber depends on a conserved loop motif which is located in the AAA domain and protrudes into the central chamber (Wang et al., 2001; Graef and Langer, 2006). The orientation of the AAA domain relative to the proteolytic domain is significantly different between adjacent subunits. In particular, one subunit exhibits extensive contact between the two domains (closed subunit), while the adjacent subunit presents a distance between the two domains due to a rotation of the AAA domain (opened subunit). In this structure the release of ADP and the binding of ATP would occur only when the subunit is in the open form because only in this condition the ATP binding site is accessible. Consequently, the complex appear constitutes of three couples of subunits (closed and opened): a trimer of dimers (Suno et al., 2006). In agreement with this hypothesis, only the ATPase catalytic site of the closed subunit seems to be active, because the arginine finger of the adjacent opened subunit is near enough to interact with the oxygen of the ATP γ-phosphate. On the contrary, in a open subunit the corresponding arginine finger is too far to promote ATP hydrolysis. These observations suggest a dynamic open-closed motion of the subunit in the hexameric structure, coupled with the ATPase cycle (Suno et al., 2006). The ATPase cycle suggested by Suno et colleagues is described in Fig.8

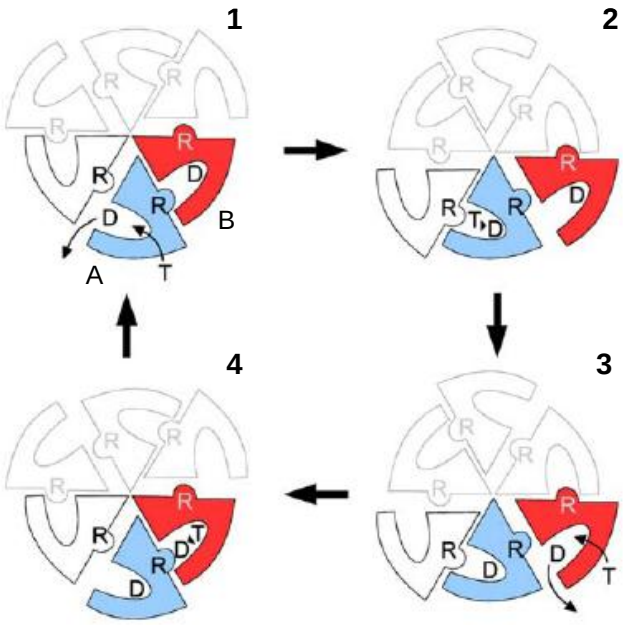

Figure 8: Coordination of ATPase cycle and open-close motion

1) The open subunit exchanges its bound ADP with ATP, and the closing motion is triggered. (2) The closing motion ac-companies rearrangement of the small subdomain, which leads to the conformational transition of the whole FtsH molecule. (3) Upon completion of the closing motion, the ATPase catalytic site becomes activated and ATP is hydrolyzed. (4) The closed subunit can return to the open form without releasing ADP, and the whole FtsH structure also returns to the original state. The ATP binding to other open subunits in the same hexamer might help this transition (modified from Suno et al., 2006).

Intersubunit coordination of ATP hydrolysis is thus emerging as a common operational principle of ring ATPase. In particular, Augustin et colleagues demonstrates that in *m*-AAA ATP binding to one AAA domain inhibits the ATPase activity of the adjacent subunit. ATP hydrolysis abolishes the inhibitory effect and allows subsequent hydrolysis of ATP in the neighboring subunit (Augustin et al., 2009). Moreover, coordinated ATP hydrolysis within the AAA ring of *m*-AAA proteases is proposed to increases the efficiency of the proteolytic machine. Substrates bind to

Yta12 subunits in the ATP-bound state. ATP hydrolysis triggers conformational changes of pore loop-1 that promote the translocation and the release of the substrate. Intersubunit coordination of ATP hydrolysis ensures that the adjacent subunit bind ATP and is able to accept the substrate, allowing efficient handover to the neighbouring subunit. In the yeast *m*-AAA protease, only the ATP-bound state of Yta12, but not that of Yta10, impairs ATP hydrolysis by neighbouring subunits, suggesting that dimers of Yta10 and Yta12 are the functional unit of the enzyme. By contrast, ATP binding to both human paraplegin and AFG3L2 inhibits ATP hydrolysis in the neighbouring subunit indicating probably a different organization of the functional unit (Augustin et al., 2009).

Role of *m*-AAA complex

In yeast *saccharomyces cerevisiae*

The functions of AAA proteases in mitochondria are best characterized in the yeast *Saccharomyces cerevisiae*. In yeast inner mitochondrial membrane, are present two different AAA proteases constituted of three protein: Afg3p (Yta10p), Yme1p (Yta11p) e Rca1p (Yta12p) (Fig. 9). The homo-oligomeric *i*-AAA protease is composed of Yme1 subunits and protrudes into the intermembrane space. It is required for respiratory growth of yeast cells at high temperatures and for fermenting growth at low temperature. The *i*-AAA protease present in yeast is also present in mammalian mitochondria, where is composed of YME1L (Leonhard et al., 1996, Tatsuta & Langer, 2009). The hetero-oligomeric *m*-AAA protease complex consists of the highly homologus subunits Yta10 (Afg3) and Yta12 (Rca1) and is active on the matrix side (Arlt et al., 1996; Leonhard et al., 1996). Both AAA proteases are a component of the mitochondrial quality control system of the IM. They do not recognise a specific sequence of cleveage, but recognize the solvent-exposed domains of membrane proteins. N- or C-terminal tails of ~20 amino acids protruding from the membrane are sufficient to allow the proteolytic attack of a membrane protein by an AAA protease (Leonhard et al. 2000). Coimmunoprecipitation studies and functional inactivation have allowed

the identification of some substrates of *m*-AAA complex. The *m*-AAA protease selectively degrades a number of non-assembeld proteins such as the mitochondrial-encoded respiratory chain subunits of Complex II, IV and V and a peripheral membrane subunit of Complex V, Atp7 (Arlt et al., 1996; Korbel et al., 2004). Moreover, *m*-AAA acts as a processing enzymes of specific mitochondrial proteins: it is involved in the maturation of the ROS scavenger cytochrome c peroxidase (Ccp1) (Esser et al., 2002) and the ribosomal subunit Mrpl32 (Arlt et al., 1996)(Fig. 9). The *m*-AAA protease mediates the proteolytic maturation of nuclear-encoded MrpL32 upon import into mitochondria (Nolden et al., 2005). MrpL32 is a component of the large mitochondrial ribosome subunit. Processing of MrpL32 by the *m*-AAA protease allows its assembly into ribosomes and subsequent protein synthesis within mitochondria, thus controlling the assembly of respiratory complexes in the inner membrane (Nolden et al., 2005). Consistently, yeast cells lacking either Yta10 (yta10Δ) or Yta12 (yta12Δ) grow on glucose but exhibit impaired growth on a nonfermentable carbon source such as glycerol, indicating a defect in respiration (OXPHOS phenotype) (Nolden et al., 2005). By contrast, the maturation of Ccp1 requires a two-step mechanism. Initially, the *m*-AAA protease dislocates the newly imported precursor of Ccp1 (pCcp1) in the inner membrane through its ATP-dependent pull down activity and removes the transmembrane segment making a second processing site accessible. Subsequently, the intermediate Ccp1 is cleaved by the intramembrane proteolytic activity of the rhomboid protease Pcp1 and is finally released as mature Ccp1 (mCcp1) into the inter membrane space (Tatsuta et al., 2007; Bonn et al., 2011). While MrpL32 is conserved from yeast to humans, a mammalian homologue of the ROS-scavenger Ccp1 does not exist.

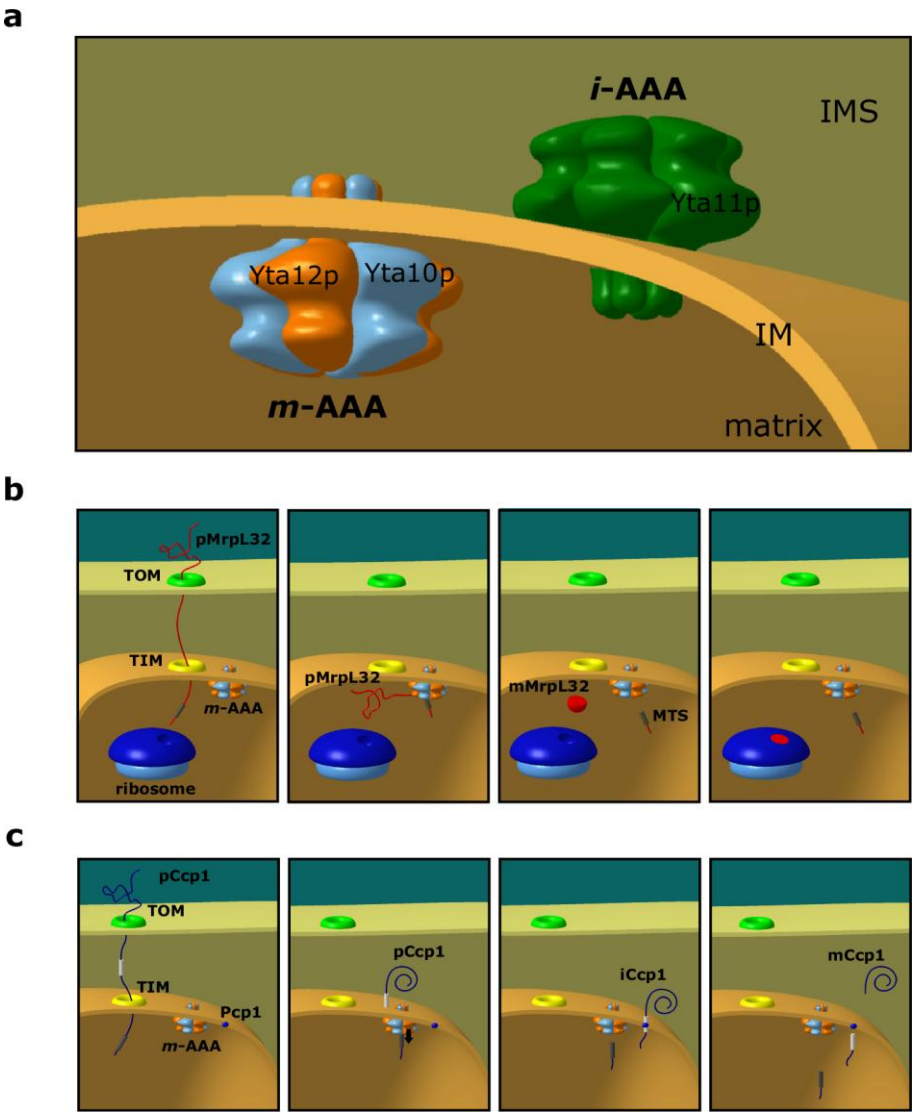

Figure 9*: i*-AAA and *m*-AAA complex in yeast

(a) Localization of *i*-AAA and *m*-AAA in yeast mitochondria. *i*-AAA protease is a homocomplex composed of Yta11p, while *m*-AAA is a heterocomplex constituted of Yta10p and Yta12p. (b) MrpL32 processing by *m*-AAA protease. (c) Two-step Ccp1 maturation by *m*-AAA protease and PcP1 rhomboid protease. pMrpL32, precursor;

mMrpL32, mature; TOM, translocase of the outer membrane; TIM, translocase of the inner membrane

In humans

AAA proteases are conserved from yeast to humans and share a high sequence identity. Functional conservation of the *i*-AAA and the *m*-AAA protease was demonstrated by complementation studies in yeast (Shah et al., 2000; Atorino et al., 2003; Nolden et al., 2005). A functional homologue of the *i*-AAA protease subunit Yme1 was identified both in mice and in humans, named YME1L1 (Yme1-like gene 1) (Coppola et al., 2000; Shah et al., 2000). Three potential subunits of the *m*-AAA protease were found in mice: the two homologues subunits Afg3l1 (AFG3-like gene 1) and Afg3l2 (AFG3-like gene 2) with a sequence identity of 70% and additionally the subunit paraplegin (Casari et al., 1998; Shah et al., 1998; Banfi et al., 1999). Whereas, AFG3L1 exists only as a pseudogene in human so that the human *m*-AAA protease is composed of AFG3L2 and paraplegin subunits (Kremmidiotis et al., 2001) (Fig. 10).

The human *m*-AAA protease exist as homo-oligomeric complexes constituted of AFG3L2 as well as hetero-oligomeric assemblies of AFG3L2 and paraplegin subunits (Fig. 10) (Koppen et al., 2007). Both the complexes has a native molecular mass of approximately 900 kDa and are present in the inner membrane of mitochondria and active on the matrix side (Banfi et al., 1999). First insights into the role of mammalian *m*-AAA protease were obtained by the involvement of paraplegin gene (SPG7) mutations in the neurodegenerative disease hereditary spastic paraplegia (HSP) (Casari et al., 1998). More recently, a study conducted in our lab indentified AFG3L2 as a novel cause of a dominant form of spinocerebellar ataxia (SCA28) (Cagnoli et al. 2006; Di Bella et al., 2010). Although AFG3L2 and paraplegin have a high sequence homology, share a common domain structure and co-assemble in an ubiquitous mitochondrial protease, mutations in these two proteins cause two neurodegenerative deseases that differ in patterns of inheritance, molecular mechanisms and degeneration of specific types of neurons. The

different phenotypes caused by mutations in AFG3L2 and paraplegin demonstrate that these proteins have at least partially distinct functions.

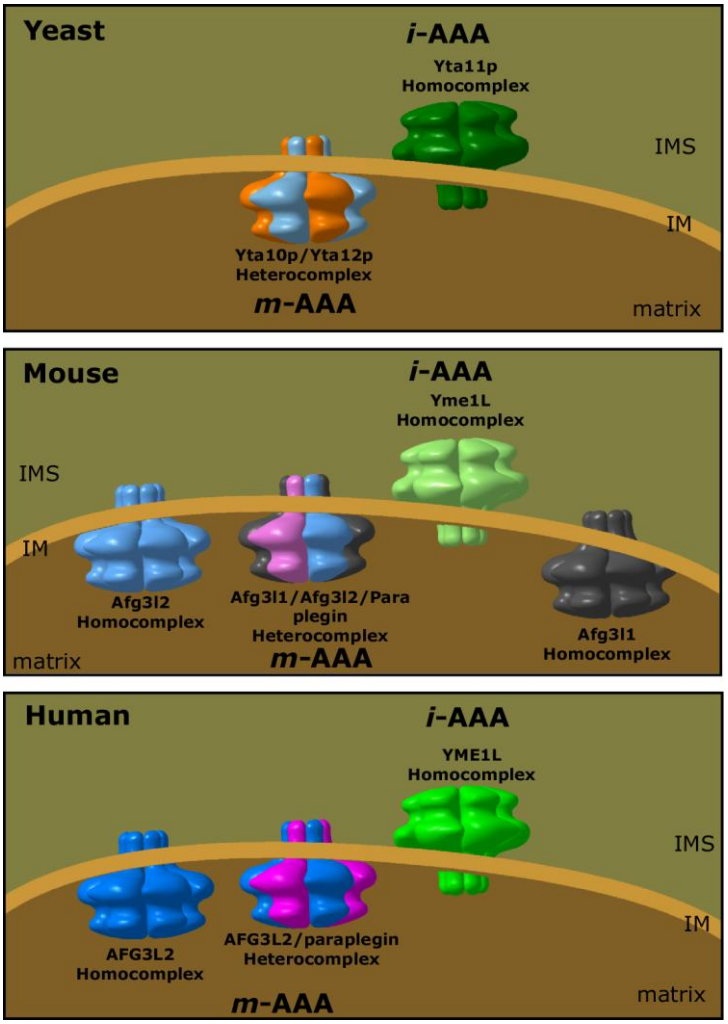

Figure 10: AAA complexes composition from yeast to human

AFG3L2

AFG3L2 was identified as thanks to its high sequence identity with paraplegin (Banfi et al., 1999). ATPase Family Gene 3-Like 2 (AFG3L2)

gene is composed of 17 exons, which encode for a protein of 797 amino acids. Northern analysis on human tissues revealed a ubiquitous expression of AFG3L2 and immunofluorescence analysis demonstrated its mitochondrial localization. AFG3L2 is evolutionarily highly conserved: it share a higher homology of sequence with Afg3p and Rca1p (69% similarity and 59% identity) than with paraplegin (58.3% sim*i*-larity and 49% identity) (Banfi et al., 1999).

Spinocerebellar ataxia

Ataxia is a neurological dysfunction of motor coordination that can affect gaze, speech, gait and balance. The aetiology of ataxia encompasses toxic causes, metabolic dysfunction, autoimmunity, paraneoplastic and genetic factors (Taroni and Di Donato, 2004). Hereditary forms are classified as: autosomal recessive and autosomal dominant. Two main mechanisms manifest autosomal recessive ataxias. Inactivating mutations result in loss of protein function, which affects control of energy output and oxidative stress (Friedreich ataxia (FRDA), ataxia with isolated vitamin E deficiency (AVED), Cayman ataxia) and control of DNA maintenance and the cell cycle (ataxia telangiectasia (AT), ataxia-OCULOMOTOR APRAXIA 1 and 2 (AOA1 and 2), spinocerebellar ataxia with axonal neuropathy (SCAN1)) (Taroni, & Di Donato, 2004).

Autosomal dominant spinocerebellar ataxias (SCAs, previously named ADCAs) are a clinically and genetically heterogeneous group of neurological disorders caused by degeneration of the cerebellum and its afferent and efferent connections (Taroni, & Di Donato, 2004; Koeppen, 2005). Affected individuals exhibit a cerebellar syndrome characterized by imbalance, progressive gait and limb ataxia, and dysarthria (Schols, et al., 2004, Harding, 2004). The clinical phenotype may appear complicated by the presence of additional neurological signs (pyramidal and extrapyramidal signs, ophthalmoparesis, dementia, pigmentary retinopathy, peripheral neuropathy, cognitive decline, and psychiatric manifestations), which are highly variable among and within families (Schols, et al., 2004). The first autosomal dominant gene for spinocerebellar ataxia type 1 (SCA1) was discovered in 1993 (Orr and Zoghbi, 2000). Since then, an increasing number of genes and

chromosomal loci have been identified, demonstrating the large genetic heterogeneity of these hereditary disorders (Duenas, et al, 2006). Thirty-one SCA loci are currently known.

The prevalence of SCAs has been estimated to be approximatly 3 in 100,000, but the relative frequency of specific genotypes may vary in different geographical areas and in populations of different ethnic origins (Schols et al., 2004, Brusco et al, 2004, Duenas et al, 2006). In particular, in Italy there is a relatively high frequency of SCA1 and SCA2 gene expansions, whereas SCA3, SCA6, SCA7 and SCA17 and DRPLA mutations are rare, compared with other European countries. No SCA10 or SCA12 and only a few SCA8 and SCA17 families are detected (Brusco et al, 2004).

SCA28

The screening of our cohort of affected individuals for the currently known SCA gene mutations has demonstrated that ~40% of the clinically identified ADCA families remain genetically unassigned. From these, we selected 225 families negative for the known SCA genes (SCA 1-2, SCA3, SCA6, SCA7, SCA17 and DRPLA) with the following selection criteria: ataxia as the principal neurological symptom, disease progression, and a positive family history. In these families, the Repeat Expansion Detection (RED) analysis excluded the presence CAG/CTG expansions >40 repeats, and linkage exclusion tests showed no evidence of linkage to most of the known SCA loci (SCA4, SCA5/20, SCA11, SCA13-16, SCA18, SCA19/22, SCA21, SCA25 and SCA27), suggesting a genetically distinct form of SCA.

From this group a four-generation Italian family (Fig.11) with a total of 30 members, including 14 affected individuals, resulted sufficient informative for statistical analysis.

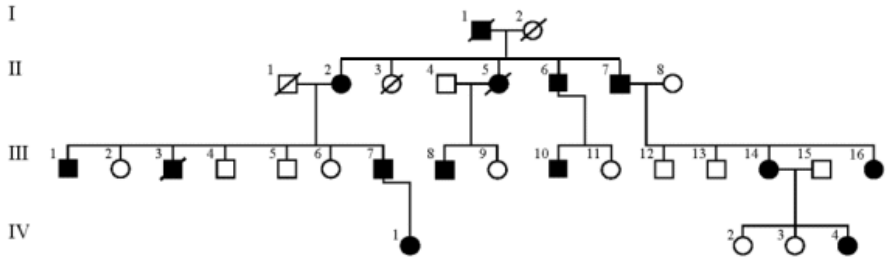

Figure 11: Pedigree of the family selected for linkage analysis.

In this family the disease occurs as a dominant ataxia with juvenile-onset with mean age at onset of 19.5 years (range 12–36) without anticipation in subsequent generations. The initial symptoms are unstable standing and ataxia and incoordination of limbs and gait. The disease is also characterized by ophthalmoparesis, lateral and vertical gaze nystagmus, Babinski sign, hyperreflexia and pyramidal signs. Disease progression is very slow. Biochemical assays on muscle biopsies revealed normal activities of the respiratory chain enzymes (complexes *I*-V), and Southern blot analysis excluded the presence of mitochondrial DNA deletions (Cagnoli et al., 2006). The genome-wide linkage analysis allowed us to map a new locus on chromosome region 18p11.22–q11.2, thus confirming that the disorder observed in this family represents a novel form of autosomal dominant SCA. This new locus has been assigned the SCA28 symbol by the Human Genome Nomenclature Committee (Cagnoli et al., 2006) (Mariotti et al., 2008) (Fig.12).

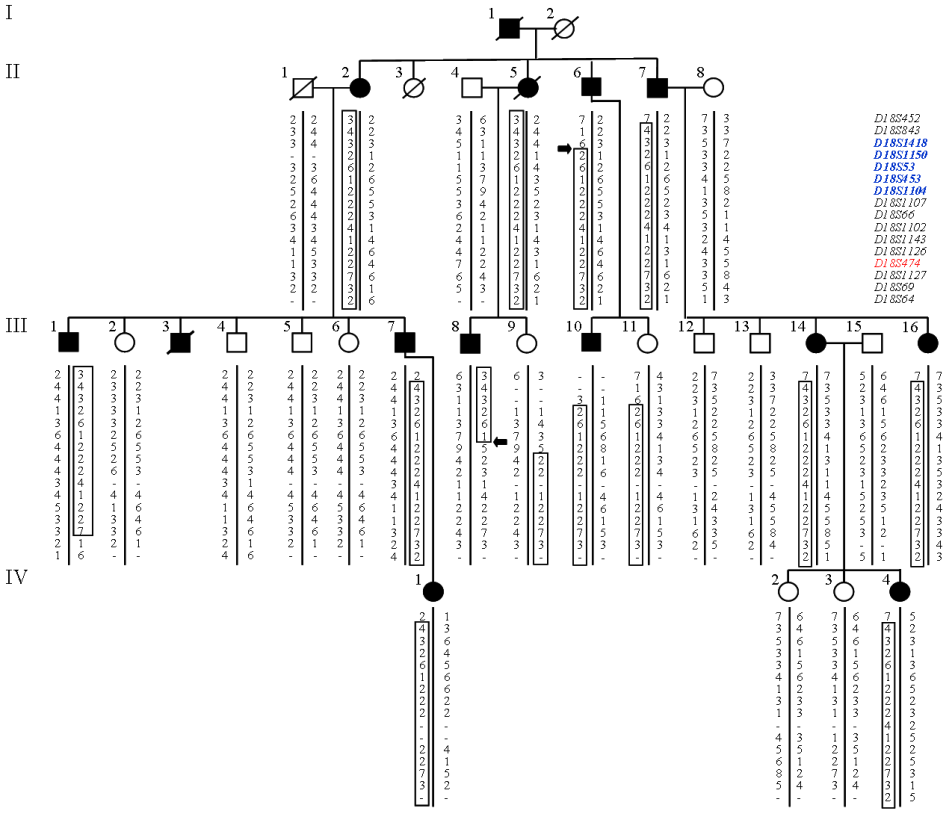

Figure 12: Linkage analysis

Pedigree of the family with 16 non-consecutive markers on chromosome 18.

This region contains approximately 70 genes (Human Genome Assembly NCBI35.1), none of which exhibits obvious similarity with any of the currently known genes causing dominant ataxias. A candidate gene approach based on expression in disease-affected tissues reduced the number of candidate genes to 12, including the gene encoding the mitochondrial metalloprotease AFG3L2 (ATPase family gene 3-like 2). Although no dominant ataxia has been thus far associated with mitochondrial dysfunction, we focused on this gene because of its partnership with paraplegin, a cognate mitochondrial protease, the loss of which causes a distinct neurodegenerative disorder, the recessively-inherited form of hereditary spastic paraplegia SPG7 (Banfi et al., 1999).

Genetic analysis of the critical region of the SCA28 locus has been conducted in all patients in this family; all the affected subjects are characterized by a missense mutation (E691K) in the exon 16 of the *AFG3L2* gene. In addition, the mutation is not found to be present in approximately 200 alleles of control of the normal population. Moreover, heterozygous AFG3L2 missense mutations were identified in other four unrelated SCA families confirming that point mutations in *AFG3L2* are associated with dominant hereditary ataxia SCA28 (Di Bella et al., 2010). Since then, AFG3L2 mutations were identified in other population of affected individual (Cagnoli et al., 2010; Edener et al., 2010). Furthermore, a homozygous mutation in AFG3L2 has been recently detected in two siblings of a consanguineous marriage who were affected by a severe early-onset syndrome characterized by severe spastic paraplegia,ataxia, ptosis, oculomotor apraxia, dystonic movements and stimulus-induced myoclonus (Pierson et al, 2011).

Paraplegin

Mutations in SPG7 gene, encoded paraplegin, were associated to an autosomal recessive form of hereditary spastic paraplegia in 1998 (Casari et al., 1998). The SPG7 gene is located on chromosome 16q24.3, it is composed of 17 exons and encodes a 795 amino acid protein (Wilkinson et al 2004, Elleuch et al. 2006).

Hereditary spastic paraparesis and SPG7

Hereditary spastic paraplegia (HSP) comprises a genetically heterogeneous group of neurodegenerative disorders (Fink, 2003; Soderblom and Blackstone, 2006; Depienne et al., 2007). The major pathological feature is a progressive degeneration of the longest axons in the body, those of the corticospinal tracts and, to a lesser extent, the fasiculi gracilis. The axonal degeneration starts from the synaptic terminal and progresses towards the cells body. Age of onset is quite variable, generally between 10 and 40 years old. According to the patient`s symptoms, the disease is classified into “pure” and “complicated” forms.

Besides progressive spasticity and weakness in the lower limbs, complicated forms are characterized by additional neurological symptoms including ataxia, mental retardation, optic atrophy, dementia and retinopathy (Harding, 1983). These diseases are genetically heterogeneous and can be autosomal dominant, autosomal recessive, or X-linked (recently reviewed in Schule and Schols, 2012) .

The phenotype of SPG7 is complicated by mild to moderate cerebellar signs as well as cerebellar atrophy on MRI in the majority of cases (Wilkinson et al., 2004; Elleuch et al., 2006). Pure cases as well as more unusual complicating symptoms, including optic atrophy, upper limb involvement, or supranuclear palsy and cognitive deficits, have been reported, however. Age at onset is usually in adulthood. The prevalence of paraplegin mutations in sporadic or autosomal recessive HSP index cases ranges from as low as 1.5% to 7%. Muscle biopsies show signs of mitochondrial disease, including ragged-red fibers and the presence of cytochrome c negative fibers in some cases. Complex I deficiency of the respiratory chain is present in muscle or fibroblasts of only some of the analysed patients. The heterogeneous pattern of mitochondrial respiratory functions in the patients seems to exclude a specific association of complex I defect with the pathology at the fibroblast level (Arnoldi et al., 2008). No systematic electrophysiologic studies have been performed in SPG7, but peripheral neuropathy has been reported in some cases. The mutational spectrum comprises missense and nonsense mutations as well as rarer small indels. Additionally, in two families a large intragenic paraplegin deletions have been identified (Casari et al., 1998; Arnoldi et al., 2008).

Mouse models

To analyze the molecular mechanisms underlying the neurodegeneration due to *m*-AAA mutations, several mouse model were generated.

At first a mouse model for HSP caused by loss-of-function mutations in the SPG7 gene was generated by deleting the first two exons of SPG7 by homologous recombination (Ferreirinha et al., 2004). Paraplegin-deficient

mice show mild and slowly progressive motor impairment associated with distal axonopathy of spinal and peripheral axons, partially recapitulating HSP patients' phenotype. Mitochondrial morphological abnormalities were found at 4,5 months of age in synaptic terminals and in distal regions of axons long before axonal degeneration and correlated with the onset of motor impairment (Ferreirinha et al., 2004). However, key mitochondrial functions, such as respiratory chain activity and ATP synthesis are not significantly impaired in spinal cords of 17-month-old Spg7-/- mice (Ferreirinha et al., 2004). Only in spinal cords of 23-month-old Spg7-/- mice a minor defect in ATP synthesis could be observed.

Subsequently, two mouse model carrying homozygous mutation or deletion in the gene coding for Afg3l2 have been described (Maltecca et al., 2008). One of these is a null mouse for Afg3l2 generated by a ecotropic reinsertion of the murine leukemia proviral Emv66 in the intron 14 of Afg3l2, while the other, named paralisè, is a spontaneous mutant strain that carries the homozygous missense mutation R389G in the same gene. Both these mouse models are affected by a severe early-onset neurological phenotype. Mice die at postnatal day 16 and exhibit a severe defect in axonal development characterized by delayed myelination and impairment of axonal radial growth in the central and peripheral nervous system (Maltecca et al., 2008). Swollen and giant mitochondria with disrupted cristae membranes are detected in motor and sensory neurons. Furthermore, a dramatic reduction of respiratory complex I and III activities were detected probably due to insufficient assembling because neither synthesis of mitochondria-encoded subunits nor import of nuclear-encoded proteins was impaired (Maltecca et al., 2008).

By contrast, heterozygous Afg3l2$^{+/Emv66}$ mice appear normal at birth and do not show a remarkable phenotype up to 3 months of age (Maltecca et al., 2009).

Finally, the double mouse model Spg7$^{-/-}$ /Afg3l2$^{+/Emv66}$ was characterized. These mice showed a severe neurological phenotype from 6 weeks of age, characterized by reduced cage activity, loss of balance, and frank uncoordinated gait, a phenotype highly reminiscent of cerebellar ataxia. Later, they lost significant weight, became immobile, and finally died

within the 4th month of life (Martinelli et al., 2009). These mice display an acceleration of the features of paraplegin-deficient mice, showing axonal degeneration in the spinal cord earlier than in the sole absence of Spg7.

Although murine MrpL32 is processed by murine *m*-AAA in a heterologous expression system (Nolden et al., 2005), a slight accumulation of the MRPL32 precursor was observed in the liver of paraplegin-deficient mice (Nolden et al., 2005) and in cerebellar mitochondria of $Spg7^{-/-}$ $Afg3l2^{Emv66/+}$ mice (Martinelli et al., 2009). However, sufficient mature MRPL32 is still present in these mitochondria and no defects of mitochondrial protein synthesis have been observed in Afg3l2 null mutants. Although still controversial, the neuron-specific phenotype of *m*-AAA defect seems to be difficult to reconcile with a housekeeping function such as the mitochondrial translation.

Scope of the thesis

Since the association of paraplegin gene with a recessive form of spastic paraparesis and even more after the identification of its partner AFG3L2 as the responsible for the spinocerebellar ataxia SCA28, the interest in the *m*-AAA complex rapidly growed up. Although several groups investigate the role of this protease in physiological and phatological condition using differet approaches, a lot of piece of the puzzle are still missing.

The aim of this work is to take a step forward in understanding the pathogenetic mechanism of *m*-AAA complex in human diseases. On one hand we screened large cohorts of patients identifying new AFG3L2 mutations and expanding the clinical spectrum of AFG3L2-associated mutations. Thus, we investigated the molecular mechanism of identified mutations characterizing the functionality of human *m*-AAAcomplexes in the budding yeast Saccharomyces cerevisiae. On the other hand we delved into the pathogenetic mechanism investigating the consequences of human *m*-AAA alterations in patient-derived cells.

References

- Arlt, H.; Steglich, G.; Perryman, R.; Guiard, B.; Neupert, W. & Langer, T. (1998), 'The formation of respiratory chain complexes in mitochondria is under the proteolytic control of the *m*-AAA protease.', *EMBO J* **17**(16), 4837--4847.

- Arlt, H.; Tauer, R.; Feldmann, H.; Neupert, W. & Langer, T. (1996), 'The YTA10-12 complex, an AAA protease with chaperone-like activity in the inner membrane of mitochondria.', *Cell* **85**(6), 875--885.

- Arnoldi, A.; Tonelli, A.; Crippa, F.; Villani, G.; Pacelli, C.; Sironi, M.; Pozzoli, U.; D'Angelo, M. G.; Meola, G.; Martinuzzi, A.; Crimella, C.; Redaelli, F.; Panzeri, C.; Renieri, A.; Comi, G. P.; Turconi, A. C.; Bresolin, N. & Bassi, M. T. (2008), 'A clinical, genetic, and biochemical characterization of SPG7 mutations in a large cohort of patients with hereditary spastic paraplegia.', *Hum Mutat* **29**(4), 522--531.

- Atorino, L.; Silvestri, L.; Koppen, M.; Cassina, L.; Ballabio, A.; Marconi, R.; Langer, T. & Casari, G. (2003), 'Loss of *m*-AAA protease in mitochondria causes complex I deficiency and increased sensitivity to oxidative stress in hereditary spastic paraplegia.', *J Cell Biol* **163**(4), 777--787.

- Augustin, S.; Gerdes, F.; Lee, S.; Tsai, F. T. F.; Langer, T. & Tatsuta, T. (2009), 'An intersubunit signaling network coordinates ATP hydrolysis by *m*-AAA proteases.', *Mol Cell* **35**(5), 574--585.

- Baker, M. J.; Tatsuta, T. & Langer, T. (2011), 'Quality control of mitochondrial proteostasis.', *Cold Spring Harb Perspect Biol* **3**(7).

- Banfi, S.; Bassi, M. T.; Andolfi, G.; Marchitiello, A.; Zanotta, S.; Ballabio, A.; Casari, G. & Franco, B. (1999), 'Identification and characterization of AFG3L2, a novel paraplegin-related gene.', *Genomics* **59**(1), 51--58.

- Benedetti, C.; Haynes, C. M.; Yang, Y.; Harding, H. P. & Ron, D. (2006), 'Ubiquitin-like protein 5 positively regulates chaperone gene expression in the mitochondrial unfolded protein response.', *Genetics* **174**(1), 229--239.

- Bieniossek, C.; Schalch, T.; Bumann, M.; Meister, M.; Meier, R. & Baumann, U. (2006), 'The molecular architecture of the metalloprotease FtsH.', *Proc Natl Acad Sci U S A* **103**(9), 3066--3071.

- Bonn, F.; Pantakani, K.; Shoukier, M.; Langer, T. & Mannan, A. U. (2010), 'Functional evaluation of paraplegin mutations by a yeast complementation assay.', *Hum Mutat* **31**(5), 617--621.

- Bota, D. A.; Ngo, J. K. & Davies, K. J. A. (2005), 'Downregulation of the human Lon protease impairs mitochondrial structure and function and causes cell death.', *Free Radic Biol Med* **38**(5), 665--677.

- Brusco, A.; Gellera, C.; Cagnoli, C.; Saluto, A.; Castucci, A.; Michielotto, C.; Fetoni, V.; Mariotti, C.; Migone, N.; Donato, S. D. & Taroni, F. (2004), 'Molecular genetics of hereditary spinocerebellar ataxia: mutation analysis of spinocerebellar ataxia genes and CAG/CTG repeat expansion detection in 225 Italian families.', *Arch Neurol* **61**(5), 727--733.

- Cagnoli, C.; Mariotti, C.; Taroni, F.; Seri, M.; Brussino, A.; Michielotto, C.; Grisoli, M.; Bella, D. D.; Migone, N.; Gellera, C.; Donato, S. D. & Brusco, A. (2006), 'SCA28, a novel form of autosomal dominant cerebellar ataxia on chromosome 18p11.22-q11.2.', *Brain* **129**(Pt 1), 235--242.

- Casari, G.; Fusco, M. D.; Ciarmatori, S.; Zeviani, M.; Mora, M.; Fernandez, P.; Michele, G. D.; Filla, A.; Cocozza, S.; Marconi, R.; Dürr, A.; Fontaine, B. & Ballabio, A. (1998), 'Spastic paraplegia and OXPHOS impairment caused by mutations in paraplegin, a nuclear-encoded mitochondrial metalloprotease.', *Cell* **93**(6), 973--983.

- Chan, D. C. (2006), 'Mitochondria: dynamic organelles in disease, aging, and development.', *Cell* **125**(7), 1241--1252.

- Chan, D. C. (2006), 'Mitochondrial fusion and fission in mammals.', *Annu Rev Cell Dev Biol* **22**, 79--99.

- Chen, H. & Chan, D. C. (2010), 'Physiological functions of mitochondrial fusion.', *Ann N Y Acad Sci* **1201**, 21--25.

- Cipolat, S.; Rudka, T.; Hartmann, D.; Costa, V.; Serneels, L.; Craessaerts, K.; Metzger, K.; Frezza, C.; Annaert, W.; D'Adamio, L.; Derks, C.; Dejaegere, T.; Pellegrini, L.; D'Hooge, R.; Scorrano, L. & De Strooper, B. (2006), 'Mitochondrial rhomboid PARL regulates cytochrome c release during apoptosis via OPA1-dependent cristae remodeling.', *Cell* **126**(1), 163--175.

- Coppola, M.; Pizzigoni, A.; Banfi, S.; Bassi, M. T.; Casari, G. & Incerti, B. (2000), 'Identification and characterization of YME1L1, a novel paraplegin-related gene.', *Genomics* **66**(1), 48--54.

- Dagda, R. K. & Chu, C. T. (2009), 'Mitochondrial quality control: insights on how Parkinson's disease related genes PINK1, parkin, and Omi/HtrA2 interact to maintain mitochondrial homeostasis.', *J Bioenerg Biomembr* **41**(6), 473--479.

- De Sagarra, M. R.; Mayo, I.; Marco, S.; Rodríguez-Vilariño, S.; Oliva, J.; Carrascosa, J. L. & Casta ñ, J. G. (1999), 'Mitochondrial localization and oligomeric structure of HClpP, the human homologue of E. coli ClpP.', *J Mol Biol* **292**(4), 819--825.

- Delettre, C.; Griffoin, J. M.; Kaplan, J.; Dollfus, H.; Lorenz, B.; Faivre, L.; Lenaers, G.; Belenguer, P. & Hamel, C. P. (2001), 'Mutation spectrum and splicing variants in the OPA1 gene.', *Hum Genet* **109**(6), 584--591.

- Depienne, C.; Stevanin, G.; Brice, A. & Durr, A. (2007), 'Hereditary spastic paraplegias: an update.', *Curr Opin Neurol* **20**(6), 674--680.

- DiBella, D.; Lazzaro, F.; Brusco, A.; Plumari, M.; Battaglia, G.; Pastore, A.; Finardi, A.; Cagnoli, C.; Tempia, F.; Frontali, M.; Veneziano, L.; Sacco, T.; Boda, E.; Brussino, A.; Bonn, F.; Castellotti, B.; Baratta, S.; Mariotti, C.; Gellera, C.; Fracasso, V.; Magri, S.; Langer, T.; Plevani, P.; Donato, S. D.; Muz*i*-Falconi, M. & Taroni, F. (2010), 'Mutations in the mitochondrial protease gene AFG3L2 cause dominant hereditary ataxia SCA28.', *Nat Genet* **42**(4), 313--321.

- Duvezin-Caubet, S.; Koppen, M.; Wagener, J.; Zick, M.; Israel, L.; Bernacchia, A.; Jagasia, R.; Rugarli, E. I.; Imhof, A.; Neupert, W.; Langer, T. & Reichert, A. S. (2007), 'OPA1 processing reconstituted in yeast

depends on the subunit composition of the *m*-AAA protease in mitochondria.', *Mol Biol Cell* **18**(9), 3582--3590.

- Edener, U.; Wöllner, J.; Hehr, U.; Kohl, Z.; Schilling, S.; Kreuz, F.; Bauer, P.; Bernard, V.; Gillessen-Kaesbach, G. & Zühlke, C. (2010), 'Early onset and slow progression of SCA28, a rare dominant ataxia in a large four-generation family with a novel AFG3L2 mutation.', *Eur J Hum Genet* **18**(8), 965--968.

- Ehses, S.; Raschke, I.; Mancuso, G.; Bernacchia, A.; Geimer, S.; Tondera, D.; Martinou, J.-C.; Westermann, B.; Rugarli, E. I. & Langer, T. (2009), 'Regulation of OPA1 processing and mitochondrial fusion by *m*-AAA protease isoenzymes and OMA1.', *J Cell Biol* **187**(7), 1023--1036.

- Elleuch, N.; Depienne, C.; Benomar, A.; Hernandez, A. M. O.; Ferrer, X.; Fontaine, B.; Grid, D.; Tallaksen, C. M. E.; Zemmouri, R.; Stevanin, G.; Durr, A. & Brice, A. (2006), 'Mutation analysis of the paraplegin gene (SPG7) in patients with hereditary spastic paraplegia.', *Neurology* **66**(5), 654--659.

- Esser, K.; Tursun, B.; Ingenhoven, M.; Michaelis, G. & Pratje, E. (2002), 'A novel two-step mechanism for removal of a mitochondrial signal sequence involves the mAAA complex and the putative rhomboid protease Pcp1.', *J Mol Biol* **323**(5), 835--843.

- Faccio, L.; Fusco, C.; Chen, A.; Martinotti, S.; Bonventre, J. V. & Zervos, A. S. (2000), 'Characterization of a novel human serine protease that has extensive homology to bacterial heat shock endoprotease HtrA and is regulated by kidney ischemia.', *J Biol Chem* **275**(4), 2581--2588.

- Ferreirinha, F.; Quattrini, A.; Pirozzi, M.; Valsecchi, V.; Dina, G.; Broccoli, V.; Auricchio, A.; Piemonte, F.; Tozzi, G.; Gaeta, L.; Casari, G.; Ballabio, A. & Rugarli, E. I. (2004), 'Axonal degeneration in paraplegin-deficient mice is associated with abnormal mitochondria and impairment of axonal transport.', *J Clin Invest* **113**(2), 231--242.

- Fink, J. K. (2003), 'The hereditary spastic paraplegias: nine genes and counting.', *Arch Neurol* **60**(8), 1045--1049.

- Graef, M. & Langer, T. (2006), 'Substrate specific consequences of central pore mutations in the *i*-AAA protease Yme1 on substrate engagement.', *J Struct Biol* **156**(1), 101--108.

- Gray, C. W.; Ward, R. V.; Karran, E.; Turconi, S.; Rowles, A.; Viglienghi, D.; Southan, C.; Barton, A.; Fantom, K. G.; West, A.; Savopoulos, J.; Hassan, N. J.; Clinkenbeard, H.; Hanning, C.; Amegadzie, B.; Davis, J. B.; Dingwall, C.; Livi, G. P. & Creasy, C. L. (2000), 'Characterization of human HtrA2, a novel serine protease involved in the mammalian cellular stress response.', *Eur J Biochem* **267**(18), 5699--5710.

- Griparic, L.; Kanazawa, T. & van der Bliek, A. M. (2007), 'Regulation of the mitochondrial dynamin-like protein Opa1 by proteolytic cleavage.', *J Cell Biol* **178**(5), 757--764.

- Hanson, P. I. & Whiteheart, S. W. (2005), 'AAA+ proteins: have engine, will work.', *Nat Rev Mol Cell Biol* **6**(7), 519--529.

- Harding, A. E. (1982), 'The clinical features and classification of the late onset autosomal dominant cerebellar ataxias. A study of 11 families, including descendants of the 'the Drew family of Walworth'.', *Brain* **105**(Pt 1), 1--28.

- Haynes, C. M.; Petrova, K.; Benedetti, C.; Yang, Y. & Ron, D. (2007), 'ClpP mediates activation of a mitochondrial unfolded protein response in C. elegans.', *Dev Cell* **13**(4), 467--480.

- Head, B.; Griparic, L.; Amiri, M.; Gandre-Babbe, S. & van der Bliek, A. M. (2009), 'Inducible proteolytic inactivation of OPA1 mediated by the OMA1 protease in mammalian cells.', *J Cell Biol* **187**(7), 959--966.

- Hegde, R.; Srinivasula, S. M.; Zhang, Z.; Wassell, R.; Mukattash, R.; Cilenti, L.; DuBois, G.; Lazebnik, Y.; Zervos, A. S.; Fernandes-Alnemri, T. & Alnemri, E. S. (2002), 'Identification of Omi/HtrA2 as a mitochondrial apoptotic serine protease that disrupts inhibitor of apoptosis protein-caspase interaction.', *J Biol Chem* **277**(1), 432--438.

- Heo, J.-M.; Livnat-Levanon, N.; Taylor, E. B.; Jones, K. T.; Dephoure, N.; Ring, J.; Xie, J.; Brodsky, J. L.; Madeo, F.; Gygi, S. P.; Ashrafi, K.;

Glickman, M. H. & Rutter, J. (2010), 'A stress-responsive system for mitochondrial protein degradation.', *Mol Cell* **40**(3), 465--480.

- Herlan, M.; Vogel, F.; Bornhovd, C.; Neupert, W. & Reichert, A. S. (2003), 'Processing of Mgm1 by the rhomboid-type protease Pcp1 is required for maintenance of mitochondrial morphology and of mitochondrial DNA.', *J Biol Chem* **278**(30), 27781--27788.

- Hooper, N. M. (1994), 'Families of zinc metalloproteases.', *FEBS Lett* **354**(1), 1--6.

- Hyde, B. B.; Twig, G. & Shirihai, O. S. (2010), 'Organellar vs cellular control of mitochondrial dynamics.', *Semin Cell Dev Biol* **21**(6), 575--581.

- Isaya, G.; Kalousek, F.; Fenton, W. A. & Rosenberg, L. E. (1991), 'Cleavage of precursors by the mitochondrial processing peptidase requires a compatible mature protein or an intermediate octapeptide.', *J Cell Biol* **113**(1), 65--76.

- Ishihara, N.; Fujita, Y.; Oka, T. & Mihara, K. (2006), 'Regulation of mitochondrial morphology through proteolytic cleavage of OPA1.', *EMBO J* **25**(13), 2966--2977.

- Johnson, F. & Kaplitt, M. G. (2009), 'Novel mitochondrial substrates of omi indicate a new regulatory role in neurodegenerative disorders.', *PLoS One* **4**(9), e7100.

- Jones, J. M.; Datta, P.; Srinivasula, S. M.; Ji, W.; Gupta, S.; Zhang, Z.; Davies, E.; Hajnóczky, G.; Saunders, T. L.; Van Keuren, M. L.; Fernandes-Alnemri, T.; Meisler, M. H. & Alnemri, E. S. (2003), 'Loss of Omi mitochondrial protease activity causes the neuromuscular disorder of mnd2 mutant mice.', *Nature* **425**(6959), 721--727.

- Juhola, M. K.; Shah, Z. H.; Grivell, L. A. & Jacobs, H. T. (2000), 'The mitochondrial inner membrane AAA metalloprotease family in metazoans.', *FEBS Lett* **481**(2), 91--95.

- Karata, K.; Inagawa, T.; Wilkinson, A. J.; Tatsuta, T. & Ogura, T. (1999), 'Dissecting the role of a conserved motif (the second region of homology)

in the AAA family of ATPases. Site-directed mutagenesis of the ATP-dependent protease FtsH.', *J Biol Chem* **274**(37), 26225--26232.

- Karata, K.; Verma, C. S.; Wilkinson, A. J. & Ogura, T. (2001), 'Probing the mechanism of ATP hydrolysis and substrate translocation in the AAA protease FtsH by modelling and mutagenesis.', *Mol Microbiol* **39**(4), 890--903.

- Karbowski, M.; Neutzner, A. & Youle, R. J. (2007), 'The mitochondrial E3 ubiquitin ligase MARCH5 is required for Drp1 dependent mitochondrial division.', *J Cell Biol* **178**(1), 71--84.

- Koeppen, A. H. (2005), 'The pathogenesis of spinocerebellar ataxia.', *Cerebellum* **4**(1), 62--73.

- Koppen, M. & Langer, T. (2007), 'Protein degradation within mitochondria: versatile activities of AAA proteases and other peptidases.', *Crit Rev Biochem Mol Biol* **42**(3), 221--242.

- Koppen, M.; Metodiev, M. D.; Casari, G.; Rugarli, E. I. & Langer, T. (2007), 'Variable and tissue-specific subunit composition of mitochondrial *m*-AAA protease complexes linked to hereditary spastic paraplegia.', *Mol Cell Biol* **27**(2), 758--767.

- Korbel, D.; Wurth, S.; Käser, M. & Langer, T. (2004), 'Membrane protein turnover by the *m*-AAA protease in mitochondria depends on the transmembrane domains of its subunits.', *EMBO Rep* **5**(7), 698--703.

- Kremmidiotis, G.; Gardner, A. E.; Settasatian, C.; Savoia, A.; Sutherland, G. R. & Callen, D. F. (2001), 'Molecular and functional analyses of the human and mouse genes encoding AFG3L1, a mitochondrial metalloprotease homologous to the human spastic paraplegia protein.', *Genomics* **76**(1-3), 58--65.

- Krzywda, S.; Brzozowski, A. M.; Verma, C.; Karata, K.; Ogura, T. & Wilkinson, A. J. (2002), 'The crystal structure of the AAA domain of the ATP-dependent protease FtsH of Escherichia coli at 1.5 A resolution.', *Structure* **10**(8), 1073--1083.

- Landes, T.; Leroy, I.; Bertholet, A.; Diot, A.; Khosrobakhsh, F.; Daloyau, M.; Davezac, N.; Miquel, M.-C.; Courilleau, D.; Guillou, E.; Olichon, A.; Lenaers, G.; Arnauné-Pelloquin, L.; Emorine, L. J. & Belenguer, P. (2010), 'OPA1 (dys)functions.', *Semin Cell Dev Biol* **21**(6), 593--598.

- Langer, T. (2000), 'AAA proteases: cellular machines for degrading membrane proteins.', *Trends Biochem Sci* **25**(5), 247--251.

- Langer, T.; Käser, M.; Klanner, C. & Leonhard, K. (2001), 'AAA proteases of mitochondria: quality control of membrane proteins and regulatory functions during mitochondrial biogenesis.', *Biochem Soc Trans* **29**(Pt 4), 431--436.

- Leonhard, K.; Guiard, B.; Pellecchia, G.; Tzagoloff, A.; Neupert, W. & Langer, T. (2000), 'Membrane protein degradation by AAA proteases in mitochondria: extraction of substrates from either membrane surface.', *Mol Cell* **5**(4), 629--638.

- Leonhard, K.; Herrmann, J. M.; Stuart, R. A.; Mannhaupt, G.; Neupert, W. & Langer, T. (1996), 'AAA proteases with catalytic sites on opposite membrane surfaces comprise a proteolytic system for the ATP-dependent degradation of inner membrane proteins in mitochondria.', *EMBO J* **15**(16), 4218--4229.

- Leonhard, K.; Stiegler, A.; Neupert, W. & Langer, T. (1999), 'Chaperone-like activity of the AAA domain of the yeast Yme1 AAA protease.', *Nature* **398**(6725), 348--351.

- Li, B.; Hu, Q.; Wang, H.; Man, N.; Ren, H.; Wen, L.; Nukina, N.; Fei, E. & Wang, G. (2010), 'Omi/HtrA2 is a positive regulator of autophagy that facilitates the degradation of mutant proteins involved in neurodegenerative diseases.', *Cell Death Differ* **17**(11), 1773--1784.

- Lin, M. T. & Beal, M. F. (2006), 'Mitochondrial dysfunction and oxidative stress in neurodegenerative diseases.', *Nature* **443**(7113), 787--795.

- Lu, B.; Yadav, S.; Shah, P. G.; Liu, T.; Tian, B.; Pukszta, S.; Villaluna, N.; Kutejová, E.; Newlon, C. S.; Santos, J. H. & Suzuki, C. K. (2007), 'Roles

for the human ATP-dependent Lon protease in mitochondrial DNA maintenance.', *J Biol Chem* **282**(24), 17363--17374.

- Maltecca, F.; Aghaie, A.; Schroeder, D. G.; Cassina, L.; Taylor, B. A.; Phillips, S. J.; Malaguti, M.; Previtali, S.; Guénet, J.-L.; Quattrini, A.; Cox, G. A. & Casari, G. (2008), 'The mitochondrial protease AFG3L2 is essential for axonal development.', *J Neurosci* **28**(11), 2827--2836.

- Maltecca, F.; Magnoni, R.; Cerri, F.; Cox, G. A.; Quattrini, A. & Casari, G. (2009), 'Haploinsufficiency of AFG3L2, the gene responsible for spinocerebellar ataxia type 28, causes mitochondria-mediated Purkinje cell dark degeneration.', *J Neurosci* **29**(29), 9244--9254.

- Mariotti, C.; Brusco, A.; Bella, D. D.; Cagnoli, C.; Seri, M.; Gellera, C.; Donato, S. D. & Taroni, F. (2008), 'Spinocerebellar ataxia type 28: a novel autosomal dominant cerebellar ataxia characterized by slow progression and ophthalmoparesis.', *Cerebellum* **7**(2), 184--188.

- Martinelli, P. & Rugarli, E. I. (2010), 'Emerging roles of mitochondrial proteases in neurodegeneration.', *Biochim Biophys Acta* **1797**(1), 1--10.

- Martins, L. M.; Morrison, A.; Klupsch, K.; Fedele, V.; Moisoi, N.; Teismann, P.; Abuin, A.; Grau, E.; Geppert, M.; Livi, G. P.; Creasy, C. L.; Martin, A.; Hargreaves, I.; Heales, S. J.; Okada, H.; Brandner, S.; Schulz, J. B.; Mak, T. & Downward, J. (2004), 'Neuroprotective role of the Reaper-related serine protease HtrA2/Omi revealed by targeted deletion in mice.', *Mol Cell Biol* **24**(22), 9848--9862.

- Matilla-Dueñas, A.; Sánchez, I.; Corral-Juan, M.; Dávalos, A.; Alvarez, R. & Latorre, P. (2010), 'Cellular and molecular pathways triggering neurodegeneration in the spinocerebellar ataxias.', *Cerebellum* **9**(2), 148--166.

- McBride, H. & Soubannier, V. (2010), 'Mitochondrial Function: OMA1 and OPA1, the Grandmasters of Mitochondrial Health.', *Curr Biol* **20**(6), R274--R276.

- McQuibban, G. A.; Saurya, S. & Freeman, M. (2003), 'Mitochondrial membrane remodelling regulated by a conserved rhomboid protease.', *Nature* **423**(6939), 537--541.

- Merkwirth, C.; Dargazanli, S.; Tatsuta, T.; Geimer, S.; Löwer, B.; Wunderlich, F. T.; von Kleist-Retzow, J.-C.; Waisman, A.; Westermann, B. & Langer, T. (2008), 'Prohibitins control cell proliferation and apoptosis by regulating OPA1-dependent cristae morphogenesis in mitochondria.', *Genes Dev* **22**(4), 476--488.

- Mogk, A.; Haslberger, T.; Tessarz, P. & Bukau, B. (2008), 'Common and specific mechanisms of AAA+ proteins involved in protein quality control.', *Biochem Soc Trans* **36**(Pt 1), 120--125.

- Mossmann, D.; Meisinger, C. & Vögtle, F.-N. (2011), 'Processing of mitochondrial presequences.', *Biochim Biophys Acta*.

- Naamati, A.; Regev-Rudzki, N.; Galperin, S.; Lill, R. & Pines, O. (2009), 'Dual targeting of Nfs1 and discovery of its novel processing enzyme, Icp55.', *J Biol Chem* **284**(44), 30200--30208.

- Nakamura, N.; Kimura, Y.; Tokuda, M.; Honda, S. & Hirose, S. (2006), 'MARCH-V is a novel mitofusin 2- and Drp1-binding protein able to change mitochondrial morphology.', *EMBO Rep* **7**(10), 1019--1022.

- Narendra, D. P. & Youle, R. J. (2011), 'Targeting mitochondrial dysfunction: role for PINK1 and Parkin in mitochondrial quality control.', *Antioxid Redox Signal* **14**(10), 1929--1938.

- Neuwald, A. F.; Aravind, L.; Spouge, J. L. & Koonin, E. V. (1999), 'AAA+: A class of chaperone-like ATPases associated with the assembly, operation, and disassembly of protein complexes.', *Genome Res* **9**(1), 27--43.

- Nolden, M.; Ehses, S.; Koppen, M.; Bernacchia, A.; Rugarli, E. I. & Langer, T. (2005), 'The *m*-AAA protease defective in hereditary spastic paraplegia controls ribosome assembly in mitochondria.', *Cell* **123**(2), 277--289.

- Nunnari, J.; Fox, T. D. & Walter, P. (1993), 'A mitochondrial protease with two catalytic subunits of nonoverlapping specificities.', *Science* **262**(5142), 1997--2004.

- Ogura, T.; Whiteheart, S. W. & Wilkinson, A. J. (2004), 'Conserved arginine residues implicated in ATP hydrolysis, nucleotide-sensing, and inter-subunit interactions in AAA and AAA+ ATPases.', *J Struct Biol* **146**(1-2), 106--112.

- Olichon, A.; Emorine, L. J.; Descoins, E.; Pelloquin, L.; Brichese, L.; Gas, N.; Guillou, E.; Delettre, C.; Valette, A.; Hamel, C. P.; Ducommun, B.; Lenaers, G. & Belenguer, P. (2002), 'The human dynamin-related protein OPA1 is anchored to the mitochondrial inner membrane facing the inter-membrane space.', *FEBS Lett* **523**(1-3), 171--176.

- Pierson, T. M.; Adams, D.; Bonn, F.; Martinelli, P.; Cherukuri, P. F.; Teer, J. K.; Hansen, N. F.; Cruz, P.; Mullikin For The Nisc Comparative Sequencing Program, J. C.; Blakesley, R. W.; Golas, G.; Kwan, J.; Sandler, A.; Fuentes Fajardo, K.; Markello, T.; Tifft, C.; Blackstone, C.; Rugarli, E. I.; Langer, T.; Gahl, W. A. & Toro, C. (2011), 'Whole-Exome Sequencing Identifies Homozygous AFG3L2 Mutations in a Spastic Ataxia-Neuropathy Syndrome Linked to Mitochondrial *m*-AAA Proteases.', *PLoS Genet* **7**(10), e1002325.

- Plun-Favreau, H.; Klupsch, K.; Moisoi, N.; Gandhi, S.; Kjaer, S.; Frith, D.; Harvey, K.; Deas, E.; Harvey, R. J.; McDonald, N.; Wood, N. W.; Martins, L. M. & Downward, J. (2007), 'The mitochondrial protease HtrA2 is regulated by Parkinson's disease-associated kinase PINK1.', *Nat Cell Biol* **9**(11), 1243--1252.

- Rawlings, N. D. & Barrett, A. J. (1995), 'Evolutionary families of metallopeptidases.', *Methods Enzymol* **248**, 183--228.

- Rugarli, E. I. & Langer, T. (2012), 'Mitochondrial quality control: a matter of life and death for neurons.', *EMBO J*.

- Sauer, R. T.; Bolon, D. N.; Burton, B. M.; Burton, R. E.; Flynn, J. M.; Grant, R. A.; Hersch, G. L.; Joshi, S. A.; Kenniston, J. A.; Levchenko, I.; Neher, S. B.; Oakes, E. S. C.; Siddiqui, S. M.; Wah, D. A. & Baker, T. A.

(2004), 'Sculpting the proteome with AAA(+) proteases and disassembly machines.', *Cell* **119**(1), 9--18.

- Savopoulos, J. W.; Carter, P. S.; Turconi, S.; Pettman, G. R.; Karran, E. H.; Gray, C. W.; Ward, R. V.; Jenkins, O. & Creasy, C. L. (2000), 'Expression, purification, and functional analysis of the human serine protease HtrA2.', *Protein Expr Purif* **19**(2), 227--234.

- Schmidt, O.; Pfanner, N. & Meisinger, C. (2010), 'Mitochondrial protein import: from proteomics to functional mechanisms.', *Nat Rev Mol Cell Biol* **11**(9), 655--667.

- Schon, E. A. & Przedborski, S. (2011), 'Mitochondria: the next (neurode)generation.', *Neuron* **70**(6), 1033--1053.

- Schöls, L.; Bauer, P.; Schmidt, T.; Schulte, T. & Riess, O. (2004), 'Autosomal dominant cerebellar ataxias: clinical features, genetics, and pathogenesis.', *Lancet Neurol* **3**(5), 291--304.

- Schüle, R. & Schöls, L. (2011), 'Genetics of hereditary spastic paraplegias.', *Semin Neurol* **31**(5), 484--493.

- Shah, Z. H.; Hakkaart, G. A.; Arku, B.; de Jong, L.; van der Spek, H.; Grivell, L. A. & Jacobs, H. T. (2000), 'The human homologue of the yeast mitochondrial AAA metalloprotease Yme1p complements a yeast yme1 disruptant.', *FEBS Lett* **478**(3), 267--270.

- Snider, J.; Thibault, G. & Houry, W. A. (2008), 'The AAA+ superfamily of functionally diverse proteins.', *Genome Biol* **9**(4), 216.

- Soderblom, C. & Blackstone, C. (2006), 'Traffic accidents: molecular genetic insights into the pathogenesis of the hereditary spastic paraplegias.', *Pharmacol Ther* **109**(1-2), 42--56.

- Song, Z.; Chen, H.; Fiket, M.; Alexander, C. & Chan, D. C. (2007), 'OPA1 processing controls mitochondrial fusion and is regulated by mRNA splicing, membrane potential, and Yme1L.', *J Cell Biol* **178**(5), 749--755.

- Steglich, G.; Neupert, W. & Langer, T. (1999), 'Prohibitins regulate membrane protein degradation by the *m*-AAA protease in mitochondria.', *Mol Cell Biol* **19**(5), 3435--3442.

- Strauss, K. M.; Martins, L. M.; Plun-Favreau, H.; Marx, F. P.; Kautzmann, S.; Berg, D.; Gasser, T.; Wszolek, Z.; Müller, T.; Bornemann, A.; Wolburg, H.; Downward, J.; Riess, O.; Schulz, J. B. & Krüger, R. (2005), 'Loss of function mutations in the gene encoding Omi/HtrA2 in Parkinson's disease.', *Hum Mol Genet* **14**(15), 2099--2111.

- Suno, R.; Niwa, H.; Tsuchiya, D.; Zhang, X.; Yoshida, M. & Morikawa, K. (2006), 'Structure of the whole cytosolic region of ATP-dependent protease FtsH.', *Mol Cell* **22**(5), 575--585.

- Suzuki, C. K.; Suda, K.; Wang, N. & Schatz, G. (1994), 'Requirement for the yeast gene LON in intramitochondrial proteolysis and maintenance of respiration.', *Science* **264**(5161), 891.

- Suzuki, Y.; Imai, Y.; Nakayama, H.; Takahashi, K.; Takio, K. & Takahashi, R. (2001), 'A serine protease, HtrA2, is released from the mitochondria and interacts with XIAP, inducing cell death.', *Mol Cell* **8**(3), 613--621.

- Tanaka, A.; Cleland, M. M.; Xu, S.; Narendra, D. P.; Suen, D.-F.; Karbowski, M. & Youle, R. J. (2010), 'Proteasome and p97 mediate mitophagy and degradation of mitofusins induced by Parkin.', *J Cell Biol* **191**(7), 1367--1380.

- Taroni, F. & DiDonato, S. (2004), 'Pathways to motor incoordination: the inherited ataxias.', *Nat Rev Neurosci* **5**(8), 641--655.

- Tatsuta, T.; Augustin, S.; Nolden, M.; Friedrichs, B. & Langer, T. (2007), '*m*-AAA protease-driven membrane dislocation allows intramembrane cleavage by rhomboid in mitochondria.', *EMBO J* **26**(2), 325--335.

- Tatsuta, T. & Langer, T. (2009), 'AAA proteases in mitochondria: diverse functions of membrane-bound proteolytic machines.', *Res Microbiol*.

- Twig, G.; Hyde, B. & Shirihai, O. S. (2008), 'Mitochondrial fusion, fission and autophagy as a quality control axis: the bioenergetic view.', *Biochim Biophys Acta* **1777**(9), 1092--1097.

- Urantowka, A.; Knorpp, C.; Olczak, T.; Kolodziejczak, M. & Janska, H. (2005), 'Plant mitochondria contain at least two *i*-AAA-like complexes.', *Plant Mol Biol* **59**(2), 239--252.

- Van Dyck, L.; Pearce, D. A. & Sherman, F. (1994), 'PIM1 encodes a mitochondrial ATP-dependent protease that is required for mitochondrial function in the yeast Saccharomyces cerevisiae.', *J Biol Chem* **269**(1), 238--242.

- Van Loo, G.; van Gurp, M.; Depuydt, B.; Srinivasula, S. M.; Rodriguez, I.; Alnemri, E. S.; Gevaert, K.; Vandekerckhove, J.; Declercq, W. & Vandenabeele, P. (2002), 'The serine protease Omi/HtrA2 is released from mitochondria during apoptosis. Omi interacts with caspase-inhibitor XIAP and induces enhanced caspase activity.', *Cell Death Differ* **9**(1), 20--26.

- Vande Walle, L.; Lamkanfi, M. & Vandenabeele, P. (2008), 'The mitochondrial serine protease HtrA2/Omi: an overview.', *Cell Death Differ* **15**(3), 453--460.

- Wang, N.; Maurizi, M. R.; Emmert-Buck, L. & Gottesman, M. M. (1994), 'Synthesis, processing, and localization of human Lon protease.', *J Biol Chem* **269**(46), 29308--29313.

- Weber, E. R.; Hanekamp, T. & Thorsness, P. E. (1996), 'Biochemical and functional analysis of the YME1 gene product, an ATP and zinc-dependent mitochondrial protease from S. cerevisiae.', *Mol Biol Cell* **7**(2), 307--317.

- Wendler, P.; Ciniawsky, S.; Kock, M. & Kube, S. (2012), 'Structure and function of the AAA+ nucleotide binding pocket.', *Biochim Biophys Acta* **1823**(1), 2--14.

- Westermann, B. (2002), 'Merging mitochondria matters: cellular role and molecular machinery of mitochondrial fusion.', *EMBO Rep* **3**(6), 527--531.

- Wilkinson, P. A.; Crosby, A. H.; Turner, C.; Bradley, L. J.; Ginsberg, L.; Wood, N. W.; Schapira, A. H. & Warner, T. T. (2004), 'A clinical, genetic and biochemical study of SPG7 mutations in hereditary spastic paraplegia.', *Brain* **127**(Pt 5), 973--980.

- Yonashiro, R.; Ishido, S.; Kyo, S.; Fukuda, T.; Goto, E.; Matsuki, Y.; Ohmura-Hoshino, M.; Sada, K.; Hotta, H.; Yamamura, H.; Inatome, R. & Yanagi, S. (2006), 'A novel mitochondrial ubiquitin ligase plays a critical role in mitochondrial dynamics.', *EMBO J* **25**(15), 3618--3626.

- Youle, R. J. & Narendra, D. P. (2011), 'Mechanisms of mitophagy.', *Nat Rev Mol Cell Biol* **12**(1), 9--14.

- Zhao, Q.; Wang, J.; Levichkin, I. V.; Stasinopoulos, S.; Ryan, M. T. & Hoogenraad, N. J. (2002), 'A mitochondrial specific stress response in mammalian cells.', *EMBO J* **21**(17), 4411--4419.

Chapter 2

Mutations in the mitochondrial protease gene AFG3L2 cause dominant hereditary ataxia SCA28

D. Di Bella[1], F. Lazzaro[2], A. Brusco[3], M. Plumari[1], G. Battaglia[4], A. Pastore[5], A. Finardi[4], C. Cagnoli[3], F. Tempia[6], M. Frontali[7], L. Veneziano[7], T.Sacco[6], E. Boda[6], A. Brussino[3], F. Bonn[8], B. Castellotti[1], S. Baratta[1], C. Mariotti[1], C. Gellera[1], V. Fracasso[1], S. Magri[1], T. Langer[8], P. Plevani[2], S. Di Donato[1], M. Muz*i*-Falconi[2], F. Taroni[1]

[1]Unit of Genetics of Neurodegenerative and Metabolic Diseases, Fondazione IRCCS Istituto Neurologico "Carlo Besta", Milan, Italy.

[2]Department of Biomolecular Sciences and Biotechnology, University of Milan, Milan, Italy.

[3]Department of Genetics, Biology, and Biochemistry, University of Turin, and Unit of Medical Genetics, San Giovanni Battista Hospital, Turin, Italy.

[4]Unit of Molecular Neuroanatomy, Fondazione IRCCS Istituto Neurologico "Carlo Besta", Milan, Italy.

[5]National Institute for Medical Research, London, UK.

[6]Section of Physiology of the Department of Neuroscience, University of Turin, and Rita Levi Montalcini Center for Brain Repair, National Institute of Neuroscience, Turin, Italy.

[7]Institute of Neurobiology and Molecular Medicine, Consiglio Nazionale delle Ricerche, Rome, Italy.

[8]Institute for Genetics and Center for Molecular Medicine Cologne, University of Cologne, Germany.

Nature Genetics 42:313–321.2010

Abstract

Autosomal dominant spinocerebellar ataxias (SCAs) are genetically heterogeneous neurological disorders characterized by cerebellar dysfunction mostly due to Purkinje cell degeneration. Here we show that AFG3L2 mutations cause SCA type 28. Along with paraplegin, which causes recessive spastic paraplegia, AFG3L2 is a component of the conserved *m*-AAA metalloprotease complex involved in the maintenance of the mitochondrial proteome. We identified heterozygous missense mutations in five unrelated SCA families and found that AFG3L2 is highly and selectively expressed in human cerebellar Purkinje cells. *m*-AAA–deficient yeast cells expressing human mutated AFG3L2 homocomplex show respiratory deficiency, proteolytic impairment
and deficiency of respiratory chain complex IV. Structure homology modeling indicates that the mutations may affect AFG3L2 substrate handling. This work identifies AFG3L2 as a novel cause of dominant neurodegenerative disease and indicates a previously unknown role for this component of the mitochondrial protein quality control machinery in protecting the human cerebellum against neurodegeneration.

Introduction

Autosomal dominant SCAs are a clinically and genetically heterogeneous group of neurological disorders primarily characterized by imbalance, progressive gait and limb ataxia, and dysarthria[1–3], caused by degeneration of the cerebellum and its afferent and efferent connections[2–5]. Twenty-eight SCA loci are currently known, and 16 seemingly unrelated disease genes have been identified thus far[3] (http://neuromuscular.wustl.edu/ataxia/domatax.html). In ten types of ataxia, the disease is caused by dynamic expansions of polyglutamine-encoding CAG repeats[4,6] (SCA types 1, 2, 3, 6, 7 and 17, and dentatorubral-pallidoluysian atrophy) or repeats falling outside the coding region[7] (SCA types 10, 12 and 31) in genes whose function is still largely unknown. In recent years, a group of SCAs have emerged that are caused by conventional mutations in specific genes (SCA types 5, 11, 13, 14, 15/16/29 and 27). The distinct functions of these disease genes have revealed the complex heterogeneity of the pathogenic mechanisms leading to cerebellar degeneration and ataxia[3].

We had mapped a previously unidentified SCA locus (*SCA28*) on chromosome 18p11.22–q11.2 in a four-generation Italian family with an autosomal dominant form of cerebellar ataxia[8] (ADCA type I (ref. 1)). On the basis of expression profiles in the nervous system, we selected 12 genes within the 7.9-megabase critical region, including that encoding the mitochondrial metalloprotease AFG3L2 (ATPase family gene 3-like 2). Although no dominant ataxia has thus far been associated with mitochondrial dysfunction, we focused on this gene because of its partnership with paraplegin, a cognate mitochondrial protease, the loss of which causes a distinct neurodegenerative disorder, the recessively inherited form of hereditary spastic paraplegia SPG7 (ref. 9).

AFG3L2 and paraplegin are highly homologous (40–45% amino acid identity) to two yeast mitochondrial proteins, Yta10p (Afg3p) and Yta12p (Rca1p), respectively, belonging to the superfamily of P-loop ATPases known as ATPases associated with various cellular activities, or AAA+ (ref. 10). They contain an ATP-binding/ATPase domain (AAA domain), the

structural hallmark of the AAA-protease subfamily[11,12], and a zinc-dependent metalloprotease domain in a single polypeptide (**Fig. 1**), and they form large proteolytic complexes in the mitochondrial inner membrane that are active on the matrix side (*m*-AAA protease)[12]. In humans, *m*-AAA is composed of paraplegin and AFG3L2. A third *m*-AAA subunit paralog, AFG3L1, is expressed in mouse but is encoded by a pseudogene in humans[13]. In yeast, the *m*-AAA is a hetero-oligomer composed of Yta10p and Yta12p subunits. By contrast, both homo-oligomeric AFG3L2-AFG3L2 and hetero-oligomeric AFG3L2-paraplegin complexes exist in mammalian mitochondria[13]. Yeast studies have demonstrated that *m*-AAA is a crucial component of the mitochondrial protein quality-control system[14]. It also has a regulatory role in mitochondrial protein synthesis and antioxidant defence, participating in protein processing and maturation both in yeast and mammals[15,16].

We report that heterozygous missense mutations in *AFG3L2* cause dominant hereditary spinocerebellar ataxia type 28 (SCA28).

Expression of mutant human AFG3L2 in yeast demonstrated that the mutations alter the proteolytic competence of the *m*-AAA complex, ultimately resulting in defective activity of cytochrome *c* oxidase (COX, also known as complex IV) and impairment of cell respiration. SCA28 is, to our knowledge, the first autosomal dominant spinocerebellar ataxia shown to be caused by alterations in a mitochondrial protein. Consistent with the clinicopathological phenotype, *AFG3L2* is highly and selectively expressed in cerebellar Purkinje cells. Our results indicate a specialized role for this component of the *m*-AAA complex in protecting the human cerebellum from neurodegeneration.

Results

Missense mutations affect functional domains of AFG3L2

Human AFG3L2 is an ~80-kDa protein encoded by a 17-exon gene (**Fig. 1**). Sequence analysis of *AFG3L2* in proband II*I*-7 of the original kindred M*I*-A0091 (ref. 8) revealed a single G2071A change in exon 16

(**Supplementary Fig. 1**), resulting in the amino acid substitution E691K within the proteolytic domain, in a region that is highly conserved in *m*-AAA and *m*-AAA–related proteins from eubacteria to humans (**Fig. 1**). The mutation was found in heterozygosis in all the affected subjects (**Supplementary Fig. 1**), consistent with the dominant pattern of inheritance, but in none of >400 unrelated ethnically matched controls.

We then examined 337 unrelated people with ataxia (Online Methods) for the presence of AFG3L2 mutations. The pattern of inheritance was dominant in 136 affected individuals and consistent with recessive transmission in 51. The disease was apparently sporadic in 150 individuals. Numerous sequence variants were identified in both affected and control subjects (**Supplementary Table 1**). Five missense mutations (**Supplementary Fig. 1**), all in heterozygous form, were detected in affected individuals only, suggesting that they may be causative mutations. Three amino acid substitutions (S674L, A694E and R702Q) found in affected individuals with dominant inheritance occurred within a portion of the proteolytic domain encoded in exon 16 (**Fig. 1**), close to the E691K substitution identified in kindred M*I*-A0091. R702Q was found in family M*I*-A0762 in the fully symptomatic index patient and in her mother and maternal uncle, both negative at neurological examination but with moderate cerebellar atrophy at magnetic resonance imaging, suggesting reduced expressivity of the mutation (**Supplementary Fig. 2**). A fourth substitution (N432T) was found in the sequence encoded by exon 10, within a highly conserved region of the ATPase domain (**Fig. 1**), in the six living affected members from a three-generation family (M*I*-A2473/R*M*-DS) presenting an ADCA type 1 phenotype. Finally, one substitution (H126Q) outside the proteolytic domain, in a region of the protein with unknown function encoded by exon 4 (**Supplementary Note**), was found in one affected individual in the possibly recessive group.

AFG3L2 substitutions impair respiration in yeast

As in silico predictions and analysis of AFG3L2 mRNA in the cells of affected individuals ruled out possible effects of the mutations on pre-mRNA splicing (Supplementary Note), we investigated the functional

consequences of the disease-segregating mutations in the facultative aerobic yeast Saccharomyces cerevisiae. Yeast cells lacking the Yta10p (yta10Δ) or Yta12p (yta12Δ) *m*-AAA subunit grow on glucose but show impaired growth on a nonfermentable carbon source such as glycerol, indicating a respiratory defect16 (OXPHOS phenotype), and they also do not process substrate proteins of the *m*-AAA complex13,15–17. Notably, this phenotype can be rescued by the expression of mammalian AFG3L2 alone, which, unlike paraplegin, can homo-oligomerize into a functional *m*-AAA complex13. We therefore tested the identified AFG3L2 variants for their ability to support respiration in an *m*-AAA–defective strain (yta10Δyta12Δ) obtained by targeted deletion of both the YTA10 and YTA12 genes (Fig. 2). Overexpression of human AFG3L2 was necessary to fully restore respiration (Fig. 2a). yta10Δyta12Δ cells were transformed with wild-type AFG3L2 (AFG3L2WT), the six identified mutants and AFG3L2E575Q, used as a positive control for inactivation of proteolytic activity13,16 (Fig.2b). When glycerol (YPG) was the only carbon source, the yta10Δyta12Δ OXPHOS phenotype was rescued by both AFG3L2WT and AFG3L2H126Q, suggesting that this substitution, located outside the conserved functional domains, probably represents a rare or private variant of no or limited pathological relevance. By contrast, despite the high levels of expression (Fig. 2g and Supplementary Fig. 3), the four variants with substitutions in the protease domain (AFG3L2E691K, AFG3L2S674L, AFG3L2A694E and AFG3L2R702Q) as well as the one with a substitution in the ATPase domain (AFG3L2N432T) did not restore respiration (Fig. 2b), indicating that these substitutions are deleterious. Given the missense nature of the mutations, we examined whether haploinsufficiency or negative dominance was the mechanism underlying these effects by coexpressing wild-type AFG3L2 with each mutant (Fig. 2c and Supplementary Fig. 4). Notably, introducing AFG3L2WT into cells carrying mutant AFG3L2E691K (Fig. 2c) or AFG3L2N432T (Supplementary Fig. 4) resulted in only a limited correction of the yta10Δyta12Δ respiratory phenotype, with an intermediately reduced growth rate of AFG3L2WT-AFG3L2mut cells, clearly indicating a dominant negative effect of these fully penetrant mutations. By contrast, coexpression of

AFG3L2WT with mutant AFG3L2S674L, AFG3L2A694E or AFG3L2R702Q fully rescued the defective growth phenotype, suggesting that haploin-sufficiency or weak negative dominance may be the disease-causing mechanism for these mutations.

To recapitulate the physiological organization of *m*-AAA in human cells, we performed a further set of experiments in which AFG3L2 and paraplegin were coexpressed (Fig. 2d–g). yta10Δyta12Δ cells carrying AFG3L2E691K (Fig. 2d,f) or the AFG3L2E575Q control (data not shown) still had a respiratory-deficient phenotype, which is consistent with a dominant negative effect of these mutations. Rescue of the AFG3L2N432T phenotype by paraplegin appeared to be temperature sensitive, with moderate growth at 28 °C that was progressively reduced and abolished at higher temperatures (Fig. 2e). By contrast, coexpression of paraplegin in the 28–37 °C range always restored respiration in cells harbouring the mutant AFG3L2S674L, AFG3L2A694E or AFG3L2R702Q, suggesting that hetero-oligomeric complexes may form between mutant AFG3L2 and paraplegin. We confirmed this with co-immunoprecipitation experiments showing that both paraplegin-responsive and paraplegin-nonresponsive mutants of AFG3L2 interact with paraplegin in a quantitative fashion (Fig. 2g).

AFG3L2 substitutions impair cytochrome *c* oxidase activity in yeast

The *m*-AAA protease is an integral protein of the inner mitochondrial membrane that has a crucial role in the quality control of mitochondrial membrane proteins, participating in both the degradation of loosely folded polypeptides and the correct assembly of other integral components of the inner membrane, including complexes of the respiratory chain[14,17,18]. To elucidate the mechanism responsible for the OXPHOS phenotype induced by SCA28 mutations, we investigated respiratory-chain activity. Whereas complex III (ubiquinol:ferricytochrome-*c* oxidoreductase) and complex V (ATPase) activities were less severely affected (data not shown), the five SCA28 mutations caused a marked reduction (≥90%) of COX activity and reduction in the levels of COX subunit proteins (**Fig. 3a**,**b** and

Supplementary Note), as observed in cells (*yta10*A*yta12*A) lacking endogenous *m*-AAA (ref. 18). The severe COX defect provides a direct explanation for the respiratory-deficient phenotype associated with AFG3L2 SCA28 mutations. In the presence of paraplegin, COX enzyme activity and subunit protein levels are restored in cells expressing AFG3L2^{S674L}, AFG3L2^{A694E} or AFG3L2^{R702}Q (paraplegin-responsive mutants) but not in cells expressing AFG3L2^{E691K} or AFG3L2^{N432T} or the control proteolytic mutant AFG3L2^{E575}Q (**Fig. 3c**,**d**). Persistent COX deficiency upon expression of paraplegin confirms the dominant effects of the AFG3L2^{E691K} and AFG3L2^{N432T} mutants in both the homo- and the hetero-oligomeric assembly of the complex.

The mutations alter the proteolytic activity of AFG3L2

As an indicator of the overall proteolytic competence of mutant AFG3L2, we analyzed the processing and maturation of the yeast nuclear-encoded ribosomal protein MrpL32 (**Fig. 4**), a known substrate of both the mammalian and yeast *m*-AAA proteases[13,16], evolutionarily conserved from yeast to mammals[16].

In *m*-AAA–deficient yeast cells (*yta10*A*yta12*A), the processing of MrpL32 is completely abolished, and the precursor species (pMrpL32) accumulates (**Fig. 4a**). Expression of AFG3L2^{WT} or AFG3L2^{H126}Q substantially reduced pMrpL32 accumulation (**Fig. 4b**). Some mature MrpL32 was produced in cells carrying the disease-associated mutants AFG3L2^{S674L} and AFG3L2^{E691K}, and, to a lesser extent, in those carrying AFG3L2^{A694E}, AFG3L2^{R702}Q and AFG3L2^{N432T}; however, for all mutants, the accumulation of unprocessed precursor, expressed as the ratio of pMrpL32 levels to total MrpL32 levels, indicated a statistically significant impairment of proteolytic activity ($P \leq 0.01$, $n = 4$; **Fig. 4b**).

When AFG3L2 and paraplegin were coexpressed (**Fig. 4c**), higher levels of pMrpL32 were observed in all transformed strains, suggesting increased MrpL32 expression in cells expressing both heterologous proteins. No statistically significant difference ($P > 0.05$, $n = 4$) was observed between the ratio of precursor to total MrpL32 in AFG3L2^{WT} harbouring cells (**Fig. 4c**) and that in SCA28 mutant strains harbouring AFG3L2^{S674L},

AFG3L2^{A694E} or AFG3L2^{R702}Q, whose defective respiration is rescued by paraplegin coexpression (**Fig. 2d**). By contrast, the respiratory-deficient strains expressing AFG3L2^{E691K}, AFG3L2^{E575}Q (ref. 13) and AFG3L2^{N432T}, whose OXPHOS phenotype is not rescued by paraplegin (**Fig. 2**), still showed proteolytic dysfunction, with a precursor- to-total ratio significantly higher than that of the AFG3L2^{WT} strain ($P \leq 0.005$, $n = 4$). Together, the results clearly indicate that the identified mutations affect AFG3L2 proteolytic activity and that alteration of this activity correlates with impairment of cellular respiratory competence.

Structural modeling of AFG3L2 mutants

To analyze the impact of the identified mutations on the structure of AFG3L2, we built a three-dimensional model using the structure of the Thermus thermophilus AAA protease FtsH (refs. 11,19) as a template (**Fig. 5**). A more detailed description of the modeling can be found in the **Supplementary Note**. AFG3L2 Glu691 is also a glutamate (Glu537) in *T. thermophilus* FtsH (ref. 19) but is not conserved in other orthologs, including paraplegin (**Fig. 1**). This residue sits in the middle of the central pore formed by the six subunits surrounding the exit from the proteolytic chamber on the matrix side of the complex (**Fig. 5a**,**b**, and **Supplementary Figs. 5a**,**b** and **6a**). Substitution of this residue to a lysine, as in AFG3L2^{E691K}, drastically changes the electrostatic potential and the chemical characteristics of the pore (**Fig. 5c**–**g** and **Supplementary Fig. 5c**–**g**). The change is evident in the AFG3L2^{WT}-AFG3L2^{E691K} compound homohexamer but is greatest in both the homohexameric mutant AFG3L2^{E691K}-AFG3L2^{E691K} and the heterohexameric AFG3L2^{E691K}-paraplegin (**Supplementary Fig. 5e**,**d**,**g**, respectively), in which paraplegin's neutral Gln693 residue, substituting for AFG3L2 Glu691, does not counteract the charge reversal of E691K. Asn432 is located within the ATPase domain in an evolutionarily conserved region and is absolutely conserved from *T. thermophilus* FtsH to human AFG3L2 (**Fig. 1**). In the hexameric assembly of FtsH, the side chain of the corresponding residue Asn280 is located in the pore and is near (~6 Å) Phe229 (Phe381 in AFG3L2) of the alternate monomer (**Supplementary Fig. 6b**), the crucial aromatic residue in the central pore loop motif @XG (pore-1 motif, where @ is an

aromatic residue and X is any residue) that is conserved in all subfamilies of the AAA family[20].

Protein expression studies in cells from affected individuals

We raised polyclonal antibodies that specifically recognize AFG3L2 and paraplegin (**Supplementary Fig. 7**). Immunoblot analysis of lymphoblastoid cells showed similar levels of AFG3L2 and paraplegin in affected and control subjects (**Supplementary Fig. 8a**). Furthermore, nondenaturing blue native gel electrophoresis revealed normal levels of a high-molecular-mass (~1 MDa) immunoreactive protein (**Supplementary Fig. 8b**). The results are consistent with co-immunoprecipitation experiments performed in yeast (**Fig. 2g**) and indicate that the mutant protein is stable and competent for supramolecular assembly and does not induce secondary depletion of paraplegin.

To examine whether AFG3L2 substitutions could induce secondary abnormalities of other proteins known to be either partners or substrates of the *m*-AAA complex, we also investigated the expression of prohibitin-1 (PHB1) and prohibitin-2 (PHB2)[12,21], MRPL32, described above, and OPA1 (ref. 22), observing no differences either in the protein levels or in the migration patterns as compared to normal controls (**Supplementary Fig. 9**).

Expression of AFG3L2 and paraplegin in the nervous system

Confocal immunofluorescence analysis (**Fig. 6a**–**h**) showed that in the human cerebellum both AFG3L2 and paraplegin are highly and selectively expressed in the Purkinje cell layer (**Fig. 6a**–**d**) and the large neurons of the deep cerebellar nuclei (data not shown), with negligible labelling in all other cerebellar structures, including the molecular layer (**Fig. 6a**–**b**). Furthermore, the intensity of staining clearly outlined not only the cell body but also the dendritic arbor of all Purkinje neurons (**Fig. 6c**,**d**). A similar staining pattern was present in neurons of the cerebellar dentate nuclei (data not shown). AFG3L2 and paraplegin were also expressed in the motor system (pyramidal cortical neurons and spinal motor neurons;

Fig. 6e–**h**). However, in contrast with observations in the cerebellum, paraplegin staining was more evident than that of AFG3L2 in both layer-V cortical neurons (compare **Fig. 6e**,**g)** and lamina-IX motor neurons (compare **Fig. 6f**,**h**). AFG3L2 staining of most spinal motor neurons was just above background levels (**Fig. 6f**, inset).

We confirmed the pattern of expression observed in the human cerebellum through *in situ* hybridization analysis of *Afg3l2* and *Spg7* transcripts in mouse (**Fig. 6i**–**k** and **l**–**n**, respectively). Both genes were strongly expressed in the Purkinje cell layer and in deep nuclei neurons. By contrast, almost no labeling was observed in the molecular layer, and in the granule cell layer, cells were labeled at an intermediate level for *Afg3l2* (**Fig. 6i**,**j)** and weakly for *Spg7* (**Fig. 6l**,**m**). Labeling of Golgi cells was strong for *Afg3l2* (**Fig. 6j**) and weak for *Spg7* (**Fig. 6m**).

Discussion

The genetic and functional data presented here demonstrate that missense mutations of *AFG3L2* are responsible for the autosomal dominant spinocerebellar ataxia SCA28 that we previously mapped on chromosome 18p11.22 (ref. 8). Furthermore, they indicate an unexpectedly essential role for AFG3L2 in protecting the human cerebellum from neurodegeneration and expand the spectrum of molecular mechanisms underlying the overlapping features of hereditary ataxias.

The finding that substitutions in AFG3L2, a metalloprotease of the mitochondrial protein quality control system[12,14], cause a dominant form of cerebellar ataxia is remarkable for several reasons. First, the vast majority of disorders of nuclear genes encoding mitochondrial proteins are recessively inherited[23]. In this group, a number of defects are known to cause different forms of early-onset ataxia, the most important of which is Friedreich's ataxia[4]. By contrast, no autosomal dominant spinocerebellar degeneration has thus far been associated with mutations affecting proteins targeted to the mitochondria, and the relatively few mitochondrial disorders having an autosomal dominant pattern of inheritance are characterized by noncerebellar phenotypes, such as progressive external ophthalmoplegia (associated with *SLC25A4* (*ANT1*;

MIM 609283), *C10orf2* (*TWINKLE*; MIM 609286) and *POLG* (MIM 157640)), optic atrophy (*OPA1*; MIM 165500), peripheral neuropathy (*MFN2* (CMT2A2; MIM 609260)) and spastic paraplegia (*HSPD1* (SPG13; MIM 605280) and *REEP1* (SPG31; MIM 610250))[23]. Second, alterations of paraplegin, a cognate AAA protease partner of AFG3L2 in the *m*-AAA metalloprotease complex, cause a distinct neurodegenerative disorder, SPG7 hereditary spastic paraplegia, by a loss-of-function recessive mechanism[9].

In total, we identified six heterozygous missense mutations in affected individuals that were absent in controls. Notably, five of them are located in highly conserved regions of the two functional domains (**Fig. 1**). Four substitutions (E691K, S674L, A694E and R702Q) reside close to each other in the proteolytic domain. Although none of these substitutions affects the catalytic zinc-binding motif HEAGH, their clustering in this small region suggests that it may be crucial in proteolysis, possibly in substrate recognition and/or handling. Expression studies in an *m*-AAA–deficient *S. cerevisiae* strain (*yta10*A*yta12*A) showed that all the substitutions except H126Q, the only one found outside the two functional domains, affect protein activity, causing a respiratory-deficient phenotype that correlates with the accumulation of unprocessed *m*-AAA substrates.

Analysis of the respiratory phenotype of cells coexpressing both normal and mutant AFG3L2 suggests that two classes of *AFG3L2* mutations exist. A first group of dominant negative mutants, exemplified by AFG3L2^{E691K} and AFG3L2^{N432T}, would affect both the homo-oligomeric (AFG3L2^{WT}-AFG3L2^{mut}) and the hetero-oligomeric (AFG3L2^{mut} paraplegin^{WT}) assemblies, as also suggested by structural models. These two mutations are expected to be highly penetrant, and the number of affected subjects observed in both families M*I*-A0091 (E691K) and MIA2473/R*M*-DS (N432T) is consistent with this hypothesis. By contrast, haploinsufficiency or a weak dominant negative effect, as no evidence of ataxia has been reported in individuals with familial syndromes caused by chromosome 18p deletion[24] could be the mechanism for a second group of AFG3L2 mutants (AFG3L2^{S674L}, AFG3L2^{A694E} and AFG3L2^{R702}Q), which are rescued in yeast by coexpression of wild-type AFG3L2 or paraplegin. In human cells, assembly of normal AFG3L2 or paraplegin with one of these mutant

AFG3L2 forms might variably mitigate the effect of the mutation, resulting in variably reduced penetrance and/or expressivity in affected people, as observed in the family bearing AFG3L2^{R702Q} (**Supplementary Fig. 2**). This hypothesis would be consistent with the limited number of affected individuals reported in families M*I*-A1948 (S674L), M*I*-A0650 (A694E) and M*I*-A0762 (R702Q). Whichever the mechanism, however, all the clinically affected individuals showed a substantially homogeneous phenotype regardless of the mutation. Thus, taken together, the results point to a model in which the cerebellar degeneration and the consequent clinical phenotype arise from the perturbation of a specific function of AFG3L2 in the Purkinje neurons, which is essentially independent from the presence of paraplegin. The selective and intense expression of both AFG3L2 and paraplegin in human and murine Purkinje cells (**Fig. 6**) is consistent with this hypothesis.

How could the identified mutations affect AFG3L2 function? Polypeptide processing by AAA proteases involves substrate recognition and ATP-dependent unfolding and disassembly of the substrate as it is threaded through the ATPase central pore into the catalytic chamber[25,26]. Analysis of both yeast and affected individuals' cells (**Supplementary Fig. 8**) indicates that there is no substantial effect on protein stability and that the mutants are competent for supramolecular assembly. The hypothesis that the mutations may disrupt specialized function(s) of AFG3L2 gains support from molecular modeling of mutants into the crystal structure of the eubacterial FtsH metalloprotease[19]. The most intriguing mutations are those affecting Glu691 (E691K) in the proteolytic domain and Asn432 (N432T) in the ATPase domain, both of which behave in a dominant negative fashion. Both affect central pore structures, either on the proteolytic side (E691K) or on the ATPase side (N432T), that may be crucial for the recognition, unfolding, translocation or release of substrate proteins. E691K drastically changes the electrostatic potential and the chemical characteristics of the pore in both the homo- and heterohexameric complexes (**Fig. 5c**–**g**), which explains why the respiratory-deficient phenotype of the AFG3L2^{E691K} strain is not rescued by AFG3L2^{WT} or paraplegin coexpression. Although several studies have investigated the structural and

functional role of the central pore in the ATPase domain[26–28], very little is known concerning the pore on the proteolytic side. On the basis of our results (**Fig. 4**), one might speculate that the mutation(s) affecting this functional domain hamper the release of processed substrate(s), thus causing upstream accumulation of unprocessed species, although one could also consider an effect on substrate recognition, on binding of adaptor proteins[21,29,30] if there are any such proteins, or even on ATPase activity[31].

The N432T substitution in the ATPase domain is also noteworthy in that it affects an absolutely conserved residue in the central pore region on the membrane side of the barrel, the channel through which substrates are translocated into the proteolytic chamber. Molecular modeling in *T. thermophilus* FtsH reveals that Asn432 is sem*i*-exposed and in proximity to Phe381 (Phe229 in FtsH), the crucial aromatic residue in the highly conserved central pore loop motif F/YVG (ref. 20) proposed to be essential for substrate recognition and ATP-dependent translocation of proteins into the proteolytic chamber[27,28,32]. Although Asn432 does not appear to make direct contact with Phe381, its extreme conservation, along with the deleterious effects of its substitution with an amino acid of the same class (uncharged polar), strongly suggest that Asn432 makes a functionally relevant contribution to forming interactions with substrates. In this case, the involvement of residues from alternate chains (monomers; **Supplementary Fig. 6b**) would be perfectly consistent with the dominant negative mechanism proposed for this mutation.

We have shown a clear correlation between respiratory deficiency and a severe defect of respiratory chain complex IV in *m*-AAA–deficient yeast cells expressing human AFG3L2 mutants. As both essential proteolytic functions and chaperone-like activity of the *m*-AAA complex have been implicated in the biogenesis and maintenance of respiratory chain complexes[17,18], the possibility exists that substitutions in the proteolytic domain may affect an activity of AFG3L2 that is poorly dependent on the proteolytic function[31]. However, we have found a good correlation between respiration and proteolytic competence of AFG3L2 (**Fig. 4**). A significant accumulation of MrpL32 precursor species was indeed observed in yeast cells expressing mutant AFG3L2. Notably, though, these cells did not respire despite the fact

that some mature MrpL32 was still produced. It is possible that mature-sized

MrpL32 generated by mutant AFG3L2 does not support respiration because it is not appropriately released from the mutant protease or does not attain a proper conformation. Whichever the mechanism, however, the accumulation of pMrpL32 indicates a general impairment of AFG3L2's substrate processing activity. As the *m*-AAA protease can act as both a processing enzyme in the biogenesis of specific mitochondrial proteins and a component of the mitochondrial protein quality control system for the degradation of misfolded polypeptides[14,33], even a partial reduction of its proteolytic competence may result in a generalized impairment of these crucial activities, with potentially lethal pleiotropic effects on mitochondrial function.

Thus, although the human pathology caused by AFG3L2 substitutions could be the result of a general impairment of the 'mitochondrial proteasome', the specificity of the lesions, particularly if compared with those associated with paraplegin substitutions, suggests that specific substrate(s) may be affected in the neurons of individuals with SCA28. No biochemical phenotype could be identified in non-neuronal cell lines and tissue obtained from affected individuals. Both MRPL32 (refs. 13,16) and OPA1, another protein recently proposed to be regulated by AFG3L2 (ref. 22), are processed normally in lymphoblasts of affected individuals (**Supplementary Fig. 9**). Similarly, there is no evidence for a defect of autocatalytic processing of *m*-AAA subunits by AFG3L2 (ref. 34; **Supplementary Fig. 8**). Furthermore, despite the high *AFG3L2* expression levels in human skeletal muscle[35], analysis of muscle biopsies from four affected individuals in families M*I*-A0091 and M*I*-A1948 did not reveal any abnormality of respiratory chain activity nor characteristic histopathological signs of mitochondrial involvement (data not shown). The lack of mitochondrial abnormalities in nonneuronal tissues is not surprising and has been observed in other disease conditions showing neuronal specificity[36]. It is conceivable that, in non-neuronal cells, the presence of one mutant *AFG3L2* allele might be insufficient to impair housekeeping functions of the *m*-AAA protease that can be carried out by proteolytic complexes with both homo- and hetero-oligomeric subunit

composition[13]. By contrast, it might be deleterious in a cellular context (such as the Purkinje neuron) more susceptible to perturbations of AFG3L2 activity or in which AFG3L2 homocomplex would perform unique or predominant functions. Thus, the data together are consistent with the purely neurological phenotype observed in all affected individuals and further support the hypothesis that specific substrates for AFG3L2 exist whose normal processing is essential to protect the cerebellum from neurodegeneration.

A specialized role of AFG3L2—both in the homo- and in the hetero- complex configuration—in the human cerebellum would well account for the phenotypic differences between SCA28, in which pyramidal dysfunction is clinically negligible, and the recessive form of hereditary spastic paraplegia (SPG7) caused by paraplegin deficiency, which is characterized by degeneration of the corticospinal tract[37]. Consistent with this model, expression analysis of AFG3L2 and paraplegin indicates a much lower expression of AFG3L2 relative to paraplegin in the human motor system (**Fig. 6**). Contrasting with the human disease, two recently described *Afg3l2*-null mouse models have a lethal motor phenotype characterized by early-onset tetraparesis leading to death at postnatal day 16 (ref. 38). In these models, however, the disease is recessive and is characterized by the complete inactivation of Afg3l2. Given the severe phenotype of *Afg3l2*-null mice and the lack of the third *m*-AAA component, Afg3l1, in human cells, we predict that complete loss of AFG3L2 is embryonically lethal in humans. Heterozygous $Afg3l2^{+/-}$ animals are apparently unaffected[38]. However, a recent re-evaluation of these mice based on our findings has revealed Purkinje cell degeneration associated with a subtle late onset decline of some motor performance[39].

In conclusion, we have identified *AFG3L2* as the gene responsible for SCA28, which appears to account for at least 3% of SCAs with unknown defects. The discovery that dominant mutations cause cerebellar ataxia by affecting AFG3L2 activity and that AFG3L2 is highly and selectively expressed in human Purkinje cells reveals its essential role in protecting the human cerebellum against neurodegeneration. The identification of neuron-specific substrates or adaptor proteins[25] of AFG3L2 will shed more

light on the normal function of this versatile component of the mitochondrial protein quality control and activation machinery and will pave the road to understanding the specificity of neuronal death in human disease.

Reference

1. Harding, A.E. The clinical features and classification of the late onset autosomal dominant cerebellar ataxias. A study of 11 families, including descendants of the 'the Drew family of Walworth'. *Brain* **105**, 1–28 (1982).
2. Schöls, L., Bauer, P., Schmidt, T., Schulte, T. & Riess, O. Autosomal dominant cerebellar ataxias: clinical features, genetics, and pathogenesis. *Lancet Neurol.* **3**, 291–304 (2004).
3. Matilla-Duenas, A. *et al.* Cellular and molecular pathways triggering neurodegeneration in the spinocerebellar ataxias. Cerebellum published online, doi:10.1007/s12311- 009-0144-2 (5 November 2009).
4. Taroni, F. & Di Donato, S. Pathways to motor incoordination: the inherited ataxias. *Nat. Rev. Neurosci.* **5**, 641–655 (2004).
5. Koeppen, A.H. The pathogenesis of spinocerebellar ataxia. *Cerebellum* **4**, 62–73 (2005).
6. Orr, H.T. & Zoghbi, H.Y. Trinucleotide repeat disorders. *Annu. Rev. Neurosci.* **30**, 575–621 (2007).
7. Soong, B.W. & Paulson, H.L. Spinocerebellar ataxias: an update. *Curr. Opin. Neurol.* **20**, 438–446 (2007).
8. Cagnoli, C. *et al.* SCA28, a novel form of autosomal dominant cerebellar ataxia on chromosome 18p11.22-q11.2. *Brain* **129**, 235–242 (2006).
9. Casari, G. *et al.* Spastic paraplegia and OXPHOS impairment caused by mutations in paraplegin, a nuclear-encoded mitochondrial metalloprotease. *Cell* **93**, 973–983 (1998).
10. Hanson, P.I. & Whiteheart, S.W. AAA+ proteins: have engine, will work. *Nat. Rev. Mol. Cell Biol.* **6**, 519–529 (2005).
11. Ito, K. & Akiyama, Y. Cellular functions, mechanism of action, and regulation of FtsH protease. *Annu. Rev. Microbiol.* **59**, 211–231 (2005).

12. Koppen, M. & Langer, T. Protein degradation within mitochondria: versatile activities of AAA proteases and other peptidases. *Crit. Rev. Biochem. Mol. Biol.* **42**, 221–242 (2007).
13. Koppen, M., Metodiev, M.D., Casari, G., Rugarli, E.I. & Langer, T. Variable and tissue-specific subunit composition of mitochondrial *m*-AAA protease complexes linked to hereditary spastic paraplegia. *Mol. Cell. Biol.* **27**, 758–767 (2007).
14. Tatsuta, T. & Langer, T. Quality control of mitochondria: protection against neurodegeneration and ageing. *EMBO J.* **27**, 306–314 (2008).
15. Esser, K., Tursun, B., Ingenhoven, M., Michaelis, G. & Pratje, E. A novel two-step mechanism for removal of a mitochondrial signal sequence involves the mAAA complex and the putative rhomboid protease Pcp1. *J. Mol. Biol.* **323**, 835–843 (2002).
16. Nolden, M. *et al.* The *m*-AAA protease defective in hereditary spastic paraplegia controls ribosome assembly in mitochondria. *Cell* **123**, 277–289 (2005).
17. Arlt, H., Tauer, R., Feldmann, H., Neupert, W. & Langer, T. The YTA10–12 complex, an AAA protease with chaperone-like activity in the inner membrane of mitochondria. *Cell* **85**, 875–885 (1996).
18. Arlt, H. *et al.* The formation of respiratory chain complexes in mitochondria is under the proteolytic control of the *m*-AAA protease. *EMBO J.* **17**, 4837–4847 (1998).
19. Suno, R. *et al.* Structure of the whole cytosolic region of ATP-dependent protease FtsH. *Mol. Cell* **22**, 575–585 (2006).
20. Yamada-Inagawa, T., Okuno, T., Karata, K., Yamanaka, K. & Ogura, T. Conserved pore residues in the AAA protease FtsH are important for proteolysis and its coupling to ATP hydrolysis. *J. Biol. Chem.* **278**, 50182–50187 (2003).
21. Tatsuta, T. & Langer, T. AAA proteases in mitochondria: Diverse functions of membrane-bound proteolytic machines. *Res. Microbiol.* **160**, 711–717 (2009).
22. Ehses, S. *et al.* Regulation of OPA1 processing and mitochondrial fusion by *m*-AAA protease isoenzymes and OMA1. *J. Cell Biol.* **187**, 1023–1036 (2009).
23. DiMauro, S. & Schon, E.A. Mitochondrial disorders in the nervous system. *Annu. Rev. Neurosci.* **31**, 91–123 (2008).
24. Nasir, J. *et al.* Unbalanced whole arm translocation resulting in loss of 18p in dystonia. *Mov. Disord.* **21**, 859–863 (2006).

25. Dougan, D.A., Mogk, A., Zeth, K., Turgay, K. & Bukau, B. AAA+ proteins and substrate recognition, it all depends on their partner in crime. *FEBS Lett.* **529**, 6–10 (2002).
26. Graef, M., Seewald, G. & Langer, T. Substrate recognition by AAA+ ATPases: distinct substrate binding modes in ATP-dependent protease Yme1 of the mitochondrial intermembrane space. *Mol. Cell. Biol.* **27**, 2476–2485 (2007).
27. Graef, M. & Langer, T. Substrate specific consequences of central pore mutations in the *i*-AAA protease Yme1 on substrate engagement. *J. Struct. Biol.* **156**, 101–108 (2006).
28. Okuno, T., Yamanaka, K. & Ogura, T. Characterization of mutants of the *Escherichia coli* AAA protease, FtsH, carrying a mutation in the central pore region. *J. Struct. Biol.* **156**, 109–114 (2006).
29. White, S.R. & Lauring, B. AAA+ ATPases: achieving diversity of function with conserved machinery. *Traffic* **8**, 1657–1667 (2007).
30. Dunn, C.D., Tamura, Y., Sesaki, H. & Jensen, R.E. Mgr3p and Mgr1p are adaptors for the mitochondrial *i*-AAA protease complex. *Mol. Biol. Cell* **19**, 5387–5397 (2008).
31. Tatsuta, T., Augustin, S., Nolden, M., Friedrichs, B. & Langer, T. *m*-AAA proteasedriven membrane dislocation allows intramembrane cleavage by rhomboid in mitochondria. *EMBO J.* **26**, 325–335 (2007).
32. Augustin, S. *et al.* An intersubunit signaling network coordinates ATP hydrolysis by *m*-AAA proteases. *Mol. Cell* **35**, 574–585 (2009).
33. Augustin, S. *et al.* Characterization of peptides released from mitochondria: evidence for constant proteolysis and peptide efflux. *J. Biol. Chem.* **280**, 2691–2699 (2005).
34. Koppen, M., Bonn, F., Ehses, S. & Langer, T. Autocatalytic processing of *m*-AAA protease subunits in mitochondria. *Mol. Biol. Cell* **20**, 4216–4224 (2009).
35. Banfi, S. *et al.* Identification and characterization of AFG3L2, a novel parapleginrelated gene. *Genomics* **59**, 51–58 (1999).
36. Amiott, E.A. *et al.* Mitochondrial fusion and function in Charcot-Marie-Tooth type 2A patient fibroblasts with mitofusin 2 mutations. *Exp. Neurol.* **211**, 115–127 (2008).
37. Stevanin, G., Ruberg, M. & Brice, A. Recent advances in the genetics of spastic paraplegias. *Curr. Neurol. Neurosci. Rep.* **8**, 198–210 (2008).
38. Maltecca, F. *et al.* The mitochondrial protease AFG3L2 is essential for axonal development. *J. Neurosci.* **28**, 2827–2836 (2008).

39. Maltecca, F. *et al.* Haploinsufficiency of AFG3L2, the gene responsible for spinocerebellar ataxia type 28, causes mitochondria-mediated Purkinje cell dark degeneration. *J. Neurosci.* **29**, 9244–9254 (2009).

Figures

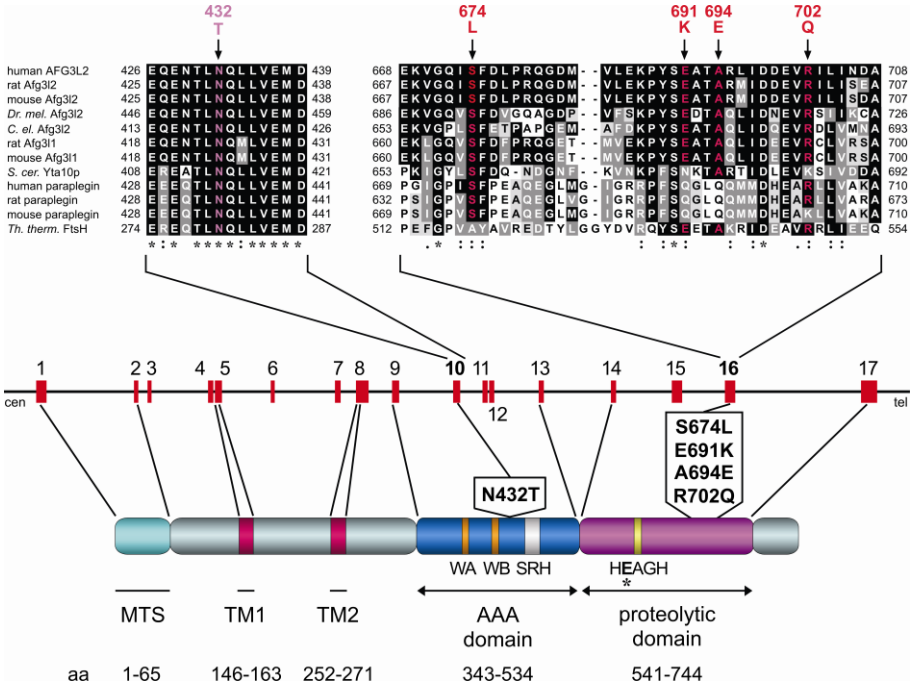

Figure 1

AFG3L2 mutations cause amino acid substitutions in highly conserved regions of the protein. Bottom, genomic organization of the human AFG3L2 gene and domain structure of the protein. AFG3L2 consists of 17 exons spanning 48 kb on chromosome 18p11.21 (5'—>3' map position: 12319108–12367194). The identified mutations in exon 10 and in exon 16 are boxed. Top, ClustalW2 multiple alignments of the human AFG3L2 regions encoded by exon 10 (residues 426–439) or exon 16 (residues 668–708) with members of the *m*-AAA family from different organisms (Dr. mel., Drosophila melanogaster; C. el., Caenorhabditis elegans; S. cer., S. cerevisiae; T. therm., T. thermophilus). The mutated residues are indicated in red (proteolytic domain) or magenta (ATPase domain) above the alignment. Residues identical to AFG3L2 are framed in black. Conserved, semiconserved and nonconserved substitutions are framed in gray, light gray and white boxes, respectively. The following consensus symbols are used in the alignment to denote the degree of conservation, as defined by the Gonnet Pam250 matrix scores observed in each column: (*), residue is identical in all sequences in the alignment;(:), conserved substitutions have been observed; (.), semiconserved substitutions have been observed. MTS, mitochondrial targeting sequence; TM1 and TM2, transmembrane domains 1 and 2, respectively (TMHMM Server v2.0); WA, Walker-A motif (GPPGTGKT, residues 348–355); WB, Walker-B motif (ILFIDEID, residues 403–410); SRH, second region of homology (TNRPDILDPALLRPGRFD, residues 453–470); HEAGH (residues 574–578), protease catalytic site (Pfam 24.0, October 2009; http://pfam.sanger.ac.uk/; the asterisk on the HEAGH site indicates the catalytic Glu575 that is mutated to glutamine in the control proteolytic mutant AFG3L2E575Q; ref. 13).

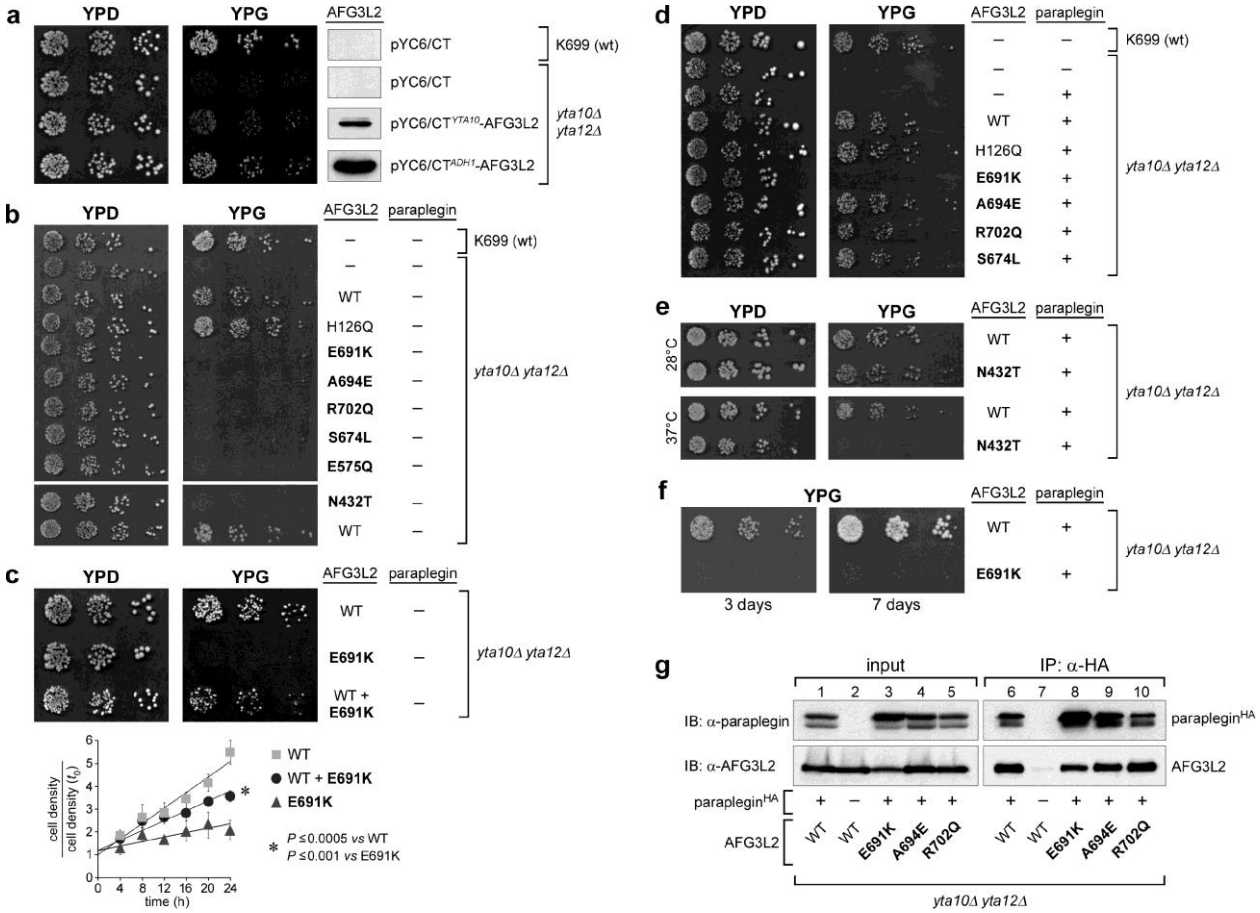
a
YPD
YPG
AFG3L2
pYC6/CT
K699 (wt)
pYC6/CT
pYC6/CT^YTA10-AFG3L2
yta10Δ yta12Δ
pYC6/CT^ADH1-AFG3L2
b
YPD
YPG
AFG3L2
paraplegin
K699 (wt)
WT
H126Q
E691K
A694E
R702Q
S674L
E575Q
N432T
yta10Δ yta12Δ
c
YPD
YPG
AFG3L2
paraplegin
WT
E691K
WT + E691K
yta10Δ yta12Δ
cell density
cell density (t0)
time (h)
WT
WT + E691K
E691K
P ≤ 0.0005 vs WT
P ≤ 0.001 vs E691K
d
YPD
YPG
AFG3L2
paraplegin
K699 (wt)
WT
H126Q
E691K
A694E
R702Q
S674L
yta10Δ yta12Δ
e
YPD
YPG
AFG3L2
paraplegin
28°C
37°C
WT
N432T
yta10Δ yta12Δ
f
YPG
AFG3L2
paraplegin
WT
E691K
yta10Δ yta12Δ
3 days
7 days
g
input
IP: α-HA
IB: α-paraplegin
IB: α-AFG3L2
paraplegin^HA
AFG3L2
WT
E691K
A694E
R702Q
yta10Δ yta12Δ

Figure 2

Complementation studies in *S. cerevisiae*. Serial dilutions of exponentially growing yeast cultures spotted on plates show oxidative growth phenotype of *yta10*Δ*yta12*Δ cells expressing normal and mutant human AFG3L2. Substitutions affecting respiration are in bold. Respiratory competence is deduced by the ability to grow on 2% glycerol (YPG). Except where indicated, we scored growth after 3 d incubation at 28 °C. YPD and YPG, YEP plates containing 2% glucose or 2% glycerol, respectively. (**a**) AFG3L2 was expressed under control of the strong *ADH1* promoter (pYC6/ CT^{ADH1}-AFG3L2) or the endogenous *YTA10* promoter (pYC6/CT^{YTA10}-AFG3L2). Right panels, AFG3L2 levels assessed by immunoblotting. K699, WT yeast strain; pYC6/CT, empty plasmid. (**b**) Respiratory phenotype of *yta10*Δ*yta12*Δ cells expressing either normal (WT) or mutant human AFG3L2. Similar results were obtained after incubation at 37 °C (data not shown). (**c**) Coexpression of $AFG3L2^{WT}$ (WT) and $AFG3L2^{E691K}$ (E691K) results in a limited correction of the respiratory-deficient phenotype, suggesting a dominant negative effect of the mutation. The graph below shows the growth rates of cells expressing either $AFG3L2^{WT}$ or $AFG3L2^{E691K}$ or coexpressing both forms (WT+E691K). We grew cells for 24 h with cell counting every 4 h. Values on the *y* axis represent the ratio between cell density (cells/ml) at a given time and cell density at start (*t*0). Growth rates are calculated by linear regression analysis (trend line). Each value represents the mean of three independent experiments. Error bars indicate ± 1 s.d. We determined statistical significance ($P \leq 0.0005$ or $P \leq 0.001$) by Student's *t*-test. (**d**) Respiratory phenotype of *yta10*Δ*yta12*Δ cells coexpressing either normal or mutant human AFG3L2 with human paraplegin. (**e**) Rescue of the $AFG3L2^{N432T}$ respiratory-deficient phenotype by paraplegin is temperature sensitive, with moderate growth at 28 °C but no growth at 37 °C; no growth difference at 37 °C was observed for the other mutants (data not shown). (**f**) No rescue of the $AFG3L2^{E691K}$ respiratory-deficient phenotype by paraplegin in long-term culture (7 d). (**g**) Both normal and mutant AFG3L2 interact with paraplegin. We immunoprecipitated hemagglutinin (HA)-tagged paraplegin ($paraplegin^{HA}$) with anti-HA from *yta10*Δ*yta12*Δ cells expressing $AFG3L2^{WT}$ alone (lanes 2 and 7) or coexpressing either wild-type or mutant AFG3L2 with $paraplegin^{HA}$. We analyzed immunoprecipitates (IP) by SDS-PAGE and immunoblotting (IB) using anti-paraplegin (á-paraplegin) or anti-AFG3L2 (á-AFG3L2). AFG3L2 was detected in all the immunoprecipitates from yeast cells coexpressing $paraplegin^{HA}$ (lanes 6 and 8–10). Lanes 1–5, immunoblot analysis of cell extracts before immunoprecipitation (input).

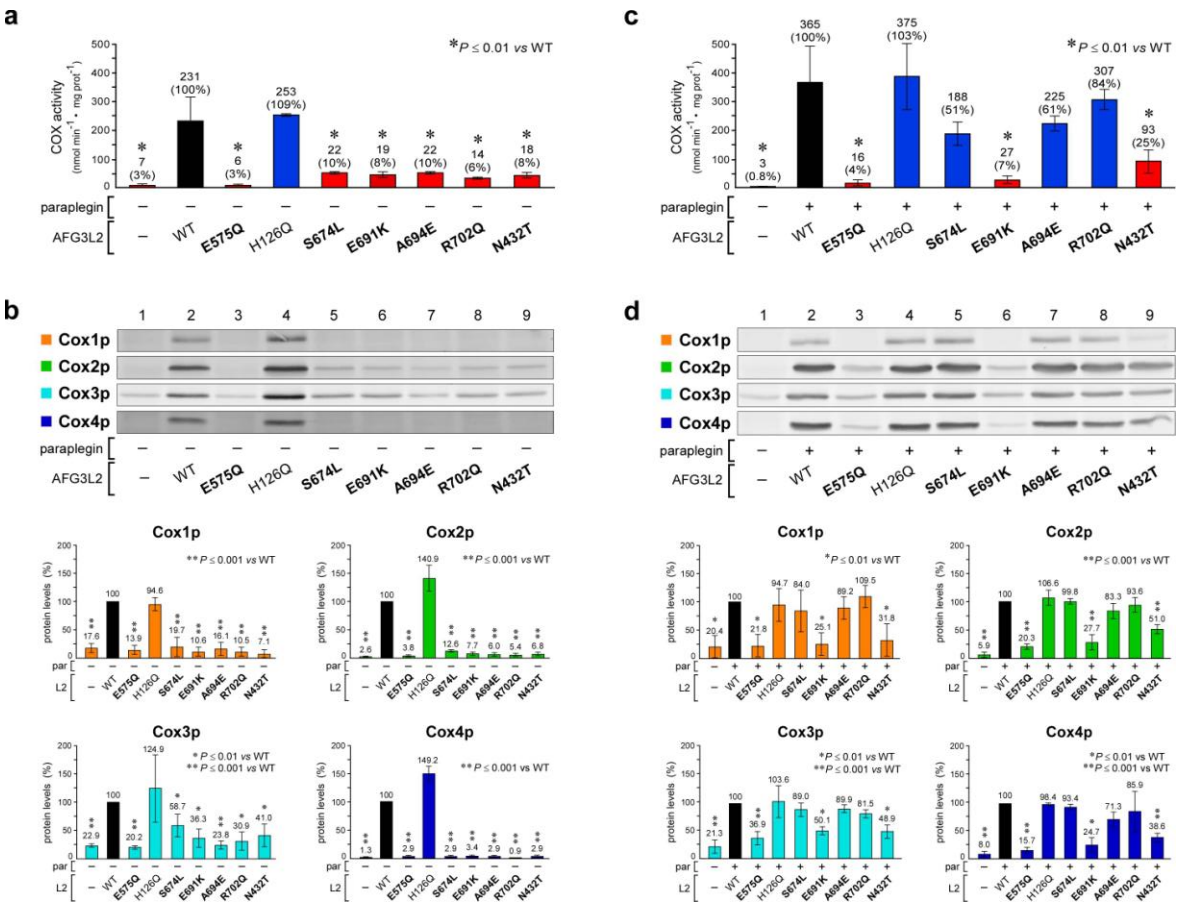
a
c
b
d
COX activity
(nmol min⁻¹ · mg prot⁻¹)
*P ≤ 0.01 vs WT
paraplegin
AFG3L2
WT
E575Q
H126Q
S674L
E691K
A694E
R702Q
N432T
Cox1p
Cox2p
Cox3p
Cox4p
protein levels (%)
**P ≤ 0.001 vs WT
par
L2

Figure 3

Cytochrome c oxidase enzyme activity and protein levels in yeast cells expressing mutant AFG3L2. Yeast strains and mutants are as described in Figure 2. Substitutions affecting respiration are in bold. (a) COX activity measured in isolated mitochondria from yta10Δyta12Δ *m*-AAA–deficient yeast cells expressing AFG3L2 alone, in the absence of paraplegin. Activity is expressed as nanomoles of cytochrome cred oxidized per minute per milligram of protein. Values in parentheses indicate percentage of activity compared to that of cells expressing AFG3L2WT (black bars). Bars and vertical lines indicate mean and ± 1 s.d., respectively. Red bars and asterisk indicate a statistically significant ($P \leq 0.01$) difference from AFG3L2WT, as determined by Student's t-test ($n = 4$). Absence of asterisk (blue bars) indicates $P > 0.05$. (b) Fluorescence immunoblot analysis and protein quantitation of mitochondria-encoded COX subunits Cox1p, Cox2p and Cox3p, and nuclear-encoded subunit Cox4p, in mitochondrial extracts from cells expressing AFG3L2 alone, in the absence of paraplegin. Single or double asterisk indicates a statistically significant difference from AFG3L2WT (black bars) with $P \leq 0.01$ or $P \leq 0.001$, respectively, as determined by Student's t-test ($n = 4$). Absence of asterisk indicate $P > 0.05$. (c,d) COX activity and fluorescence immunoblot analysis as in a and b for AFG3L2 in the presence of paraplegin.

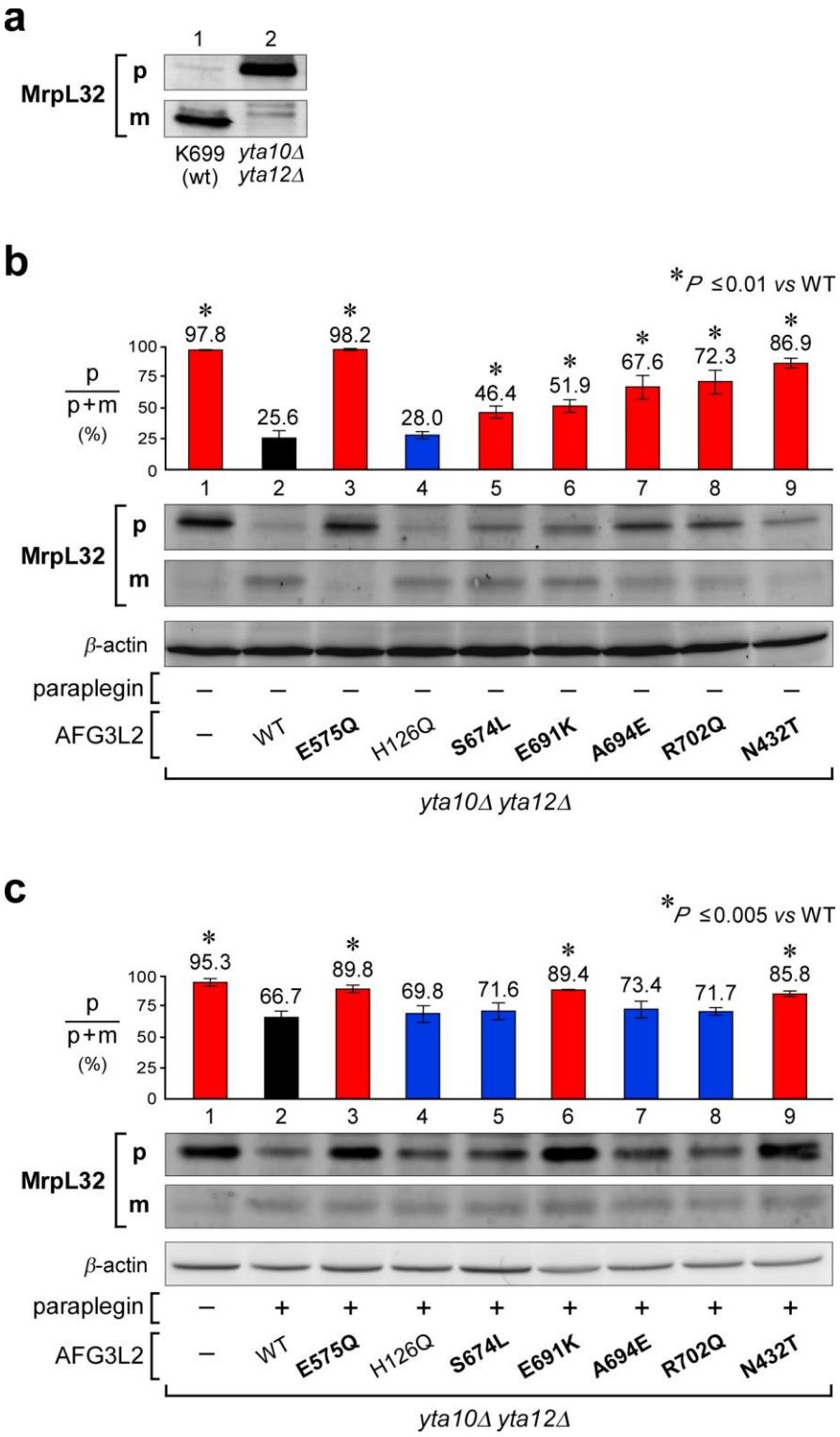
a
1
2
MrpL32
p
m
K699 (wt)
yta10Δ yta12Δ
b
*P ≤0.01 vs WT
p / p+m (%)
97.8
25.6
98.2
28.0
46.4
51.9
67.6
72.3
86.9
1 2 3 4 5 6 7 8 9
MrpL32
β-actin
paraplegin
AFG3L2
WT
E575Q
H126Q
S674L
E691K
A694E
R702Q
N432T
yta10Δ yta12Δ
c
*P ≤0.005 vs WT
95.3
66.7
89.8
69.8
71.6
89.4
73.4
71.7
85.8
1 2 3 4 5 6 7 8 9
MrpL32
β-actin
paraplegin
AFG3L2
WT
E575Q
H126Q
S674L
E691K
A694E
R702Q
N432T
yta10Δ yta12Δ

Figure 4

Proteolytic activity of normal and mutant AFG3L2 in yeast. Yeast strains and mutants are as in Figure 2. Substitutions affecting respiration are in bold. (a) Fluorescence immunoblot analysis with ant*i*-MrpL32 shows that yeast MrpL32 precursor (p) accumulates in yta10Ayta12A *m*-AAA–deficient cells (lane 2). m, mature MrpL32. (b) Fluorescence immunoblot analysis of MrpL32 in yeast cells expressing AFG3L2 homo-oligomeric *m*-AAA, showing accumulation of MrpL32 precursor in AFG3L2 mutants. Histograph reports quantitative results. AFG3L2 proteolytic competence is expressed as the ratio of pMrpL32 level to total (p + m) MrpL32 level. MrpL32 levels were normalized to the loading control protein f3-actin. Bars and vertical lines indicate mean and ± 1 s.d., respectively. Red bars and asterisks indicate a statistically significant (P ~ 0.01) difference from AFG3L2WT (lane 2, black bar) as determined by Student's t-test (n = 4). Blue bars and absence of asterisk indicate P > 0.05. (c) Fluorescence immunoblot analysis of MrpL32 in *m*-AAA–deficient yeast cells, showing the effects of AFG3L2 and paraplegin coexpression on the accumulation of pMrpL32 (indicated by p/(p + m) ratio as in b). MrpL32 levels were normalized to the loading control protein f3-actin. Bars and vertical lines indicate mean and ± 1 s.d., respectively. No statistically significant difference (P > 0.05) was observed between AFG3L2WT-harboring cells (lane 2, black bar) and strain AFG3L2H126Q or mutant strains AFG3L2S674L, AFG3L2A694E and AFG3L2R702Q (lanes 4, 5, 7 and 8, blue bars). By contrast, asterisk (red bars) indicates a statistically significant difference (P ~ 0.005, n = 4; Student's t-test) between AFG3L2WT cells and SCA28 mutants AFG3L2E691K or AFG3L2N432T, or the control mutant AFG3L2E575Q (ref. 13).

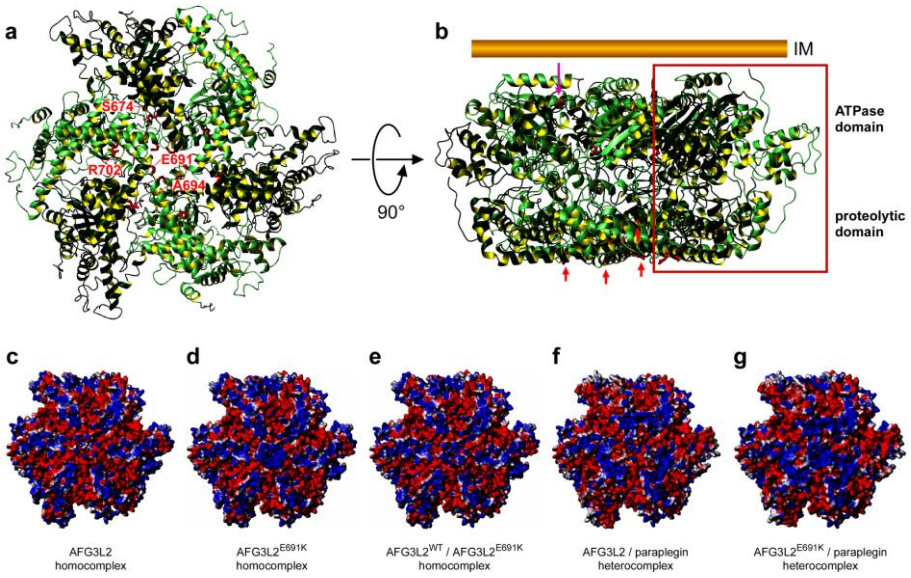
a
S674
R702
E691
A694
90°
b
IM
ATPase domain
proteolytic domain
c
d
e
f
g
AFG3L2 homocomplex
AFG3L2E691K homocomplex
AFG3L2WT / AFG3L2E691K homocomplex
AFG3L2 / paraplegin heterocomplex
AFG3L2E691K / paraplegin heterocomplex

Figure 5

Molecular modeling of normal and mutant AFG3L2. (a,b) Orthogonal views of the hexameric ring of AFG3L2 built by homology using the coordinates of T. thermophilus FtsH (PDB 2DHR) as a template. Panel a shows the view from the protease domain (matrix) side. The monomers are alternately shown in light and dark green. The side chains of the proteolytic domain residues mutated in the affected individuals are shown in red. In b, it is clear that the hexamer adopts a flat-cylinderlike shape divided into two disks. The lower disk, containing the protease domain, forms a sixfold-symmetric structure with a zinc binding site. The upper disk is composed of six AAA domains, each of which contains ADP. Short red arrows indicate the locations of substitutions on the matrix side of the protease domain (lower disc); long magenta arrow indicates the location of the N432T substitution in the ATPase domain (upper disc). The monomer (Supplementary Fig. 5a) is boxed in red. IM, inner mitochondrial membrane. (c–g) Surface representations of the protease side of the homo- and hetero-oligomeric homology models, showing the effect of the E691K substitution on the electrostatic potential of the complex (see also Supplementary Fig. 5c–g). Shown are electrostatic surfaces of wild-type AFG3L2 homohexamer (c); homohexamer of AFG3L2E691K (d); homohexamer obtained by alternating wild-type AFG3L2 (AFG3L2WT) and mutant AFG3L2E691K (e); and heterohexamer obtained by alternating paraplegin with either AFG3L2WT (f) or AFG3L2E691K (g). Blue, positive charge; red, negative charge. The change induced by the E691K charge reversal in the central pore is greatest in the homohexameric mutant AFG3L2E691K-AFG3L2E691K (d) and in the heterohexameric complex of AFG3L2E691K and paraplegin (g), in which the positively charged Lys691 of AFG3L2E691K is not counteracted by the neutral Gln693 of paraplegin.

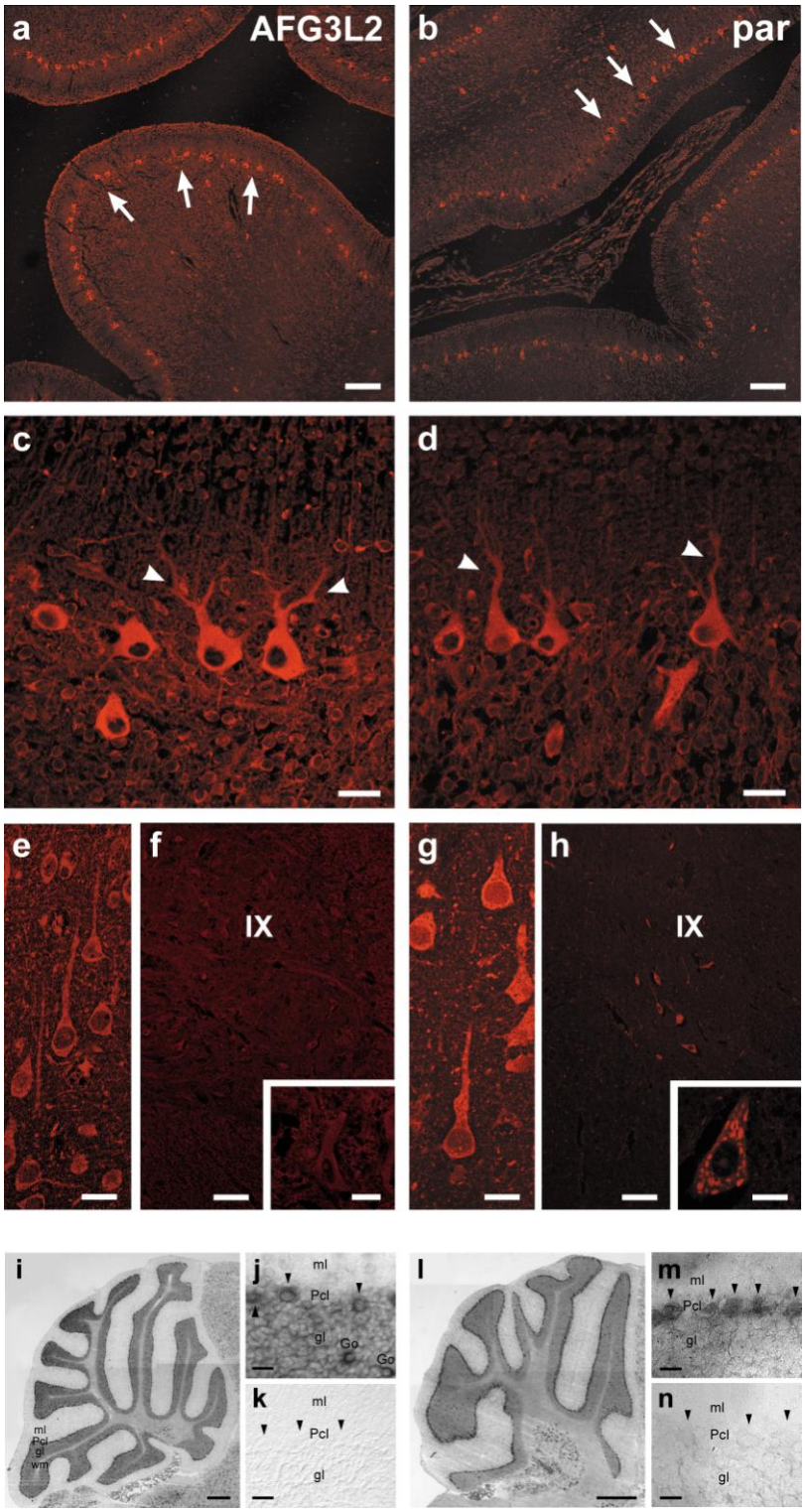
a
AFG3L2
b
par
c
d
e
f
IX
g
h
IX
i
ml
Pcl
gl
wm
j
ml
Pcl
gl
Go
Go
k
ml
Pcl
gl
l
m
ml
Pcl
gl
n
ml
Pcl
gl

Figure 6

Expression of AFG3L2 and paraplegin in human and mouse nervous systems. (a–h) Confocal immunofluorescence of human nervous tissue. In the cerebellum (a–d), both AFG3L2 (a,c) and paraplegin (b,d) are selectively expressed in the Purkinje cell layer (a,b, arrows). Note the intense expression in the soma and apical dendrites of Purkinje neurons (c,d, arrowheads). In the cerebral cortex (e,g) and spinal cord (f,h), as compared to AFG3L2 (e,f), paraplegin is more intensely expressed in layer-V pyramidal neurons (g) and lamina-IX motor neurons (h). AFG3L2 staining in spinal motor neurons (f) is just above background level. Insets in f and h show enlarged detail. Scale bars, 100 .tm (a,b,f,h) or 20 .tm (c–e,g, insets of f and h). (i–n) In situ hybridization of mouse cerebellum with Afg3l2 (i–k) and Spg7 (l–n) riboprobes. Low (i,l) and high (j,m) magnification of parasagittal sections of the cerebellar vermis showing a strong expression in Purkinje cells (j,m, arrowheads) and a weaker expression in granule and Golgi cells. (k,n) Control sections adjacent to j and m, hybridized with sense probes. Scale bars, 400 .tm (i,l) or 25 .tm (j,k,m,n). ml, molecular layer; Pcl, Purkinje cell layer; gl, granule cell layer; Go, Golgi cell; wm, white matter.

Online Methods

Affected individuals, DNA samples and cell lines.

Affected individuals and members from family M*I*-A0091 were as described[8]. We further studied 337 unrelated index cases (136 with autosomal dominant inheritance, 51 compatible with autosomal recessive inheritance because of parental consanguinity or occurrence of the disease in one or more siblings in a single generation, and 150 sporadic cases) selected from a large cohort of individuals with a diagnosis of ataxia referred to our center from throughout Italy. Inclusion criteria were the presence of a progressive clinical phenotype in which ataxia was the prominent symptom and a positive familial history, or, for sporadic cases, the absence of acquired causes of cerebellar dysfunction[40]. All affected individuals were of Italian origin and showed a progressive ataxic phenotype and cerebellar atrophy variably associated with additional features such as pyramidal signs and minor abnormalities in ocular movements. Autosomal dominant and sporadic cases were negative for SCA1 and SCA2, the most frequent Italian SCA mutations[41]. The genes associated with SCA3, SCA6, SCA7, SCA10, SCA12, SCA17 and DRPLA were tested whenever a suggestive phenotype was present[2]. In most of the dominant index cases, the presence of a CAG expansion had also been excluded by repeat expansion detection analysis[41]. Possibly recessive cases and sporadic cases were negative for *FRDA1* GAA expansion. Control subjects were individuals who presented for work-up of unrelated neurologic conditions.

We prepared Epstein-Barr-virus-stabilized lymphoblastoid cell lines and genomic DNA from peripheral-blood lymphocytes and lymphoblastoid cells as previously described[42].

We obtained written informed consent from each individual providing a biological sample. All procedures involving human subjects were approved by the Institutional Review Board of the Fondazione IRCCS Istituto Neurologico "Carlo Besta", Milan, Italy.

Mutation analysis.

All *AFG3L2* genotyping protocols took into account the presence, revealed by *in silico* analysis (NCBI Genome Assembly Build 36.2) and confirmed by genomic DNA sequencing, of a previously unrecognized *AFG3L2* pseudogene on chromosome 8p22 (5′→3′ map position: 13447603–13445733) encompassing *AFG3L2* exons 1–14. We analyzed sequences of the 17 exons of 18p11 *AFG3L2*, including flanking intron sequences and the 5′ and 3′ untranslated regions, on an automated capillary sequencer (ABI Prism 3100 Genetic Analyzer, Applied Biosystems) using the BigDyeDeoxy Terminator Cycle Sequencing Kit (Applied Biosystems) according to the manufacturer's recommendations.

For mutation screening of the selected affected population, we analyzed PCR products by automated sequencing and/or denaturing HPLC (**Supplementary Note**).

PCR conditions and sequences of the oligonucleotide primers used for PCR amplification, sequencing and denaturing HPLC analysis are detailed in **Supplementary Table 2** online.

Nucleotides are numbered so that the first nucleotide of the first in-frame ATG codon is nucleotide +1. Amino acid residues are numbered so that the methionine encoded by the first in-frame ATG codon is Met1.

AFG3L2 and paraplegin yeast expression plasmids.

We generated plasmids for heterologous expression of human AFG3L2 and paraplegin in yeast as described in the **Supplementary Note**. We verified AFG3L2 and paraplegin protein expression levels in each strain by immunoblot analysis of trichloroacetic acid cell protein extracts (see 'Protein immunoblot analysis' below and **Supplementary Fig. 3**).

Yeast strains and growth conditions.

All the strains used in this study are derivatives of W303 (K699; **Supplementary Table 3** online). To generate the *yta10*Δ*yta12*Δ strain, we deleted *YTA10* and *YTA12* using the one-step PCR strategy[43]. We

followed standard procedures for strain generation and cultures[44]. We transformed yeast strains with the described vectors and grew cells at 28 °C on YEP medium (1% yeast extract, 2% Bacto-peptone, 2% agar for plates) or selective medium supplemented with 2% (wt/vol) glucose according to standard procedures. We selected blasticidin-resistant transformants on YPD medium supplemented with 50 µg of blasticidin S per ml. For complementation experiments, we spotted equal amounts of fivefold serial dilutions of cells from exponentially grown cultures onto YEP plates containing 2% (wt/vol) glucose (YPD) or 2% (vol/vol) glycerol (YPG) and incubated them at 28 °C or 37 °C.

For growth rate analysis, we precultured yeast cells from the stock cultures overnight in selective medium, inoculated at a standard density of approximately 1×10^6 cells/ml and then grew them in YEP medium supplemented with 2% (vol/vol) glycerol for 24 h. Except where indicated, we removed samples every 4 h and determined cell density, expressed as cells/ml, in a Bürker chamber.

Assay of cytochrome c oxidase activity.

For *in vitro* activity assay of COX, we prepared yeast cell mitochondria by differential centrifugations[45,46] (**Supplementary Note**) and determined COX activity spectrophotometrically as described in ref. 46 and **Supplementary Note**.

Antibodies.

We raised polyclonal antisera directed against human AFG3L2 and paraplegin in rabbit using glutathione *S*-transferase fusion proteins that carried protein fragments of AFG3L2 (residues 67–305) and paraplegin (residues 89–304) showing no homology to each other (see **Supplementary Note**). The antisera against AFG3L2 and paraplegin showed no cross-reactivity against the two proteins (**Supplementary Fig. 7a**,**b**) and demonstrated colocalization of AFG3L2 and paraplegin with the mitochondrial protein PHB1 (**Supplementary Fig. 7c**–**h**).

We prepared antibodies to HA from mouse hybridoma clone 12CA5. Anti-yeast MrpL32 (ref. 13) and anti–medium-chain acyl-CoA dehydrogenase (MCAD)[42] were as previously reported. Anti-human MRPL32 were polyclonal antibodies raised in rabbit (T.L., unpublished data). Anti-tubulin, anti-PHB1, anti-PHB2 and anti-OPA1 were from Santa Cruz Biotechnology. Anti–α-actin was from Abcam. Mouse monoclonal antibodies to Cox1p, Cox2p, Cox3p and Cox4p were from MitoSciences.

Protein immunoblot analysis.

For protein blot analysis of yeast cells, we prepared trichloroacetic acid protein extracts as described[43] and separated them by SDS-PAGE in 10% or 15% acrylamide gels. We performed protein blotting with anti-AFG3L2 (1:12,000 dilution) and anti-paraplegin (1:6,000 dilution) using standard techniques. We probed filters with anti-yMrpL32 (1:1,000 dilution; ref. 13) and anti–α-actin (1:1,500 dilution), and revealed them with Alexa Fluor 647-conjugated goat anti-rabbit IgG (H+L) and Alexa Fluor 488-conjugated goat anti-mouse IgG (H+L) (Molecular Probes). We normalized MrpL32 signal to that of α-actin as the loading control protein.

For protein blot analysis of respiratory chain complex IV (COX) subunits, we prepared yeast mitochondria as described above and in **Supplementary Note**. We electrophoresed equal amounts of mitochondrial proteins on 15% SDS polyacrylamide gels and transferred them to a polyvinylidene difluoride membrane (PVDF; Immobilon FL, Millipore). We probed filters with antiCox1p (1:300 dilution), anti-Cox2p (1:1,500 dilution), anti-Cox3p (1:300 dilution) and anti-Cox4p (1:1,500 dilution), and revealed them with Alexa Fluor 488-conjugated goat anti-mouse IgG (H+L) (Molecular Probes). We acquired fluorescence signals using a VersaDoc Imaging System (Bio-Rad) and performed quantitative analysis using Quantity One software (Bio-Rad) in four independent experiments.

Co-immunoprecipitation of AFG3L2 and paraplegin.

For immunoprecipitation experiments[47], we grew cells of strains harboring the different AFG3L2 substitutions to late log phase, resuspended them in PBS, 1 mM PMSF, 1 mM $NaVO_4$ and 50 mM NaF supplemented with Complete Protease Inhibitor Cocktail (Roche), and homogenized them using the FastPrep System (Qbiogene-MP Biomedicals). We spun homogenates for 20 min at 16,000*g* and incubated the resulting supernatants with 12CA5 monoclonal ant*i*-HA (2 h at 4 °C under gentle shaking). We then incubated antigen-antibody complexes with protein G–Sepharose (2 h at 4 °C under gentle shaking). After extensive washes, we eluted samples from beads and analyzed them by SDS-PAGE and immunoblotting.

Homology modeling.

We built a model of AFG3L2 using the automated homology modeling server SWISS-MODEL[48] and the structure of the cytosolic region of the ATP-dependent metalloprotease FtsH from *T. thermophilus*[19] (mutant G399L; PDB 2DHR; UniProt Q72IK4) as the coordinate template.
We first aligned the two sequences with the ClustalX program (http://www. clustal.org/) to optimize insertions and deletions, then visualized and analyzed the model with the Molmol program. We built a similar model for the heterohexameric complex, assuming that AFG3L2 and paraplegin form an alternating heterodimer.

Confocal immunofluorescence analysis of human nervous tissue.

We obtained autopsy paraffin sections from the cerebellum of an infant who died immediately after birth owing to respiratory failure, and from the spinal cords of a 6-month-old infant and an adult who died from respiratory failure and medulloblastoma, respectively. We also used cortical vibratome sections obtained from a temporal-lobe specimen of a 47-year-old individual during brain surgery for a low-grade glioma. We cut paraplast-embedded autopsy specimens in 5- to 10-µm

sections with a rotary microtome (Leica), whereas we fixed the cortical sample by immersion in 4% (wt/vol) paraformaldehyde and then cut it in 50-µm sections with a vibratome (Leica). We performed immunofluorescence assays with anti-AFG3L2 or anti-paraplegin (1:500 dilution) followed by incubation with biotinylated goat anti-rabbit IgG/rhodamine avidin D (Jackson ImmunoResearch Labs) essentially as previously described[49]. We acquired fluorescence images on a Radiance 2100 confocal microscope (Bio-Rad) at a resolution of 1,024 × 1,024 pixels.

In situ hybridization on mouse cerebellum.

We performed nonradioactive *in situ* hybridization with digoxigenin-labeled riboprobes spanning the transcripts of *Afg3l2* and *Spg7* on brains collected from adult CD-1 mice and prepared as previously described[50]. We cut sections (15 µm) with a cryostat, mounted them on glass slides, fixed them in 4% (wt/vol) paraformaldehyde and treated them with 0.5% Triton X-100 PBS and then with triethanolamineacetic anhydride solution. We carried out pre-hybridization and hybridization according to standard procedures[51]. Sense probes served as negative controls. We examined slides using a Zeiss Axiophot light microscope (Zeiss) equipped with a Nikon Coolpix 950 digital camera (Nikon).

URLs.

National Center for Biotechnology Information, http://www.ncbi.nlm.nih.gov/; Washington University Neuromuscular Disease Center database (dominant ataxia section), http://www.neuro.wustl.edu/neuromuscular/ataxia/domatax.html; ClustalW2, http://www.ebi.ac.uk/Tools/clustalw2/ index.html; ClustalX, http://www.clustal.org/; Pfam, http://pfam.sanger. ac.uk/; TMHMM Server v2.0, http://www.cbs.dtu.dk/services/TMHMM-2.0/; RCSB Protein Data Bank, http://www.rcsb.org/pdb/; SWISS-MODEL, http:// swissmodel.expasy.org/; UniProt, http://www.uniprot.org/.

40. Manto, M. & Marmolino, D. Cerebellar ataxias. *Curr. Opin. Neurol.* **22**, 419–429 (2009).
41. Brusco, A. *et al.* Molecular genetics of hereditary spinocerebellar ataxia: mutation analysis of spinocerebellar ataxia genes and CAG/CTG repeat expansion detection in 225 Italian families. *Arch. Neurol.* **61**, 727–733 (2004).
42. Gellera, C. *et al.* Frataxin gene point mutations in Italian Friedreich ataxia patients. *Neurogenetics* **8**, 289–299 (2007).
43. Puddu, F. *et al.* Phosphorylation of the budding yeast 9–1-1 complex is required for Dpb11 function in the full activation of the UV-induced DNA damage checkpoint. *Mol. Cell. Biol.* **28**, 4782–4793 (2008).
44. Adams, A., Gottschling, D.E., Kaiser, C.A. & Stearns, T. *Methods in Yeast Genetics: A Cold Spring Harbor Laboratory Course Manual* (Cold Spring Harbor Laboratory Press, Cold Spring Harbor, New York, 1997).
45. Lemaire, C. & Dujardin, G. Preparation of respiratory chain complexes from *Saccharomyces cerevisiae* wild-type and mutant mitochondria: activity measurement and subunit composition analysis. *Methods Mol. Biol.* **432**, 65–81 (2008).
46. Magri, S., Fracasso, V., Rimoldi, M. & Taroni, F. Preparation of yeast mitochondria and *in vitro* assay of respiratory chain complex activities. *Nat. Protoc.* published online, doi:10.1038/nprot.2010.25 (7 March 2010).
47. Fracasso, V., Lazzaro, F. & Muzi-Falconi, M. Co-immunoprecipitation of human mitochondrial proteases AFG3L2 and paraplegin heterologously expressed in yeast cells. *Nat. Protoc.* published online, doi:10.1038/nprot.2010.26 (7 March 2010).
48. Schwede, T., Kopp, J., Guex, N. & Peitsch, M.C. SWISS-MODEL: An automated protein homology-modeling server. *Nucleic Acids Res.* **31**, 3381–3385 (2003).
49. Finardi, A. *et al.* NMDA receptor composition differs among anatomically diverse malformations of cortical development. *J. Neuropathol. Exp. Neurol.* **65**, 883–893 (2006).
50. Sacco, T., De Luca, A. & Tempia, F. Properties and expression of Kv3 channels in cerebellar Purkinje cells. *Mol. Cell. Neurosci.* **33**, 170–179 (2006).
51. Darby, I.A. & Hewitson, T.D. (eds) *In Situ Hybridization Protocols.* (Humana Press, Totowa, New Jersey, 2006).

Supplementary Information

Genetic studies

RNA analysis

To verify that the mutations were present in the transcripts, when feasible, total RNA was extracted from transformed lymphoblastoid cell lines derived from affected individuals using the RNAeasy Mini Kit (Qiagen). cDNA synthesis was carried out using the Cloned AMV First-Strand Synthesis Kit (Invitrogen) with an *AFG3L2*-specific primer. PCR primer pairs were designed to amplify fragments spanning from exon 9 to exon 11 and exon 15 to exon 17.

In silico analysis of the identified AFG3L2 mutations

The four mutations in exon 16 cause the amino acid substitutions S674L, E691K, A694E, and R702Q within the proteolytic domain, in a region that is highly conserved in *m*-AAA and *m*-AAA-related proteins of multiple species, ranging from eubacteria to humans (Fig. 1). In particular, conservation for Ser674, Arg702, Ala694, and Glu691 is 92%, 83%, 75%, and 66%, respectively. Notably, however, Glu691, Ala694, and Arg702 are conserved from the ancestral eubacterial protein FtsH11. The N432T substitution, found in the sequence encoded by exon 10, occurs in the ATPase (AAA) domain and also resides within an evolutionarily highly conserved region. In particular, all *m*-AAA and *m*-AAA-related proteins from eubacteria to humans exhibit an absolute conservation of a 5-amino acid motif (TLNQ) encompassing AFG3L2 Asn432 (Fig. 1). By contrast, the H126Q substitution, caused by the 378C>G mutation in exon 4, occurs in the N-terminal part of the mature protein which precedes the 1st transmembrane domain and protrudes into the matrix, a region of unknown functional properties which exhibits high homology (100% identity between residue 113 and residue 133) with rodent AFG3L2 but is not evolutionarily conserved in orthologs from more distantly-related species (data not shown). Predictions on the effects of the substitutions on

protein function using the algorithms SIFT52 and PolyPhen53 did not give univocal results. Both programs predicted the S674L, R702Q, and H126Q substitutions to be tolerated, and the A694E substitution to affect protein function. By contrast, the E691K change was predicted to be benign by PolyPhen but not tolerated by SIFT. Both programs predicted the N432T not to be tolerated. Possible effects of the mutations on pre-mRNA splicing were assessed using the algorithms ESEfinder54 (Release 3.0) for changes in exonic splicing enhancers (ESE) and PESX55 for changes in putative exonic splicing silencers (PESS). None of the mutations is predicted to change putative silencer sequences. No effect on ESE sequences is predicted for the 4 mutations on exon 16. The 1296A>C mutation causing N432T is predicted to alter the ESE pattern in exon 10 by abolishing one SF/ASF site and creating 3 novel ones. However, RT-PCR analysis of AFG3L2 transcript in lymphoblastoid cells from patients carrying this mutation or the mutations in exon 16 demonstrated equal dosage of normal and mutant mRNA, with no evidence of aberrant splicing induced by the mutations. Two modest changes were predicted for the 378C>G mutation (H126Q), namely, the mild attenuation of a putative SRp40 ESE sequence along with the creation of a novel similar sequence with a just above the threshold score. Unfortunately, no mRNA source was available from the patient and the effect of the 378C>G mutation (H126Q) on splicing could not be directly tested.

Mutation screening

For mutation screening of the selected patient population, PCR products were analyzed by automated sequencing and/or Denaturing High-Performance Liquid Chromatography (DHPLC)[56,57]. Sequences of the oligonucleotide primers and conditions used for PCR amplification, DNA sequencing, and DHPLC analysis are detailed in **Supplementary Table 2**. For DHPLC analysis on the 3500HT WAVE® system (Transgenomic), melting profiles of each PCR product sequence were predicted using the Navigator 6.4 software (Transgenomic). For each exon, DHPLC mutation analysis was performed at at least two different temperatures (**Supplementary Table 2b**), based on the

melting profiles. PCR products encompassing frequent polymorphic sites or PCR fragments not suitable for DHPLC analysis were directly sequenced.

Structural modeling of AFG3L2 mutations

A three-dimensional model of AFG3L2 was built using the structure of the *Th. thermophilus* (*Tth.*) AAA protease FtsH[11,19] as a template (**Fig. 5**). This protein is a homohexamer (**Fig. 5a**) which adopts a flat-cylinder-like shape divided into two disks (**Fig. 5b**). The lower disk, containing the protease domain, forms a six-fold-symmetric structure with a Zn^{2+} binding site. The upper disk is composed of six AAA+ domains, each of which contains ADP. ***E691K.*** AFG3L2 Glu691 is also a glutamate (Glu537) in *T. thermophilus* FtsH[19], but is not conserved in other orthologs including paraplegin (**Fig. 1**). This residue is at the N-terminus of helix a17 (**Supplementary Figs. 5a** and **6a**) and sits in the middle of the central pore formed by the six subunits surrounding the exit from the pore on the matrix side of the proteolytic domain (**Fig. 5a**-**b** and **Supplementary Figs. 5a**-**b** and **6a**). While overall exposed and therefore not evidently contributing to subunit interactions or fold stability, this residue could be relevant for protease specificity[57]. Substitution of this residue with a lysine as in AFG3L2^{E691K} could have severe consequences on protein function as it drastically changes the electrostatic potential and the chemical characteristics of the pore (**Fig. 5c-g** and **Supplementary Fig. 5c-g**). The change is evident in the AFG3L2^{WT}-AFG3L2^{E691K} compound homohexamer (**Supplementary Fig. 5e**) but is greatest in both the homohexameric mutant AFG3L2^{E691K}-AFG3L2^{E691K} (**Supplementary Fig. 5d**) and the heterohexameric AFG3L2^{E691K}-paraplegin (**Supplementary Fig. 5g**) in which the charge reversal of E691K is not counteracted by the neutral residue (Gln693) that substitutes AFG3L2 Glu691 in paraplegin.

A694E and ***R702Q***, the other two AFG3L2 mutations which produce a variation in the protein charge, appear to have smaller effects on the electrostatic potential of the protein surface (not shown). Ala694 (Ala540 in FtsH) is also close to the pore and nonconserved. Despite

being rather superficial, its side chain points towards the pore inside and is overall rather buried, therefore not influencing significantly the electrostatic potential. Substitution of this alanine with a glutamate as in AFG3L2^{A694E} requires burial of a charged group in the protein interior which can be achieved only at a high energetic cost. We may therefore predict that this mutation would have a strong effect on destabilizing the fold. Arg702 is Arg548 in FtsH. This side chain packs with the next subunit, although it does not appear to establish specific interactions with it. Also in this case, the effect of its replacement by a glutamine in AFG3L2^{R702Q} could be the destabilization of the assembly.

S674L. Ser674 is an alanine (A518) in FtsH. This residue is in a loop region between a16 and 39 and while it is exposed in the monomer (**Supplementary Fig. 5a**), it is buried in the subunit interface. In FtsH, the side chain of A518 is sandwiched between the conserved T498 and R494 of the adjacent subunit. While a serine can easily substitute the alanine, mutation of this residue in the bulkier leucine as in AFG3L2^{S674L} is expected to destabilize the hexamer assembly.

N432T. N432 is located within the ATPase domain in an evolutionarily conserved region and is absolutely conserved from eubacterial *Tth.* FtsH (N280) to human AFG3L2 (**Fig. 1**). This residue, which lies in the middle of a7, between Walker B and SRH motifs, is relatively exposed in the monomer (46 Å^2 accessible surface area) (**Supplementary Fig. 5a**) and is rather superficial also in the hexameric assembly (**Fig. 5** and **Supplementary Fig. 6b**). The side chain does not seem to form significant specific interactions with the surrounding. Although replacement of Asn432 by threonine in AFG3L2^{N432T} represents an exchange of two amino acids of the same class (uncharged polar), the asparagine side chain could have an important role in forming the required characteristics for substrate recognition and specificity. In the hexameric assembly of *T. thermophilus* FtsH, the side chain of the corresponding residue Asn280 is located in the pore and is near (~6 Å) the conserved Phe229 (Phe381 in AFG3L2) of the alternate monomer (**Supplementary Fig. 6b**). Notably, this phenylalanine is the crucial aromatic residue in the central pore loop motif @XG (pore-1 motif, where

@ is an aromatic residue and X is any residue) that is conserved in all subfamilies of the AAA family[20] and has been proposed to play an essential role for substrate recognition and ATP-dependent translocation of proteins into the proteolytic chamber[27,32].

Expression studies

AFG3L2 and paraplegin yeast expression plasmids

To generate yeast plasmids for heterologous expression of human AFG3L2, the sequence encoding residues 35-797 of human AFG3L2 was amplified by PCR from a full-length human *AFG3L2* cDNA clone (clone IMAGp998I0513535Q1, RZPD Consortium), fused to the sequence encoding the mitochondrial targeting peptide of Yta10p (amino acids 1-63), and cloned into the *Bam*HI/*XbaI*-digested low-copy-number centromeric vector pYC6/CT (Invitrogen) which carries the blasticidin resistance gene (plasmid pYC6/CT^{GAL1}-AFG3L2). To obtain high constitutive levels of AFG3L2 expression under control of the *ADH1* promoter, the glucose/galactose-regulated *GAL1* promoter on pYC6/CT was substituted with the 1-kb region upstream from the *ADH1* translation initiation codon, amplified by PCR and cloned into the *Spe*I/*Bam*H*I*-digested pYC6/CT^{GAL1}-AFG3L2 plasmid. This plasmid [pYC6/CT^{ADH1}-Yta10p(1-63)-AFG3L2(35-797)-V5/HIS, abbreviated into pYC6/CT^{ADH1}- AFG3L2-V5/HIS] was used in all expression experiments except when differently indicated. For AFG3L2 expression under control of the weaker *YTA10* promoter, plasmid pYC6/CT^{YTA10}-AFG3L2-V5/HIS was likewise generated by replacing the pYC6/CT *GAL1* promoter with a PCR fragment amplified from the 1-kb region upstream from the *YTA10* translation initiation. To investigate dominance of the mutations, plasmid pYC2/CT^{ADH1}- AFG3L2-V5/HIS carrying wild-type AFG3L2 and the *URA3* gene for selection was constructed by subcloning the *Spe*I/*Xba*I fragment [*ADH1*-Yta10p(1-63)-AFG3L2(35-797)] from pYC6/CT^{ADH1}-AFG3L2-V5/HIS into the *Spe*I/*XbaI*-digested centromeric pYC2/CT vector (Invitrogen).

The mutations causing the six substitutions identified in patients (AFG3L2^{H126Q}, AFG3L2^{S674L}, AFG3L2^{E691K}, AFG3L2^{A694E}, AFG3L2^{R702Q}, and AFG3L2^{N432T}) or the control proteolytic substitution AFG3L2^{E575Q} (ref. 13) were introduced into the yeast AFG3L2 expression construct pYC6/CT^{ADH1}-AFG3L2-V5/HIS using the QuikChange XL Site-Directed Mutagenesis Kit (Stratagene) and the following oligonucleotide primer pairs. Mutagenized plasmids were verified by DNA sequencing.

Mutant		**Primer pairs (5'->3')**
AFG3L2^{E575Q}	Forward	CTGTGGCATACCACCAAGCAGGCCATGCGG
		CCGCATGGCCTGCTTGGTGGTATGCCACAG
AFG3L2^{E691K}	Forward	TATTGGAGAAACCTTACAGTAAAGCCACTGCAAGATTGATAGA
		TCTATCAATCTTGCAGTGGCTTTACTGTAAGGTTTCTCCAATA
AFG3L2^{H126Q}	Forward	GGCAAGAAAGTAGATTCTCAGTGGTGGTCCAGGTTTCAGAA
		TTCTGAAACCTGGACCACCACTGAGAATCTACTTTCTTGCC
AFG3L2^{R702Q}	Forward	GATGATGAAGTACAAATACTTATTAATGATG
		CATCATTAATAAGTATTTGTACTTCATCATC
AFG3L2^{A694E}	Forward	TTACAGTGAAGCCACTGAAAGATTGATAGATGATG
		CATCATCTATCAATCTTTCAGTGGCTTCACTGTAA
AFG3L2^{S674L}	Forward	GGTTGGGCAAATCTTATTTGACCTCCCACGTCAGG
		CCTGACGTGGGAGGTCAAATAAGATTTGCCCAACC
AFG3L2^{N432T}	Forward	GAGAACACACTCACCCAGCTGCTGGTGGAG
		CTCCACCAGCAGCTGGGTGAGTGTGTTCTC

For human paraplegin expression, plasmid YCplac111^{ADH1}-Yta10p(1-63)- paraplegin(59-795)-HA (abbreviated into YCplac111^{ADH1}-paraplegin-HA) was used, in which the sequence corresponding to the mature form of paraplegin (amino acids 59-795) is tagged at the C-terminus with the HA epitope, fused to the Yta10p mitochondrial

leader peptide (amino acids 1-63), and expressed under control of the *ADH1* promoter[59].

Plasmids and strains generated in this study are available upon request following the execution of an MTA agreement.

Cytochrome c oxidase analysis in yeast

For in-vitro activity assay of cytochrome c oxidase (COX) or immunoblot analysis of its subunits, yeast cells were grown at 28°C in YEP medium supplemented with 2% (wt/vol) galactose-0.1% (wt/vol) glucose[45,46]. Following differential centrifugation of the cells, the resulting mitochondrial pellet was resuspended in 10-mM potassium phosphate buffer and freezed and thawed for three times. COX activity was determined spectrophotometrically at 30°C following for 2 minutes the decrease of absorbance at 550 nm because of oxidation of cytochrome c^{red} (refs. 46,60). Activity was expressed as nanomoles of cytochrome cred oxidized per minute per milligram of protein. Protein concentration was determined by Bradford microplate microassay (Bio-Rad) with bovine serum albumin as the standard.

In yeast, COX is composed of 11 subunits, three of which (Cox1p, Cox2p, and Cox3p) are encoded in the mitochondrial genome and form the catalytic core of the enzyme[61]. Immunoblot analysis with antibodies directed against the three mitochondrial-encoded subunits and one nuclear-encoded subunit (Cox4p) demonstrated mult*i*-subunit deficiency, with a drastic reduction (80 - >95%) of Cox1p, Cox2p, and Cox4p protein levels and a milder decrease (40-75%) of Cox3p levels (Fig. 3b). Upon co-expression of paraplegin, COX activity (Fig. 3c) was partially recovered in mutants AFG3L2^{S674L} (51%), AFG3L2^{A694E} (61%), and AFG3L2^{R702Q} (84%) but remained significantly low (P 0.01 n=4) in mutants AFG3L2^{E691K} (7%), AFG3L2^{N432T} (25%), or the control mutant AFG3L2^{E575Q} (ref. 13) (4%), consistently with the observed respiratory phenotypes (Fig. 2d and e). As illustrated by immunoblot analysis in Fig. 3d, COX subunit protein levels paralleled enzyme activity, returning nearly normal in mutants AFG3L2^{S674L}, AFG3L2^{A694E}, and AFG3L2^{R702Q} (Fig. 3d, lanes 5, 7, and 8), but remaining significantly low (P 0.01 n=4) in mutants AFG3L2^{E691K},

AFG3L2^{N432T}, or the control mutant AFG3L2^{E575Q} (Fig. 3d, lanes 6, 9, and 3, respectively).

Generation of antibodies against AFG3L2 and paraplegin

To raise rabbit polyclonal antisera against human AFG3L2 and paraplegin, GST fusion proteins were generated with protein fragments of AFG3L2 and paraplegin showing no homology to each other. The regions encoding amino acids 67-305 of AFG3L2 and amino acids 89-304 of paraplegin were PCR amplified from IMAGE clones (clone IMAGp998I0513535Q1 for *AFG3L2* and clone IMAGp998D1211693Q1 for *SPG7*, RZPD Consortium) and subcloned into the pGEX-6P-1 vector (Amersham Biosciences), in order to generate GST-AFG3L2 and GST-paraplegin fusion proteins. Recombinant proteins were expressed in *Escherichia coli* and purified by glutathione affinity chromatography. After preparative SDS-PAGE and electroelution[62], recovered proteins were injected into rabbits (200-300 tg of protein per injection). The ant*i*-AFG3L2 and ant*i*-paraplegin antisera collected from the animals showed no cross-reaction when tested against each protein individually expressed in *yta10Ayta12A* yeast cells (**Supplementary Fig. 7a**) nor when used in Western blot analysis of protein extracts from human cells (**Supplementary Fig. 7b**).
Antibodies generated in this study are available upon request following the execution of an MTA agreement.

SK-N-SH cell culture and confocal immunofluorescence analysis

Human neuroblastoma SK-N-SH cells[63] were grown in Dulbecco's modified Eagle's medium (DMEM) supplemented with nonessential amino acids and 10% fetal bovine serum and plated on coverslip in 12-well plates. Prior to immunofluorescence (**Supplementary Fig. 7**), cells were fixed in 4% (wt/vol) paraformaldehyde for 5 minutes, repeatedly rinsed in phosphatebuffered saline (PBS), and incubated overnight at 4°C with the primary antisera[48] (rabbit polyclonal ant*i*-

AFG3L2 or anti-paraplegin, 1:500 dilution). For sequential double-labeling, cells were incubated for 2 hours with Alexa Fluor 546-conjugated goat anti-rabbit IgG (Molecular Probes; 1:2,000 dilution), then with monoclonal anti-prohibitin-1 (PHB1) antibody (Santa Cruz Biotechnology; 1:50 dilution) as mitochondrial marker, followed by Alexa Fluor 488-conjugated goat anti-mouse secondary antibody (Molecular Probes; 1:2,000 dilution). Finally, cells were repeatedly rinsed and coverslipped with Fluorsave (Calbiochem). Immunofluorescence images were acquired on a Radiance 2100 confocal microscope (BioRad) at 1,024 x 1,024-pixel resolution.

Immunoblot analysis of patients' cells

Epstein-Barr-virus-stabilized lymphoblastoid cell lines from patients, their relatives and control subjects were established and cultured as previously described[42]. For Western blot analysis of patients' lymphoblasts (**Supplementary Figs. 8a** and **9**), 50-150 tg of lymphoblastoid cell lysate from each line were electrophoresed on 10%-15%-SDSpolyacrylamide gels and transferred to a nitrocellulose membrane (Amersham Biosciences) by electroblotting. Filters were probed with polyclonal antibodies as indicated in the text and in the figure legends, and developed by HRP-conjugated secondary antibodies using a chemiluminescent substrate (ECL Kit, Amersham Biosciences) followed by autoradiography. The signals were normalized by probing filters with antibodies directed against tubulin (Santa Cruz Biotechnology) as a loading control protein.

Blue native gel electrophoresis

Blue native polyacrylamide gel electrophoresis (BNE) (**Supplementary Fig. 8b**) was carried out essentially as described[64]. To obtain mitochondria-enriched extracts, lymphoblastoid cell pellets were resuspended in a cold digitonin solution (20-mM MOPS, 250-mM sucrose, pH 7.4, 0.2-mg/ml digitonin), kept on ice for 10 min, and

centrifuged at 600 X g for 10 min at 4°C. Supernatants were centrifuged at 7000 x g for 7 min at 4°C. The resulting pellets were solubilized in NativePAGETM Sample Buffer (Invitrogen) with 1% (wt/vol) digitonin, 1-mM ATP, 5-mM E-amino-*n*-caproic acid, and COMPLETETM Protease Inhibitor Cocktail (Roche). The solution was incubated on ice for 90 min and then centrifuged at 125,000 x g for 30 min at 4°C. After addition of NativePAGETM 5%-G-250 Sample Additive (Invitrogen), samples were loaded onto 3-12% NativePAGETM Novex® Bis-Tris Gels (Invitrogen). Electrophoresis was performed at 4°C according to the manufacturer's protocol.

Supplementary Table 1. AFG3L2 polymorphic variants observed in this study

Nucleotide change[a]	**Amino acid change**[b]	**NCBI SNP Reference Cluster ID**[c]	**Allele frequency (%) (n=300)**
-96G>C		rs12327346	G=97.4; C=2.6
293$^{-61A>G}$		rs8093375	nd[d]
400$^{-95G>A}$		rs2298542	nd[d]
400$^{-14C>G}$		not reported	C=99.4; G=0.6
752$^{+6C>T}$		rs8097342	C=18.4; T=81.6
753$^{-55T>C}$		rs7407640	nd[d]
1026$^{+8G>A}$		rs8091858	G=93.9; A=6.1
1165$^{-21T>A}$		rs9966470	nd[d]
1319$^{-59G>T}$		not reported	G=99.7; T=0.3
1319$^{-55T>G}$		not reported	T=99.1; G=0.9
1389G>A	L463L	rs11080572	G=32; A=68
1650A>G	E550E	not reported	A=18; G=82
1664$^{-39G>A}$		not reported	G=98.1; A=1.9
1664$^{-9T>C}$		not reported	T=99.7; C=0.3

2394G>C		rs1129115	nd[d]

[a]Nucleotide numbering refers to the AFG3L2 cDNA [GenBank accession No. NM_006796.1 (GI:5802969)].

Nucleotides are numbered so that the first nucleotide (nt) of the first in-frame ATG codon is nucleotide +1.

[b]Amino acids are numbered so that methionine encoded by the first in-frame ATG codon is Met1. *c* http://www.ncbi.nlm.nih.gov/projects/SNP/.

[d]nd, not determined.

Supplementary Table 2. Oligonucleotide primers used for PCR amplification, DNA sequencing, and DHPLC analysis of AFG3L2 exons

2a. DNA sequence analysis

Exon amplicons		**Primer pairs (5'->3')**	**PCR annealing temperature** *a*
1	Forward Reverse	TTGAGAGCTTG GGCTCCT	57°C
2-3	Forward Reverse	TTATGACCAGGAAAT GAAGC	56°C
4-5	Forward Reverse	AGCCTCCCTGATTG GTAAG	58°C
6	Forward Reverse	TGGGGGCATCT TTATCTG	58°C
7	Forward Reverse	AATGAGTGACATTTA ATCACC	57°C
8	Forward Reverse	GCCTTTGAAGAA CACTTGC	56°C
9	Forward Reverse	AATGTTCTACCATAGCTC AGATG	57°C
10	Forward Reverse	GGCCGATTTATTT CATTTCT	56°C
11-12	Forward Reverse	GCTATGAATTTGCA GTGCTC	56°C
13	Forward Reverse	ACTATGGATTTGGCT GTCC	57°C

14	Forward Reverse	TTGTGATAGGCAGCTCAGTC CTTTGCAGGAGTGTAGCTTG	58°C
15	Forward Reverse	CCACTAAGGCTGA TGAACT TCCTTCCCTAAAAA	57°C
16	Forward Reverse	TGGGATTTGCGTCCTA AC CCACACAACCAAACATC	59°C
17	Forward Reverse	TGGGGTCACCTGTAA ATAAAA TCCTGTAGAAAACCA	56°C

[a]PCR conditions included an initial denaturation step at 95°C for 3 min, followed by 35 cycles of denaturation at 94°C for 1 min, annealing for 45 s at the temperature indicated in the table, and extension at 72°C for 1 min, with a final extension step at 72°C for 10 min.

Supplementary Table 3. Saccharomyces cerevisiae strains used in this study

Strain	**Relevant genotype** [a]	**Source**
K699 (source:	*MAT***a** *ade2-1 trp1-1 can1-100 leu2-3,112 his3-11,15 ura3-52*	Refs. 43 65
yDDB64 [b]	K699 *yta10::NAT yta12::KanMX6*	This study
yDDB79	yDDB64 (pYC6/CT^{ADH1}-AFG3L2-V5/HIS)	This study
yDDB94	yDDB64 (pYC6/CT^{YTA10}-AFG3L2-V5/HIS)	This study
yDDB 1 1 1b	yDDB64 (pYC6/CT^{YTA10}-AFG3L2-V5/HIS) (YCplac 1 1 1^{YTA10}-paraplegin-HA)	This study
yDDB122	yDDB64 (pYC6/CT^{ADH1}-AFG3L2^{H126Q}-V5/HIS)	This study
yDDB 123	yDDB64 (pYC6/CT^{ADH1}-AFG3L2^{E691K}-V5/HIS)	This study
yDDB124	yDDB64 (pYC6/CT^{ADH1}-AFG3L2^{A694E}-V5/HIS)	This study
yDDB125	yDDB64 (pYC6/CT^{ADH1}-AFG3L2^{R702Q}-V5/HIS)	This study
yDDB126	yDDB64 (pYC6/CT^{ADH1}-AFG3L2^{S674L}-V5/HIS)	This study
yDDB158	yDDB64 (pYC6/CT^{ADH1}-AFG3L2^{N432T}-V5/HIS)	This study

yDDB127	yDDB64 (pYC6/CT*ADH1*-AFG3L2E575Q-V5/HIS)	This study
yDDB 1 09	yDDB64 (pYC2/CT^{ADH1}-AFG3L2-V5/HIS)	This study
yDDB 1 9 0	yDDB64 (pYC6/CT^{ADH1}-AFG3L2^{E691K}-V5/HIS) (pYC2/CT^{ADH1}-AFG3L2-V5/HIS)	This study
yDDB191	yDDB64 (pYC6/CT^{ADH1}-AFG3L2^{A694E}-V5/HIS) (pYC2/CT^{ADH1}-AFG3L2-V5/HIS)	This study
yDDB 1 92	yDDB64 (pYC6/CT^{ADH1}-AFG3L2^{R702Q}-V5/HIS) (pYC2/CT^{ADH1}-AFG3L2-V5/HIS)	This study
yDDB 1 89	yDDB64 (pYC6/CT^{ADH1}-AFG3L2^{S674L}-V5/HIS) (pYC2/CT^{ADH1}-AFG3L2-V5/HIS)	This study
yDDB201	yDDB64 (pYC6/CT^{ADH1}-AFG3L2^{N432T}-V5/HIS) (pYC2/CT^{ADH1}-AFG3L2-V5/HIS)	This study
yDDB138	yDDB64 (YCplac111^{ADH1}-paraplegin-HA)	This study
yDDB 1 65	yDDB64 (pYC6/CT^{ADH1}-AFG3L2-V5/HIS) (YCplac1 1 1^{ADH1}-paraplegin-HA)	This study
yDDB 1 74	yDDB64 (pYC6/CT^{ADH1}-AFG3L2^{R702Q}-V5/HIS) (YCplac111^{ADH1}-paraplegin-HA)	This study
yDDB75b	yDDB64 (pYC6/CT^{ADH1}-AFG3L2^{H126Q}-V5/HIS) (YCplac111^{ADH1}-paraplegin-HA)	This study
yDDB200	yDDB64 (pYC6/CT^{ADH1}-AFG3L2^{A694E}-V5/HIS) (YCplac111^{ADH1}-paraplegin-HA)	This study
yDDB 1 6 6	yDDB64 (pYC6/CT^{ADH1}-AFG3L2^{E691K}-V5/HIS) (YCplac111^{ADH1}-paraplegin-HA)	This study
yDDB 129	yDDB64 (pYC6/CT^{ADH1}-AFG3L2^{E575Q}-V5/HIS) (YCplac111^{ADH1}-paraplegin-HA)	This study
yDDB 1 6 7	yDDB64 (pYC6/CT^{ADH1}-AFG3L2^{S674L}-V5/HIS) (YCplac111^{ADH1}-paraplegin-HA)	This study
yDDB 1 75	yDDB64 (pYC6/CT^{ADH1}-AFG3L2^{N432T}-V5/HIS) (YCplac111^{ADH1}-paraplegin-HA)	This study

[a] See **Supplementary Note** for plasmid description.

[b] *yta10dyta12.* parental strain generated using the one-step PCR strategy (refs. 43,66).

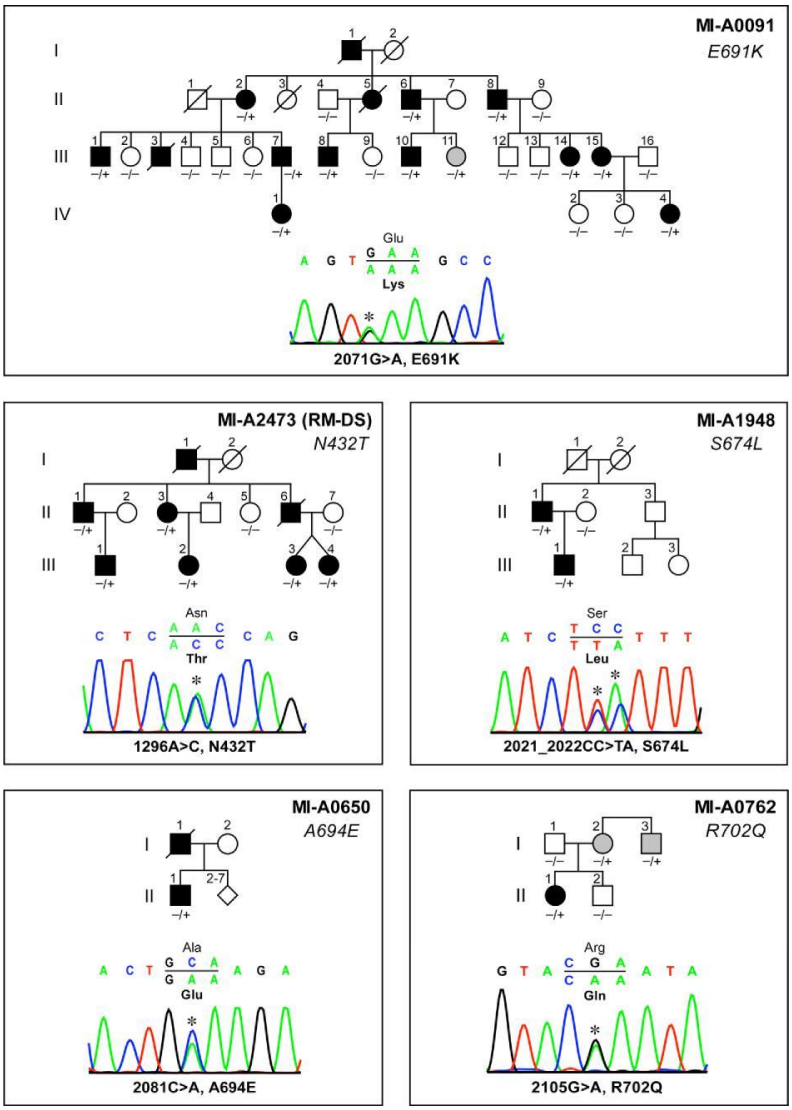

Supplementary Figure 1

Pedigrees and segregation of the mutations detected in *AFG3L2.*

Square and circle symbols are male and female individuals, respectively. Symbols filled in black are affected individuals. Symbols filled in gray are asymptomatic or paucisymptomatic individuals carrying an *AFG3L2* mutation. *AFG3L2* genotype is indicated under the symbols of the sampled individuals: - = normal sequence;

+ = mutation. Electropherograms of mutated *AFG3L2* sequences are shown under each pedigree. Mutated nucleotides are indicated by an asterisk (*). Amino acid changes are indicated in boldface. Nucleotide numbering refers to the AFG3L2 cDNA. Nucleotides are numbered so that the first nucleotide of the first in-frame ATG codon is nucleotide +1. In family M*I*-A0091, one asymptomatic individual (II*I*-11), previously reported to have the disease haplotype[8], was indeed mutated. Further clinical evaluation demonstrated the presence of nystagmus and very mild cerebellar signs. In family M*I*-A1948, the S674L substitution (TCC>TTA) was caused by the 2-nt mutation 2021_2022CC>TA. The occurrence of the two changes on the same allele was demonstrated both by segregation in the family (the two nucleotide substitutions were also carried by the affected father) and by sequencing of the subcloned PCR fragment. In family M*I*-A0762, individuals *I*-2 and *I*-3, heterozygous for the R702Q substitution, had a chronic subjective sense of unsteadiness, in the absence of objective neurological signs at clinical examination but with moderate cerebellar atrophy at MRI (see also **Supplementary Fig. 2**).

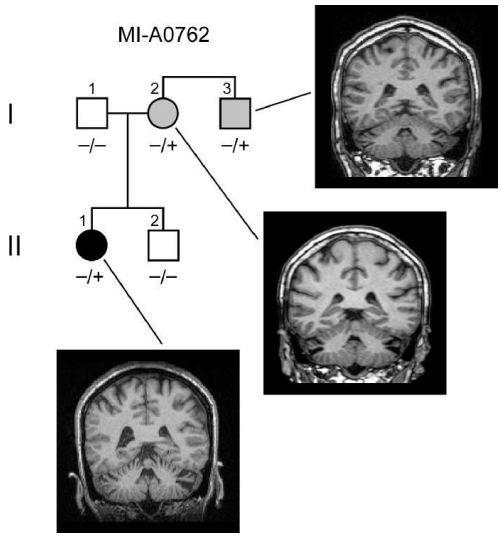

Supplementary Figure 2

Variable expressivity of AFG3L2^{R702Q} in family M*I*-A0762.

Pedigree of family M*I*-A0762 (see also **Supplementary Fig. 1**) showing segregation of the R702Q substitution. Symbols are as in **Supplementary Fig. 1**. *AFG3L2* genotype is indicated under the symbols of the tested individuals (- = normal sequence; + = mutated sequence). The index case (II-1) is a 40-year-old woman with a full-blown cerebellar phenotype that manifested at 28 years of age with progressive gait and limb ataxia. She now presents severe ataxia and dysarthria, ophthalmoplegia, and pyramidal signs with increased muscle tone, brisk reflexes, and Babinski sign. MRI shows the presence of marked atrophy of the vermis and the cerebellar hemispheres. Her 78-years-old father, who does not carry the AFG3L2^{R702Q} substitution, is completely asymptomatic and does not exhibit any clinical sign at neurological examination. MRI is negative (not shown). AFG3L2^{R702Q} is carried in heterozygous form by the mother (I2, 76 years old) and the maternal uncle (*I*-3, 74 years old). Both are negative at neurological examination, exhibiting none of the clinical signs observed in the index case II-1. In particular, there are no abnormalities of gait and speech, and no signs of corticospinal involvement. Despite negative neurological examination, though, both report to have been suffering of a chronic subjective sense of unsteadiness since

many years. Interestingly, in both subjects, MRI shows the presence of a moderate cerebellar atrophy in comparison to age-matched controls.

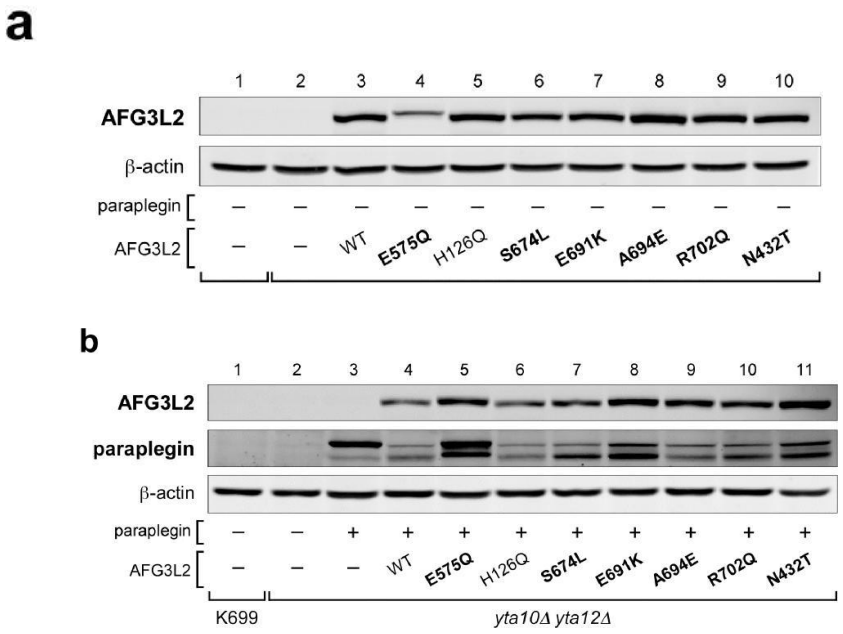

Supplementary Figure 3

Protein levels of heterologous AFG3L2 and paraplegin expressed in yeast cells.

Yeast strains and mutants as in **Fig. 4**. Mutations affecting respiration are in bold. (**a**) Fluorescence immunoblot analysis (VersaDoc Imaging System, BioRad) of TCA protein extracts of yeast cells expressing wild-type or mutant human AFG3L2 only. Filters were probed with antibodies against AFG3L2 (upper panel) or the loading control protein *fl*-actin (lower panel). (**b**) Fluorescence immunoblot analysis of TCA protein extracts of yeast cells co-expressing wild-type or mutant human AFG3L2 with human paraplegin. Filters were probed with antibodies against AFG3L2 (upper panel), paraplegin (middle panel), or the loading control protein *fl*-actin (lower panel). The two protein species in the paraplegin panel (middle panel) result from two-step processing of paraplegin upon import into mitochondria[34].

K699, wild-type yeast strain; *yta10Ayta12A*, yeast strains lacking endogenous *m*-AAA subunits Yta10p and Yta12p.

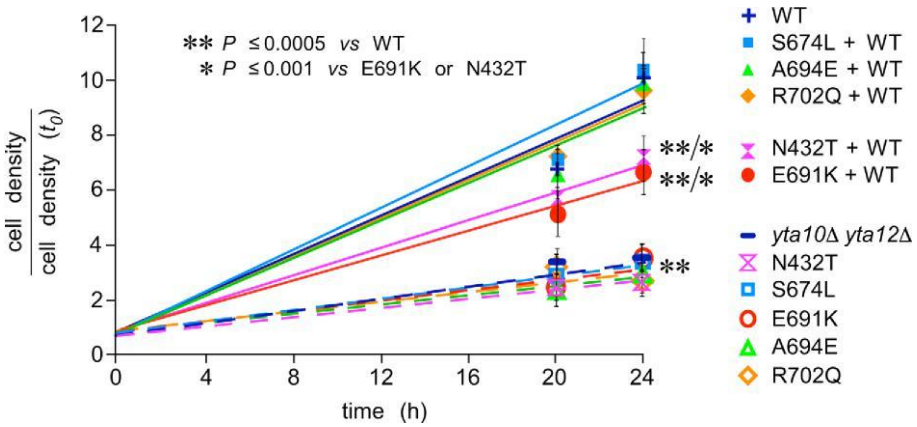

Supplementary Figure 4

Effect of co-expression of normal and mutant AFG3L2 on the growth of *yta10A yta12A* yeast cells.

To determine whether the identified *AFG3L2* mutations exert a dominant-negative effect, as observed for AFG3L2^{E691K} (see **Fig. 2c**), the growth rates of *m*-AAA-deficient yeast cells (*yta10Ayta12A*) harboring the different mutant forms of AFG3L2 were analysed both in the absence and in the presence of normal AFG3L2 (WT). The graph shows the growth rates of cells expressing either AFG3L2^{WT} or each mutant or co-expressing both the normal and the mutant form. Cells were grown for 24 hours with cell counting at 0, 20, and 24 hours. Values on the *y*-axis represent the ratio between cell density (= number of cells/ml) at a given time and cell density at start (*t0*). Growth rates are calculated by linear regression analysis (trend line). Each value represents the mean of four independent experiments. Error bars indicate s.d. Asterisk(s) indicate statistical significance (one asterisk, *P* 0.001; two asterisks, *P* 0.0005) as determined by Student's t-test. Introducing AFG3L2^{WT} into cells carrying mutant AFG3L2^{E691K} or AFG3L2^{N432T} resulted in a limited correction of the *yta10Ayta12A* respiratory phenotype, indicating a dominant-negative effect of these mutations (see also **Fig. 2c**). By contrast, co-expression of AFG3L2^{WT} with mutants AFG3L2^{S674L}, AFG3L2^{A694E}, and AFG3L2^{R702Q} appears to fully rescue the defective growth phenotype, suggesting that haploinsufficiency, rather than a dominant-negative effect, may be the disease-causing mechanism for these mutations.

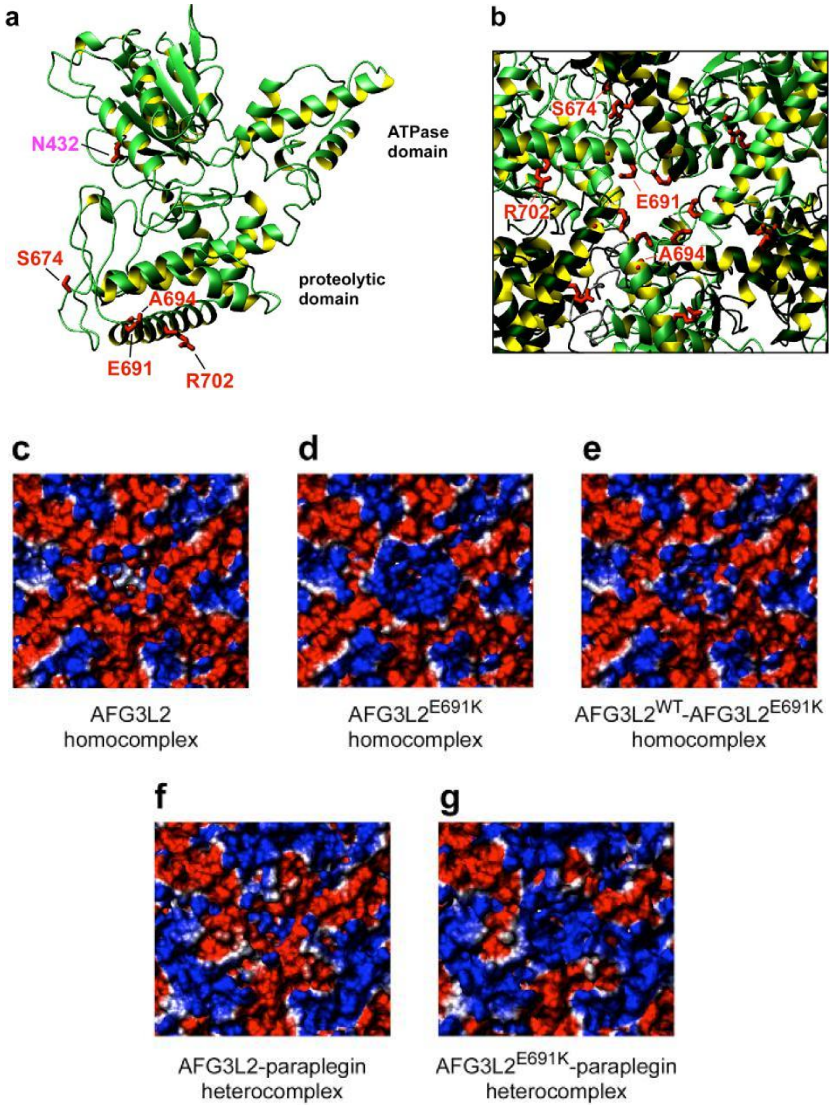

Supplementary Figure 5

Molecular modeling of normal and mutant AFG3L2.

The structure of AFG3L2 was built by homology using the coordinates of T. thermophilus FtsH (PDB 2DHR) as a template. A similar hetero-oligomeric model was built assuming that AFG3L2 and paraplegin form an alternate heterodimer (f, g). (a) The panel shows the structure of one of the subunits corresponding to the monomer boxed in red in Fig. 5b. The side chains of the residues substituted in the

proteolytic domain are indicated in red whereas the Asn432, located in the ATPase domain, is highlighted in magenta. Residues are labeled using the AFG3L2 numbering. (b) A blow-up of the hexameric structure in Fig. 5a to show details of the central pore from the matrix side and the location of the amino acid substitutions in the proteolytic domain. (c-g) Surface representations of the protease side of the homo-oligomeric and heterooligomeric homology models showing the effect of the E691K substitution on the electrostatic potential of the protein. The blow-ups of the structures in Fig. 5c-g show a detailed view of the electrostatic changes in the central pore formed by the six subunits surrounding the exit from the pore on the matrix side of the proteolytic domain. (c) Electrostatic surface of the homohexamer of AFG3L2; (d) homohexamer of AFG3L2E691K; (e) homohexamer obtained by alternating wild-type AFG3L2 and mutant AFG3L2E691K; (f) heterohexamer obtained by alternating AFG3L2 and paraplegin; (g) as in f but after substituting Glu691 with a lysine in AFG3L2. The surfaces are coloured according to electrostatic potential with blue indicating positive and red indicating negative charge. The E691K substitution drastically changes the electrostatic and chemical characteristics of the pore. The change induced by the E->K charge reversal is greatest in the homohexameric mutant (d) and in the heterohexameric complex of AFG3L2E691K and paraplegin (g), in which the negatively charged Glu691 of AFG3L2WT is substituted by the neutral Gln693 of paraplegin.

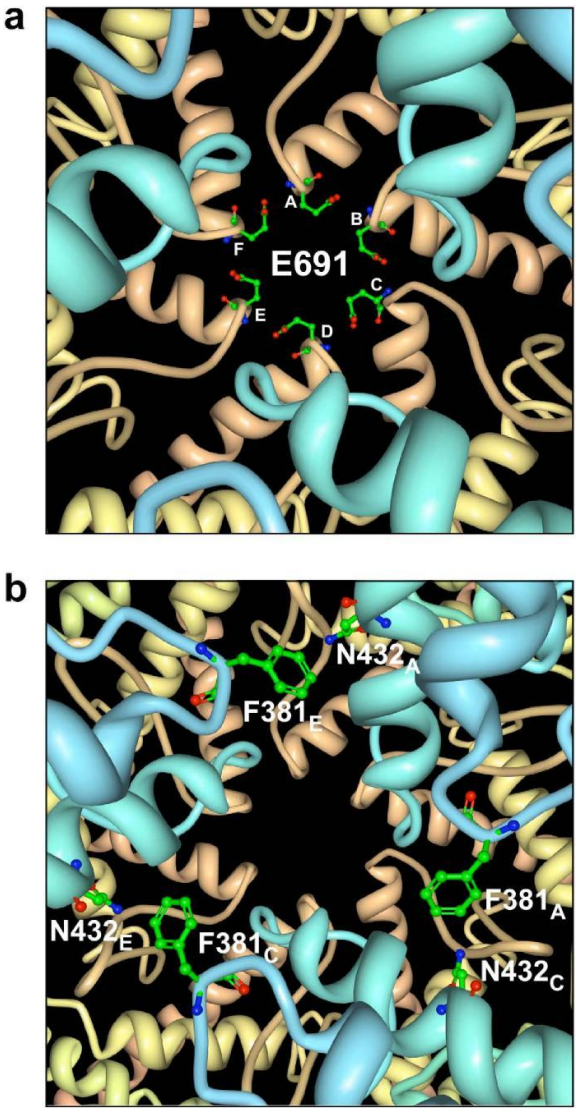

Supplementary Figure 6

Molecular modeling of Glu691 and Asn432 central pore residues substituted in SCA28 patients.

The model is based on *T. thermophilus* FtsH structure (PDB 2DHR). The figures are viewed from the ATPase side. (**a**) Wireframe display of Glu691 lining the central pore of the protease ring (*light brown* ribbons). The six monomers are indicated by capital letters from A to F. (**b**) The panel shows the central pore of the ATPase ring (*light blue* ribbons) with wireframe visualization of Asn432 and Phe381. Asn432 is substituted with threonine in patients from family M*I*-A2473/R*M*-DS.

Phe381 is the crucial aromatic residue in the conserved pore-1 loop motif FVG that protrudes into the central pore and may play an essential function for the ATP-dependent translocation of proteins into the proteolytic cavity[27,32]. The side chain of Asn432 is also located in the pore and is near (~6 Å) Phe381 of the alternate monomer (F381A-N432C, F381C-N432E, F381E-N432A). Atoms are colored as follows: carbon is *green*, oxygen is *red*, and nitrogen is *blue*.

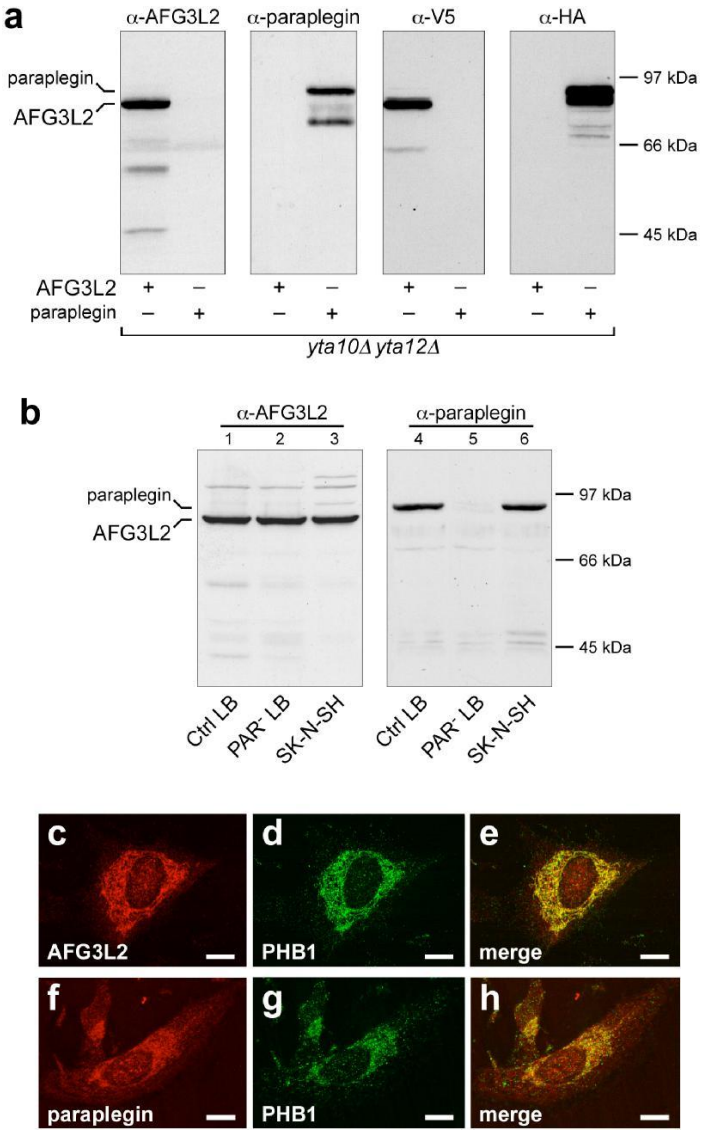

Supplementary Figure 7

Characterization of anti-AFG3L2 and anti-paraplegin antibodies.

To investigate expression of the *m*-AAA subunits in normal and diseased human cells and tissue, we raised polyclonal antisera that specifically recognize human AFG3L2 and paraplegin. Western blot analysis shows that the antibodies exhibit no cross reactivity against the two proteins (**a**, **b**). In both cases, immunofluorescence patterns are consistent with mitochondrial localization of the two proteins (**e** and **h**). (**a**) Immunoblot analysis of extracts from *yta10Ayta12A* yeast cells expressing either $AFG3L2^{WT}$ or $paraplegin^{WT}$ (left panels) or epitope-tagged $AFG3L2^{V5}$ or $paraplegin^{HA}$ (right panels). Blots were probed with anti-AFG3L2 (a-AFG3L2) or anti-paraplegin (a-paraplegin) polyclonal antibodies (left panels), or anti-V5 (a-V5) or anti-HA (a-HA) monoclonal antibodies. (**b**) Immunoblot analysis of AFG3L2 and paraplegin in human cells. Ctrl LB, lymphoblastoid cells from a normal control; PAR^- LB, lymphoblastoid cells from a spastic paraplegia patient carrying a homozygous null mutation in the *SPG7* gene; SK-N-SH, human neuroblastoma cells[63]. (**c**-**h**) Confocal immunofluorescence of cultured human neuroblastoma SK-N-SH cells showing the mitochondrial subcellular localization of both AFG3L2 (**c**) and paraplegin (**f**) by double-labeling with either antiAFG3L2 or anti-paraplegin antibodies and antibodies against the mitochondrial marker prohibitin-1 (PHB1; **d**, **g**). Note the high degree of colocalization, as indicated by the yellow signal in the merged images (**e**, **h**). Scale bars: 10 tm.

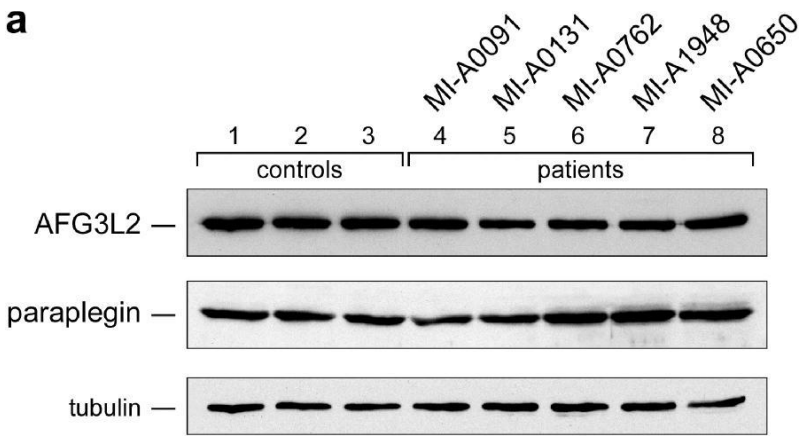

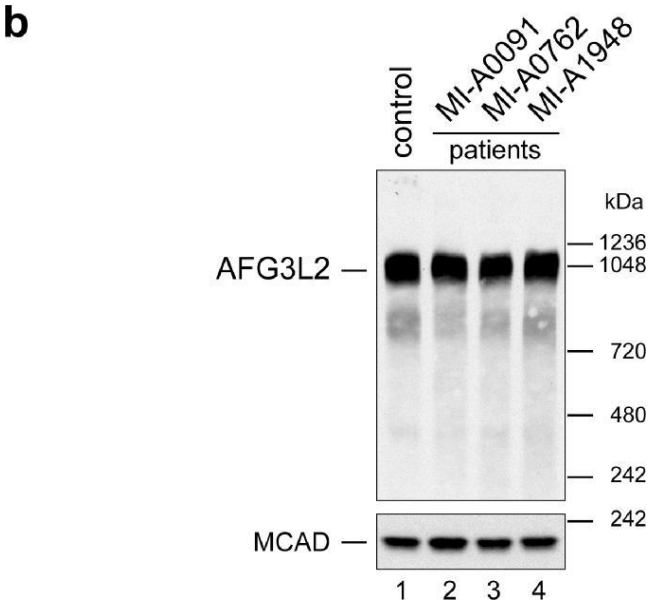

Supplementary Figure 8

Analysis of AFG3L2 and paraplegin protein expression in patients' cells.

(**a**) Western blot analysis of lymphoblastoid cell extracts (50 tg) following SDS-PAGE showed normal levels of AFG3L2 and paraplegin in five patients from the four families. Lanes 1-3: control subjects; lanes 4 and 5: probands from family M*I*-A0091 (AFG3L2^{E691K}); lanes 6-8: probands from families M*I*-A762 (AFG3L2^{R702Q}) (lane 6), M*I*-A1948 (AFG3L2^{S674L}) (lane 7), M*I*-A0650 (AFG3L2^{A694E}) (lane 8). Filters were probed with ant*i*-AFG3L2 or ant*i*-paraplegin antibody and an antibody directed against tubulin as a loading control protein. (**b**) Western blot analysis of lymphoblastoid cell extracts following nondenaturing blue native electrophoresis demonstrated normal levels of a high-molecular-mass immunoreactive protein of approx. 1 MDa, indicating that the substitutions affect neither the amount nor the size of the supramolecular assembly of AFG3L2. Lymphoblastoid cells were solubilized in digitonin and 100 tg of cell protein were loaded on a 3-12% polyacrylamide gradient gel. Immunoblotting was carried out with ant*i*-AFG3L2 antibody or antibody against medium-chain acyl-CoA dehydrogenase (MCAD) as a loading control protein (native molecular mass = ~230 kDa). NativeMarkTM Protein Standard (Invitrogen) were used as molecular weight markers ranging 242-1,236 kDa.

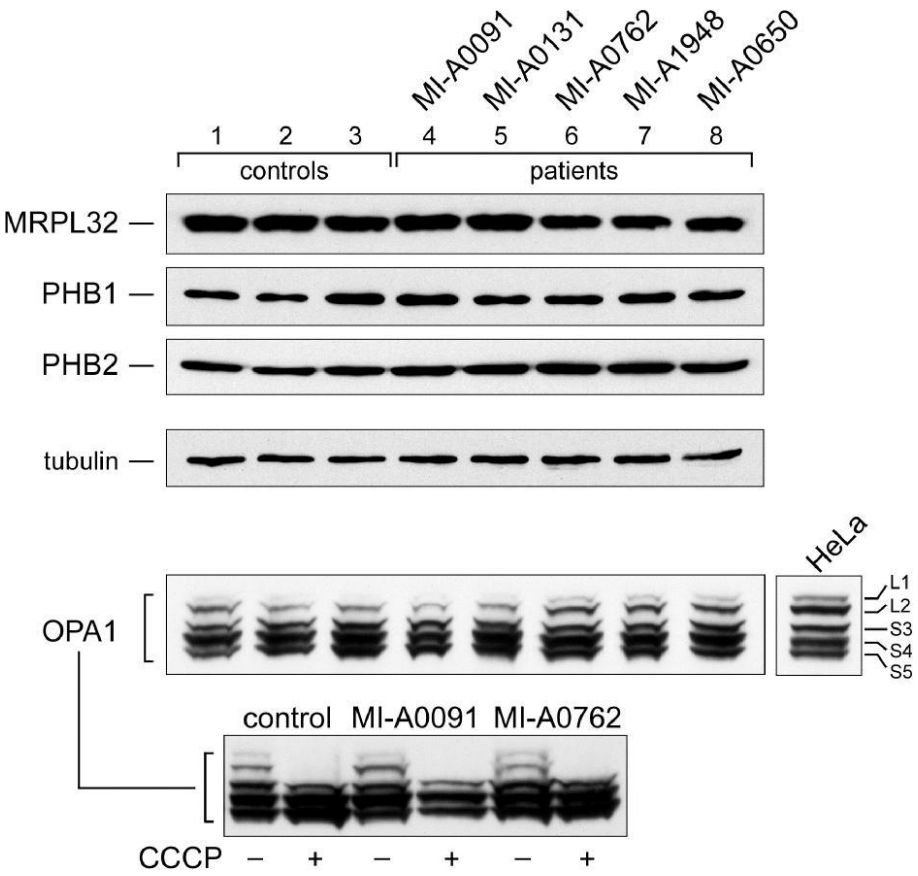

Supplementary Figure 9

Expression analysis of MRPL32, prohibitin 1 and 2, and OPA1 in patients' lymphoblasts.

To examine whether mutations affecting AFG3L2 could induce secondary abnormalities of other proteins known for being either partners or substrates of the *m*-AAA complex, we investigated the expression of prohibitin 1 (PHB1) and 2 (PHB2), MRPL32, and OPA1, observing no differences both in the protein levels and in the migration pattern as compared to normal controls. MRPL32 is a subunit of human mitochondrial ribosomes, homolog of yeast MrpL32, a previously reported substrate of *m*-AAA (ref. 16); prohibitin 1 (PHB1) and 2 (PHB2) have been shown to form ring-shaped assemblies that associate with *m*-AAA in a supercomplex of ~1.2 MDa and modulate *m*-AAA proteolytic activity[12]; OPA1, a dynamin-like GTPase that causes human dominant optic

atrophy and functions in mitochondrial fusion and inner membrane remodeling, has been recently proposed to be regulated by the *m*-AAA protease[22,67,68]. Cell extracts were subjected to Western blotting with the antibody indicated. HeLa cell extracts were used as a control for OPA1 processing. Expression of eight OPA1 splice variants and proteolytic processing leads to the formation of at least five different isoforms of OPA1, two long forms designated L1 and L2, which can be proteolytically converted into three short forms, designated S3-S5[67,68]. Dissipation of mitochondrial membrane potential, as that caused by the uncoupler carbonyl cyanide 3- chlorophenylhydrazone (CCCP), stimulates OPA1 processing[67,68] and may thereby reveal impairment of processing, if any.

Supplementary References

52. Ng, P. C. & Henikoff, S. SIFT: Predicting amino acid changes that affect protein function. *Nucleic Acids Res* **31**, 3812-3814 (2003).
53. Ramensky, V., Bork, P. & Sunyaev, S. Human non-synonymous SNPs: server and survey. *Nucleic Acids Res* **30**, 3894-3900 (2002).
54. Cartegni, L., Wang, J., Zhu, Z., Zhang, M. Q. & Krainer, A. R. ESEfinder: A web resource to identify exonic splicing enhancers. *Nucleic Acids Res* **31**, 3568-3571 (2003).
55. Zhang, X. H. & Chasin, L. A. Computational definition of sequence motifs governing constitutive exon splicing. *Genes Dev* **18**, 1241-1250 (2004).
56. Xiao, W. & Oefner, P. J. Denaturing high-performance liquid chromatography: A review. *Hum Mutat* **17**, 439-474 (2001).
57. Takashima, H., Boerkoel, C. F. & Lupski, J. R. Screening for mutations in a genetically heterogeneous disorder: DHPLC versus DNA sequence for mutation detection in multiple genes causing Charcot-Marie-Tooth neuropathy. *Genet Med* **3**, 335-342 (2001).
58. Bieniossek, C. *et al*. The molecular architecture of the metalloprotease FtsH. *Proc Natl Acad Sci U S A* **103**, 3066-3071 (2006).
59. Atorino, L. *et al*. Loss of *m*-AAA protease in mitochondria causes complex I deficiency and increased sensitivity to oxidative stress in hereditary spastic paraplegia. *J Cell Biol* **163**, 777-787 (2003).
60. Rimoldi, M. *et al*. Cytochrome-*c*-oxidase deficiency in muscles of a floppy infant without mitochondrial myopathy. *J Neurol* 227, 201-207 (1982).
61. Fontanesi, F., Soto, I. C. & Barrientos, A. Cytochrome c oxidase biogenesis: new levels of regulation. *IUBMB Life* **60**, 557-568 (2008).
62. Plumari, M., Gellera, C. & Taroni, F. Production of polyclonal antibodies against protein antigens purified by electroelution from SDS-polyacrylamide gel. *Nat. Protoc.* published online, doi:10.1038/nprot.2010.27 (7 March 2010).
63. Ciccarone, V., Spengler, B. A., Meyers, M. B., Biedler, J. L. & Ross, R. A. Phenotypic diversification in human neuroblastoma cells: expression of distinct neural crest lineages. *Cancer Res* **49**, 219-225 (1989).
64. Schägger, H. Blue-native gels to isolate protein complexes from mitochondria. *Methods Cell Biol* **65**, 231-244 (2001).

65. Nasmyth, K., Adolf, G., Lydall, D. & Seddon, A. The identification of a second cell cycle control on the HO promoter in yeast: cell cycle regulation of SW15 nuclear entry. *Cell* **62**, 631-647 (1990).
66. Longtine, M. S. *et al*. Additional modules for versatile and economical PCR-based gene deletion and modification in Saccharomyces cerevisiae. *Yeast* **14**, 953-961 (1998).
67. Ishihara, N., Fujita, Y., Oka, T. & Mihara, K. Regulation of mitochondrial morphology through proteolytic cleavage of OPA1. *EMBO J* **25**, 2966-2977 (2006).
68. Duvezin-Caubet, S. *et al*. OPA1 processing reconstituted in yeast depends on the subunit composition of the *m*-AAA protease in mitochondria. *Mol Biol Cell* **18**, 3582- 3590 (2007).

Co-immunoprecipitation of human mitochondrial proteases AFG3L2 and paraplegin heterologously expressed in yeast cells

Valentina Fracasso[1], Federico Lazzaro PhD[2] and Marco Muz*i*-Falconi PhD[2]

1)Lab/Group: Neurodegenerative & Metabolic Disease Lab Fondazione IRCCS Istituto Neurologico Carlo Besta, Milan, Italy
2)DNA Metabolism & Cell Cycle Lab University of Milan, Italy

Nature protocols (2010) DOI: 10.1038/nprot.2010.26
Related Journal & Article Information
Journal: Nature Genetics
Article Title: Mutations in the mitochondrial protease gene AFG3L2 cause dominant hereditary ataxia SCA28

Introduction

AFG3L2 and paraplegin are cognate ATP-dependent metalloproteases that constitute the *m*-AAA protease complex in the inner mitochondrial membrane. Co-immunoprecipitation (CoIP) is a useful technique for the analysis of protein-protein interaction. Here, we illustrate a protocol to precipitate the complex formed by human epitope-tagged AFG3L2 and paraplegin heterologously expressed in the yeast Saccharomyces cerevisiae. The procedure employs polyclonal ant*i*-AFG3L2 and ant*i*-paraplegin, and monoclonal ant*i*-HA antibodies to investigate the interaction between the two proteins. The protocol can be adapted to the analysis of other protein complexes.

Materials

Reagents

YPD medium for yeast culture

1% (w/v) yeast extract

2% (w/v) Bacto™ Peptone

2% (w/v) D-glucose

10X Phosphate-Buffered Saline (PBS)

1.37 M NaCl, 27 mM KCl, 100 mM Na2HPO4, 17.6 mM KH2PO4, pH 7.4

1X PBS/BSA

1X PBS with 0.1 mg/ml bovine serum albumin (BSA) (keep ice-cold)

Inhibitors Buffer

PBS buffer supplemented with protease and phosphatase inhibitors (keep ice-cold):

30 ml of 1X PBS containing:

1 mM PMSF

1 mM NaVO4

50 mM NaF

1 tablet of COMPLETE™ Protease Inhibitor Cocktail (Roche)

Protein G Resin

10 ml of 50% slurry in 1X PBS/20% ethanol (GenScript Co.)

Loading Buffer

7 ml Stacking Buffer (0.5M Tris-HCl, pH 6.8, 0.4% SDS)

3 ml glycerol

1 g SDS

0.93 g dithiothreitol

1.2 mg bromophenol blue

Equipment

Shaking incubator at 28°C

Refrigerated centrifuges

FastPrep® System (Qbiogene-MP Biomedicals)

Time Taken

Three days

Procedure

Day 1

Inoculate yeast cells from a solid culture (agar plate) into 5 ml of YPD medium or appropriate selective medium supplemented with 2% (w/v) D-glucose and incubate at 28°C overnight with shaking.

Day 2

A) Cell pellet preparation

1. Transfer overnight culture into 100 ml of YPD and incubate at 28°C with shaking. OD600 nm should be 0.3-0.5 (=1 × 107 cell/ml)

2. Place cells in 50-ml tubes and centrifuge at 3,000g for 4 min at 4°C.

3. Discard the supernatant and resuspend cell pellets by vortexing in 25 ml of sterile H2O. Combine two cell pellets and centrifuge at 3,000g for 2 min at 4°C.

4. Discard the supernatant and resuspend the cell pellet in 1 ml of 1X PBS. Transfer into 2-ml screw-cap eppendorf tube and centrifuge at 2,000g for 2 min at 4°C.
5. Discard the supernatant and store the pellet at -80°C.

B) Resin and pre-saturated tube preparation

1. Pre-saturate Protein G Resin: place 20 µl of Protein G Resin per sample to be immunoprecipitated in one 1.5-ml eppendorf tube and add 1 ml of 1X PBS/BSA. Mix well.
2. Centrifuge at 800g for 2 min at 4°C.
3. Gently remove supernatant and wash three times with 1 ml of 1X PBS/BSA.
4. Resuspend resin with 1 ml of 1X PBS/BSA and incubate overnight at 4°C under gentle shaking.
5. Pre-saturate eppendorf tubes with BSA: aliquot 1 ml of 1X PBS/BSA into 1.5-ml eppendorf tubes (two tubes for each sample) and incubate overnight at 4°C under gentle shaking. Wash with 1 ml of 1X PBS just before use.

Day 3

1. Thaw cell pellets (from step A5 of Day 2) on ice and resuspend each pellet in 1 ml of ice-cold Inhibitors Buffer.
2. Centrifuge at 800g for 2 min at 4°C. Discard the supernatant and resuspend the cell pellet in 500 µl of Inhibitors Buffer.
3. Add 1 g of 425-600-µm glass beads.
4. Homogenize using the FastPrep® System (Qbiogene-MP Biomedicals): shake for 15 sec and then keep on ice for 1 min. Repeat 10 times.
5. Check cell breakage under a microscope.
6. Pierce the tube bottom with a needle.
7. Insert the tube into a new 2-ml eppendorf tube and spin at top speed to transfer the cell extract into the lower tube.
8. Centrifuge at 16,000g for 20 min at 4°C.

9. Transfer the supernatant into a new 1.5-ml eppendorf tube and adjust the volume to 1 ml with Inhibitors Buffer.
10. Determine sample protein concentration.
11. Normalize samples for protein concentration (optimal concentration: 2.5-3 mg/ml). Transfer 1 ml of each sample into the pre-saturated eppendorf tubes washed with 1 ml of 1X PBS (see "Day-2, B-5").
12. Transfer 50 µl of each normalized cellular extract into a new eppendorf tube and add 10 µl of Loading Buffer. Heat samples at 95°C for 5 min. Store at -20°C (INPUT sample).
13. Add primary antibody to normalized samples and incubate for 2 hr at 4°C under gentle shaking to allow formation of antigen-antibody complexes. (We use 10 µg of monoclonal ant*i*-HA antibodies).
14. Centrifuge pre-saturated Protein G Resin at 800g for 2 min at 4°C. Gently remove supernatant with pipette.
15. Wash resin twice with Inhibitors Buffer (gently remove supernatant with pipette).
16. Following the second wash, resuspend Protein G Resin 1:1 with 1X PBS.
17. Wash a pre-saturated eppendorf tube with 1 ml of 1X PBS for each sample. In each tube, add 1 ml of 1X PBS and 40 µl of Protein G Resin suspension from previous step.
18. Centrifuge at 800g for 2 min at 4°C. Remove supernatant with pipette.
19. Add 1 ml of antigen-antibody complex (from step 13) and incubate for 2 hr at 4°C under gentle shaking.
20. Centrifuge at 800g for 2 min at 4°C.
21. Transfer 50 µl of supernatant in a new eppendorf tube and add 10 µl of Loading Buffer. Heat samples at 95°C for 5 min. Store samples at -20°C (IMMUNODEPLETED sample).
22. Discard the remaining supernatant and wash resin with 1 ml of a freshly prepared Inhibitors Buffer. Shake gently for 2 min and centrifuge at 800g for 2 min at 4°C.
23. Repeat step 22 three times. Remove supernatant with pipette.

24. Add 20 µl of 1:3 diluted Loading Buffer. Heat samples at 95°C for 5 min.
25. Centrifuge at top speed for 5 min at room temperature.
26. Transfer the supernatant into a new 1.5-ml eppendorf tube. Store samples at -20°C [IMMUNOPRECIPITATED (IP) sample].
27. Analyze samples by SDS-PAGE and immunoblotting (IB) (Figure 1).

Troubleshooting

SDS-PAGE of immunoprecipitates may result in the co-migration of antibody heavy (approx. 50 kDa) and light (approx. 25 kDa) chains with target proteins. To circumvent the issue of IgG chain detection in the immunoblots, it is recommended that antibodies used for co-immunoprecipitation and immunoblotting originate from two different hosts [in the protocol described here: mouse monoclonal (ant*i*-HA) Ab for immunoprecipitation and rabbit polyclonal (ant*i*-AFG3L2 or ant*i*-paraplegin) Ab for immunoblotting (IB)].

Critical Steps

Day 3: keep samples on ice during the entire procedure.
Day 3, Step 21: in the presence of antigen excess (as it occurs when target proteins are overexpressed), immunoprecipitation may not result in the complete immunodepletion of input sample(s).

Keywords

immunoprecipitation, mitochondria, protease, yeast, Saccharomyces cerevisiae, antibody

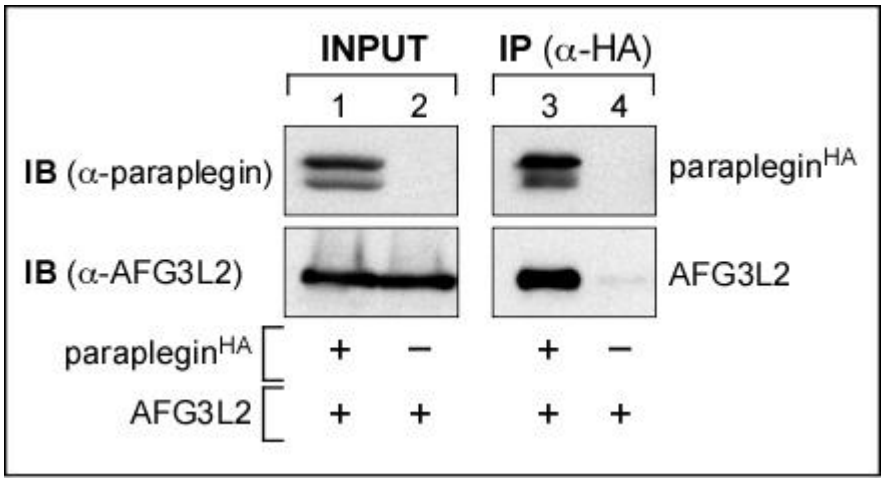

Figure 1

Co-immunoprecipitation of AFG3L2 and HA-tagged paraplegin heterologously expressed in Saccharomyces cerevisiae

HA-tagged paraplegin (parapleginHA) was immunoprecipitated with mouse monoclonal anti*-*HA antibodies from yeast cells co-expressing AFG3L2 and parapleginHA (lanes 1 and 3) or AFG3L2 alone (lanes 2 and 4). Lanes 1-2: immunoblot analysis of cell extracts before immunoprecipitation (INPUT). Immunoprecipitates (IP) were analyzed by SDS-PAGE and immunoblotting (IB) using rabbit polyclonal anti*-*paraplegin (α-paraplegin) or anti*-*AFG3L2 (α-AFG3L2) antibodies. AFG3L2 was detected in the immunoprecipitate from yeast cells co-expressing parapleginHA (lane 3), indicating AFG3L2-paraplegin interaction.

Preparation of yeast mitochondria and in vitro assay of respiratory chain complex activities

Stefania Magri, Valentina Fracasso, Marco Rimoldi and Franco Taroni

Unit of Genetics of Neurodegenerative and Metabolic Diseases
Fondazione IRCCS Istituto Neurologico Carlo Besta, Milan, Italy

Nature protocols (2010) DOI: 10.1038/nprot.2010.25
Related Journal & Article Information
Journal: Nature Genetics
Article Title: Mutations in the mitochondrial protease gene AFG3L2 cause dominant hereditary ataxia SCA28

Introduction

The aim of the protocol is to obtain an enriched fraction of intact mitochondria from the yeast Saccharomyces cerevisiae to perform quantitative determination of the activity of respiratory chain enzymes. All the strains used to perform this protocol are derivatives of W303 (K699: MATa ade2-1 trp1-1 can1-100 leu2-3,112 his3-11,15 ura3-52).

Materials

Reagents

Cell culture

- Selective medium (as appropriate) supplemented with 2% (w/v) D-glucose
- YPGAL medium: YEP medium (1% yeast extract, 2% Bactopeptone) supplemented with 2% (w/v) D-galactose and 0.1% (w/v) D-glucose

Preparation of mitochondria by differential centrifugations

- 10 mM ethylenediaminetetraacetic acid (EDTA)
- Sorbitol Buffer A: 1.2 M sorbitol, 50 mM Tris-HCl, pH7.5, 10 mM EDTA (stored at 4°C), 0.3% (v/v) 2-mercaptoethanol added before use
- Sorbitol Buffer B: 0.7 M sorbitol, 50 mM Tris-HCl, pH 7.5, 0.2 mM EDTA (stored at 4°C)
- Zymolyase-100T (Seikagaku Biobusiness Corporation) 4 mg/ml (stored at -20°C)
- Complete™ Protease Inhibitor Cocktail EDTA-free Tablets (Roche)

Sample preparation

- 10 mM potassium phosphate (PK) buffer, pH 7.4 (stored at -20°C)
- Bradford microplate microassay (Bio-Rad)

Ubiquinol:cytochrome c oxidoreductase assay

- 250 mM potassium phosphate (PK) buffer, pH 7.4 (stored at -20°C)
- 50 mM sodium azide (NaN_3) (stored at -20°C)
- 1 mM cytochrome c (freshly prepared)
- 1 mg/ml antimycin A in 50% ethanol (stored at -20°C)

- sodium borohydride (NaBH4)
- decylubiquinone (DB)
- decylubiquinol (DBH2) (stored at 4°C and freshly diluted 1:1 with H2O)

Cytochrome c oxidase assay

- 100 mM potassium phosphate (PK) buffer, pH 7.0 (stored at -20°C)
- 0.8 mM cytochrome c (freshly prepared). Dissolve cytochrome c in H2O containing 10% of 100 mM potassium phosphate buffer, pH 7.0, and reduce it with sodium dithionite)
- 40 mM potassium cyanide (KCN) (stored at -20°C)

ATP synthase assay

- Buffer H-Mg: 10 mM MgSO4 in 100 mM Hepes-KOH, pH 8.0 (stored at -20°C)
- 30 mM NADH (freshly prepared)
- 50 mM phosphoenolpyruvic acid (freshly prepared)
- 10 mg/ml pyruvate kinase
- 5 mg/ml lactate dehydrogenase (stored at 4°C)
- 0.2 mg/ml antimycin A in 50% ethanol (stored at -20°C)
- 25 mM ATP buffered at pH 7.0 with 3M KHCO3 (freshly prepared)
- 0.2 mg/ml oligomycin in 50% ethanol (stored at -20°C)

Equipment

- Shaking incubator at 28°C
- Water bath at 37°C
- Refrigerated centrifuges
- Spectrophotometer

Time Taken

3 days:

- Cell culture: 8h (pre-culture in selective medium) + 20h (overnight culture in YPGAL)
- Preparation of mitochondria by differential centrifugations: 4-6h
- Sample preparation: 1h

- Respiratory chain activity assay: variable, depending on the number of samples

Procedure

Cell culture

1. Pre-inoculate yeast cells in 5 ml of liquid selective medium supplemented with 2% (w/v) glucose with shaking at 28°C for 8h.
2. Harvest cells and inoculate in 200 ml of YPGAL medium. Incubate overnight with shaking at 28°C.
3. Harvest cells by centrifuging when OD600nm of the culture reaches a value of 2.
4. Wash the pellet in 20 ml of sterile H2O. The resulting pellet can be stored at -80°C.

Preparation of mitochondria by differential centrifugations

Yeast cell mitochondria are prepared by differential centrifugations. This protocol is adapted from Ref. 1.
1. Rinse the pellet with 5ml of 10 mM EDTA.
2. Centrifuge at 400g for 3 min.
3. Discard the supernatant and resuspend the pellet in 4.5 ml of ice-cold Sorbitol Buffer A supplemented with 0.3% (v/v) 2-mercaptoethanol.
4. Digest the cell wall with approx. 250 µl of 4 mg/ml Zymolyase-100T (1 mg per g of cells) at 37°C for 45 min.
5. Verify wall digestion under the microscope.
6. Harvest spheroplasts by centrifugation at 1,800g for 15 min at 4°C.
7. Discard the supernatant and resuspend the pellet gently in 7 ml of ice-cold Sorbitol Buffer B.
8. Centrifuge at 2,500g for 15 min at 4°C.
9. Transfer the supernatant in a new tube and centrifuge at 20,000g for 15 min at 4°C.

10. Discard the supernatant and resuspend the pellet by pipetting in 4 ml of ice-cold Sorbitol Buffer B supplemented with EDTA-free Complete™ Protease Inhibitor Cocktail (Roche).
11. Centrifuge at 800g for 5 min at 4°C.
12. Transfer the supernatant in a new tube and centrifuge at 15,000g for 15 min at 4°C.
13. Discard the supernatant and resuspend the pellet by pipetting in 4 ml of ice-cold Sorbitol Buffer B.
14. Centrifuge at 800g for 5 min at 4°C.
15. Transfer the supernatant in a new tube and centrifuge at 15,000g for 15 min at 4°C.
16. Discard the supernatant and resuspend the pellet by pipetting in 1.5 ml of ice-cold Sorbitol Buffer B.
17. Centrifuge at 800g for 5 min at 4°C.
18. Decant the supernatant in a new 2-ml-tube and centrifuge at 15,000g for 15 min at 4°C.
19. Store the pellet at -80°C.

Sample preparation

1. Resuspend the resulting mitochondrial pellet in 300-500 µl of 10 mM PK buffer, pH 7.4.
2. Freeze and thaw three times.
3. Determine protein concentration with Bradford microplate microassay (Bio-Rad).
4. Normalize samples for protein concentration (recommended concentration: between 0.3 and 0.6 µg/µl).

Ubiquinol:cytochrome c oxidoreductase (Complex III) activity assay

The protocol is adapted from Refs. 2 and 3.
A) Chemically reduce decylubiquinone (DB) to decylubiquinol (DBH2)
1. Prepare a 10-mM solution of DB in HCl-acidified ethanol (pH ≤4).

2. Add a few milligrams of sodium borohydride to reduce quinone. Reaction is completed when solution's color changes from yellow to colorless.
3. Add 2 ml of cyclohexane to the reduced solution and stir it.
4. Transfer the upper (organic) phase to a clean tube.
5. Add 2 ml of cyclohexane to the remaining lower phase and stir it. Transfer the upper phase adding it to the previous one.
6. Repeat point 5 another time.
7. Wash the organic fraction with 2 M NaCl.
8. Dry the pellet under nitrogen and resuspend it with a volume of HCl-acidified ethanol (pH ≤4) corresponding to the initial one.

B) Determine ubiquinol:cytochrome c oxidoreductase activity

Activity is determined by measuring spectrophotometrically, at 550 nm at 30°C, the rate of reduction of cytochrome c by ubiquinol. Measure complex III activity at several protein concentrations paying attention to the linearity of the reaction. To determine the reduction of cytochrome c due to the specific activity of complex III, for each sample, perform parallel measurements of activity in the presence and in the absence of antimycin A, an inhibitor of complex III.
1. Prepare two cuvettes containing 200 µl of 250 mM PK buffer, pH 7.4, 40 µl of 50 mM NaN_3, and 50 µl of 1 mM cytochrome c. Add 10 µl of 1 mg/ml antimycin A in one of them and an equal volume of H_2O in the other one.
2. Add 2-10 µg of mitochondrial proteins.
3. Adjust the volume to 990 µl with H_2O.
4. Record the baseline for 2 min.
5. Start the reaction by adding 10 µl of DBH_2.
6. Measure absorbance of the sample at 550 nm for 2 min.
7. Calculate complex III specific activity using the Beer-Lambert law equation (Fig.1). Express the activity as nanomoles of cytochrome c reduced per minute per milligram of protein.

Cytochrome c oxidase (Complex IV) activity assay

Determine cytochrome c oxidase activity by measuring spectrophotometrically at 30°C for 2 minutes the oxidation of cytochrome cred as indicated by the decrease of absorbance at 550 nm (Refs. 2-3). For each sample, measure complex IV activity twice at at least two protein concentrations that ensure the linearity of the reaction.

1. Reduce cytochrome c by adding tiny amounts of sodium dithionite until the absorbance at 550 nm of 100 µl of cytochrome c in 1 ml of H2O is between 1.8 and 1.9.
2. In a cuvette, add 100 µl of 100 mM PK buffer, pH 7.0, 100 µl of reduced cytochrome c and adjust the volume with H2O (800 µl minus sample volume).
3. Incubate the cuvette at 30°C for 2 min.
4. Start the reaction by adding 2-10 µg of mitochondrial proteins.
5. Measure absorbance of the sample at 550 nm for 2 min.
6. Verify the specificity of cytochrome c reduction by inhibiting cytochrome c oxidase activity with 50 µl of 40 mM KCN.
7. Calculate complex IV specific activity using the Beer-Lambert law equation (Fig. 1). Express the activity as nanomoles of cytochrome c oxidised per minute per milligram of protein.

ATP synthase (Complex V) activity assay

Determine complex V activity by measuring spectrophotometrically at 30°C for 2 minutes the oxidation of NADH as indicated by the decrease of absorbance at 340 nm (Refs. 2-3). Repeat each measurement twice at at least two protein concentrations that ensure the linearity of the reaction.

1. In a cuvette add 500 µl of Buffer H-Mg, 10 µl of 30 mM NADH, 50 µl of 50 mM phosphoenolpyruvic acid, 5 µl of 10 mg/ml of pyruvate kinase, 10 µl of 5 mg/ml of lactate dehydrogenase, and 10 µl of antimycin A.
2. Add 2-10 µg of mitochondrial proteins.
3. Adjust the volume to 900 µl with H2O.
4. Incubate the cuvette at 30°C for 2 minutes
5. Record the baseline for 2 min.
6. Start the reaction by adding 100 µl of 25 mM ATP.

7. Measure absorbance of the sample for 2 min (ΔAbs340nmwithout oligomycin)
8. Add 10 µl of oligomycin.
9. Measure absorbance for 2min (ΔAbs340nmwith oligomycin).
10. Calculate complex V specific activity using the Beer-Lambert law equation (Fig. 1). Express complex V activity as nanomoles of NADH oxidised per minute per milligram of protein.

Critical Steps

Preparation of mitochondria by differential centrifugations
Keep samples on ice during the entire procedure.
Following wall digestion, resuspend the pellets by gentle pipetting (not vortexing) to avoid mitochondria fragmentation.

References

1. Lemaire, C. & Dujardin, G. Preparation of respiratory chain complexes from Saccharomyces cerevisiae wild-type and mutant mitochondria: activity measurement and subunit composition analysis. Methods Mol Biol 432, 65-81 (2008).
2. Rimoldi, M. et al. Cytochrome-c-oxidase deficiency in muscles of a floppy infant without mitochondrial myopathy. J Neurol 227, 201-207 (1982).
3. Dionis*i*-Vici, C. et al. Fulminant Leigh syndrome and sudden unexpected death in a family with the T9176C mutation of the mitochondrial ATPase 6 gene. J. Inherit Metab Dis 21, 2-8 (1998).

Keywords

yeast, Saccharomyces cerevisiae, mitochondria, respiratory chain complexes, ATP synthase, cytochrome c oxidase, ubiquinol:cytochrome c oxidoreductase

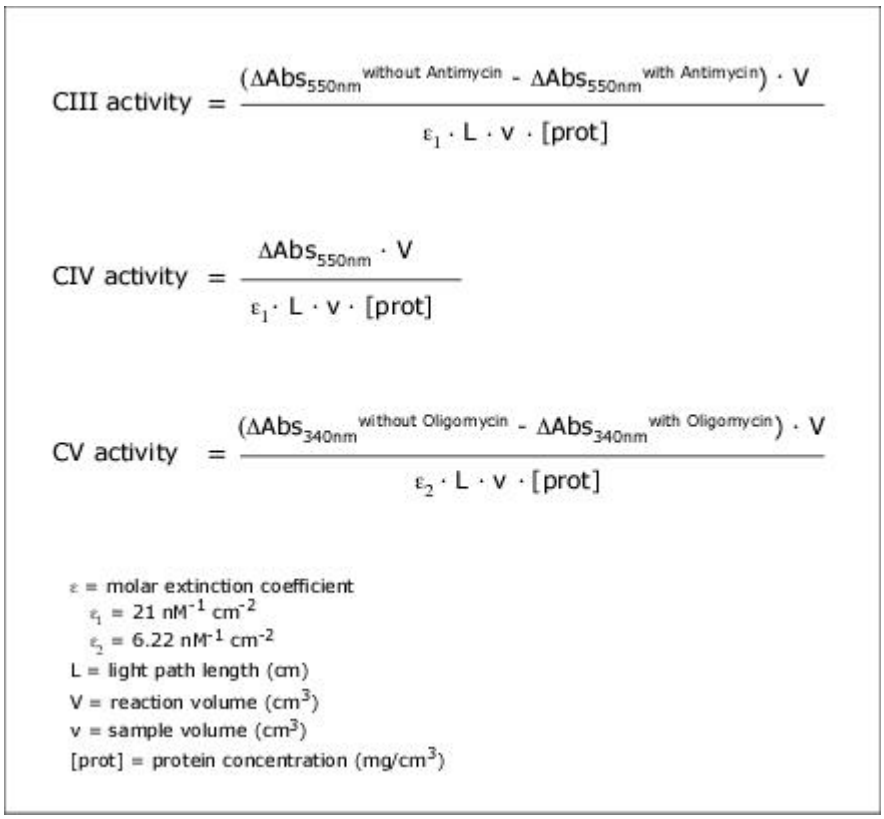

Figure 1

Formulae to calculate Complex III, Complex IV, and Complex V activity
Formulae are derived from the Beer-Lambert law equation. Activities are expressed as nanomoles per minute per milligram of protein.

Chapter 3

Spinocerebellar ataxia type 28: identification and functional analysis of novel AFG3L2 mutations

V. Fracasso[1], S. Magri[1], M.Plumari[1], P. Giunti,[2] S. Boesch,[3] M. Muzi-Falconi[4], F. Lazzaro[4], D. Di Bella[1], and F. Taroni[1]*

[1]Unit of Genetics of Neurodegenerative and Metabolic Disease, Fondazione IRCCS Istituto Neurologico "Carlo Besta", Milan, Italy
[2]Institute of Neurology and The National Hospital for Neurology and Neurosurgery, London, UK
[3]Department of Neurology, Innsbruck Medical University, Innsbruck, Austria
[4]Department of Biomolecular Sciences and Biotechnology, University of Milan, Milan, Italy

* Corresponding author

Address correspondence to:
Franco Taroni, MD
Unit of Genetics of Neurodegenerative and Metabolic Disease
Fondazione IRCCS Istituto Neurologico "Carlo Besta"
via Amadeo 42 *I*-20133 Milan Italy
Phone: +39-02-23944580
Fax: +39-02-700548648
email: taroni.f@istituto-besta.it

submitted

Abstract

Autosomal dominant spinocerebellar ataxias (SCAs) are a clinically and genetically heterogeneous group of diseases caused by progressive degeneration of the cerebellum and its afferent and efferent paths. We have recently identified missense mutations in the *AFG3L2* gene (ATPase Family Gene 3-Like 2) as the cause of spinocerebellar ataxia type 28 (SCA28). AFG3L2 and paraplegin are components of the inner mitochondrial membrane metalloprotease AAA (*m*-AAA). This protease complex is known to exert chaperon-like activity and to participate in protein quality control. We screened 233 individuals with ataxia for mutations in the *AFG3L2* gene. We identified 3 heterozygous missense mutations and 1 small in-frame deletions, establishing a minimum frequency of 1.7% for patients with a SCA phenotype. Function analysis of these mutations were analyzed in a yeast cellular model confirming the pathogenic role of the amino acid substitutions identified in AFG3L2.

Introduction

Cerebellar ataxias are a heterogeneous group of diseases caused by progressive degeneration of the cerebellum which leads to a complex movement disorder, whose principal symptoms are the progressive loss of motor coordination and difficulties in executing voluntary movements. Autosomal dominant spinocerebellar ataxias (SCAs) are clinically and genetically heterogeneous [Dürr, 2010]. Thirty-one SCA loci are currently known (http://neuromuscular.wustl.edu/ataxia/domatax.html). These diseases may be caused by expansions of tr*i*- or pentanucleotide repeats or deletions, missense, nonsense or frameshift mutations in the corresponding genes [Taroni and DiDonato, 2004]. We have recently identified missense mutations in the gene encoding the mitochondrial protease AFG3L2 (ATPase Family Gene 3-Like 2) as the cause of spinocerebellar ataxia type 28 (SCA28) [Di Bella et al., 2010]. Mutations in the AFG3L2 gene are interesting because no dominant ataxia has been thus far associated with mitochondrial dysfunction, and because its partner protein is paraplegin. Mutations in the SPG7 gene encoding paraplegin cause an autosomal recessive form of hereditary spastic paraparesis [Casari et al., 1998]. Both AFG3L2 and paraplegin are metalloproteases that are components of the mitochondrial AAA (*m*-AAA) protease complex. These proteases belong to the family of the AAA proteins (ATPases Associated with different cellular Activities). In the subfamily AAA+, proteins have a common structural domain composed by one AAA-domain with ATPase activity followed by a highly conserved proteolytic domain. They exert chaperone-like activity and are implicated in the degradation of macromolecular structures involved in different cellular processes. Studies in the yeast Saccharomyces cerevisiae have demonstrated a dual role for the *m*-AAA protease [Tatsuta and Langer 2008]. First, it is implicated in the quality control of mitochondrial inner membrane proteins selectively degrading improperly folded or unassembled polypeptides [Koppen and Langer, 2007). Second, it plays a regulatory role in mitochondrial protein synthesis participating in the processing and maturation of some mitochondrial proteins including

cytochrome c peroxidase (Ccp1) in yeast [Esser et al., 2002] and the ribosomal subunit Mrpl32 in both yeast and mammals cells [Nolden et al., 2005]. The importance of *m*-AAA in humans is underlined by the evidence that mutations in both genes are responsible for important neurodegenerative diseases. *m*-AAA is well characterized in yeast. Yeast *m*-AAA is composed of Yta10p and Yta12p which show high homology with AFG3L2 and paraplegin, respectively [Arlt et al., 1996; Banfi et al., 1999].

Here, we report the AFG3L2 variations identified in the genetic study of a new cohort of affected individuals with ataxic phenotype. We also describe the results of a functional study using a yeast cellular model to evaluate the functional effects and the pathogenic role of the amino acid substitutions identified in AFG3L2. Functional analysis of the respiratory competence and the proteolytic activity of human mutant AFG3L2 expressed in yeast *Saccharomyces cerevisiae* represents a necessary tool to discriminate between real pathogenic mutations and rare/unique polymorphic variants.

Results

Mutation analysis

Two hundred and thirty-three unrelated individuals with a chronic progressive ataxic phenotype were screened for *AFG3L2* mutations. In this patient series, 153 index cases were Italian (108 with autosomal dominant inheritance and 45 sporadic cases) whereas other probands came from European collaborating groups: 75 were British (with positive family history), 2 were Austrian (from 2 unrelated families), and 3 were Spanish (from 3 unrelated families). All affected individuals showed a progressive ataxic phenotype and cerebellar atrophy variably associated with additional features such as pyramidal signs and minor abnormalities in ocular movements, consistent with a SCA28 phenotype [Cagnoli et al., 2010; Mariotti et al., 2008]. The 17 coding exons of the *AFG3L2* gene were analysed by denaturing high performance liquid chromatography (dHPLC) and direct sequencing. We identified 7 heterozygous AFG3L2 missense substitutions and 2 heterozygous small in-frame deletions in 9 affected individuals. Most AFG3L2 variations are located in functional domains of the protein involving highly conserved residues: 2 variations (T444A and I473V) are located in a portion of the AAA-domain encoded by exon 11, 5 variations (K569del, M666V, R679C, K687T, and L772F) are located in the proteolytic domain, whereas only 2 variations (82N_84Kdel and A86P) were found in exon 3 in a region of the protein with unknown function (**Figs. 1** and **2**). The affected individual with the R679C substitution presented another variation, a transition T>C at position c.1779+2C changing the splice donor site from GT to GC. The two mutations are likely to be on distinct alleles since RT-PCR analysis of total RNA from this patient demonstrated the presence of the R679C variant only, which suggests that transcript from the c.1779+2C-carrying allele is degraded. The substitution M666V identified in this analysis has also been observed in two previously reported families [Cagnoli et al., 2010].

None of the substitutions identified in this study are reported as polymorphisms in the dbSNP database nor were they found in >400 control chromosomes, except for the L772F variant, that was recently annotated as rs117182113 (http://www.ncbi.nlm.nih.gov/projects/SNP/). *In silico* prediction by PolyPhen (http://genetics.bwh.harvard.edu/pph/) and SIFT (http://blocks.fhcrc.org/sift/SIFT.html) of the effects of the substitutions on protein structure/function did not give univocal results. Both programs predicted as benign the substitutions A86P, T444A, and I473V, and as probably damaging the M666V and R679C. By contrast the substitutions K687T and L772F were predicted to be benign by PolyPhen but not tolerated by SIFT. Computational analysis by ESE Finder (ESE, exonic splicing enhancers) (http://rulai.cshl.edu/cgi-bin/tools/ESE3/esefinder.cgi?process=home), FAS-ESS web server (ESS, exonic splicing silencers) (http://genes.mit.edu/fas-ess/), and RESCUE-ESE web server (http://genes.mit.edu/burgelab/rescue-ese/) of the possible effects of the mutations on splicing excluded the formation of ESS in all cases but gave nonunivocal results regarding the generation or abolition of exon splicing enhancers.

As for the mutations described previously [Cagnoli et al., 2010; Di Bella et al., 2010], most of the substitutions identified are located in exons, mostly in exon 16, that encode the proteolytic domain, indicating that this region of AFG3L2 is a hot spot for mutations (**Fig. 1**). Fewer mutations were located in the ATPase domain.

The SPG7 gene encoding paraplegin was also sequenced in all patients. Interestingly, two patients were found to be positive for mutations in this gene. An Italian patient heterozygous for the A86P mutation in *AFG3L2* also carried a homozygous nonsense mutation (R457X) in SPG7 exon 10, which is predicted to result in a truncated protein. Western blot analysis of paraplegin in the patient's peripheral blood lymphocytes showed the absence of the protein (not shown). In a second patient of British origin, SPG7 sequence analysis revealed heterozygosis for a frameshift mutation (c.1052dupC) in exon 8, which is predicted to cause premature termination of the protein (G352RfsX43) encoded by the mutant allele.

Respiratory competence of AFG3L2 variants in yeast model

We have used a yeast *(Saccharomyces cerevisiae)* cellular model to evaluate the functional effects and to validate the pathogenic role of the amino acid substitutions identified in AFG3L2. Yeast *YTA10*/*YTA12*-defective strains have been widely used in previous studies on the characterization of the *m*-AAA protease [Di Bella et al., 2010; Koppen et al., 2007]. Yeast cells lacking either Yta10 (*yta10*Δ) or Yta12 (*yta12*Δ) grow on glucose but exhibit impaired growth on a nonfermentable carbon source such as glycerol, indicating a respiratory defect (OXPHOS phenotype) [Arlt et al., 1996]. Yta10p and Yta12p exhibit high homology with AFG3L2 and paraplegin, respectively [Banfi et al., 1999]. Complementation studies in yeast have shown that human AFG3L2 homocomplex or AFG3L2/paraplegin heterocomplex, but not paraplegin homocomplex, if any, are able to functionally replace the Yta10p/Yta12p complex and to restore the respiratory competence of the yeast cell [Koppen et al., 2007]. The functional effects of the 9 substitutions identified in the present study and of 5 mutations identified by a collaborating group [Cagnoli, et al, 2010] were analysed by expressing normal and mutant AFG3L2 under the control of the strong yeast *ADH1* promoter. We evaluated the human AFG3L2 substitutions for their ability to support respiration in an *m*-AAA-defective strain (double-deletion mutant *Δyta10/Δyta12*) (**Figs. 3** and **4**). All transformants exhibited normal growth in glucose-containing medium (YPD). When glycerol was the only carbon source, five mutants (AFG3L282N_84Kdel, AFG3L2A86P, AFG3L2T444A, AFG3L2I473V, and AFG3L2L772F) were able to grow, suggesting that these variations may represent rare AFG3L2 polymorphic variants. In particular, the mutations AFG3L2T444A, AFG3L2I473V, and AFG3L2L772F seem to present growing faster than the WT. Some mutants (AFG3L2K569del, and AFG3L2K687T) were partially able to rescue respiration, showing a slower growth than the strain carrying normal AFG3L2 (AFG3L2^{WT}). By contrast, the other amino acid substitutions in the highly-conserved proteolytic domain (AFG3L2^{T654I}, AFG3L2^{M666R}, AFG3L2^{M666T}, AFG3L2^{M666V}, AFG3L2^{G671E}, AFG3L2^{G671R} , and AFG3L2^{R679C})

were not able to restore respiratory competence of *Δyta10/Δyta12* cells (**Fig. 3a**). These results clearly indicate a pathogenic role for these mutations. Results at 28°C and 37°C (not shown) were comparable. To better evaluate the intermediate growth of strains AFG3L2K569del, and AFG3L2K687T, growth rate was measured in liquid medium for 24h at 28°C. The results confirmed the data obtained on solid medium showing a statistically significant slower growth as compared with AFG3L2WT. (**Fig. 3b**).

In human, the *m*-AAA exist as homo-oligomeric AFG3L2 complexes as well as hetero-oligomeric complexes composed of AFG3L2 and paraplegin subunits [Koppen et al., 2007]. We analyzed the phenotype of strains carrying mutant AFG3L2 also in the presence of normal human paraplegin. When AFG3L2 and paraplegin were coexpressed, cells harboring AFG3L2^{82N_84Kdel}, AFG3L2^{A86P}, AFG3L2^{T444A}, AFG3L2^{I473V}, and AFG3L2^{L772F} maintained respiratory competence, as expected. By contrast, the strains (AFG3L2^{K569del} and AFG3L2^{K687T}) showing intermediate growth when carrying AFG3L2mut alone, were fully rescued by paraplegin coexpression.

As regards the AFG3L2 substitutions that abolished respiration competence when expressed alone, coexpression of paraplegin resulted in four respiratory phenotypes. All the experiments were carried out at 28°C, but similar results were obtained at 37 °C (not shown). A full rescue of respiratory competence was observed in the case of AFG3L2^{G671R} while a partial rescue (intermediately reduced growth rate) was the effect of paraplegin coexpression in the case of AFG3L2^{M666V}, AFG3L2^{M666T}, AFG3L2^{G671E}, and AFG3L2^{R679C} (**Fig. 4a**). These strains with intermediate growth phenotype were further characterized in liquid medium, which allowed to further identify two subgroups: I1 (intermediate group 1, slow-growing strains; AFG3L2^{M666T}, AFG3L2^{R679C}) and I2 (intermediate group 2, slower-growing strains; AFG3L2^{M666V}, AFG3L2^{G671E}) (**Fig. 4b**). For all these mutants, the mutation mechanism is likely to be haploinsufficiency or a weak dominant negative effect, resulting in variably reduced penetrance or expressivity in affected people. In the last group of mutants, coexpression of paraplegin did not rescue the defective phenotype

(AFG3L2^{T654I}, AFG3L2^{M666R}) suggesting a dominant-negative effect of the mutations (**Fig. 4a**).

Notably, different amino acid substitutions at the same residue may lead to different phenotypes. In the case of glycine 671 (G671), substitution with the negatively-charged glutamic acid (G671E) leads to a respiratory phenotype with slower growth than substitution with the positively-charged arginine (G671R) that results in the complete recovery of the respiratory phenotype following paraplegin coexpression. The substitution of methionine 666 with arginine (M666R) is particularly interesting since it leads to a total loss of respiration, while the other two substitutions identified (threonine, M666T, and valine, M666V) result in I1 and I2 phenotypes, respectively (**Fig. 4b**).

Proteolytic activity of AFG3L2 variants

To determine the proteolytic competence of AFG3L2 substitutions, we analysed the processing of two mitochondrial precursor proteins: MrpL32 and cytochrome *c* peroxidase (Ccp1). Lack of *m*-AAA, as in *Δyta10/Δyta12* cells, causes respiratory defect and also completely abolishes the processing of MrpL32 and Ccp1 with accumulation of unprocessed precursor proteins [Nolden et al., 2005; Esser et al., 2002]. MrpL32 is a ribosomal protein, encoded by nuclear genome, whose maturation is necessary for ribosome assembly and subsequent protein synthesis within mitochondria, thus controlling the assembly of respiratory complexes in the inner membrane. MrpL32 is known to be matured by the yeast as well as the mammalian *m*-AAA protease [Nolden et al., 2005]. Ccp1 is localized to mitochondrial intermembrane space and it is required for peroxide and toxic radical scavenging. In yeast, Ccp1 precursor (pCcp1) contains a bipartite N-terminal targeting sequence which is sequentially processed to an intermediate form (iCcp1) by the *m*-AAA protease and to a mature form by the intramembrane rhomboid protease Pcp1 [Esser et al., 2002]. Recent studies, however, have shown that the major role of *m*-AAA in the maturation of Ccp1 is the ATP-dependent dislocation of the pCcp1 precursor from the inner mitochondrial membrane rather than its processing to an intermediate form iCcp1 [Tatsuta et al., 2007].

We evaluated the human AFG3L2 substitutions for their ability to support proteolytic activity in the *m*-AAA-defective strain (*Δyta10/Δyta12*). AFG3L2 proteolytic competence is expressed as the ratio of precursor protein level (p) to total protein level (p + m; m=mature) for both proteins [Di Bella et al., 2010]. Data are summarized in **Table 1**. We observed a good correlation between the respiratory competence of the cells and the maturation of MrpL32, both when AFG3L2^{mut} was expressed alone and when AFG3L2^{mut} was coexpressed with paraplegin (**Fig. 5**).

Notably, two strains with intermediate growth phenotype (AFG3L2K569del, and AFG3L2K687T) are partially impaired in a processing of MrpL32 precursor (yellow bars). In the set of experiments where paraplegin was coexpressed with AFG3L2, all transformed strains showed higher levels of pMrpL32, suggesting either increased MrpL32 expression in cells expressing both heterologous proteins or reduced processing by AFG3L2/paraplegin heterocomplex as compared with that by AFG3L2 homocomplex.

For Ccp1, the results indicated that some mutant strain harbouring mutant AFG3L2 homocomplex or AFG3L2/paraplegin heterocomplex (AFG3L2^{R679C}, AFG3L2^{M666T}/paraplegin, AFG3L2^{M666V}/paraplegin, and AFG3L2^{G671E}/paraplegin) showed a dissociation between respiratory growth and processing of the substrate. Surprisingly, Ccp1 was processed in the strain harbouring mutant AFG3L2^{R679C}, which exhibited respiratory deficiency (see **Fig. 3**). On the contrary, proteolysis of Ccp1 was impaired in strains carrying AFG3L2^{M666T}/paraplegin, AFG3L2^{M666V}/paraplegin, or AFG3L2^{G671E}/paraplegin which exhibited an intermediate growth phenotype (see **Fig. 4**).

Evaluation of mitochondrial amount

These data show clearly that distinct mutations cause different defects in substrate processing.

This effect could be due to a direct impairment of *m*-AAA activity or a more general mitochondrial damage. To discriminate between these two

hypothesis we measure indirectly the mitochondrial amount evaluating the ratio between Porin and β-actin. Porin is a mitochondrial protein; we use Porin antibody to assess the quantity of mitochondria present compared to β-actin, a cytosol housekeeping protein. Quantitative analysis of Porin and β-actin proteins by fluorescence immunoblot exhibit that the most strains do not present any statistically significant difference from WT strain. By contrast, homocomplex mutant strains harbouring AFG3L2^{T654I}, AFG3L2^{M666R} and AFG3L2^{R679C} show a reduction of Porin-Actin ratio (20-40%) compared to AFG3L2 WT. Consistently these three substitutions present the most severe respiratory phenotype in yeast. In particular, AFG3L2^{T654I}, AFG3L2^{M666R} are the only two non-paraplegin-responsive mutations, whereas AFG3L2^{R679C} is one of the mutations partially rescued by paraplegin expression.
Accumulation of unprocessed precursor proteins seems to be the direct consequence of AFG3L2 mutations because the most mutated strains show any variation in quantity of mitochondria.

AFG3L2 mutations assemble with paraplegin

Functional studies in yeast demonstrate that AFG3L2 mutations have different behaviors upon paraplegin coexpressing. This effect could be due a diverse molecular mechanism of some mutations. In particular, the mutations with no- or only partial paraplegin response could be not able to form a complex with paraplegin. To confirm this hypothesis, we perform co-immunoprecipitation experiment in strain with hetero-oligomeric AFG3L2-paraplegin complexes. V5-tagged AFG3L2 was immunoprecipitated with mouse monoclonal anti-V5 antibody. The input and the immunoprecipitates (IP) were analyzed by Western Blot using specific antibodies against AFG3L2 and paraplegin. The input data underline immediately that yeast strain carrying AFG3L2^{M666R} mutation show only a precursor form of paraplegin as the yeast strain carrying paraplegin alone (negative control). Moreover this strain evidence also a major electrophoretic height and a minor level of AFG3L2 protein compared to other mutants and WT form. This mutation interferes with the stability of the protein, probably. Immunoprecipitation shows that

AFG3L2^{R679C} interact mainly with mature paraplegin as AFG3L2 WT, while the most AFG3L2^{M666R} interact with the intermediate paraplegin form. Finally, AFG3L2^{T654I}, AFG3L2^{M666V} are associated with both form of paraplegin suggesting a partially impairment of paraplegin processing. Moreover, it is interesting to compare the two Methionine 666 substitutions: AFG3L2^{M666V} is partially able to mature paraplegin, whereas the AFG3L2^{M666R} mutation does not support paraplegin maturation, constituting inactive heterocomplexes, in agreement with the respiratory and proteolytic data previously described. Immunoprecipitation results indicate that all mutations analyzed are able to form a complex with paraplegin, but not all are able to process it in the mature form.

Discussion

In this work, we screened a large series of patients with a SCA-like chronic-progressive ataxic phenotype [Dürr, 2010] to identify novel mutations in the *AFG3L2* gene and to evaluate the frequency of *AFG3L2* mutations in this large group of people with ataxia. Moreover, we wanted to characterize the function of the protein involved in the pathogenesis of this new form of dominant spinocerebellar ataxia.

We have identified four novel heterozygous mutations in AFG3L2 in individuals with ataxic phenotype, further confirming that mutations in AFG3L2 cause spinocerebellar ataxia SCA28. Most mutations are located in the proteolytic domain, one mutation in exon 14 ($AFG3L2^{K569del}$) and three mutations in exon 16 ($AFG3L2^{M666V}$, $AFG3L2^{R679C}$ and $AFG3L2^{K687T}$), confirming that this region is a mutational hot spot for SCA28 and underlining the crucial importance of the peptidase domain for *m*-AAA activity. No mutation was found in the metal-binding motif HEXGH. In this study, for the first time we have identified two small in-frame deletions in addition to missense mutations. All the mutations identified, except for $AFG3L2^{M666V}$, are novel and have not been found in previous studies [Di Bella et al., 2010; Cagnoli et al., 2010; Edener et al., 2010].

The pathogenicity of the identified mutations is suggested by the following: 1) in families with more than one affected subject, the identified mutation segregated with the disease and was not present in healthy members of the family; 2) the mutations were not found in more than 400 control chromosomes; and 3) the mutations affect residues that are highly conserved or occur in regions with high degree of conservation through evolution. However, most mutations occurred only in a single patient/family and, in some cases, segregation could not be adequately assessed due to the limited size of the family. Thus, the possibility exists that, at least in some cases, the identified substitutions represent very rare or private polymorphic variants. Functional studies are ultimately necessary to confirm the pathogenicity of the identified amino acid

substitutions. The yeast *S. cerevisiae* has been previously used as an *in vivo* model to validate the pathogenic significance of mutations in genes involved in mitochondrial diseases, thanks to the similarity of orthologous yeast *vs.* human OXPHOS-related genes, and the ability of the yeast to survive in spite of mitochondrial dysfunction, provided that a fermentable carbon source is made available [Fontanesi et al., 2009]. In addition to functional proof of pathogenicity, expression studies may provide clue to genotype-phenotype correlations. Finally, the interesting question of negative dominance *vs.* haploinsufficiency of mutations can be defined by using yeast heteroallelic strains that contain both the mutant and the wild-type allele, thus mimicking the human diploid condition.

Human AFG3L2 and paraplegin have high homology with Yta10p and Yta12p yeast proteins, respectively. Complementation studies in yeast have shown that human *m*-AAA is able to restore the respiratory competence in *m*-AAA-deficient cells *ΔYta10*/*ΔYta12* [Koppen et al., 2007]. In order to provide a complete picture of the functional effects of AFG3L2 mutations causing SCA28, we functionally tested the 9 substitutions identified in the present study as well as the 5 mutations previously reported by a collaborating group [Cagnoli, et al, 2010]. Expression studies of mutant AFG3L2 in yeast cells lacking *m*-AAA showed that all the substitutions analysed, except 82N_84Kdel, A86P, T444A, I473V and L772F, were not able to restore a functional *m*-AAA. These data strongly suggested that the substitutions K569del, T654I, M666R, M666T, M666V, G761E, G671R, R679C and K687T are pathogenic mutations while substitutions 82N_84Kdel, A86P, T444A, I473V, and L772F are likely to be rare/unique benign variants. Interestingly, some of these apparently nonpathogenic substitutions are also located in the crucial functional regions of the protein, two (T444A and I473V) in the AAA (ATPase) domain and one (L772F) in the proteolytic domain.

Some interesting results were provided from coexpression of mutant AFG3L2 and its partner paraplegin. Analysis of the respiratory phenotype of cells coexpressing both proteins showed three respiratory phenotypes: 1) a full restore of respiratory competence; 2) a partial rescue of respiratory phenotype, that we call intermediate growth rate

with subgroups I1 and I2; and 3) no rescue of the defective phenotype. Altogether, these phenotypes suggest that two classes of AFG3L2 mutations exist. The majority of mutations are "paraplegin-responsive", namely K569del, M666T, M666V, G761E, G671R, R679C, and K687T. In these cases, the mechanism is likely to be haploinsufficiency, which may result in variably reduced penetrance and/or expressivity in affected people. Two mutations (T654I and M666R) are not rescued by paraplegin coexpression. These variants behave as dominant-negative mutations with a likely full penetrance in the family. Segregation of the T654I mutation in the family pedigree lends support to this hypothesis [Cagnoli et al. 2010]. The M666R mutation exhibited the most severe phenotype in yeast, with the highest impairment of MrpL32 and Ccp1 processing. Interestingly, this mutation was identified in a very small family with early onset of the disease (6 and 8 years of age) and severe clinical features [Cagnoli et al. 2010]. Structural modeling of the M666R mutation had showed significant decrease of the electrostatic potential difference between the inner mitochondrial membrane side and the matrix side of the hexamer [Cagnoli et al. 2010].

The proteolytic competence of AFG3L2 variants was assessed analysing the processing of two known substrates, MrpL32 and Ccp1. MrpL32 is a component of the large mitochondrial ribosomal particle 54S. The correct assembly of mitochondrial ribosomes is required for the translation of proteins encoded by mitochondrial DNA, including the core subunits of the respiratory chain. The correct maturation of MrpL32 is therefore crucial for the control of mitochondrial protein synthesis, in particular for the assembly of respiratory chain and F_1F0-ATP-synthase complexes [Nolden et al., 2005]. Overall, our data on processing of MrpL32 in strains harboring AFG3L2^{mut} correlate well with the respiratory phenotype, consistent with the other results described above. The different ability of MrpL32 processing in the strains with intermediate growth indicates that a small amount of the mature protein is sufficient to ensure aerobic growth in yeast. However, this might not be sufficient for nerve cells. Neurons, in particular the cerebellar Purkinje cells, large cells with long axons where AFG3L2 is highly and selectively expressed [Di

Bella et al., 2010], need high and constant levels of energy to perform their activities. Therefore, they could particularly suffer of the energy deficit and undergo a degenerative process such as that occurring in affected individuals.Interestingly, some mutant strains showed inconsistency between respiratory growth and processing of the substrate. Thus, Ccp1 was processed in the respiratory-deficient mutant strain AFG3L2^{R679C}. This behavior could be explained by function of *m*-AAA: the maturation of Ccp1 depends only on the ATPase but not the proteolytic activity of the *m*-AAA protease. The complex dislocate the precursor form of Ccp1 into the inner membrane where it is cleaved by intramembrane rhomboid protease Pcp1. Subsequently, mature Ccp1 is released into the intermembrane space [Tatsuta et al, 2007].On the contrary, processing of Ccp1 was impaired in strains carrying AFG3L2^{M666T}/paraplegin, AFG3L2^{M666V}/paraplegin, or AFG3L2^{G671E}/paraplegin which exhibited an intermediate growth phenotype. Altogether, these results raise the intriguing possibility that the mutations may differentially affect distinct and specialized functions of the *m*-AAA complex.

Co-immunoprecipitation experiment has demonstrated that all the AFG3L2^{mut} analyzed are able to form a complex with paraplegin. However, the no-paraplegin-response mutations (AFG3L2^{T654I}, AFG3L2^{M666V}) are not completely able to process paraplegin into the mature form. The mutations that affect AFG3L2 more severely lead to an impaired processing of paraplegin causing also the loss of paraplegin activity. This mechanism could explain their non-responsiveness to paraplegin coexpression. These data confirm that the human paraplegin is substrate of human AFG3L2 in our yeast model. Moreover, these results are consistent with data observed by expression of mouse *m*-AAA in yeast cells [Koppen et al., 2009]. Therefore, if functionality of the *m*-AAA complex is lost, even partially, several mitochondrial proteins may not be correctly processed and/or degraded creating an accumulation of unassembled/undegraded polypeptides potentially toxic for the cell.

The toxicity caused by a non-correct *m*-AAA activity may explain the mitochondrial loss seen by measuring the Porin-Actin ratio. Taken together functional studies in yeast indicate that mutations can act

through distinct pathomechanisms at the molecular level with a different role in shaping homo- and hetero-mAAA complex activity.

In conclusion, we identified 9 substitutions in AFG3L2 in patients with autosomal dominant spinocerebellar ataxia and analyzed the functional effects of them. The discovery of the genetic cause of SCA28 is extremely important for the diagnosis of SCA allowing a molecular diagnosis of the disease. Our data allow to establish a minimum frequency of AFG3L2 mutations of 1.7% (4 /233) in a raw series of patients with chronic progressive neurodegenerative ataxia negative for the most common SCA mutations (SCA1, SCA2, SCA3, SCA11, and SCA17). Functional data have clearly shown the pathogenic role of $AFG3L2^{K569del}$, $AFG3L2^{M666V}$, $AFG3L2^{R679C}$ and $AFG3L2^{K687T}$ and have instead suggested that the $AFG3L2^{82N\_84Kdel}$, $AFG3L2^{A86P}$, $AFG3L2^{T444A}$, $AFG3L2^{I473V}$, and $AFG3L2^{L772F}$ represents a rare benign variants of the gene AFG3L2. Our results demonstrate that the yeast *Saccharomyces cerevisiae* is an appropriate and useful functional model for assessing the pathogenicity of substitutions, particularly in the critical cases of mutations identified in sporadic cases or small families where segregation analysis is not informative.

Materials and methods

Patients and DNA samples

We studied 233 unrelated index cases with a diagnosis of ataxia. 153 individuals (108 with autosomal dominant inheritance, and 45 sporadic cases) were selected from a large cohort of patients referred to our Centre from throughout Italy. The other individuals were selected by European collaborating group: 75 British, 2 Austrian, 3 Spanish. Inclusion criteria were the presence of a progressive ataxic phenotype and cerebellar atrophy variably associated with additional features such as pyramidal signs and minor abnormalities in ocular movements, in according with SCA28 phenotype. Control subjects were individuals who presented for work-up of unrelated neurologic conditions. Genomic DNA was prepared from peripheral-blood lymphocytes using standard procedures as previously described [Gellera et al., 2007]. Written informed consent was obtained from each individual providing a biological sample. All procedures involving human subjects were approved by the Institutional Review Board of the Fondazione IRCCS Istituto Neurologico "Carlo Besta", Milan, Italy.

Mutation analysis

For mutation screening of the selected patient population, PCR products were analyzed by automated sequencing and/or Denaturing High-Performance Liquid Chromatography (DHPLC). Sequences of the oligonucleotide primers and conditions used for PCR amplification, DNA sequencing, and DHPLC analysis are as previously described [Di Bella et al., 2010].

Except when noted differently, nucleotides were numbered so that the first nucleotide of the first in-frame ATG codon was nucleotide +1. Amino acids were numbered so that methionine encoded by the first in-frame ATG codon was Met1.

AFG3L2 and paraplegin yeast expression plasmids

Plasmids for heterologous expression of human AFG3L2 and paraplegin in yeast were generated as previously described [Di Bella et al.2010]. Seven of the nine mutations identified in our patients (AFG3L2^{T444A}, AFG3L2^{L772F}, AFG3L2^{I473V}, AFG3L2^{K569del} AFG3L2^{K687T}, AFG3L2G6^{M666V}, AFG3L2^{K687T}) were introduced into the yeast AFG3L2 expression construct pYC6/CT*ADH1*-AFG3L2-V5/HIS using the QuikChange XL Site-Directed Mutagenesis Kit (Stratagene) (**Supplementary Table 1**).The other two mutations (AFG3L2^{A86P}, AFG3L2$^{82-84del}$,) were obtained by Gene Synthesis Service (Eurofins MWGoperon); the gene region between EcoRI and AspI carring these mutation were synthesised and subsequently subcloned into our plasmid. Mutagenized plasmids were verified by DNA sequencing. The yeast AFG3L2 expression construct carring the five mutations previously described in [Cagnoli et al., 2010], (AFG3L2^{T654I}, AFG3L2^{G671R}, AFG3L2^{G671E}, AFG3L2^{M666T} AFG3L2^{M666R}), were performed by Brusco Lab using the QuikChange XL Site-Directed Mutagenesis Kit (Stratagene).

For human paraplegin expression, plasmid YCplac111*ADH1*-Yta10(1-63)-paraplegin(59-795)-HA (abbreviated into YCplac111*ADH1*-paraplegin-HA) was used as previously described [Di Bella et al., 2010].

Yeast strains and growth conditions

All the strains used in this study are derivatives of W303 (K699, *MATa ho ade2-1 trp1-1 can1-100 leu2-3,12 his3-11,15 ura3 ssd1*) (**Supplementary Table 2**). Deletions of *YTA10* and *YTA12* (*yta10Δyta12Δ* strain) were generated using the one-step PCR system [Longtine et al., 1998]. Standard genetic procedures were followed for strain generation [Adams et al. 1997]. Yeast strains were transformed with the described vectors. Cells were grown at 28°C on YEP medium (1%-yeast extract, 2%-peptone, 2%-agar for plates) or selective medium supplemented with 2% (wt/vol) glucose according to standard procedures. Blasticidin-resistant transformants were selected on YEP medium supplemented with 50 µg of blasticidin S per ml. For complementation experiments, equal amounts of five-fold serial dilutions of cells from exponentially grown

cultures were spotted onto YEP plates containing 2% (wt/vol) glucose (YPD) or 2% (wt/vol) glycerol (YPG) and incubated at 28°C or 37°C.

For growth rate analysis, we precultured overnight yeast cells in selective medium supplemented with 2% (wt/vol) galactose and 0.1% (wt/vol) glucose and then cultured them in YEP medium supplemented with 2% (wt/vol) glycerol for 24 h, inoculated at a standard density of approximately 1×10^6 cells/ml. We removed samples at 0, 20 and 24h and determined cell density spectrophotometrically, expressed as OD_{600}.

For Western blot analysis yeast cells were cultured overnight in selective medium supplemented with 2% (wt/vol) galactose and 0.1% (wt/vol) glucose and normalized spectrophotometrically at OD_{600}.

Protein blot analysis

For Western blot analysis of yeast cells, trichloroacetic acid (TCA) protein extracts were prepared as described [Muz*i*-Falconi et al., 1993]. Protein extracts were separated by SDS-PAGE in 10% or 15% acrylamide gels and transferred to a PVDF membrane (Immobilon LF, Millipore). Filters were probed with ant*i*-yMrpL32 and ant*i*-Ccp1 (1:1,000 dilution) [Koppen et al., 2007], ant*i*-ß actin antibodies (1:1,500 dilution) ant*i*-Porin antibodies (1:1,000 dilution) and revealed by Alexa Fluor®647-coniugated goat ant*i*-rabbit IgG (H+L) and antibody and Alexa Fluor®488-coniugated goat ant*i*-mouse IgG (H+L) antibody (Molecular probes). Fluorescence signals were acquired using G:BOX iChemi (Syngene); quantification was performed using Gene Tools software (Syngene) on four independent Western Blots normalizing the signals to the ß-actin loading control.

Co-immunoprecipitation of AFG3L2 and paraplegin.

For immunoprecipitation experiments we grew cells of strains harboring the different AFG3L2 substitutions as previously described [Fracasso et al., 2010] We spun homogenates for 20 min at 16,000*g* and incubated the resulting supernatants with monoclonal ant*i*-V5 antibody (Over night at 4 °C under gentle shaking). We then incubated antigen-antibody complexes with protein G Mag Sepharose magnetic beads (GE Healthcare)

(2 h at 4 °C under gentle shaking). After extensive washes, we eluted samples from beads and analyzed them by SDS-PAGE and immunoblotting.

Antibodies

Polyclonal antisera directed against human AFG3L2 and paraplegin were raised in rabbit as previously described [Di Bella et al., 2010]. Ant*i*-yeast MrpL32 and ant*i*-Ccp1 [Koppen et al., 2007] were as previously reported. Ant*i*-ß actin antibody was from Abcam. Ant*i*-VDAC/Porin antibody was from MitoSciences. Ant*i*-V5 monoclonal antibody was from Life Science Technologies.

Supplementary Material

Supplementary Table 1. Oligonucleotide primers used for site-directed mutagenesis of *AFG3L2* cDNA

Mutant		Primer pairs (5'->3')
AFG3L2T444A	Forward Reverse	GAGATGGATGGTTTTAATACACAACAAATGTCGTCATTTTGG CCAAAATGACGACATTTGTTGTGTATTAAAACCATCCATCTC
AFG3L2L772F	Forward Reverse	GGATGAGGACACCTCATTTCCAGAAGGCCTTAA CTTAAGGCCTTCTGGAAATGAGGTGTCCTCATC
AFG3L2I473V	Forward Reverse	CGTTTCGACAGGCAGGTCTTTATTGGACCAC GTGGTCCAATAAAGACCTGCCTGTCGAAACG
AFG3L2K687T	Forward Reverse	ACATGGTATTGGAGACACCTTACAGTGAAGCC GGCTTCACTGATAGGTGTCTCCAATACCATGTC
AFG3L2K569del	Forward Reverse	GCCTGAGGAGAAGACTGTGGCATACCAC GTGGTATGCCACAGTCTTCTCCTCAGGC
AFG3L2M666V	Forward Reverse	CCAATTGTTCAGTTTGGCGTGAATGAAAAGGTTGGGC GCCCAACCTTTTCATTCACGCCAAACTGAACAATTGG
AFG3L2R679C	Forward Reverse	CTTTGACCTCCCATGTCAGGGGGACATG ATGTCCCCCTGACATGGGAGGTCAAAGG

Supplemenatry Table 2. *Saccharomyces cerevisiae* strains used in this study

Strain	Relevant genotype	Origin
K699	*MATa ho ade2-1 his3-11,15 leu2-3,112 trp1-1 ura3-52 can1-100 ssd1*	Ref. [Nasmyth et al., 1990]
yDDB64	*MATa ade2-1 his3-11,15 leu2-3,112 trp1-1 ura3-52 can1-100 yta10::NAT yta12::KanMX6*	Ref. [Di Bella 2010]
yDDB79	*MATa ade2-1 his3-11,15 leu2-3,112 trp1-1 ura3-52 can1-100 yta10::NAT yta12::KanMX6* pYC6/CT^{ADH1}-Yta10(1-63)-AFG3L2(66-797)-V5/HIS	Ref. [Di Bella 2010]
yDDB165	*MATa ade2-1 his3-11,15 leu2-3,112 trp1-1 ura3-52 can1-100 yta10::NAT yta12::KanMX6* pYC6/CT^{ADH1}-Yta10(1-63)-AFG3L2(66-797)-V5/HIS YCpLac111^{ADH1}-Yta10(1-63)-paraplegin(59-795)-HA	Ref. [Di Bella 2010]
yDDB159	*MATa ade2-1 his3-11,15 leu2-3,112 trp1-1 ura3-52 can1-100 yta10::NAT yta12::KanMX6* pYC6/CT^{ADH1}-Yta10(1-63)-AFG3L2(66-797)^{T444A}-V5/HIS	This study
yDDB176	*MATa ade2-1 his3-11,15 leu2-3,112 trp1-1 ura3-52 can1-100 yta10::NAT yta12::KanMX6* pYC6/CT^{ADH1}-Yta10(1-63)-AFG3L2(66-797) ^{T444A}-V5/HIS YCpLac111^{ADH1}-Yta10(1-63)-paraplegin(59-795)-HA	This study
yDDB193	*MATa ade2-1 his3-11,15 leu2-3,112 trp1-1 ura3-52 can1-100 yta10::NAT yta12::KanMX6* pYC6/CT^{ADH1}-Yta10(1-63)-AFG3L2(66-797)^{L772F}-V5/HIS	This study
yDDB195	*MATa ade2-1 his3-11,15 leu2-3,112 trp1-1 ura3-52 can1-100 yta10::NAT yta12::KanMX6* pYC6/CT^{ADH1}-Yta10(1-63)-AFG3L2(66-797) ^{L772F} -V5/HIS YCpLac111^{ADH1}-Yta10(1-63)-paraplegin(59-795)-HA	This study
yDDB226	*MATa ade2-1 his3-11,15 leu2-3,112 trp1-1 ura3-52 can1-100 yta10::NAT yta12::KanMX6* pYC6/CT^{ADH1}-Yta10(1-63)-AFG3L2(66-797)^{A86P}-V5/HIS	This study
yDDB222	*MATa ade2-1 his3-11,15 leu2-3,112 trp1-1 ura3-52 can1-100 yta10::NAT yta12::KanMX6* pYC6/CT^{ADH1}-Yta10(1-63)-AFG3L2(66-797) ^{A86P} -V5/HIS YCpLac111^{ADH1}-Yta10(1-63)-paraplegin(59-795)-HA	This study

Strain	Relevant genotype	Origin
yDDB232	*MATa ade2-1 his3-11,15 leu2-3,112 trp1-1 ura3-52 can1-100 yta10::NAT yta12::KanMX6* pYC6/CT^{ADH1}-Yta10(1-63)-AFG3L2(66-797)^{I473V}-V5/HIS	This study
yDDB223	*MATa ade2-1 his3-11,15 leu2-3,112 trp1-1 ura3-52 can1-100 yta10::NAT yta12::KanMX6* pYC6/CT^{ADH1}-Yta10(1-63)-AFG3L2(66-797) ^{I473V} -V5/HIS YCpLac111^{ADH1}-Yta10(1-63)-paraplegin(59-795)-HA	This study
yDDB220	*MATa ade2-1 his3-11,15 leu2-3,112 trp1-1 ura3-52 can1-100 yta10::NAT yta12::KanMX6* pYC6/CT^{ADH1}-Yta10(1-63)-AFG3L2(66-797)$^{82.84del}$-V5/HIS	This study
yDDB221	*MATa ade2-1 his3-11,15 leu2-3,112 trp1-1 ura3-52 can1-100 yta10::NAT yta12::KanMX6* pYC6/CT^{ADH1}-Yta10(1-63)-AFG3L2(66-797)$^{82.84del}$-V5/HIS YCpLac111^{ADH1}-Yta10(1-63)-paraplegin(59-795)-HA	This study
yDDB162	*MATa ade2-1 his3-11,15 leu2-3,112 trp1-1 ura3-52 can1-100 yta10::NAT yta12::KanMX6* pYC6/CT^{ADH1}-Yta10(1-63)-AFG3L2(66-797)^{K687T}-V5/HIS	This study
yDDB179	*MATa ade2-1 his3-11,15 leu2-3,112 trp1-1 ura3-52 can1-100 yta10::NAT yta12::KanMX6* pYC6/CT^{ADH1}-Yta10(1-63)-AFG3L2(66-797) ^{K687T} -V5/HIS YCpLac111^{ADH1}-Yta10(1-63)-paraplegin(59-795)-HA	This study
yDDB146	*MATa ade2-1 his3-11,15 leu2-3,112 trp1-1 ura3-52 can1-100 yta10::NAT yta12::KanMX6* pYC6/CT^{ADH1}-Yta10(1-63)-AFG3L2(66-797)^{T654I}-V5/HIS	This study
yDDB149	*MATa ade2-1 his3-11,15 leu2-3,112 trp1-1 ura3-52 can1-100 yta10::NAT yta12::KanMX6* pYC6/CT^{ADH1}-Yta10(1-63)-AFG3L2(66-797) ^{T654I} -V5/HIS YCpLac111^{ADH1}-Yta10(1-63)-paraplegin(59-795)-HA	This study
yDDB203	*MATa ade2-1 his3-11,15 leu2-3,112 trp1-1 ura3-52 can1-100 yta10::NAT yta12::KanMX6* pYC6/CT^{ADH1}-Yta10(1-63)-AFG3L2(66-797)^{K659del}-V5/HIS	This study
yDDB204	*MATa ade2-1 his3-11,15 leu2-3,112 trp1-1 ura3-52 can1-100 yta10::NAT yta12::KanMX6* pYC6/CT^{ADH1}-Yta10(1-63)-AFG3L2(66-797) ^{K659del}-V5/HIS YCpLac111^{ADH1}-Yta10(1-63)-paraplegin(59-795)-HA	This study

Strain	Relevant genotype	Origin
yDDB148	*MATa ade2-1 his3-11,15 leu2-3,112 trp1-1 ura3-52 can1-100 yta10::NAT yta12::KanMX6* pYC6/CT^{ADH1}-Yta10(1-63)-AFG3L2(66-797)^{G671R}-V5/HIS	This study
yDDB154	*MATa ade2-1 his3-11,15 leu2-3,112 trp1-1 ura3-52 can1-100 yta10::NAT yta12::KanMX6* pYC6/CT^{ADH1}-Yta10(1-63)-AFG3L2(66-797)^{G671R}-V5/HIS YCpLac111^{ADH1}-Yta10(1-63)-paraplegin(59-795)-HA	This study
yDDB147	*MATa ade2-1 his3-11,15 leu2-3,112 trp1-1 ura3-52 can1-100 yta10::NAT yta12::KanMX6* pYC6/CT^{ADH1}-Yta10(1-63)-AFG3L2(66-797) ^{G671E}-V5/HIS	This study
yDDB153	*MATa ade2-1 his3-11,15 leu2-3,112 trp1-1 ura3-52 can1-100 yta10::NAT yta12::KanMX6* pYC6/CT^{ADH1}-Yta10(1-63)-AFG3L2(66-797) ^{G671E}-V5/HIS YCpLac111^{ADH1}-Yta10(1-63)-paraplegin(59-795)-HA	This study
yDDB161	*MATa ade2-1 his3-11,15 leu2-3,112 trp1-1 ura3-52 can1-100 yta10::NAT yta12::KanMX6* pYC6/CT^{ADH1}-Yta10(1-63)-AFG3L2(66-797) ^{R679C}-V5/HIS	This study
yDDB178	*MATa ade2-1 his3-11,15 leu2-3,112 trp1-1 ura3-52 can1-100 yta10::NAT yta12::KanMX6* pYC6/CT^{ADH1}-Yta10(1-63)-AFG3L2(66-797) ^{R679C}-V5/HIS YCpLac111^{ADH1}-Yta10(1-63)-paraplegin(59-795)-HA	This study
yDDB144	*MATa ade2-1 his3-11,15 leu2-3,112 trp1-1 ura3-52 can1-100 yta10::NAT yta12::KanMX6* pYC6/CT^{ADH1}-Yta10(1-63)-AFG3L2(66-797)^{M666V}-V5/HIS	This study
yDDB151	*MATa ade2-1 his3-11,15 leu2-3,112 trp1-1 ura3-52 can1-100 yta10::NAT yta12::KanMX6* pYC6/CT^{ADH1}-Yta10(1-63)-AFG3L2(66-797) ^{M666V}-V5/HIS YCpLac111^{ADH1}-Yta10(1-63)-paraplegin(59-795)-HA	This study
yDDB143	*MATa ade2-1 his3-11,15 leu2-3,112 trp1-1 ura3-52 can1-100 yta10::NAT yta12::KanMX6* pYC6/CT^{ADH1}-Yta10(1-63)-AFG3L2(66-797) ^{M666T}-V5/HIS	This study
yDDB150	*MATa ade2-1 his3-11,15 leu2-3,112 trp1-1 ura3-52 can1-100 yta10::NAT yta12::KanMX6* pYC6/CT^{ADH1}-Yta10(1-63)-AFG3L2(66-797) ^{M666T}-V5/HIS YCpLac111^{ADH1}-Yta10(1-63)-paraplegin(59-795)-HA	This study

Strain	Relevant genotype	Origin
yDDB145	*MATa ade2-1 his3-11,15 leu2-3,112 trp1-1 ura3-52 can1-100 yta10::NAT yta12::KanMX6* pYC6/CT^{ADH1}-Yta10(1-63)-AFG3L2(66-797) ^{M666R}-V5/HIS	This study
yDDB152	*MATa ade2-1 his3-11,15 leu2-3,112 trp1-1 ura3-52 can1-100 yta10::NAT yta12::KanMX6* pYC6/CT^{ADH1}-Yta10(1-63)-AFG3L2(66-797) ^{M666R}-V5/HIS YCpLac111^{ADH1}-Yta10(1-63)-paraplegin(59-795)-HA	This study

References

- Adams A, Gottschling DE, Kaiser CA, Stearns T. 1997. Methods in Yeast Genetics. A Cold Spring Harbor Laboratory Course Manual (Cold Spring Harbor Laboratory Press, Cold Spring Harbor, NY).
- Arlt H, Tauer R, Feldmann H, Neupert W, Langer T. 1996. The YTA10-12 complex, an AAA protease with chaperone-like activity in the inner membrane of mitochondria. Cell 85:875-885.
- Banfi S et al. 1999. Identification and characterization of AFG3L2, a novel paraplegin-related gene. Genomics 59:51-58.
- Cagnoli C et al. 2010. Missense Mutations in the AFG3L2 Proteolytic Domain Account for ~1.5% of European Autosomal Dominant Cerebellar Ataxias. Hum Mutat 31:1117–1124.
- Casari G et al. 1998. Spastic paraplegia and OXPHOS impairment caused by mutations in paraplegin, a nuclear-encoded mitochondrial metalloprotease. Cell 93:973-983.
- Di Bella D et al. 2010. Mutations in the mitochondrial protease gene AFG3L2 cause dominant hereditary ataxia SCA28. Nat Genet 42:313-321.
- Dürr A. 2010. Autosomal dominant cerebellar ataxias: polyglutamine expansions and beyond. Lancet Neurol 9:885-894.
- Esser K, Tursun B, Ingenhoven M, Michaelis G, Pratje E. 2002. A novel two-step mechanism for removal of a mitochondrial signal sequence involves the mAAA complex and the putative rhomboid protease Pcp1. J Mol Biol 323:835-843.
- Fontanesi F, Diaz F, Barrientos A. 2009. Evaluation of the mitochondrial respiratory chain and oxidative phosphorylation system using yeast models of OXPHOS deficiencies. Curr Protoc Hum Genet Chapter 19:Unit19.5.
- Fracasso, V., Lazzaro, F. & Muz*i*-Falconi, M. Co-immunoprecipitation of human mitochondrial proteases AFG3L2 and paraplegin heterologously expressed in yeast cells. *Nat. Protoc.* published online, doi:10.1038/nprot.2010.26 (7 March 2010).
- Gellera C et al. 2007. Frataxin gene point mutations in Italian Friedreich ataxia patients. Neurogenetics 8:289-299.
- Koppen M, Langer T. 2007. Protein degradation within mitochondria: versatile activities of AAA proteases and other peptidases. Crit Rev Biochem Mol Biol 42:221-242.

- Koppen M, Metodiev MD, Casari G, Rugarli EI, Langer T. 2007. Variable and tissue-specific subunit composition of mitochondrial *m*-AAA protease complexes linked to hereditary spastic paraplegia. Mol Cell Biol 27:758-767.
- Koppen, M., Bonn, F., Ehses, S. & Langer, T. 2009.Autocatalytic processing of *m*-AAA protease subunits in mitochondria. Mol. Biol. Cell 20: 4216–4224
- Longtine MS et al. 1998. Additional modules for versatile and economical PCR-based gene deletion and modification in Saccharomyces cerevisiae. Yeast 14:953-961.
- Mariotti C et al. 2008. Spinocerebellar ataxia type 28: A novel autosomal dominant cerebellar ataxia characterized by slow progression and ophthalmoparesis. Cerebellum 7:184-188.
- Muz*i*-Falconi M et al. 1993. De novo synthesis of budding yeast DNA polymerase alpha and POL1 transcription at the G1/S boundary are not required for entrance into S phase. Proc Natl Acad Sci USA 90:10519-10523.
- Nolden M et al. 2005. The *m*-AAA protease defective in hereditary spastic paraplegia controls ribosome assembly in mitochondria. Cell 123:277-289.
- Taroni F, DiDonato S. 2004. Pathways to motor incoordination: the inherited ataxias. Nature Rev Neurosci 5:641-655.
- Tatsuta T, Augustin S, Nolden M, Friedrichs B and Langer T. 2007. *m*-AAA protease-driven membrane dislocation allows intramembrane cleavage by rhomboid in mitochondria. EMBO J 26:325-335.
- Tatsuta T, Langer T. 2008. Quality control of mitochondria: protection against neurodegeneration and ageing. EMBO J. 27:306–314.

Figures

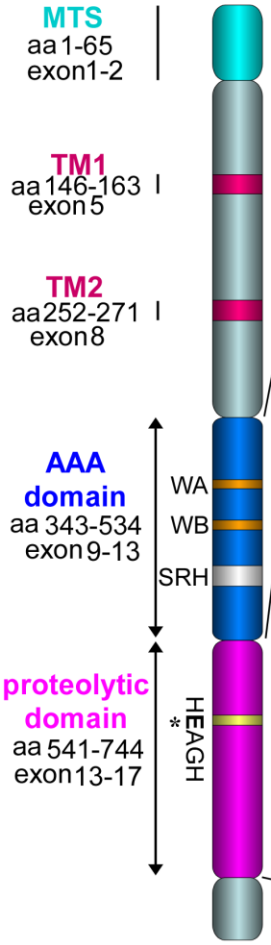

Variant	Exon location	Reference
N82_K84del	3	This study
A86P	3	This study
H126Q	4	Di Bella 2010
N432T	10	Di Bella 2010
T444A	11	This study
I473V	11	This study
K569del	14	This study
T654I	15	Cagnoli 2010
M666R	16	Cagnoli 2010
M666T	16	Cagnoli 2010
M666V	16	This study - Cagnoli 2010
G671E	16	Cagnoli 2010
G671R	16	Cagnoli 2010
S674L	16	Di Bella 2010
R679C	16	This study
K687T	16	This study
E691K	16	Di Bella 2010
A694E	16	Di Bella 2010
E700K	16	Edener 2010
R702Q	16	Di Bella 2010
L772F	17	This study

Figure 1

Figure 1: All variants identified in AFG3L2 gene

The human *AFG3L2* domain structure of the protein is shown in the left part of the figure. MTS, mitochondrial targeting sequence; TM1 and TM2, transmembrane domains 1 and 2, respectively, AAA domain with WA (Walker-A motif), WB (Walker-

B motif) SRH (second region of homology). Proteolytic domain with HEAGH (protease catalytic site). In the right part of figure is reported variant (in blue variants in AAA domain and in magenta variants in proteolytic domain), exon location and reference.

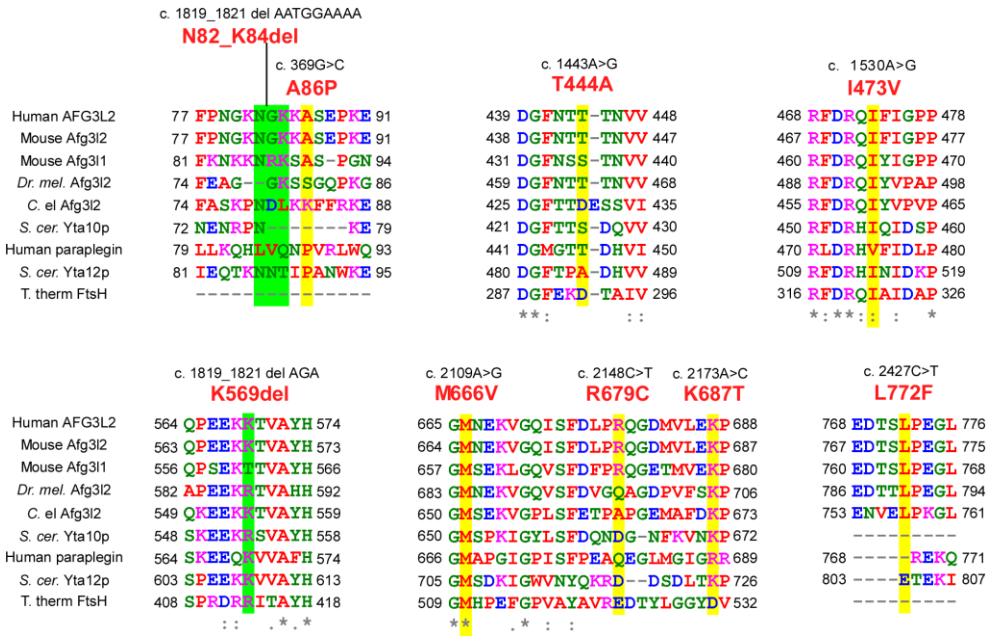

Figure 2

Figure 2: Amino acids conservation

ClustalW2 multiple alignment of variants of human AFG3L2 with members of the *m*-AAA family from different organisms: Human AFG3L2, Mouse afg3l2, Mouse afg3l1, *Dr. mel.* (*Drosophila melanogaster*); *C. el.* (*Caenorhabditis elegans*); *S. cer.*Yta10p (*Saccharomyces cerevisiae*); *Human paraplegin*, *S. cer.*Yta12p (*Saccharomyces cerevisiae*)and *Th. therm*. FtsH (*Thermus thermophilus*). The nucleotide position, nucleotide change and mutated residues are indicated above the alignment.

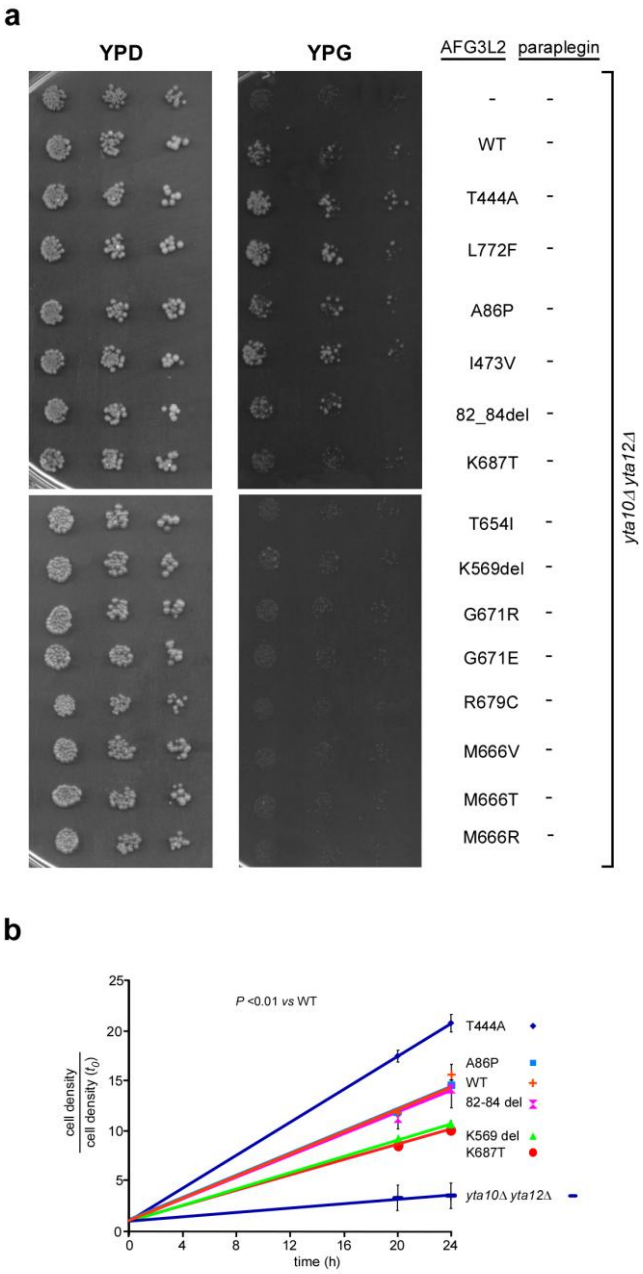
a
YPD
YPG
AFG3L2 paraplegin
-
WT
T444A
L772F
A86P
I473V
82_84del
K687T
T654I
K569del
G671R
G671E
R679C
M666V
M666T
M666R
yta10Δ yta12Δ
b
P <0.01 vs WT
cell density / cell density (t0)
time (h)
T444A
A86P
WT
82-84 del
K569 del
K687T
yta10Δ yta12Δ

Figure 3

Figure 3: Complementation studies in *Saccharomyces cerevisiae*

(**a**) Serial dilutions of cells from exponentially grown cultures were spotted onto YEP plates containing either 2%(wt/vol) glucose (left panels, YPD) or 2%(wt/vol) glycerol (right panels, YPG) and they are incubated at 28°C. Respiratory competence is deduced by the ability to grow on glycerol (YPG). We analyse the respiratory phenotype of yta10Δyta12Δ cells expressing either normal (WT) or mutant human AFG3L2 at 28°C.

(**b**) The graph shows the growth rates of cells expressing either $AFG3L2^{WT}$ or some mutants. Cells were grown in YEP medium supplemented with 2% (wt/vol) galactose-0.1% (wt/vol) glucose for 24 hours at 28°C. Values on the *y*-axis represent the ratio between cell density (= number of cells/ml) at a given time and cell density at start (*t0*). The cells are counted at 0, 20, and 24 hours. Each value represents the mean of five independent experiments. Error bars indicate s.d.. Statistical significance, determined by Student's t-test, is $P < 0.05$ for mutants vs WT Growth rates are calculated by linear regression analysis (trend line).

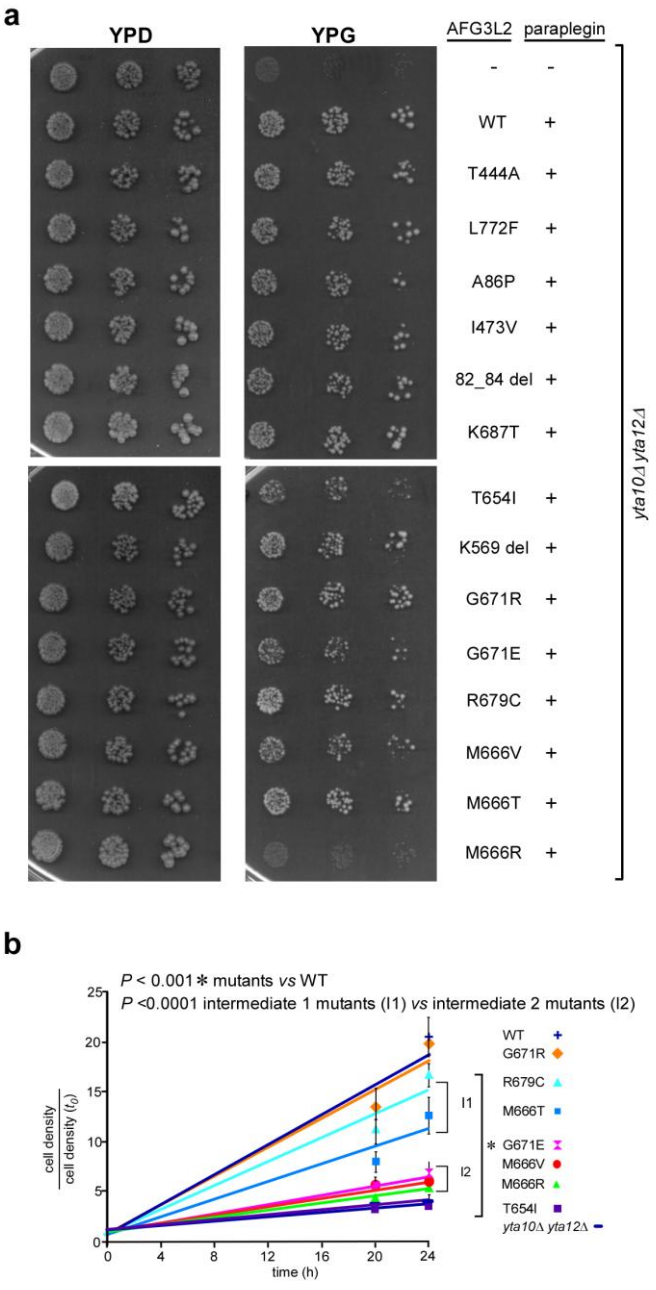
a
YPD
YPG
AFG3L2
paraplegin
-
-
WT
+
T444A
+
L772F
+
A86P
+
I473V
+
82_84 del
+
K687T
+
T654I
+
K569 del
+
G671R
+
G671E
+
R679C
+
M666V
+
M666T
+
M666R
+
yta10Δ yta12Δ
b
P < 0.001 * mutants vs WT
P <0.0001 intermediate 1 mutants (I1) vs intermediate 2 mutants (I2)
cell density / cell density (t0)
time (h)
0
4
8
12
16
20
24
0
5
10
15
20
25
I1
I2
WT
G671R
R679C
M666T
* G671E
M666V
M666R
T654I
yta10Δ yta12Δ

Figure 4

Figure 4: Complementation studies in *Saccharomyces cerevisiae*

(**a**) Serial dilutions of cells from exponentially grown cultures were spotted onto YEP plates containing either 2% (wt/vol) glucose (left panels, YPD) or 2%(wt/vol) glycerol (right panels, YPG). and they are incubated at 28°C. Respiratory competence is deduced by the ability to grow on glycerol (YPG). Respiratory phenotype of yta10Δyta12Δ cells coexpressing either normal or mutant human AFG3L2 with human paraplegin at 28°C.

(**b**) The graph shows the growth rates of cells coexpressing either normal or some mutants human AFG3L2 with human paraplegin. Cells were grown in YEP medium supplemented with 2% (wt/vol) galactose-0.1% (wt/vol) glucose for 24 hours at 28°C. Values on the *y*-axis represent the ratio between cell density (= number of cells/ml) at a given time and cell density at start (*t0*). The cells are counted at 0, 20, and 24 hours. Each value represents the mean of five independent experiments. Error bars indicate s.d.. Asterisk indicate statistical significance, determined by Student's t-test. For strains grow at 28°C is $P < 0.001$ for mutants vs WT and $P < 0.0001$ for intermediate 1 mutants (I1) vs intermediate 2 mutants (I2). Growth rates are calculated by linear regression analysis (trend line).

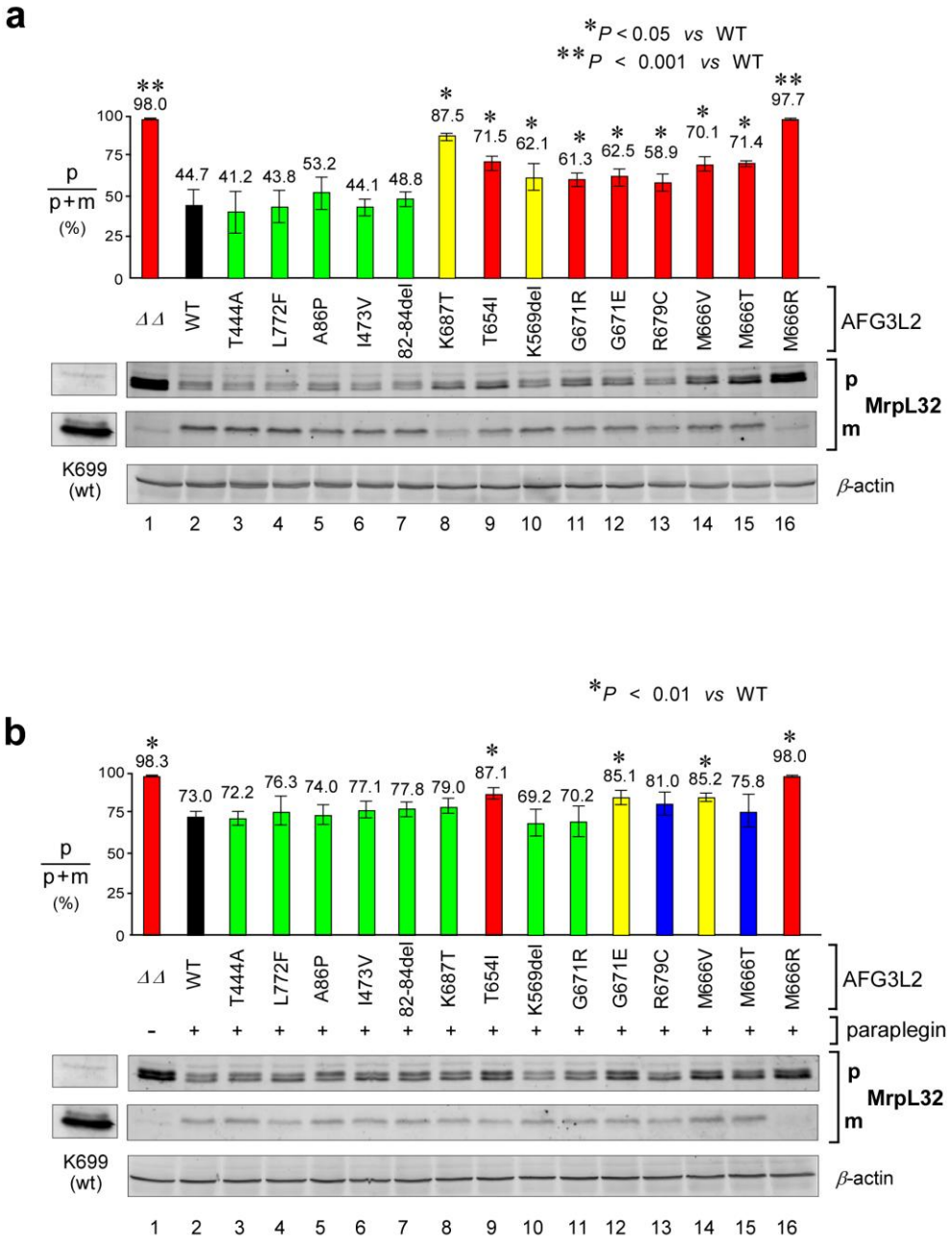
a
*P < 0.05 vs WT
**P < 0.001 vs WT
p / p+m (%)
98.0
44.7
41.2
43.8
53.2
44.1
48.8
87.5
71.5
62.1
61.3
62.5
58.9
70.1
71.4
97.7
ΔΔ
WT
T444A
L772F
A86P
I473V
82-84del
K687T
T654I
K569del
G671R
G671E
R679C
M666V
M666T
M666R
AFG3L2
p
MrpL32
m
K699 (wt)
β-actin
1 2 3 4 5 6 7 8 9 10 11 12 13 14 15 16
b
*P < 0.01 vs WT
98.3
73.0
72.2
76.3
74.0
77.1
77.8
79.0
87.1
69.2
70.2
85.1
81.0
85.2
75.8
98.0
paraplegin
- + + + + + + + + + + + + + + +

Figure 5

Figure 5: Proteolytic activity of normal and mutant AFG3L2 expressed in yeast

(**a**) Fluorescence immunoblot analysis with ant*i*-MrpL32 in yeast cells expressing mutant AFG3L2. Immunoblotting was performed using polyclonal antisera directed against MrpL32. p (precursor form); m (mature form). AFG3L2 proteolytic competence is expressed as the ratio of pMrpL32 level to total (p + m) MrpL32 level. MrpL32 levels were normalized to the loading control protein β-actin. Bar graph above immunoblot reports quantitative results and it represents the mean of four experiments. The colours of histograms symbolize the respiratory growth: wt in black, grow strains in green, slower strains in yellow and no grow strainsin red. Error bars indicate s.d.. Asterisks indicate a statistically significant (P <0.05 or P <0.001) difference from AFG3L2^{WT} as determined by Student's t-test.

(**b**) Proteolytic activity of normal and mutant AFG3L2 in the presence of paraplegin coexpression. Analysis performed under the same conditions described above. The histograms in blue colour symbolize the slow strains intermediate 1 mutants (I1) and the histograms in yellow colour represent the slower strains intermediate 2 mutants (I2). In these experiments statistically significant difference from AFG3L2^{WT} is P <0.01).

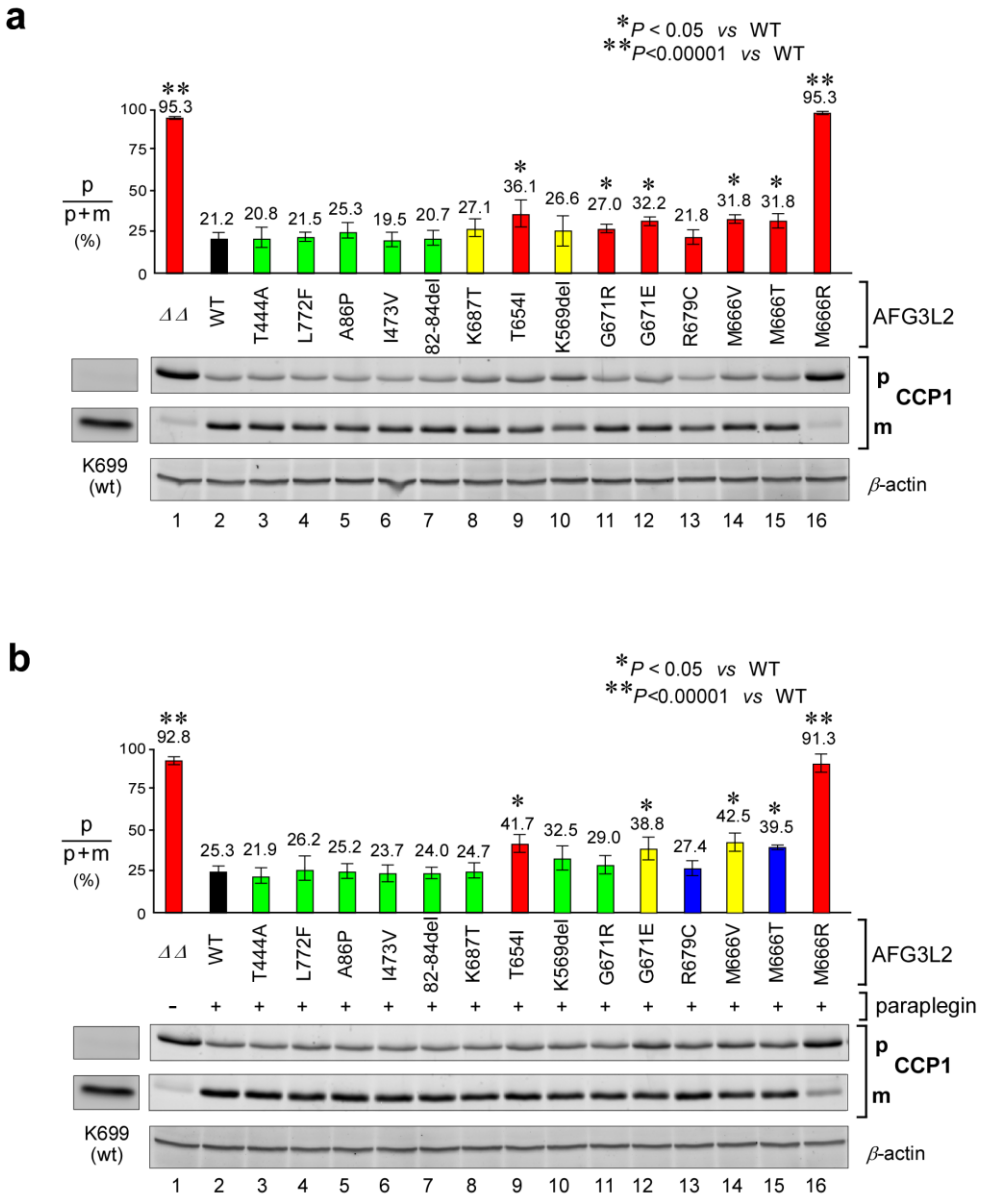
a
*P < 0.05 vs WT
**P<0.00001 vs WT
p / p+m (%)
**95.3
21.2
20.8
21.5
25.3
19.5
20.7
27.1
*36.1
26.6
*27.0
*32.2
21.8
*31.8
*31.8
**95.3
ΔΔ
WT
T444A
L772F
A86P
I473V
82-84del
K687T
T654I
K569del
G671R
G671E
R679C
M666V
M666T
M666R
AFG3L2
p
CCP1
m
K699 (wt)
β-actin
1 2 3 4 5 6 7 8 9 10 11 12 13 14 15 16
b
*P < 0.05 vs WT
**P<0.00001 vs WT
p / p+m (%)
**92.8
25.3
21.9
26.2
25.2
23.7
24.0
24.7
*41.7
32.5
29.0
*38.8
27.4
*42.5
*39.5
**91.3
ΔΔ
WT
T444A
L772F
A86P
I473V
82-84del
K687T
T654I
K569del
G671R
G671E
R679C
M666V
M666T
M666R
AFG3L2
- + + + + + + + + + + + + + + +
paraplegin
p
CCP1
m
K699 (wt)
β-actin
1 2 3 4 5 6 7 8 9 10 11 12 13 14 15 16

Figure 6

Figure 6: Proteolytic activity of normal and mutant AFG3L2 expressed in yeast

(**a**) Fluorescence immunoblot analysis with ant*i*-Ccp1 in yeast cells expressing mutant AFG3L2. Immunoblotting was performed using polyclonal antisera directed against Ccp1. p (precursor form); m (mature form). AFG3L2 proteolytic competence is expressed as the ratio of p Ccp1level to total (p + m) Ccp1 level. Ccp1 levels were normalized to the loading control protein β-actin. Histogram above immunoblot reports quantitative results and it represents the mean of five experiments. Error bars indicate s.d. Asterisks indicate a statistically significant (P <0.05 or P <0.00001) difference from $AFG3L2^{WT}$ as determined by Student's t-test. (**b**) Proteolytic activity of normal and mutant AFG3L2 in the presence of paraplegin coexpression. Analysis performed under the same conditions described above.

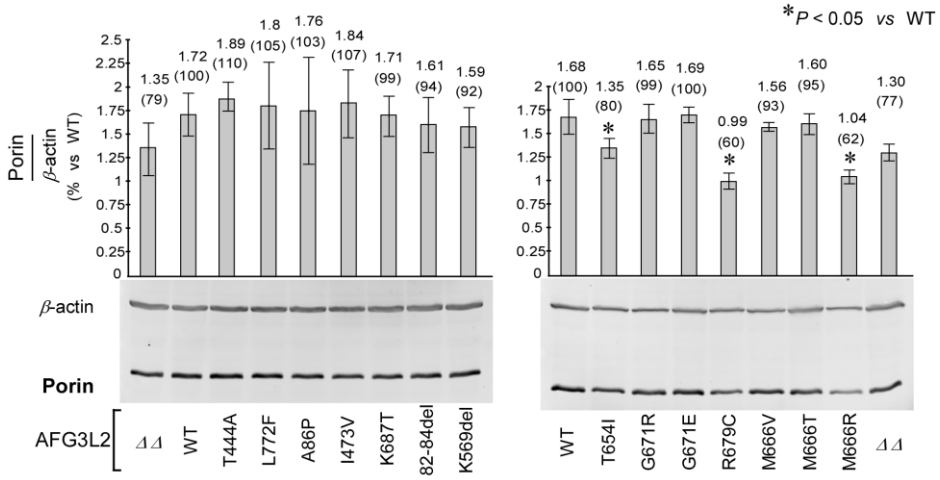

Figure 7

Figure 7: Mitochondrial quantification in mutant AFG3L2 homocomplex expressed in Saccharomyces cerevisiae

Fluorescence immunoblot analysis of Actin and Porin proteins in yeast cells expressing WT and mutant AFG3L2. Immunoblotting was performed using porin antibody as mitochondrial marker and β-actin antibody as cellular marker. The graphs above immunoblot report the quantitative results and they represent the mean of three independent experiments. Error bars indicate s.d.. Asterisks indicate a statistically significant (P <0.05) difference from AFG3L2^{WT} as determined by Student's *t*-test.

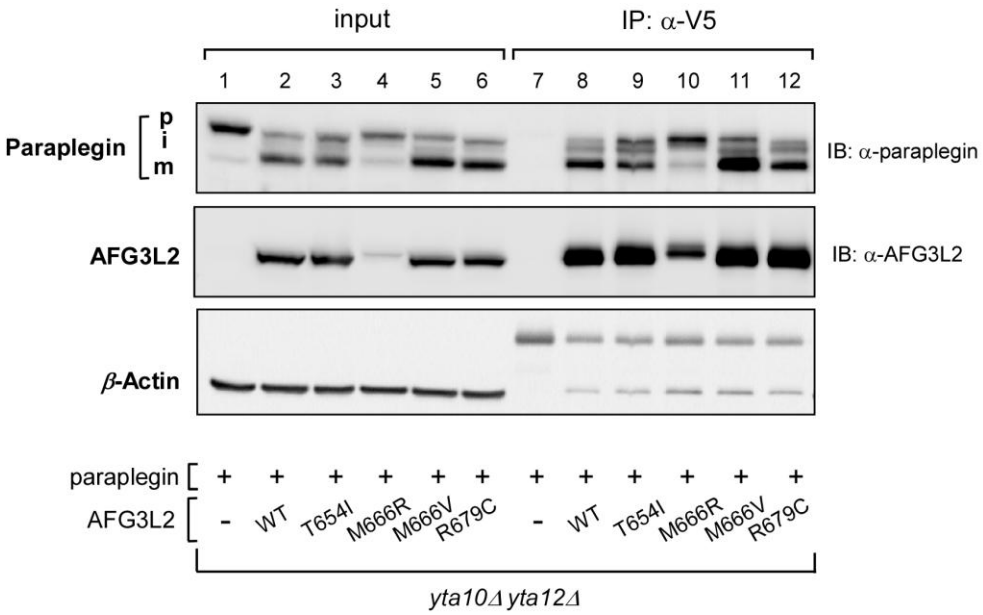

Figure 8

Figure 8: Co-immunoprecipitation of paraplegin and V5 tagged AFG3L2 WT and mutated heterocomplexes.

V5-tagged AFG3L2 was immunoprecipitated with mouse monoclonal anti-V5 antibody. Cell extracts before immunoprecipitation (INPUT) and immunoprecipitates (IP) were analyzed by SDS-PAGE and immunoblotting (IB) using rabbit polyclonal anti-paraplegin (α-paraplegin) or anti-AFG3L2 (α-AFG3L2) antibodies.

We can see three forms of paraplegin: p=precursor, i=intermediate and m=mature.

Chapter 4

Concurrent mutations in AFG3L2 and paraplegin cause mitochondrial dysfunction in patients with spinocerebellar degeneration

S. Magri[1],V. Fracasso[1], M. Plumari[1] P. Rusmini[4], C. Gellera[1], C. Pantaleoni[3], S. De Biasi[2], A. Poletti[4], P. Plevani[2], F. Lazzaro[2], M. Muzi-Falconi[2], D. DiBella[1], F. Taroni[1]

(1) Unit of Genetics of Neurodegenerative and Metabolic Diseases, Fondazione IRCCS Istituto Neurologico Carlo Besta, Milan, Italy;
(2) Dept. Biomolecular Sciences and Biotechnology, University of Milan, Italy;
(3) Unit of Developmental Neurology, Fondazione IRCCS Istituto Neurologico Carlo Besta, Milan, Italy
(4) Dept. of Endocrinology, Physiopathology and Applied Biology, and Centre of Excellence on Neurodegenerative Diseases, University of Milan, Italy;

Submitted

Abstract

Autosomal dominant spinocerebellar ataxias (SCA) are a heterogeneous group of neurological disorders characterized by cerebellar dysfunction. We recently showed that AFG3L2 mutations cause dominant ataxia SCA28. AFG3L2 and its partner protein paraplegin, which causes recessive spastic paraparesis SPG7, are components of the *m*-AAA complex, involved in mitochondrial protein quality control. Since yeast functional studies showed that paraplegin coexpression can modulate AFG3L2 mutations, we investigated the possible coinheritance of AFG3L2 and SPG7 mutations in patients with spinocerebellar syndromes. We identified 3 probands with heterozygous mutations in both the AFG3L2 and the SPG7 genes. Two ataxic patients carry an *AFG3L2* mutation affecting highly conserved amino acids located in the ATPase or in the proteolytic domains of the protein along with the paraplegin^{A510V}. The third proband carries a *de novo AFG3L2* mutation in the highly conserved SRH region of the ATPase domain along with the inherited deletion of *SPG7* exons 4-6. The clinical presentation of this patient is characterized by early onset optic atrophy and a L-dopa-responsive spastic-ataxic syndrome with extrapyramidal signs. A muscle biopsy revealed an isolated complex I deficiency. Moreover, evaluation of substrates processing in patient's fibroblasts showed abnormal processing pattern of OPA1. In conclusion, our data indicate that the presence of a loss-of-function mutation in paraplegin may act as a disease modifier for heterozygous AFG3L2 mutations. Concurrent mutations in both components of the mitochondrial *m*-AAA complex may result in a complex phenotype, thus expanding the clinical spectrum of AFG3L2-associated mutations. Moreover, biochemical and cell biology studies revealed a crucial role of the *m*-AAA complex in the processing of OPA1 and the maintenance of mitochondrial morphology.

Introduction

Autosomal dominant spinocerebellar ataxias (SCAs) are a group of genetically heterogeneous neurodegenerative diseases characterized by a progressive cerebellar syndrome mostly due to Purkinje cell degeneration. From a clinical point of view cerebellar gait and limb ataxia is often associated with other neurological signs such as pyramidal or extrapyramidal signs, ophthalmoplegia, and cognitive impairment (Durr et al., 2010). Recently, we have identified AFG3L2 as the gene responsible for SCA28 and found heterozygous missense mutation in five unrelated SCA families (Di Bella et al., 2010). Afterward, we screened a new large cohort of affected individuals with ataxic phenotype confirming a minimum frequency of ~1.7% (Fracasso et al., submitted). The finding that AFG3L2 mutations cause dominant ataxia is remarkable also because alterations of paraplegin, partner of AFG3L2 in the *m*-AAA metalloprotease complex, cause a distinct neurodegenerative disorder, SPG7 hereditary spastic paraplegia, by a loss-of-function recessive mechanism (Casari et al., 1998). The *m*-AAA metalloprotease is an ATP-dependent proteolytic complex located in the inner mitochondrial membrane. It carries out protein quality control by degrading non-assembled or damaged proteins and also participates in the processing and maturation of some mitochondrial proteins (Koppen and Langer 2007; Esser et al., 2002; Nolden et al., 2005). In humans, *m*-AAA exists in two different subunit composition: a heterocomplex composed of AFG3L2 and paraplegin and a homocomplex constituited of AFG3L2 only (Di Bella et al., 2010).

Yeast *m*-AAA is composed of Yta10p and Yta12p which exhibit high sequence homology with AFG3L2 and paraplegin. In the absence of the *m*-AAA protease, yeast cells are respiratory deficient and cannot grow on non-fermentable carbon sources such as glycerol (Atorino et al., 2003). Complementation studies demonstrate that *m*-AAA protease is functionally conserved from yeast to human: human *m*-AAA complexes (both homo- and heterocomplex) are able to replace the Yta10p/Yta12p complex and to restore the respiratory competence (Atorino et al., 2003; Koppen et al., 2007). According to these data, we expressed mutant human *m*-AAA in a

yeast cellular model to investigate the functional effects of the mutations causing amino acid substitution and to discriminate between disease-causing mutations and rare benign variants. AFG3L2 mutations were evaluated in both the homocomplex (AFG3L2 without paraplegin) and the heterocomplex (AFG3L2/paraplegin). The mutations were classified as benign variants, paraplegin-responsive mutations, and paraplegin-non responsive mutations on the basis of the capacity to restore respiratory competence in the presence and in the absence of paraplegin (Di Bella et al., 2010; Fracasso et al., submitted). Since yeast functional studies showed that paraplegin coexpression can complement or modulate AFG3L2 mutations, we investigated the possible coinheritance of *SPG7* mutations in patients with *AFG3L2* mutations. We report here the identification of 3 probands with heterozygous mutations in both the *AFG3L2* and the SPG7 genes.

We performed functional analysis and cell biology studies on one genotype because of the severity and complexity of the relative clinical phenotype and the crucial role of the mutated AFG3L2 residue.

Materials and Methods

Patients and DNA samples

We studied 16 unrelated index cases with a genetic diagnosis of SCA28 previously established in our laboratory. Six of them have been previously described by Di Bella et al. (2010), while the identification of other 9 SCA28 patients was reported by Fracasso et al. (submitted). The remaining proband is a sporadic case carrying a *de novo* mutation in AFG3L2 (R468C). Genomic DNA was prepared from peripheral-blood lymphocytes using standard procedures as previously described (Gellera et al., 2007). Each individual providing a biological sample signed written informed consent. All procedures involving human subjects were approved by the Institutional Review Board of the Fondazione IRCCS Istituto Neurologico "Carlo Besta", Milan, Italy.

Mutation analysis

Mutation screening of SPG7 gene was performed by automated sequencing, while copy number variation was detected by MLPA (Multiplex Ligation-dependent Probe Amplification). Sequences of the oligonucleotide primers are described in Table 1. Nucleotides were numbered so that the first nucleotide of the first in-frame ATG codon is nucleotide +1. Amino acids were numbered so that methionine encoded by the first in-frame ATG codon is Met1.

SPG7 amplicons	bp	Annealing temp.	Primer fw 5'-3'	Primer rw 5-3˙
1	615	61°C	TGTGACCGAACCCTGCGGGTGA	TAAGGCCCAGCCCGGCGGGGCG
2	242	61°C	TTAGTCTGCATTGCTTTGGTACT	CACACTTACCGCCT*CAGCTACT*
4	375	61°C	TGGATGTCGCCCGTGTCTGTTG	*TGGCAGCCTGT*GAGAGTGAGG
5	275	61°C	TTGACTGTAGGGTTGCTCGTCT	TTGTAATCTGAGAAACAGATTGC
6	304	61°C	TGGAAACA*TTGCCAGCAGTGGT*	AGGGAAAACCTGTTGCAGAGAG
7	273	61°C	TCAGGTGCGTGGGCTGAGCGCT	CGGCCGTCCTCCTCTCCCAGAA
8	312	61°C	GTGACCCAGAGAGACCTTACCT	CTGGCTCCTTTCACACATCCTT
9	343	61°C	CTGGCCCGGGTACAGGAAGAGG	*TG*GTGAGCCAAGATCGTGTCACT
10	262	61°C	AACCTGCAGGGGAAATCTGTTG	CACTCGCTCTGAGTGGTCTGGC
11	249	61°C	GACAAACATGCCGCACCTGTG	TCACCTGCGCAAACAGCATCGA
12	265	61°C	TCCCTTGAGGGCCCCTTCCTCCT	AGAAATACCCAGGCAGGTATTG
13	330	61°C	GTCTCGAACTCCTGTCCTCA	GCCTGTGTCTGTAGCTGACT
14	295	61°C	CCTCTTAGTCCCACACCTTCCT	GCTTTTCCCTGCATGACTCCTT
15	334	61°C	CAGTGCTCTGACCGGGACACCT	*GGTCTACCACACAA*GGGTCGCCCA
16	247	61°C	AGTCTGCCATTTCTTTTCTGTG	ACCCCTCTCGTGAAGTATTTCC
17	412	61°C	CTTGCCACCTCCCCAGGACATA	TAGTCCCTGCACAGTGACTTCT

Table 1. Oligonucleotide primers for SPG7 screening

AFG3L2 and paraplegin yeast expression plasmids

Plasmids for heterologous expression of human AFG3L2 and paraplegin in yeast were generated as previously described (Di Bella et al., 2010). The R468C mutation was introduced into the yeast construct pYC6/CT*ADH1*-AFG3L2-V5/HIS using the QuikChange XL Site-Directed Mutagenesis Kit (Stratagene). Table 2 contains oligonucleotide primers used for site-directed mutagenesis. The plasmid YCplac111*ADH1*-Yta10(1-63)-paraplegin(59-795)-HA was used to express human paraplegin as previously described (Di Bella et al., 2010)

Mutant		**Primer pairs (5'->3')**
AFG3L2^{E575Q}	Forward	CTGTGGCATACCACCAAGCAGGCCATGCGG
	Reverse	CCGCATGGCCTGCTTGGTGGTATGCCACAG
AFG3L2^{E691K}	Forward	TATTGGAGAAACCTTACAGTAAAGCCACTGCAAGATTGATAGA
	Reverse	TCTATCAATCTTGCAGTGGCTTTACTGTAAGGTTTCTCCAATA
AFG3L2^{S674L}	Forward	GGTTGGGCAAATCTTATTTGACCTCCCACGTCAGG
	Reverse	CCTGACGTGGGAGGTCAAATAAGATTTGCCCAACC
AFG3L2^{R468C}	Forward	CTTAGGCCGGGGTGTTTCGACAGGCAG
	Reverse	TGCCTGTCGAAACACCCCGGCCTAAGC

Table 2: Oligonucleotide primers used for site-directed mutagenesis of *AFG3L2* cDNA

Yeast strains and growth conditions

All strains used in this study (Table 3) derived from W303 (K699, *MATa ho ade2-1 trp1-1 can1-100 leu2-3,12 his3-11,15 ura3 ssd1*). Deletions of *YTA10* and *YTA12* (*yta10Δyta12Δ* strain) were generated using the one-step PCR system; the obtained strain was transformed as previous described. Cells were grown at 28°C on YEP medium (1%-yeast extract, 2%-peptone, 2%-agar for plates) or selective medium supplemented with 2% (wt/vol) glucose according to standard procedures. Blasticidin-resistant transformants were selected on YEP medium supplemented with 50 µg of blasticidin S per ml. For complementation experiments, equal amounts of five-fold serial dilutions of cells from exponentially grown cultures were spotted onto YEP plates containing 2% (wt/vol) glucose (YPD) or 2% (wt/vol) glycerol (YPG) and incubated at 28°C or 37°C. For growth rate analysis, we precultured overnight yeast cells in selective medium supplemented with 2% (wt/vol) galactose and 0.1% (wt/vol) glucose and then cultured them in YEP medium supplemented with 2% (wt/vol) glycerol for 24 h, inoculated at a standard density of approximately 1×10^6 cells/ml. We removed samples at 0h, 20h and 24h and determined cell density spectrophotometrically, expressed as OD_{600}. For western blot analysis, yeast cells were cultured overnight in selective medium supplemented with 2% (wt/vol) galactose and 0.1% (wt/vol) glucose and normalized spectrophotometrically at OD_{600}.

Strain	Relevant genotype	Origin
K699	*MATa ho ade2-1 his3-11,15 leu2-3,112 trp1-1 ura3-52 can1-100 ssd1*	Nasmyth et al.1990
yDDB64	*MATa ade2-1 his3-11,15 leu2-3,112 trp1-1 ura3-52 can1-100 yta10::NAT yta12::KanMX6*	DiBella et al.2010
yDDB79	*MATa ade2-1 his3-11,15 leu2-3,112 trp1-1 ura3-52 can1-100 yta10::NAT yta12::KanMX6* pYC6/CT^{ADH1}-Yta10(1-63)-AFG3L2(66-797)-V5/HIS	DiBella et al.2010
yDDB205	*MATa ade2-1 his3-11,15 leu2-3,112 trp1-1 ura3-52 can1-100 yta10::NAT yta12::KanMX6* pYC6/CT^{ADH1}-Yta10(1-63)-AFG3L2(66-797)^{R468C}-V5/HIS	This study
yDDB123	*MATa ade2-1 his3-11,15 leu2-3,112 trp1-1 ura3-52 can1-100 yta10::NAT yta12::KanMX6* pYC6/CT^{ADH1}-Yta10(1-63)-AFG3L2(66-797)^{E691K}-V5/HIS	DiBella et al.2010
yDDB126	*MATa ade2-1 his3-11,15 leu2-3,112 trp1-1 ura3-52 can1-100 yta10::NAT yta12::KanMX6* pYC6/CT^{ADH1}-Yta10(1-63)-AFG3L2(66-797)^{S674L}-V5/HIS	DiBella et al.2010
yDDB127	*MATa ade2-1 his3-11,15 leu2-3,112 trp1-1 ura3-52 can1-100 yta10::NAT yta12::KanMX6* pYC6/CT^{ADH1}-Yta10(1-63)-AFG3L2(66-797)^{E575Q}-V5/HIS	DiBella et al.2010
yDDB211	*MATa ade2-1 his3-11,15 leu2-3,112 trp1-1 ura3-52 can1-100 yta10::NAT yta12::KanMX6* pYC2/CT^{ADH1}-Yta10(1-63)-AFG3L2(66-797)-V5/HIS pYC6/CT^{ADH1}-Yta10(1-63)-AFG3L2(66-797)^{H125Q}-V5/HIS	This study
yDDB212	*MATa ade2-1 his3-11,15 leu2-3,112 trp1-1 ura3-52 can1-100 yta10::NAT yta12::KanMX6* pYC2/CT^{ADH1}-Yta10(1-63)-AFG3L2(66-797)-V5/HIS pYC6/CT^{ADH1}-Yta10(1-63)-AFG3L2(66-797)^{R468C}-V5/HIS	This study
yDDB190	*MATa ade2-1 his3-11,15 leu2-3,112 trp1-1 ura3-52 can1-100 yta10::NAT yta12::KanMX6* pYC2/CT^{ADH1}-Yta10(1-63)-AFG3L2(66-797)-V5/HIS pYC6/CT^{ADH1}-Yta10(1-63)-AFG3L2(66-797)^{E691K}-V5/HIS	DiBella et al.2010
yDDB138	*MATa ade2-1 his3-11,15 leu2-3,112 trp1-1 ura3-52 can1-100 yta10::NAT yta12::KanMX6* YCpLac111^{ADH1}-Yta10(1-63)-paraplegin(59-795)-HA	DiBella et al.2010

Strain	Relevant genotype	Origin
yDDB165	*MATa ade2-1 his3-11,15 leu2-3,112 trp1-1 ura3-52 can1-100 yta10::NAT yta12::KanMX6* pYC6/CT^{ADH1}-Yta10(1-63)-AFG3L2(66-797)-V5/HIS YCpLac111^{ADH1}-Yta10(1-63)-paraplegin(59-795)-HA	DiBella et al.2010
yDDB177	*MATa ade2-1 his3-11,15 leu2-3,112 trp1-1 ura3-52 can1-100 yta10::NAT yta12::KanMX6* pYC6/CT^{ADH1}-Yta10(1-63)-AFG3L2(66-797)^{R468C}-V5/HIS YCpLac111^{ADH1}-Yta10(1-63)-paraplegin(59-795)-HA	This study
yDDB166	*MATa ade2-1 his3-11,15 leu2-3,112 trp1-1 ura3-52 can1-100 yta10::NAT yta12::KanMX6* pYC6/CT^{ADH1}-Yta10(1-63)-AFG3L2(66-797)^{E691K}-V5/HIS YCpLac111^{ADH1}-Yta10(1-63)-paraplegin(59-795)-HA	DiBella et al.2010
yDDB167	*MATa ade2-1 his3-11,15 leu2-3,112 trp1-1 ura3-52 can1-100 yta10::NAT yta12::KanMX6* pYC6/CT^{ADH1}-Yta10(1-63)-AFG3L2(66-797)^{S674L}-V5/HIS YCpLac111^{ADH1}-Yta10(1-63)-paraplegin(59-795)-HA	DiBella et al.2010
yDDB129	*MATa ade2-1 his3-11,15 leu2-3,112 trp1-1 ura3-52 can1-100 yta10::NAT yta12::KanMX6* pYC6/CT^{ADH1}-Yta10(1-63)-AFG3L2(66-797)^{E575Q}-V5/HIS YCpLac111^{ADH1}-Yta10(1-63)-paraplegin(59-795)-HA	DiBella et al.2010

Table 3. Saccharomyces cerevisiae strains used in this study

Western blot analysis and antibodies

For Western blot analysis of yeast cells, trichloroacetic acid (TCA) protein extracts were prepared as described (Muz*i*-Falconi et al., 1993). Western blot analysis of COX subunit was performed on mitochondrial extracts. Protein extracts were separated by SDS-PAGE in 10% or 15% acrylamide gels as indicated and transferred to a PVDF membrane (Immobilon LF, Millipore). Filters were

probed with antibodies as indicated in the text and in the figure legends (Table 4). Fluorescent blot was performed using Alexa Fluor®647-coniugated goat anti-rabbit IgG (H+L) antibody and Alexa Fluor®488-coniugated goat anti-mouse IgG (H+L) antibody (Molecular probes). Fluorescence signals were acquired using G:BOX iChemi (Syngene); quantification was performed using Gene Tools software (Syngene) on four independent western blots normalizing the signals to the ß-actin loading control. For western blot analysis of patient-derived lymphoblasts and fibroblasts, cell lysates from each line were electrophoresed on 10%-15%-SDS-polyacrylamide gels and transferred to a nitrocellulose membrane (Amersham Biosciences) by electroblotting. Filters were probed with indicated antibodies and developed by HRP-conjugated secondary antibodies using a chemiluminescent substrate (ECL Prime, Amersham). Signals were detected by G:BOX iChemi (Syngene).

Antibody	**Reacivity**	**Dilution**	**Distributor/producer**
Anti-ßactin	Yeast	1:1.500	Abcam
Anti-MrpL32	Yeast	1:1000	Koppen et al. 2007
Anti-Ccp1	Yeast	1:1000	Koppen et al. 2007
Anti-porin	Yeast	1:1000	Mitosciences
Anti-Cox1p	Yeast	1:300	MitoSciences
Anti-Cox2p	Yeast	1:1.500	MitoSciences
Anti-Cox3p	Yeast	1:300	MitoSciences
Anti-Cox4p	Yeast	1:1.500	MitoSciences

Anti-AFG3L2	Human	1:12000	DiBella et al. 2010
Anti-par	Human	1:6000	DiBella et al. 2010
Anti-OPA1	Human	1:1000	BD Bioscences
Anti-MrpL32	Human	1:1000	Koppen et al. 2007
Anti-HSP60	Human	1:1000	SantaCruz Biotechnology
Anti-glutathione reductase	Human	1:1000	Labfrontier

Table 4. Antibodies

Assays of respiratory chain complexes activity

For in vitro activity assay of Complex III, IV and V and immunoblot analysis of COX subunits, yeast cells were grown at 28°C in YEP medium supplemented with 2% (wt/vol) galactose-0.1% (wt/vol) glucose. Yeast cell mitochondria were prepared by differential centrifugations. The resulting mitochondrial pellet was resuspended in 10-mM potassium phosphate buffer and freezed and thawed for three times. Protein concentration was determined by Bradford microplate microassay (Bio-Rad) with bovine serum albumin as the standard. Respiratory chain enzymes activity were determined spectrophotometrically as previously described (Magri et al., 2010). Activity was expressed as nanomoles per minute per milligram of protein.

Coimmunoprecipitation of AFG3L2 e paraplegin

For immunoprecipitation experiments, yeast cells were precultured overnight in a selective medium and then grown in 100 ml of YPD medium until 1x 10^7 cell/ml as previously described (Fracasso et al., 2010). Normalized cells were resuspended in PBS, 1 mM PMSF, 1 mM NaVa, 50 mM NaF supplemented with protease inhibitor cocktail (Roche), and homogenized using the FastPrep® System (Qbiogene-MP Biomedicals).

Homogenates were centrifuged and the resulting supernatants were incubated with ant*i*-V5 antibodies. Antigen-antibody complexes were then incubated with protein G MAG-sepharose (GE Healthcare). Samples were eluted from beads and analysed by SDS-PAGE and immunoblotting.

Patient-derived cell lines

Epstein-Barr-virus-stabilized lymphoblastoid cell lines from patients, their relatives and control subjects were established and cultured as previously described (Gellera et al., 2007). Fibroblasts from patient and controls were grown in the DME*M*-High glucose media as described previously(Wong et al., 1999).

Analysis of mitochondrial morphology

For analysis of mitochondrial morphology fibroblasts were grown on coverslips inside a petri dish filled with the appropriate culture medium. When reached the desired confluence, cells were incubated for 15 minutes with a medium containing Mito Tracker Red™(50 nm). The stained cells were fixed using a 1:1 solution of 4% saccharose and 4% paraformaldeyde for 25 min at 37°C under weak agitation, and then in ice-cold methanol for 10 min at room temperature. Samples were analyzed with a TCS NT confocal laser scanning microscope (Leica Lasertecknik GmbH, Heidelberg, Germany) equipped with a 75 mW Kripton/Argon mixed gas laser.

To quantitative analysis, acquired images of mitochondria were analyzed using NIH-developed Image J software (Wayne Rasband, NIH). Row images were first enhanced by 2D deconvolution (Iterative Deconvolve 2D by Robert Dougherty- Copyright (c) 2005, OptiNav, Inc.) and then converted into black and white (binary) images. Particles were analyzed determining AspectRatio (AR) and FormFactor (FF) as quantitative descriptors of mitochondrial morphology.

Results

Concurrent paraplegin mutations occur in AFG3L2-mutated patients

The finding that respiratory competence of yta10Δyta12Δ cells expressing some of the AFG3L2 mutants could be restored by paraplegin (Di Bella et al., 2010) prompted us to analyze whether SCA28 patients could carry abnormalities in the paraplegin-encoding gene. Sixteen SCA28 patients were screened by direct sequencing and MLPA for mutations and deletions in SPG7 gene. Fifteen of them were previously described (Di Bella et al., 2010 and Fracasso et al., submitted). They present with a progressive ataxic phenotype and cerebellar atrophy variably associated with additional features, consistent with the SCA28 phenotype (Cagnoli et al., 2008; Mariotti et al., 2008). The remaining proband, carrying a *de novo* AFG3L2 mutation (R468C), has a more severe phenotype.

Very interestingly, heterozygous mutations in the paraplegin gene were discovered in three index patients. In particular, patient M*I*-A0762 I*I*-1 (Di Bella et al., 2010) heterozygous for the AFG3L2 R702Q mutation presents an SPG7 mutation (c.1529C>T) resulting in the substitution of alanine-510 with valine (p.A510V). Notably, genetic analysis of the available M*I*-A0762 family members demonstrated that the AFG3L2 R702Q and paraplegin A510V mutations cosegregated only in patient I*I*-1, the only positive member of family M*I*-A0762 to exhibit a full-blown ataxic phenotype (Fig.1a). The second index patient presents a deletion of three nucleotides in the *AFG3L2* gene (del c.1706-1708), resulting in the deletion of lysine 569 (Fracasso et al., submitted), along with an heterozygous duplication of a cytosine (c.1052dupC) in the *SPG7* gene causing a frameshift from amino acid 352 (G352fsX43). Unfortunately, very little information is currently available about his clinical phenotype except that he suffers of a chronic progressive form of cerebellar ataxia. Finally, a deletion of SPG7 exons 4-6 was discovered in the patient carrying the AFG3L2 R468C mutation (Fig.1b). The clinical presentation of this patient is characterized by early-onset optic atrophy and a L-dopa-

responsive spastic-ataxic syndrome with extrapyramidal signs. Moreover, a muscle biopsy revealed an isolated complex I deficiency.
While R468C is a *de novo* mutation, the SPG7 deletion is maternally-inherited. The mother and the two brothers of the patient, who present only the paraplegin deletion, were completely unaffected, consistently with the recessive nature of *SPG7* mutations. Since the proband is the only family member carrying the R468C mutation, it is not possible to establish which is the relative role of AFG3L2 and SPG7 mutations in phenotype determination. Arginine 468 is a crucial residue for intersubunit communication and catalysis; its substitution with a cystein abolishes the arginine finger in the ATP-binding site which is necessary for ATP hydrolysis (Ogura et al., 2004). Therefore, functional studies in yeast were performed to better characterize this mutation and investigate genotype-phenotype correlation. Furthermore, to get insight into the pathogenic mechanisms in a native genetic context, we performed biochemical and cell biology studies in patient-derived cells.

The AFG3L2 mutation R468C functionally inactivates both homo- and heterocomplexes

Our previous studies demonstrated that the facultative aerobic yeast *Saccharomyces cerevisiae* is an appropriate and useful model for assessing the functional consequences of disease-segregating mutations in human *m*-AAA proteases (Di Bella et al., 2010). Therefore, we used this model to investigate the effect of the R468C variant, overexpressing the human AFG3L2^{R468C} in a *m*-AAA–defective strain (*yta10Δyta12Δ*). As reference mutations, we used the yeast strains carring AFG3L2^{E691} and AFG3L2^{S674L}, two previously described pathogenic substitutions (Di Bella et al., 2010). First, we evaluated the ability of the mutated homocomplex (composed of AFG3L2^{R468C} only) to support respiration (Fig.2a). Yeast cell lacking the endogenous *m*-AAA protease are not able to grow on a nonfermentable carbon source such as glycerol (YPG) indicating a respiratory defect (OXPHOS phenotype). As expected, the respiratory defect is complemented by the expression of human AFG3L2^{WT}. On the

contrary, AFG3L2^{R468C} , like AFG3L2^{E691} and AFG3L2^{S674L}, did not restore respiration suggesting that this substitution is deleterious for homocomplex function.

Since in human mithochondria the *m*-AAA complex exists also in a hetero-oligomeric form containing AFG3L2 and paraplegin subunits in equimolar ratios, we examined the effect of R468C mutation on heterocomplex function coexpressing AFG3L2^{R468C} and paraplegin (Fig.2b). The *yta10Δyta12Δ* strain carrying AFG3L2^{R468C}/paraplegin still had a respiratory-deficient phenotype indicating that the R468C mutation is not rescued by paraplegin, similarly to the reference mutation E691K. On the contrary, the other reference mutation, S674L, belongs to the group of the paraplegin-responsive mutations as previous described (Di Bella et al., 2010).

In order to discriminate between haploinsufficiency and negative dominant mechanism, we investigated whether mutant subunits can suppress the *m*-AAA complex activity also in the presence of wild-type subunits (Fig.2c). To better evaluate growth rates, we determined yeast cells concentration by measuring the optical density (OD) of a 24h culture in liquid YPG medium. Coexpression of AFG3L2^{WT} in cells carrying AFG3L2^{R468C} resulted in a limited recovery of respiratory capacity. Altogehter, these experiments demonstrate the pathogenicity of R468C variant and that this amino acid change functionally inactivates both homo- and heterocomplex with a dominant negative mechanism.

In vitro activity and immunoblot analysis of respiratory chain complexes reveal a defect comparable to cells lacking endogenous *m*-AAA

Several study demonstrate that the yeast *m*-AAA is involved in the assembly and maintenance of respiratory complexes (Tauer et al., 1994; Arlt et al., 1996; Arlt et al., 1998). To better elucidate the mechanism responsible for the OXPHOS phenotype induced by this SCA28 mutation, we quantitatively determined respiratory-chain activity (Fig.3a). *In vitro* activity assay for complex III, IV, and V were evaluated

separately in the yeast *m*-AAA-deficient strain and in strains carrying the R468C and the reference mutations both in the presence and in the absence of paraplegin. The activity of complex III and V in AFG3L2^{R468C} strain is reduced by at ≥80% with respect to AFG3L2^{WT}. Complex IV activity is even more affected with ≥90% reduction. Notably, R468C shows the same reduction observed in cells (*yta10Δyta12Δ*) lacking endogenous *m*-AAA, whereas the two reference mutations caused a lower decrease of specific activity. Respiratory enzymes deficiency persists unchanged upon coexpression of paraplegin confirming the dominant effect of the R468C mutation. Moreover, in order to verify if the respiratory defect is due to a selective deficit of some subunits, we evaluated the levels of the mitochondria-encoded cytochrome *c* oxidase (COX) subunits Cox1p, Cox2p and Cox3p, which constitutes the catalytic core of the enzyme, and of the nuclear-encoded subunit Cox4p (Fig.3b). Protein quantitation of fluorescent immunoblots shows a severe reduction of all the analyzed subunits indicating a general downregulation of the whole enzyme. Quantitative evaluation of the OXPHOS phenotype allowed us to highlight the severity of R468C mutation.

Impairment of proteolytic and dislocase activity in AFG3L2^{R468C} yeast

The activity of human *m*-AAA proteases in yeast cells can be monitored directly by western blot analysis of substrates of the endogenous protease, namely, the ribosomal subunit MrpL32 and the ROS-scavenger protein Ccp1 (Nolden et al., 2005; Esser et al., 2002). We used the conversion of MrpL32 from its precursor form (pMrpL32) to its mature form (mMrpL32) as an indicator of the overall proteolytic competence. The fluorescent immunoblot analysis of MrpL32 allowed the quantification of accumulated unprocessed precursor, expressed as the ratio of pMrpL32-to-total MrpL32 levels (Fig.4a). pMrpL32 accumulates in AFG3L2^{R468C} strains both in the presence and in the absence of paraplegin at the same level of yta10Δyta12Δ cells.

Moreover, we evaluated the maturation of Ccp1 as a detector of the ATP-dependent dislocase activity of *m*-AAA complex. In fact, while the N-terminal targeting sequence of MrpL32 is cleaved off directly by the *m*-AAA complex after completion of mitochondrial import, the maturation of Ccp1 requires a two-step mechanism. Initially, the *m*-AAA protease dislocates the newly imported precursor of Ccp1 (pCcp1) in the inner membrane through its ATP-dependent pull out activity and removes the transmembrane segment making a second processing site accessible. Subsequently, the intermediate Ccp1 is cleaved by the intramembrane proteolytic activity of the rhomboid protease Pcp1 and is finally released as mature Ccp1 (mCcp1) into the inter membrane space (Tatsuta et al., 2007; Bonn et al., 2011). We quantified precursor accumulation as the ratio of pCcp1 levels to total Ccp1 levels in yeast strains harbouring R468C and the two reference mutations of AFG3L2 alone or coexpressing paraplegin (Fig.4b). In AFG3L2^{R468C} strain the processing of Ccp1 is abolished at the same level as in *m*-AAA–deficient yeast cells and pCcp1 accumulates. On the contrary, the two reference AFG3L2 mutations, E691K and S674L, are able to partially restore Ccp1 processing: pCcp1 accumulates at a lesser, but statistically significant extent. The presence of paraplegin does not improve Ccp1 maturation in the R468C strain confirming the dominant effect of this mutation. Surprisingly, paraplegin coexpression completely rescues the mild S647L defect, but worsens the E691K ones. Notably, the defect of Ccp1 maturation does not always correlate with the defect of MrpL32 processing indicating not only that these two substrates involve different *m*-AAA activities, but also that different mutations can differently affect the proteolytic and the ATP-dependent dislocase activity. The results clearly indicate that the R468C mutation disrupts completely both *m*-AAA activities.

AFG3L2^{R468C} compromises autoprocessing and paralegin maturation.

Since mouse Afg3l1 and Afg3l2 mediate their own maturation in an autocatalytic manner (Koppen et al., 2009), we analysed human *m*-AAA

subunits processing in yeast (Fig.5a-b). Initially, we performed immunoblot analysis of strains expressing homocomplex carrying the disease-causing mutation R468C, the reference mutations E691K and S674L, and the proteolytic inactive mutant E575Q. The yeast strain expressing paraplegin alone was used as negative control. AFG3L2^{WT} accumulates as the mature form (m) whereas the proteolytically inactive AFG3L2^{E575Q} accumulates as a larger form (p, precursor)(Fig.5a). These data indicate that human AFG3L2 undergoes autocatalytic processing when expressed in yeast, as the homolog mouse subunits Afg3l2 and Afg3l1. Both reference mutations E691K e S674L show a doublet band in which the slightly larger form likely represents an intermediate (i) processing product, while the smaller band corresponds to the mature (m) form. AFG3L2^{R468C} is present not only as mature and intermediate forms, but also as precursor protein, indicating that this disease-causing mutation substantially impairs autoprocessing.

Moreover, in order to evaluate paraplegin processing and AFG3L2 autoprocessing in the heterocomplex, we repeated the same experiment in the presence of paraplegin (Fig.5b). AFG3L2^{WT} coexpressed with paraplegin appears as a doublet composed of the intermediate and the mature forms equally represented. The reference mutant AFG3L2^{S674L} exhibits the same band pattern of AFG3L2^{WT} confirming its paraplegin-responsive nature. On the contrary, AFG3L2 with the second reference mutation E691K, which is not rescued by paraplegin, is present mainly as intermediate form. Finally proteolytic inactive AFG3L2 E575Q accumulates as intermediate form and to a small degree as precursor, but not as mature form confirming that AFG3L2 maturation required its own proteolytic activity. Notably, the R468C mutation appears to behave in a different manner from the other mutations: in this case the AFG3L2^{R468C} protein is almost completely unprocessed and exists as a precursor species only.

Since newly imported paraplegin is cleaved by MPP in mouse, giving rise to an intermediate form that is subsequently converted into the mature protein by Afg3l1 and Afg3l2 (Koppen et al., 2009), we evaluated if also in the human heterocomplex AFG3L2 is able to process the cognate subunit

(Fig.5b). In yeast cells, paraplegin alone accumulates mostly into a larger form (p, precursor) and to a lesser extent into a smaller band. As paraplegin alone is inactive and not able to assembly in a functional homocomplex (Koppen et al., 2007), the smaller band may represents a product of degradation. AFG3L2^{WT}/paraplegin expression results in the accumulation of two forms of paraplegin, both smaller than the precursor protein. We termed the larger one intermediate (i) and the smaller one mature (m). All strain carrying mutated AFG3L2 (R468C, E691K, S674L and E575Q) present an accumulation of paraplegin intermediate form, but only E691K and S674L show also the presence of the mature paraplegin. In strain expressing R468C, paraplegin exhibits a second band smaller than the mature form, while paraplegin coexpressed with the AFG3L2 proteolytic mutant E575Q shows a different pattern composed of several bands, none of them corresponding to the mature form. These data indicate that AFG3L2^{WT}, AFG3L2^{E691K}, and AFG3L2^{S674L} are able to process paraplegin into the mature form, while AFG3L2 carrying the R468C mutation and the proteolytically inactive mutant does not process paraplegin that likely undergoes a different degradation process.

In order to verify this hypothesis, we investigated which paraplegin forms interact with AFG3L2 subunits by co-immunoprecipitating heterocomplexes in strain carrying AFG3L2^{R468C} (Fig.5c). In particular, wild-type or R468C AFG3L2 was pulled down with ant*i*-V5 antibody and immunoprecipitates (IP) were analyzed by western blot using specific antibodies against AFG3L2 and paraplegin. In the yeast strain carrying paraplegin alone, used as negative control, no immunoprecipitation with ant*i*-V5 Ab can be observed. By contrast, in yeast cells expressing wild-type or mutant AFG3L2 with paraplegin, immunoprecipitation experiments show that AFG3L2^{WT} interacts mainly with mature paraplegin, while AFG3L2^{R468C} interacts mostly with the intermediate form. These results indicate that both the intermediate and the mature form of paraplegin assembly with AFG3L2. Although AFG3L2^{R468C} interacts with intermediate paraplegin, this mutation is not able to support paraplegin maturation, leading to the formation of inactive heterocomplexes.

Taken together, functional studies in yeast reveal that *m*-AAA complexes affected by R468C mutation do not retain any activity, with proteolytic activity, dislocase activity and autocatalytic processing being almost completely abolished. Furthermore, this mutation impairs active complex assembling. Therefore, yeast strain expressing AFG3L2R468C are comparable from a functional point of view to cells lacking endogenous *m*-AAA (*yta10Δyta12Δ* strain). In order to verify whether expression of human AFG3L2^{R468C} affects mitochondria to the same degree as the absence of *m*-AAA does, we evaluated the reduction of mitochondrial content (Fig.5d). Total amount of mitochondria was indirectly measured as ratio between a mitochondrial and a cytosol housekeeping protein. To this purpose, actin and porin were quantified by fluorescence immunoblotting in yeast strains lacking *m*-AAA or expressing human WT and R468C AFG3L2. The yeast strain carrying R468C shows 40% reduction of the porin:actin ratio as compared to WT, due to a decrease of porin level. On the contrary, the *yta10Δyta12Δ* strain does not present any statistically significant difference from WT strain. These data suggest that the expression of AFG3L2^{R468C} affects mitochondria more than the lack of *m*-AAA. The negative effect of AFG3L2^{R468C} could be due to an overload of mitochondrial quality control system. In fact, the lack of endogenous *m*-AAA complex impairs the mitochondrial quality control system. Since R468C impairs AFG3L2 correct assembling, its overexpression may results in the accumulation of a misfolded mitochondrial protein, thus constituting an additional load for the already defective mitochondrial quality control system.

Immunoblot analysis reveal an altered processing of OPA1 in patient's lymphoblasts and fibroblasts

In order to evaluate the impairment of non-neuronal cell lines and tissue, protein extract from lymphoblasts were analyzed by western blot under denaturing conditions (Fig.6a). In the patient carrying both AFG3L2^{R468C} and SPG7$^{ex4\text{-}6del}$, lymphoblasts AFG3L2 level is comparable to control cells', while the level of paraplegin is mildly reduced, consistent with the

heterozygous condition. Moreover, in order to examine whether patient cells show aberrant processing of protein known to be substrates of the *m*-AAA complex in mice, we analysed both Mrpl32 and OPA1 by western blot. MrpL32 is a nuclear-encoded protein of the mitochondrial ribosome processed by *m*-AAA in yeast (Nolden et al., 2005). Although both Mrpl32 and *m*-AAA are highly conserved in eukaryotes, their interaction is not clearly demonstrated in mammals (Nolden et al., 2005; Maltecca et al., 2008; Martinelli et al., 2009). OPA1 is a dynamin-related protein essential for mitochondrial fusion machinery in mammals (Chan, 2006; Duvezin-Caubet et al., 2006; Ishihara et al., 2006). Alternative splicing and post-translational proteolytic processing produces several OPA1 isoforms. At least five different forms are detected in mammals: two long forms (L1 e L2) and three short forms (S3, S4 and S5). Several proteases of the inner mitochondrial membrane have been linked to OPA1 processing, including *m*-AAA, but their respective roles still have to be clarified (Cipolat et al., 2006; Ishihara et al., 2006; Duvezin-Caubet et al., 2007; Ehses et al., 2009).

Western blot analysis on lymphoblast extracts revealed normal processing of MrpL32, while OPA1 showed an abnormal processing pattern (Fig.6a). In particular, we observed a reduction of the long form L2 and the short one S4. In order to delve deeper into this issue, we evaluated substrate processing also in fibroblasts cultured under different conditions (Fig 6b). In particular, we treated fibroblasts grown in high-glucose medium with: (1) MG132, a specific proteasome inhibitor which impairs the degradation of unprocessed precursors by the ubiquitin-proteasome machinery thus promoting their accumulation; (2) valinomycin, a ionophore that makes the inner membrane permeable to potassium and destroys the membrane potential, thus preventing correct import and processing of mitochondrial precursor proteins. Additionally, in order to expose fibroblasts to a mild metabolic stress, we performed the same treatments on cells grown in a medium containing galactose, which enhances the effects of a mitochondrial dysfunction (Palmfeldt et al., 2009). In high glucose-medium, MG132 treatment allows accumulation of two MrpL32 forms larger than the mature one, the precursor (p) and the intermediate (i)

form. On the contrary, the addiction of valinomycin causes a reduction of mature level probably as a consequence of mitochondrial damage. The combined used of MG132 and valinomycin results in a greater accumulation of precursor and intermediate forms to the expense of mature protein. While fibroblasts cultured in galactose medium present only mature protein after proteasome inhibition with MG132, in the presence of valinomycin they die within few hours and cannot be analyzed.

Although cultured in conditions allowing precursor detection, patient's fibroblasts show the same MrpL32 immunoblot pattern as that of control cells and accumulate MrpL32 precursor and intermediate at the same level.

Galactose-induced mild metabolic stress allowed to enhance OPA1 aberrant processing (Fig. 6b). Although a difference between patient and control OPA1 pattern can be appreciated also in high-glucose medium both in the presence and in the absence of MG132, a 48h-incubation in galactose medium enhances the reduction of OPA1 long forms and the accumulation of the short ones. From these experiments, we can conclude that there is no alteration of MrpL32 level or processing in patient's fibroblasts and lymphoblasts. By contrast, *m*-AAA impairment causes loss of OPA1 long forms also in non-neural tissues. These findings reveal for the first time an aberrant mitochondrial phenotype in cells from individuals affected by *m*-AAA defects.

Abnormal mitochondrial morphology in patient's fibroblasts

Since a balance of short and long OPA1 forms is required for mitochondrial fusion activity in mammals (Song et al., 2007; Lenaers et al., 2009), we investigated the functional consequence of impaired OPA1 processing evaluating morphology of the mitochondrial network. Patient and control fibroblasts were grown in high glucose medium and pyruvate-enriched medium. The addition of pyruvate enhances cellular respiration increasing TCA cycle flux. Cells were stained with Red MitoTracker®, a dyes that selective accumulates in mitochondria regardless of their membrane

potential. Analysis by confocal microscopy revealed a drastic fragmentation of the mitochondrial network in patient's fibroblasts as compared to control cells (Fig.7a). In particular, mitochondria appear as a branched reticulum of connected tube-like filaments in most control cells. On the contrary, patient fibroblasts present an almost completely fragmentation of the network: mitochondria appear as ellipsoid-shaped vesicles, short tubes or take the form of a tennis racket.

In order to quantitate these changes in mitochondrial morphology, acquired images of mitochondria were analyzed using NIH-developed Image J software (Wayne Rasband, NIH). Raw images were first enhanced by 2D deconvolution (Iterative Deconvolve 2D by Robert Dougherty-Copyright (c) 2005, OptiNav, Inc.) and then converted into black and white (binary) images. Finally all particles were analyzed determining for each object several parameters such as area (Am), perimeter (Pm), maximal and minimal radius. In particular we used AspectRatio (AR) and FormFactor (FF) as quantitative descriptors of mitochondrial morphology. AspectRatio is the ratio between the major and minor axis of the ellipse equivalent to the mitochondrion and reports changes in length, whereas FormFactor (defined as [Pm2]/[4πAm]) allows to quantify the degree of branching (Koopman et al., 2006). Both parameters are independent from image magnification and have a minimal value of 1, corresponding to a circular mitochondrion. Higher values of AR and FF correspond to longer and more branching mitochondria respectively. Scatter graphs in Fig.7b and c plot AR as a function of FF. Each scatter plot in panel c illustrates mitochondria shapes of a single cell in one of the four conditions: patients or control cells; incubated with or without pyruvate. Overlapping the four graphs (panel b) highlights the differences between patient and control mitochondria shape. Control cells grown without pyruvate present mitochondria with high degree of branching (high FF value), while in the presence of pyruvate they show longer and more filamentous mitochondria (high AR value). On the contrary, patient's cells present mostly short and less branched mitochondria either in the presence and in the absence of pyruvate. Accordingly, bar graphs in Fig.7d, which represent average AR and FF values calculated on at least four randomly

selected cells in the different conditions, display lower average values of FF and AR in patient's cells than in control cells.

In conclusion, analysis of mitochondrial morphology shows a drastic fragmentation of mitochondrial network in patient fibroblasts, very likely resulting from loss of long-OPA1 forms.

Discussion

SCA28 is an autosomal dominant form of cerebellar ataxia characterized by juvenile onset, slow disease progression, eye movement abnormalities, and, in some cases, pyramidal signs. Mutation screening allowed to establish a minimum frequency of ~1.7% in our cohort of patients (Di Bella et al., 2010, Fracasso et al., submitted). The functional characterization of the identified mutations in a yeast model demonstrated that coexpression of paraplegin has a different effect on different AFG3L2 mutations. The majority of AFG3L2 mutations is fully rescued by paraplegin expression in yeast, while a second group of mutations are non responsive or only partially responsive to paraplegin (Di Bella et al., 2010, Fracasso et al., submitted). This observation suggests the idea that paraplegin could modulate the phenotype of AFG3L2 mutations also in humans. In particular, co-inherited paraplegin mutations could explain more severe clinical presentation within the same family and/or different phenotypes of some individuals. Interestingly, three of the sixteen SCA28 probands that we screened present a concurrent *SPG7* heterozygous mutation (~18%). Initially, the A510V mutation of *SPG7* was found in family M*I*-A0762 in association with the *AFG3L2* mutation R702Q. Notably, the segregation of the paraplegin mutation is consistent with the phenotypic variability observed in this family: the proband carrying both *AFG3L2*^{R702Q} and *SPG7*^{A510V} shows a full-blown ataxic phenotype, whereas her mother and her maternal uncle, carrying only the *AFG3L2* mutation present only a moderate cerebellar atrophy at MRI. This genotype-phenotype correlation suggests that the SCA28 cerebellar degeneration is aggravated by the presence of a loss-of-function mutation in the AFG3L2 partner paraplegin. The second patient carries *AFG3L2*^{K569del} in association with a single nucleotide insertion in *SPG7* exon 8 causing a frameshift (G352fsX43). Unfortunately, DNA from the patient's parents was not available for segregation studies. Finally, the third proband presents the missense mutation R468C of *AFG3L2* and the deletion of exons 4, 5, and 6 of *SPG7*. She is the only affected member of family M*I*-PPS0722 because of the *de novo* nature of AFG3L2 mutation. On the contrary, the

maternally inherited *SPG7* deletion was present also in her two brothers. Interestingly, this patient presents a novel early-onset phenotype characterized by an important optic atrophy since the age of 5 years, a L-dopa-responsive spastic paraparesis from the age of 6, extrapyramidal signs and dysarthria. Moreover, unlike any other previously described SCA28 affected individuals, this patient presents evidence of mitochondrial involvement. In fact, analysis of muscle biopsy revealed an isolated Complex I deficiency. The severity of her clinical presentation prompted us to functionally characterize the R468C mutation. Furthermore, availability of patient's fibroblasts allowed us to investigate the molecular mechanism in the native genotype. *In silico* analysis revealed that arginine 468 belongs to the highly conserved SRH region of the ATPase domain. Site-directed mutagenesis of the corresponding arginine of various AAA/AAA+ ATPases had showed that this residue is essential for ATP hydrolysis. Moreover in the crystal structure model, this arginine protrudes in the ATP-binding pocket of the adjacent subunit in such a way that its planar and positively charged side chain can interact with the γ-phosphate of ATP (Ogura et al., 2004). In order to verify the crucial role of this residue in the human *m*-AAA, we assessed the functionality of human mutated AFG3L2 in a yeast model. Since human *m*-AAA protease can complement the loss of the homologous yeast complex, we investigated the ability of the mutated AFG3L2 to carry out the activity of the endogenous complex. The respiratory phenotype of the *m*-AAA-lacking strain is not rescue by AFG3L2^{R468C} demonstrating the pathogenicity of this variants. Consistently, yeast strain expressing AFG3L2^{R468C} shows 80% reduction of respiratory chain activity due to decreased levels of both mitochondrial- and nuclear-encoded protein. To delve deeper into the molecular mechanism of this mutation, we evaluated specifically the proteolytic activity of the mutated protease by measuring MrpL32 processing, and the dislocase activity by determining the ability to pull Ccp1 precursor out of the inner membrane. The results showed clearly a dramatic impairment of both proteolytic and dislocase activities comparable to that observed in the absence of functional protease (*yta10Δyta12Δ* strain). Furthermore, these defective phenotypes persist unchanged upon expression not only of

wild-type paraplegin, but also of wild-type AFG3L2 subunits, which strongly suggests a dominant negative mechanism. The deleterious effect of this mutation on the other subunits, either paraplegin or AFG3L2, could be explained by the role of this residue in intersubunit communication. Functional studies on orthologue preoteases suggest that this arginine acts as a sensor for the presence of ATP in the neighbour subunit (Ogura et al., 2004). According to the hypothesis of coordinate ATP hydrolysis between adjacent subunit and synchronized open-close motions of subunits that drive the translocation of a substrate polypeptide to the protease catalytic sites (Suno et al., 2006), this residue could contribute to couple the free energy of ATP hydrolysis to the conformational changes necessary for protease functioning.

The characterization of the yeast Yta10/Yta12 complex demonstrate that ATP binding is essential for *m*-AAA assembling, whereas ATP hydrolysis and its own proteolytic activity are not necessary for the *m*-AAA complex correct folding (Arlt et al., 1996). On the contrary, in mammals ATP-dependent preoteolytic activity is necessary for the formation of an active *m*-AAA. In particular, both Afg3l1, that in human is a pseudogene, and Afg3l2 undergo autocatalytic processing and mediate paraplegin maturation upon assembly into complexes (Koppen et al., 2009). In consideration of the above, we investigated if the formation of a functional *m*-AAA in humans requires its proteolytic activity as in mammals. Western blot analysis of wild-type and proteolytically inactive protease demonstrate that human AFG3L2 mediate both their own maturation and paraplegin processing. Moreover, co-immunoprecipitation experiments reveal that also unprocessed forms of AFG3L2 and paraplegin interact and can assemble into an inactive complex. We can therefore conclude that AFG3L2 induces its own and paraplegin maturation through its ATP-dependent proteolytic activity. Consistently with its inability to process substrates, R468C mutation impairs both AFG3L2 autoprocessing and paraplegin maturation. Although the expression of human *m*-AAA protease in heterologous hosts as the budding yeast *Saccharomyces cerevisiae* is very useful to investigate the functionality of the complex, it tells us little about its physiological and pathological function in human cells. In order

to get insight into the pathogenic mechanism, we investigated the consequence of human *m*-AAA alterations in patient-derived cells. Since some substrates of the yeast and murine *m*-AAA complex are known, we evaluated the impairment of the homologous substrates in human cells. While there is no mammalian homologue of the yeast ROS-scavenger Ccp1, the nuclear-encoded subunit of the mitochondrial ribosome protein MrpL32 is highly conserved from yeast to human. In yeast the *m*-AAA protease mediates the proteolytic maturation of MrpL32 upon import into mitochondria allowing the completion of ribosome assembly (Nolden et al., 2005). Thus, impaired MrpL32 maturation could be sufficient to explain the respiratory phenotypes observed in *m*-AAA -deficient yeast cells. In mammals the role of *m*-AAA in MrpL32 processing is still controversial. Although murine MrpL32 is processed by murine *m*-AAA in a heterologous expression system (Nolden et al., 2005), its processing is only slightly reduced in the liver of paraplegin-deficient mice (Nolden et al., 2005) and in the cerebellum of $Spg7^{-/-}/Afg3l2^{Emv66/+}$ mice (Martinelli et al., 2009). Moreover, an impairment of mitochondrial translation was observed in the liver of $Spg7^{-/-}$ mice (Nolden et al., 2005), but not in the brain of $Afg3l2^{Emv66/Emv66}$ and $Spg7^{-/-}/Afg3l2^{Emv66/+}$ (Maltecca et al., 2008; Martinelli et al., 2009). Western Blot analysis of human MrpL32 in lymphoblasts and fibroblasts did not reveal any differences in protein level and processing between patient and controls. Furthermore, we treated fibroblasts with MG132 to prevent protease degradation and promote the accumulation of unprocessed precursor. Since also in this condition MrpL32 precursor accumulates at the same level in patient's and control's cells, we conclude that *m*-AAA mutations does not affect MrpL32 processing in patient's lymphoblasts and fibroblasts.

Although the SCA28 patients previously analysed in our lab did not show any abnormality of OPA1 isoform pattern (Di Bella et al., 2010, Supplementary Figure 9), we evaluated OPA1 processing in this proband because of the presence of severe optic atrophy since five years of age. In fact, mutations in the *OPA1* gene cause a dominantly-inherited form of optic atrophy. OPA1 is a dynamin-like GTPase involved in mitochondrial fusion and inner membrane remodelling. Interestingly it has been recently

proposed to be regulated by the *m*-AAA protease in mice (Duvezin-Caubet et al., 2007; Ehses et al., 2009). OPA1 exists in at least five forms generated by alternative splicing and proteolytic processing events at two sites, S1 and S2 (Ishihara et al., 2006). Since both long and short forms are required for mitochondrial fusion (Song et al., 2007), the highly regulated OPA1 processing is strictly linked with mitochondrial morphology. In mice, Yme1L1, which constitutes the *i*-AAA protease, regulates OPA1 cleavage at S2, whereas Parl, Oma1 and the *m*-AAA protease seems to be involved in cleavege at S1, though their relative roles are not still elucidated (Cipolat et al., 2006; Ishihara et al., 2006; Duvezin-Caubet et al., 2007; Ehses et al., 2009). Western blot analysis of patient-derived cells reveals an aberrant OPA1 processing. In particular, the long form L2 and the short form S4 are reduced in both lymphoblasts and fibroblasts. Moreover, incubation in galactose medium, which generates a mild metabolic stress, enhances the aberrant processing of OPA1 in the patient's fibroblasts. This could be due to the increased workload of the respiratory pathway. In fact, fibroblasts incubation with galactose results in increased levels of respiratory chain proteins, but not of quality control system proteins such as AFG3L2 and mitochondrial morphology-related proteins such as OPA1 (Palmfeldt et al., 2009). Consistently with the loss of long OPA1 forms, analysis of mitochondrial morphology in patient's cell lines revealed an important fragmentation of the mitochondrial network compared to control cells. Furthermore, quantitative evaluation of mitochondrial fragmentation underlines the effect of pyruvate on fibroblast. In healthy cells, the majority of mitochondria are organized in a branched reticulum, whereas the addition of pyruvate in the medium results in linearization and elongation of mitochondria. By contrast, in patient cells, mitochondria appear as ellipsoid and circle particles, short tubes or take the form of a tennis racket both in the absence and in the presence of pyruvate. The observed fragmentation is presumably due to the impairment of fusion events caused by an unbalance between long and short OPA1 forms. It has still to be elucidated if this mitochondrial fragmentation is a direct consequence

of the loss of *m*-AAA activity on OPA1, or a secondary effect caused by another mitochondrial injury.

In conclusion, this study reveals the presence of concurrent loss-of-function mutations in the *SPG7* gene in a significant percentage of SCA28 patients (~18%). Since in the family with more than one affected individuals the presence of SPG7 mutation consistently segregates with the more severe phenotype, we can hypothesize that the presence of a loss-of-function mutation in paraplegin may act as a disease modifier for heterozygous AFG3L2 mutations. Moreover, cosegregation of a mutation in a crucial residue of AFG3L2 and of a haploinsufficiency mutation in the partner protein paraplegin results in a complex phenotype, thus expanding the clinical spectrum of AFG3L2-associated mutations. Functional studies allowed us to identify the aberrant OPA1 processing as the first disease-related alteration observed in patient cells. These findings may shed light on the pathogenetic mechanism of spinocerebellar degeneration due to SCA28 mutations. We can hypothesize that the pathogenic mechanism in the nervous system is the same in all the SCA28 patients, even if only the more severely affected individuals show a phenotype in non-neuronal-tissue. In fact, until now, this is the only SCA28 patient presenting an aberrant phenotype in peripheral cells probably because of the crucial function of the mutated AFG3L2 residue and the concurrent heterozygous mutation of SPG7. Finally, the observation of an altered processing of OPA1 but not of MrpL32 in non-neuronal-tissue suggests that MrpL32 is not likely to be the first cause of mitochondrial impairment in human.

Figures

a

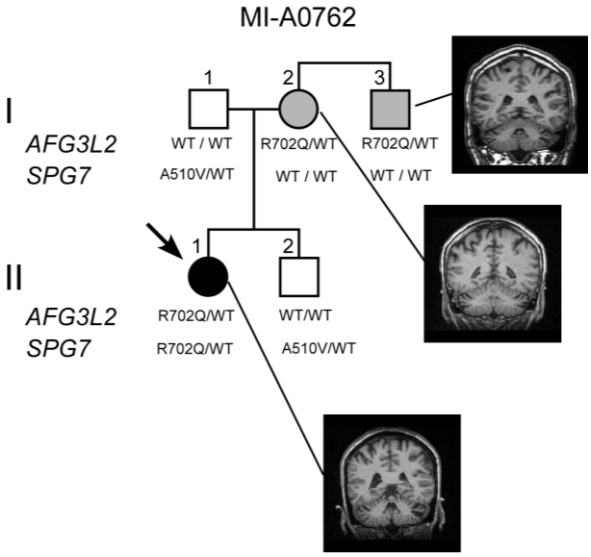
MI-A0762
I
II
AFG3L2
SPG7
1
2
3
WT / WT
A510V/WT
R702Q/WT
WT / WT
R702Q/WT
WT / WT
1
2
R702Q/WT
R702Q/WT
WT/WT
A510V/WT

b

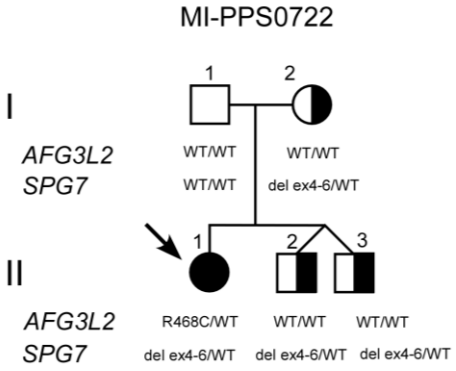
MI-PPS0722
I
II
AFG3L2
SPG7
1
2
WT/WT
WT/WT
WT/WT
del ex4-6/WT
1
2
3
R468C/WT
del ex4-6/WT
WT/WT
del ex4-6/WT
WT/WT
del ex4-6/WT

Figure 1 Segregation of SPG7 and AFG3L2 mutations.

(a) Pedigree and MRI of family M*I*-A0762. (b) Pedigree of families M*I*-PPS0722. Square and circle symbols are male and female individuals, respectively. Symbols filled in black represent affected individuals, while symbols filled in gray are paucisymptomatic individuals. AFG3L2 and SPG7 genotypes are indicated under the symbols of the sampled individuals.

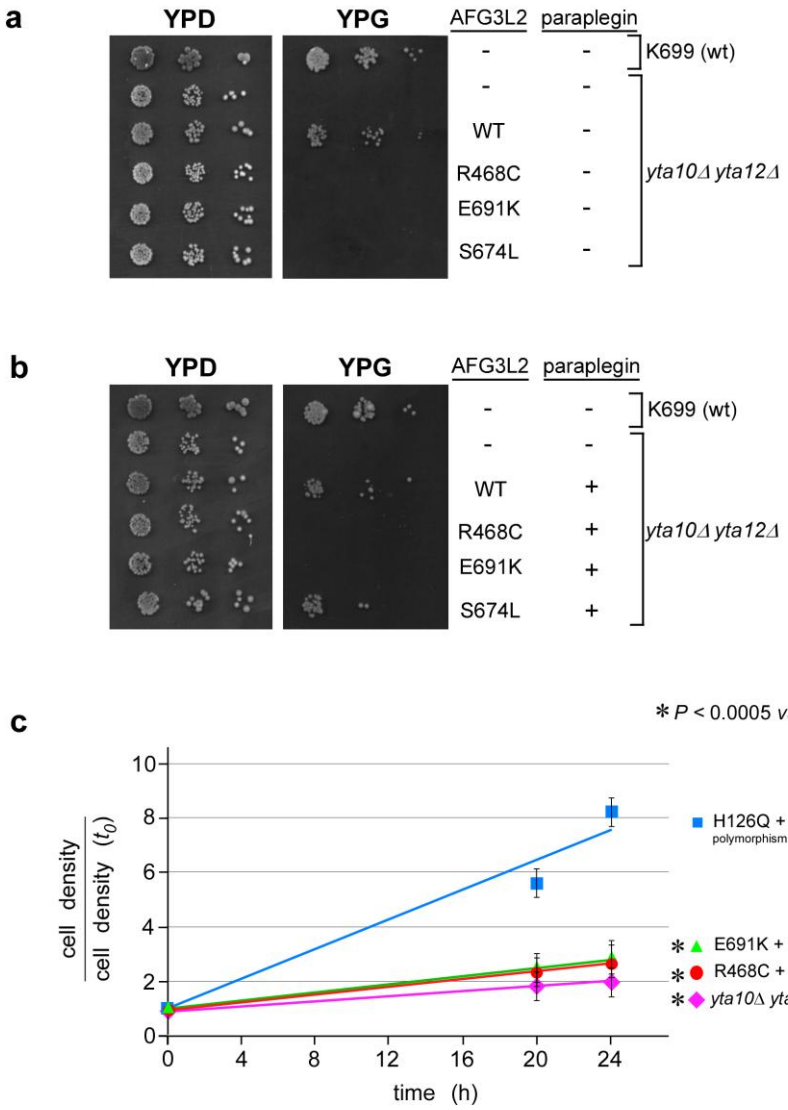
a
YPD
YPG
AFG3L2
paraplegin
-
-
K699 (wt)
-
-
WT
-
R468C
-
E691K
-
S674L
-
yta10Δ yta12Δ
b
YPD
YPG
AFG3L2
paraplegin
-
-
K699 (wt)
-
-
WT
+
R468C
+
E691K
+
S674L
+
yta10Δ yta12Δ
c
* P < 0.0005 vs H126Q+WT
cell density / cell density (t0)
time (h)
0
2
4
6
8
10
0
4
8
12
16
20
24
H126Q + WT
polymorphism
* E691K + WT
* R468C + WT
* yta10Δ yta12Δ

Figure 2 Respiratory phenotype of *yta10*Δ*yta12*Δ cells expressing AFG3L2^{R468C}.

(a,b) Serial dilutions of normalized yeast cultures were spotted on YEP plates containing 2% glucose (YPD) or 2% glycerol (YPG) and incubated ay 28°C for 3 days. Respiratory competence was deduced by the ability to grow on 2% glycerol (YPG). **(a)** Respiratory phenotype of K699 (WT yeast strain) and *yta10*Δ*yta12*Δ cells expressing either normal (WT) or mutant human AFG3L2 (R468C and the two reference mutations E691K and S674L previously described in Di Bella et al. 2010). **(b)** Respiratory phenotype of K699 and *yta10*Δ*yta12*Δ cells coexpressing either normal or mutant human AFG3L2 with human paraplegin. **(c)** Growth rates of cells coexpressing mutated and wild type AFG3L2. Yeast strains were grown in YEP medium supplemented with 2% (wt/vol) galactose and 0.1% (wt/vol) glucose for 24 hours at 28°C. Cell density were evaluated at 0, 20, and 24 hours by measure spectrometrically the optic density at 600nm. Values on the *y*-axis represent the ratio between cell density at a given time and cell density at start (*t0*). Each value represents the mean of five independent experiments. Graph represents the growth rates expressed as tendency lines. Bars indicate ± 1 standard deviation. Asterisks represent statistical significance ($P < 0.0005$) vs the wt strain.

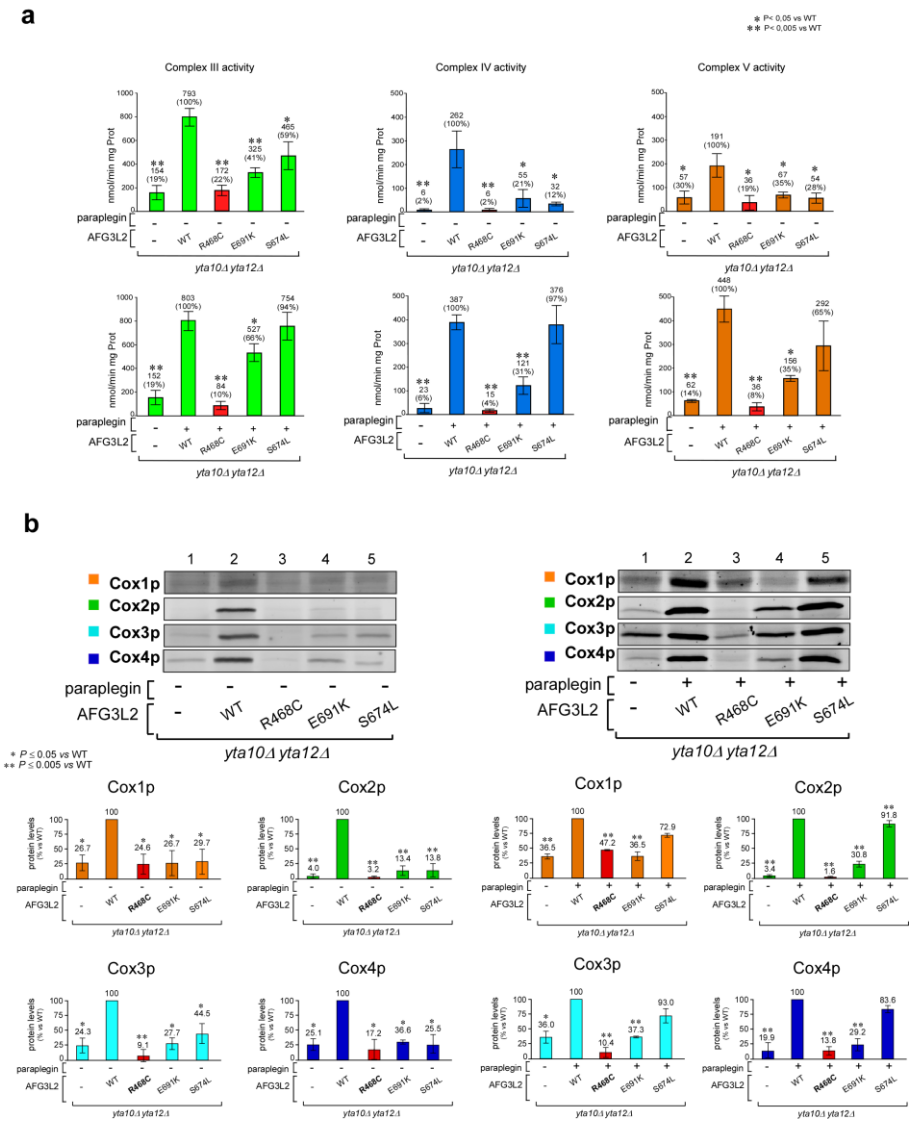
a
* P< 0,05 vs WT
** P< 0,005 vs WT
Complex III activity
Complex IV activity
Complex V activity
nmol/min mg Prot
paraplegin
AFG3L2
WT
R468C
E691K
S674L
yta10Δ yta12Δ
b
Cox1p
Cox2p
Cox3p
Cox4p
* P ≤ 0.05 vs WT
** P ≤ 0.005 vs WT
protein levels (% vs WT)

Figure 3 Respiratory chain activity and Cytochrome *c* oxidase protein levels.

(a) Enzyme activity of complexes III–IV-V in isolated mitochondria from *yta10*Δ*yta12*Δ *m*-AAA–deficient yeast cells expressing normal or mutated AFG3L2 in absenceand in the presence of paraplegin. Ubiquinol *c* oxido reductase (CIII) specific activity is expressed as nanomoles of cytochrome *c* reduced per minute per milligram of protein. Cytochrome *c* oxidase (CIV) specific activity is expressed as nanomoles of cytochrome c^{red} oxidized per minute per milligram of protein. ATPase (CV) specific activity is expressed as nanomoles of NADH oxidized per minute per milligram of protein. Bars and vertical lines indicate mean and ±1 standard deviation of 3 independent experiments. Values in parentheses indicate percentage of activity compared to AFG3L2WT. Asterisks indicate a statistically significant (*$P \leq 0.05$; **$P \leq 0.005$) difference from AFG3L2WT, as determined by Student's *t*-test. **(b)** Fluorescence immunoblot analysis of mitochondrial-encoded COX subunits Cox1p, Cox2p and Cox3p, and nuclear-encoded subunit Cox4p, in mitochondrial extracts from cells expressing normal or mutant AFG3L2 (left panel) and in the presence of paraplegin (right panel). Bar graphs represent densitometric analysis of 3 independent western blots. Protein levels are expressed as percentage of wild-type. Bars and vertical lines indicate mean ± 1 standard deviation. Asterisks indicate a statistically significant difference from $AFG3L2^{WT}$ determined by Student's *t*-test (*$P \leq 0.05$ or **$P \leq 0.005$). Yeast strains and mutants are as described in Figure 2.

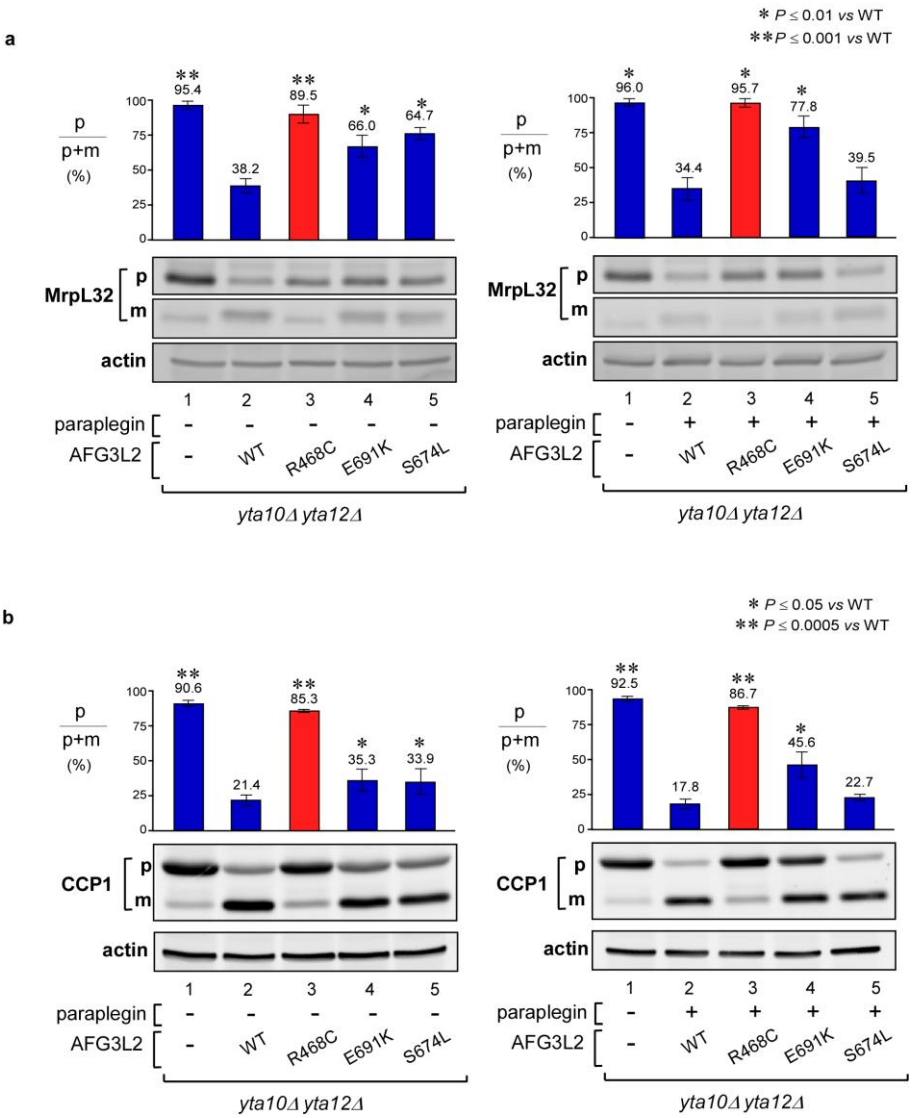
a
* P ≤ 0.01 vs WT
** P ≤ 0.001 vs WT
p
p+m
(%)
MrpL32
p
m
actin
paraplegin
AFG3L2
WT
R468C
E691K
S674L
yta10Δ yta12Δ
b
* P ≤ 0.05 vs WT
** P ≤ 0.0005 vs WT
CCP1

Figure 4 Proteolytic and dislocase activity of AFG3L2^{R468C} in yeast.

(a) Fluorescence immunoblot analysis of MrpL32 precursor (p) and mature (m) form in yeast cells expressing either WT or mutant human AFG3L2 (left panel) and coexpressed with paraplegin (right panel). Proteolytic competence is measured as precursor accumulation expressed as the percent ratio of precursor level to total (p + m) level. MrpL32 levels were normalized to the loading control protein β-actin. Histograph reports desitometric quantification of precursor accumulation (indicated by p/(p + m) %) of 3 independent experiments. Asterisks indicate a statistically significant (* $P \leq 0.01$;** $P \leq 0.001$) difference from AFG3L2WT (lane 2) as determined by Student's *t*-test. **(b)** Fluorescence immunoblot analysis of CCP1 precursor (p) and mature (m) forms in yeast cells expressing either WT or mutant human AFG3L2 (left panel) and coexpressed with paraplegin (right panel). The dislocase competence is measured as precursor accumulation expressed as the percent ratio of precursor level to total (p + m) level. CCP1 levels were normalized to the loading control protein β-actin. Bar graph reports desitometric quantification of precursor accumulation (indicated by p/(p + m) %) of 3 independent experiments. Asterisks indicate a statistically significant (* $P \leq 0.05$;** $P \leq 0.0005$) difference from AFG3L2^{WT} (lane 2) as determined by Student's *t*-test. Red bars= strain expressing AFG3L2^{R468C}; Blue bars= reference strains: *yta10*Δ*yta12*Δ, AFG3L2^{WT} and control mutants as in figure 2. Bars and vertical lines indicate mean and ± 1 s.d., respectively.

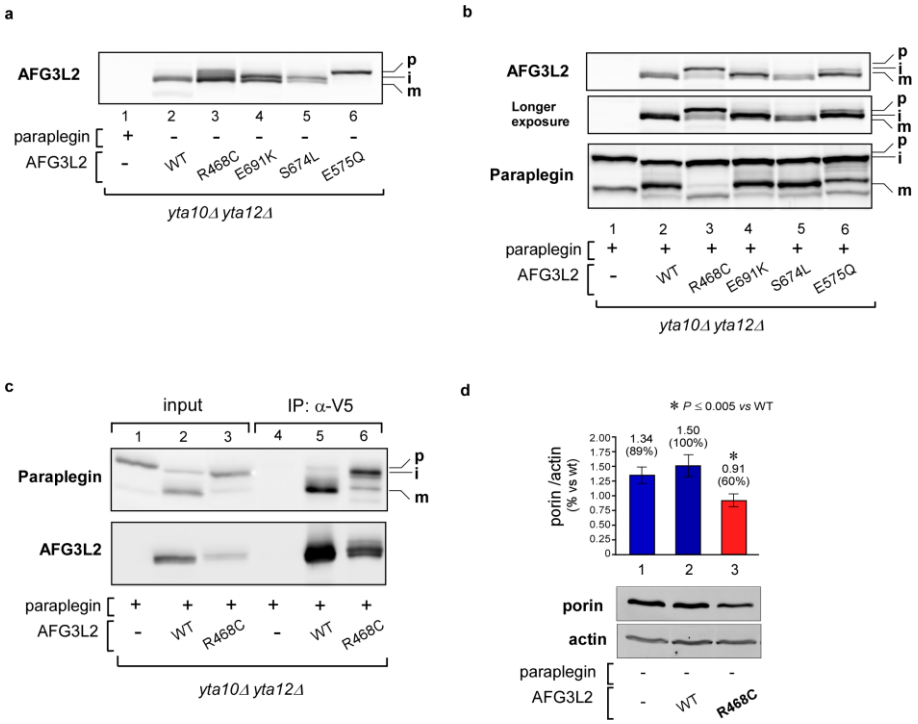
a
AFG3L2
p
i
m
1 2 3 4 5 6
paraplegin + - - - - -
AFG3L2 - WT R468C E691K S674L E575Q
yta10Δ yta12Δ
b
AFG3L2
Longer exposure
Paraplegin
p
i
m
1 2 3 4 5 6
paraplegin + + + + + +
AFG3L2 - WT R468C E691K S674L E575Q
yta10Δ yta12Δ
c
input
IP: α-V5
1 2 3 4 5 6
Paraplegin
AFG3L2
p
i
m
paraplegin + + + + + +
AFG3L2 - WT R468C - WT R468C
yta10Δ yta12Δ
d
* P ≤ 0.005 vs WT
porin /actin (% vs wt)
2.00
1.75
1.50
1.25
1.00
0.75
0.50
0.25
0
1.34 (89%)
1.50 (100%)
* 0.91 (60%)
1 2 3
porin
actin
paraplegin - - -
AFG3L2 - WT R468C

Figure 5 *m*-AAA maturation impairment in yeast strain expressing AFG3L2^{R468C}.

(a) Immunoblot analysis of human AFG3L2 autocatalytic processing. Yeast strains are as described in figure 2a, with the addiction of the proteolytic inactive mutant E575Q. **(b)** Immunoblot analysis of human AFG3L2 autocatalytic processing and paraplegin maturation in strains coexpressing paraplegin. m=mature; p=precursor; i=intermediate. **(c)** Co-immunoprecipitation of WT and mutated (R468C) heterocomplexes. V5-tagged AFG3L2 was immunoprecipitated with anti-V5 antibody. Inputs and immunoprecipitates (IP) were analyzed by SDS-PAGE and detected using anti-paraplegin and anti-AFG3L2. m=mature; p=precursor; i=intermediate. **(d)** Fluorescent immunoblot analysis of Actin and Porin in yeast strain carrying AFG3L2 wt and R468C. Bar graph reports desitometric quantification of the total amount of mitochondria indirectly measured as a ratio between porin and actin levels in 4 independent experiments (n=4). Asterisks indicate a statistically significant (*$P \leq 0.005$) difference from AFG3L2WT (lane 2) as determined by Student's *t*-test. Bars and vertical lines indicate mean and ± 1 s.d., respectively. Red bar= strain expressing AFG3L2R468C; Blue bars= reference strain.

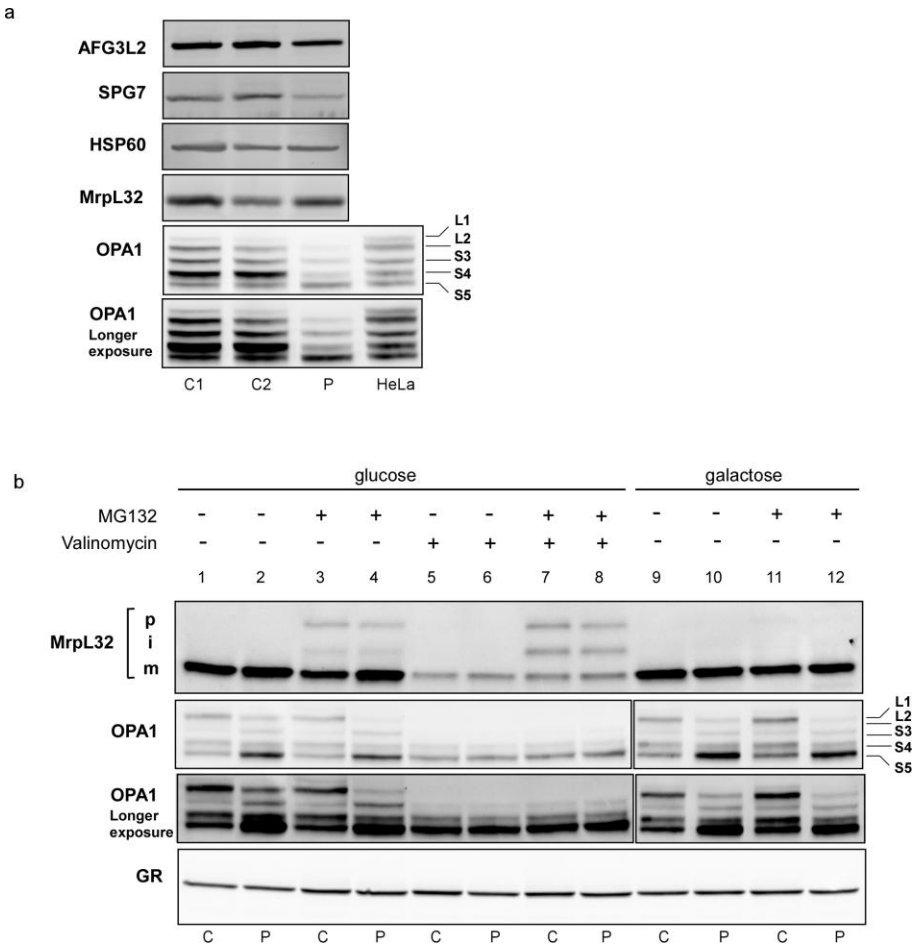
a
AFG3L2
SPG7
HSP60
MrpL32
OPA1
L1
L2
S3
S4
S5
OPA1
Longer
exposure
C1
C2
P
HeLa
b
glucose
galactose
MG132
Valinomycin
1 2 3 4 5 6 7 8 9 10 11 12
MrpL32
p
i
m
OPA1
L1
L2
S3
S4
S5
OPA1
Longer
exposure
GR
C P C P C P C P C P C P

Figure 6 Expression analysis in patients' lymphoblasts and fibroblasts.

(a) In order to evaluate the impairment of non-neuronal cell lines and tissue, protein extracts from lymphoblasts were analyzed by Western blot under denaturing conditions. Protein level were analysed by immunblotting with antibodies against AFG3L2, paraplegin, MrpL32 and OPA1. Hsp60 was used as a loading control. **(b)** Immunoblot analysis of fibroblasts extracts cultured with different treatment. Fibroblasts were treated for 24h with 10μM MG132 (specific proteasome inhibitor) and/or 1μM Valinomycin (in the presence of potassium it is a potent uncoupler of mitochondria). Moreover fibroblasts were exposed to mild metabolic stress by cultivation in galactose for 48h. MrpL32 and OPA1 were detected with specific antibodies, Glutatione reductase (GR) was used as a loading control. MrpL32: p=precursor, i=intermediate, m=mature. OPA1: long forms (L1 and L2) short forms (S3,S4 and S5). P= patient; C, C1 and C2= controls.

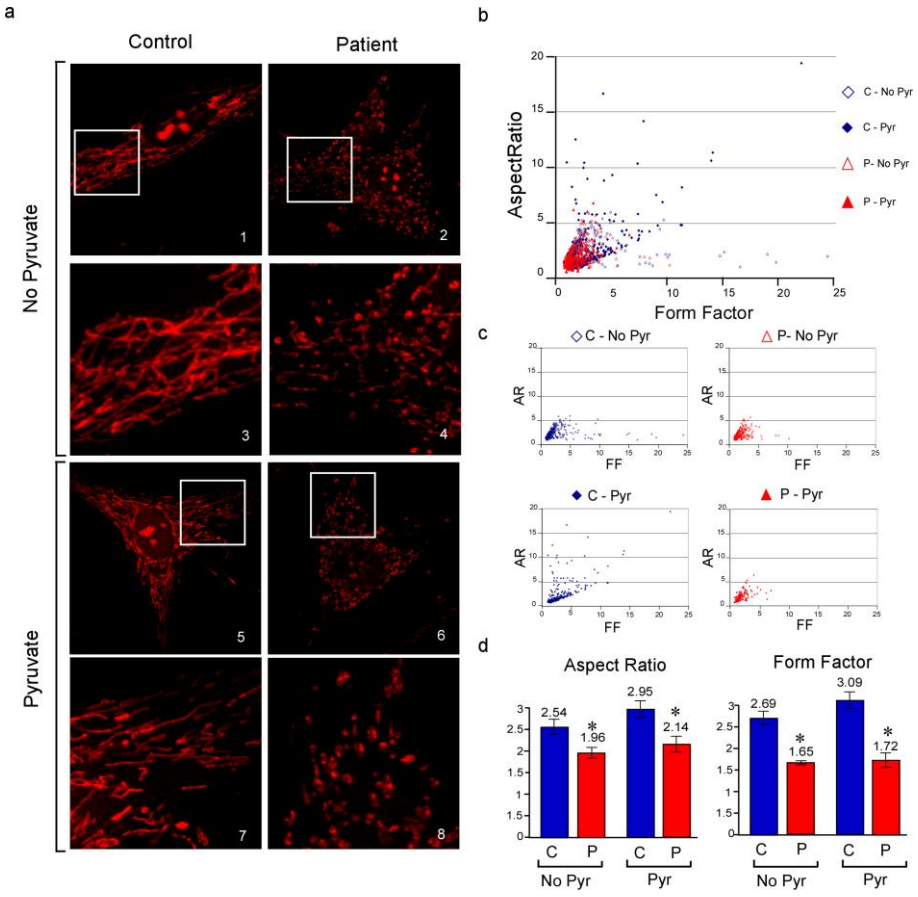
a
Control
Patient
No Pyruvate
Pyruvate
1
2
3
4
5
6
7
8
b
AspectRatio
Form Factor
C - No Pyr
C - Pyr
P- No Pyr
P - Pyr
c
C - No Pyr
P- No Pyr
C - Pyr
P - Pyr
AR
FF
d
Aspect Ratio
Form Factor
2.54
1.96
2.95
2.14
2.69
1.65
3.09
1.72
C
P
No Pyr
Pyr

Figure 7 Analysis of mitochondrial morphology in patient-derived fibroblasts.

(a) Representative confocal images of mitochondria stained with Mitotracker Red. Control and patient fibroblasts cultured both in absence and in presence of pyruvate were stained with Mitotracker Red. Images 1, 2, 5 and 6 are 40x; 3, 4, 7, 8 are insets of the previous. **(b-c)** Scatter graphs show FormFactor (FF) versus AspectRatio (AR) values for individual mitochondrion. Higher values of AR and FF correspond to longer and more branching mitochondria respectively. Each scatter plot in panel c illustrates mitochondrial shapes of a single cell in one of the four conditions: patients or control cell; cultivated with or without pyuvate. The overlapping of the four graphs (panel b) highlights the differences between patient and control mitochondria shape. **(d)** The graph shows average FF and AR values for mitochondria in the four condition (n=4). Bars and vertical lines indicate means and ± 1 s.d., respectively. Red bars= patient; Blue bars= control. Asterisks indicate a statistically significant (*P ≤ 0.005) difference from control as determined by Student's t-test. P= patient; C, C1 and C2= controls.

References

- Arlt, H.; Steglich, G.; Perryman, R.; Guiard, B.; Neupert, W. & Langer, T. (1998), 'The formation of respiratory chain complexes in mitochondria is under the proteolytic control of the *m*-AAA protease.', *EMBO J* **17**(16), 4837--4847.

- Arlt, H.; Tauer, R.; Feldmann, H.; Neupert, W. & Langer, T. (1996), 'The YTA10-12 complex, an AAA protease with chaperone-like activity in the inner membrane of mitochondria.', *Cell* **85**(6), 875--885.

- Atorino, L.; Silvestri, L.; Koppen, M.; Cassina, L.; Ballabio, A.; Marconi, R.; Langer, T. & Casari, G. (2003), 'Loss of *m*-AAA protease in mitochondria causes complex I deficiency and increased sensitivity to oxidative stress in hereditary spastic paraplegia.', *J Cell Biol* **163**(4), 777--787.

- Bonn, F.; Pantakani, K.; Shoukier, M.; Langer, T. & Mannan, A. U. (2010), 'Functional evaluation of paraplegin mutations by a yeast complementation assay.', *Hum Mutat* **31**(5), 617--621.

- Casari, G.; Fusco, M. D.; Ciarmatori, S.; Zeviani, M.; Mora, M.; Fernandez, P.; Michele, G. D.; Filla, A.; Cocozza, S.; Marconi, R.; Dürr, A.; Fontaine, B. & Ballabio, A. (1998), 'Spastic paraplegia and OXPHOS impairment caused by mutations in paraplegin, a nuclear-encoded mitochondrial metalloprotease.', *Cell* **93**(6), 973--983.

- Chan, D. C. (2006), 'Mitochondria: dynamic organelles in disease, aging, and development.', *Cell* **125**(7), 1241--1252.

- Cipolat, S.; Rudka, T.; Hartmann, D.; Costa, V.; Serneels, L.; Craessaerts, K.; Metzger, K.; Frezza, C.; Annaert, W.; D'Adamio, L.; Derks, C.; Dejaegere, T.; Pellegrini, L.; D'Hooge, R.; Scorrano, L. & De Strooper, B. (2006), 'Mitochondrial rhomboid PARL regulates cytochrome c release during apoptosis via OPA1-dependent cristae remodeling.', *Cell* **126**(1), 163--175.

- DiBella, D.; Lazzaro, F.; Brusco, A.; Plumari, M.; Battaglia, G.; Pastore, A.; Finardi, A.; Cagnoli, C.; Tempia, F.; Frontali, M.; Veneziano, L.; Sacco, T.; Boda, E.; Brussino, A.; Bonn, F.; Castellotti, B.; Baratta, S.; Mariotti, C.; Gellera, C.; Fracasso, V.; Magri, S.; Langer, T.; Plevani, P.; Donato, S. D.; Muz*i*-Falconi, M. & Taroni, F. (2010), 'Mutations in the mitochondrial protease gene AFG3L2 cause dominant hereditary ataxia SCA28.', *Nat Genet* **42**(4), 313--321.

- Durr, A. (2010), 'Autosomal dominant cerebellar ataxias: polyglutamine expansions and beyond.', *Lancet Neurol* **9**(9), 885--894.

- Duvezin-Caubet, S.; Koppen, M.; Wagener, J.; Zick, M.; Israel, L.; Bernacchia, A.; Jagasia, R.; Rugarli, E. I.; Imhof, A.; Neupert, W.; Langer, T. & Reichert, A. S. (2007), 'OPA1 processing reconstituted in yeast depends on the subunit composition of the *m*-AAA protease in mitochondria.', *Mol Biol Cell* **18**(9), 3582--3590.

- Esser, K.; Pratje, E. & Michaelis, G. (1996), 'SOM 1, a small new gene required for mitochondrial inner membrane peptidase function in Saccharomyces cerevisiae.', *Mol Gen Genet* **252**(4), 437--445.

- Esser, K.; Tursun, B.; Ingenhoven, M.; Michaelis, G. & Pratje, E. (2002), 'A novel two-step mechanism for removal of a mitochondrial signal sequence involves the mAAA complex and the putative rhomboid protease Pcp1.', *J Mol Biol* **323**(5), 835--843.

- Fracasso; Magri; Plumari; Giunti; Boesch; Muz*i*-Falconi, M.; Lazzaro; Bella, D. & Taroni (submitted), 'Spinocerebellar ataxia type 28: identification and functional analysis of novel AFG3L2 mutations', .

- Fracasso, V., L. F. &. M.-F. M. (2010), 'Co-immunoprecipitation of human mitochondrial proteases AFG3L2 and paraplegin heterologously expressed inyeast cells.', Technical report, Nat. Protoc. published online,.

- Gellera, C.; Castellotti, B.; Mariotti, C.; Mineri, R.; Seveso, V.; Didonato, S. & Taroni, F. (2007), 'Frataxin gene point mutations in Italian Friedreich ataxia patients.', *Neurogenetics* **8**(4), 289--299.

- Ishihara, N.; Fujita, Y.; Oka, T. & Mihara, K. (2006), 'Regulation of mitochondrial morphology through proteolytic cleavage of OPA1.', *EMBO J* **25**(13), 2966--2977.

- Koopman, W. J. H.; Visch, H.-J.; Smeitink, J. A. M. & Willems, P. H. G. M. (2006), 'Simultaneous quantitative measurement and automated analysis of mitochondrial morphology, mass, potential, and motility in living human skin fibroblasts.', *Cytometry A* **69**(1), 1--12.

- Koppen, M.; Bonn, F.; Ehses, S. & Langer, T. (2009), 'Autocatalytic Processing of *m*-AAA Protease Subunits in Mitochondria.', *Mol Biol Cell*.

- Koppen, M. & Langer, T. (2007), 'Protein degradation within mitochondria: versatile activities of AAA proteases and other peptidases.', *Crit Rev Biochem Mol Biol* **42**(3), 221--242.

- Koppen, M.; Metodiev, M. D.; Casari, G.; Rugarli, E. I. & Langer, T. (2007), 'Variable and tissue-specific subunit composition of mitochondrial *m*-AAA protease complexes linked to hereditary spastic paraplegia.', *Mol Cell Biol* **27**(2), 758--767.

- Lenaers, G.; Reynier, P.; Elachouri, G.; Soukkarieh, C.; Olichon, A.; Belenguer, P.; Baricault, L.; Ducommun, B.; Hamel, C. & Delettre, C. (2009), 'OPA1 functions in mitochondria and dysfunctions in optic nerve.', *Int J Biochem Cell Biol* **41**(10), 1866--1874.

- Magri, S., F. V. R. M. &. T. F. (2010), 'Preparation of yeast mitochondria and in vitro assay of respiratory chain complex activities.', Technical report, Nat. Protoc. published online,.

- Maltecca, F.; Aghaie, A.; Schroeder, D. G.; Cassina, L.; Taylor, B. A.; Phillips, S. J.; Malaguti, M.; Previtali, S.; Guénet, J.-L.; Quattrini, A.; Cox, G. A. & Casari, G. (2008), 'The mitochondrial protease AFG3L2 is essential for axonal development.', *J Neurosci* **28**(11), 2827--2836.

- Mariotti, C.; Brusco, A.; Bella, D. D.; Cagnoli, C.; Seri, M.; Gellera, C.; Donato, S. D. & Taroni, F. (2008), 'Spinocerebellar ataxia type 28: a novel autosomal dominant cerebellar ataxia characterized by slow progression and ophthalmoparesis.', *Cerebellum* **7**(2), 184--188.

- Martinelli, P.; Mattina, V. L.; Bernacchia, A.; Magnoni, R.; Cerri, F.; Cox, G.; Quattrini, A.; Casari, G. & Rugarli, E. I. (2009), 'Genetic interaction between the *m*-AAA protease isoenzymes reveals novel roles in cerebellar degeneration.', *Hum Mol Genet* **18**(11), 2001--2013.

- Muzi Falconi, M.; Piseri, A.; Ferrari, M.; Lucchini, G.; Plevani, P. & Foiani, M. (1993), 'De novo synthesis of budding yeast DNA polymerase alpha and POL1 transcription at the G1/S boundary are not required for entrance into S phase.', *Proc Natl Acad Sci U S A* **90**(22), 10519--10523.

- Nolden, M.; Ehses, S.; Koppen, M.; Bernacchia, A.; Rugarli, E. I. & Langer, T. (2005), 'The *m*-AAA protease defective in hereditary spastic paraplegia controls ribosome assembly in mitochondria.', *Cell* **123**(2), 277--289.

- Ogura, T.; Whiteheart, S. W. & Wilkinson, A. J. (2004), 'Conserved arginine residues implicated in ATP hydrolysis, nucleotide-sensing, and inter-subunit interactions in AAA and AAA+ ATPases.', *J Struct Biol* **146**(1-2), 106--112.

- Palmfeldt, J.; Vang, S.; Stenbroen, V.; Pedersen, C. B.; Christensen, J. H.; Bross, P. & Gregersen, N. (2009), 'Mitochondrial proteomics on human fibroblasts for identification of metabolic imbalance and cellular stress.', *Proteome Sci* **7**, 20.

- Song, Z.; Chen, H.; Fiket, M.; Alexander, C. & Chan, D. C. (2007), 'OPA1 processing controls mitochondrial fusion and is regulated by mRNA splicing, membrane potential, and Yme1L.', *J Cell Biol* **178**(5), 749--755.

- Suno, R.; Niwa, H.; Tsuchiya, D.; Zhang, X.; Yoshida, M. & Morikawa, K. (2006), 'Structure of the whole cytosolic region of ATP-dependent protease FtsH.', *Mol Cell* **22**(5), 575--585.

- Tatsuta, T.; Augustin, S.; Nolden, M.; Friedrichs, B. & Langer, T. (2007), '*m*-AAA protease-driven membrane dislocation allows intramembrane cleavage by rhomboid in mitochondria.', *EMBO J* **26**(2), 325--335.

- Tauer, R.; Mannhaupt, G.; Schnall, R.; Pajic, A.; Langer, T. & Feldmann, H. (1994), 'Yta10p, a member of a novel ATPase family in yeast, is essential for mitochondrial function.', *FEBS Lett* **353**(2), 197--200.

- Wong, A.; Yang, J.; Cavadini, P.; Gellera, C.; Lonnerdal, B.; Taroni, F. & Cortopassi, G. (1999), 'The Friedreich's ataxia mutation confers cellular sensitivity to oxidant stress which is rescued by chelators of iron and calcium and inhibitors of apoptosis.', *Hum Mol Genet* **8**(3), 425--430.

Chapter 5

Summary

The mitochondrial *m*-AAA metalloprotease, belonging to the superfamily of the AAA proteins (ATPases Associated with different cellular Activities), carries out protein quality control and degrades non-assembled or damaged mitochondrial inner-membrane proteins. This metalloprotease is a hexameric proteolytic complex located in the inner mitochondrial membrane active on the matrix side. In humans, *m*-AAA exists in two different subunit compositions: a heterocomplex composed of AFG3L2 and paraplegin as well as a homocomplex constituted of AFG3L2 only. The importance of *m*-AAA in humans is underlined by the evidence obtained in my laboratory that mutations in *AFG3L2* are associated with a new dominant form of spinocerebellar ataxia (SCA28) (Di Bella et al., 2010), while *SPG7* gene encoding paraplegin causes an autosomal recessive form of hereditary spastic paraparesis (SPG7)(Casari et al., 1998). The cellular functions of *m*-AAA protease have been mostly studied in the yeast *Saccharomyces cerevisiae*. Yeast *m*-AAA is composed of Yta10p and Yta12p, which exhibit high sequence homology with AFG3L2 and paraplegin, respectively. In the absence of the *m*-AAA protease, yeast cells are respiratory deficient and cannot grow on non-fermentable carbon sources such as glycerol. Complementation studies demonstrate that *m*-AAA protease is functionally conserved from yeast to human: human *m*-AAA complexes (both homo and heterocomplex) are able to replace the Yta10p/Yta12p complex and to restore the respiratory competence. After the identification of *AFG3L2* as the gene responsible for SCA28, we examined 337 unrelated people with ataxia for the presence of *AFG3L2* mutations (Di Bella et al., 2010). Five heterozygous missense mutations were detected in affected individuals but not in controls, suggesting that

they may be causative mutations. Thanks to the high conservation of this complex from yeast to human, we were able to set a yeast model to functionally validate *m*-AAA mutations. Mutant human *m*-AAA complexes were expressed in yeast to investigate the functional effects of the mutations causing amino acid substitution and to discriminate between pathogenic mutations and rare benign variants. We tested the first group of 6 AFG3L2 variants (H126Q, S674L, E691K, R694A, R702Q and N432T) in this yeast model. AFG3L2 mutations were evaluated in both the homocomplex (AFG3L2 without paraplegin) and the heterocomplex (AFG3L2/paraplegin) and were classified as benign variants, paraplegin-responsive mutations, and paraplegin-non responsive mutations based on the capacity to restore respiratory competence in the presence and in the absence of paraplegin. Recently, we screened a second group of 233 patients for mutations in the *AFG3L2* gene identifying nine heterozygous variants (Fracasso et al., submitted). We therefore tested these nine variants identified in our lab and five mutations identified by a collaborating group (Cagnoli et al., 2010) using our yeast model. Expression studies in an *m*-AAA–deficient *S. cerevisiae* strain (*yta10Δyta12Δ)* allowed to establish the functional role of the amino acid variants discriminating between real mutations and rare/unique benign variants. Functional analysis of mutated AFG3L2 in the heterocomplex ($AFG3L2^{mut}$/paraplegin) suggested that two classes of AFG3L2 mutations exist: "paraplegin-responsive" and "non-paraplegin responsive" mutations based on the ability of paraplegin to complement AFG3L2 mutations.

Since paraplegin can modulate the phenotype of AFG3L2 mutations in yeast, we investigated the possible coinheritance of *AFG3L2* and *SPG7* mutations in patients with spinocerebellar syndromes. Interestingly, we identified three SCA28 patients carrying concurrent mutations in *SPG7* (Magri et al., submitted). We performed functional analysis and cell biology studies on one genotype because of the severity and complexity of the relative clinical phenotype and the crucial role of the mutated AFG3L2 residue. We observed for the first time an impairment of mitochondrial dynamics in cell lines of a SCA28 patient: OPA1, a dynamin-like GTPase necessary for mitochondrial fusion, presents an abnormal pattern of

processing in patient lymphoblasts and fibroblasts. This finding represents a step forward to the understanding of *m*-AAA-related diseases.

Conclusions and future perspectives

The importance of *m*-AAA in humans is underlined by the evidence that mutations in both the subunits of this mitochondrial protease are associated with important neurodegenerative diseases. While the *SPG7* gene encoding paraplegin is associated with an autosomal recessive form of hereditary spastic paraparesis (SPG7) (Casari et al., 1998), evidences recently obtained in our lab demonstrate that mutations in *AFG3L2* cause a new dominant form of spinocerebellar ataxia (SCA28) (Di Bella et al., 2010). Since that discovery, we screened 571 unrelated individuals with progressive ataxic phenotype. We identified 14 heterozygous *AFG3L2* missense variants and 2 heterozygous small in-frame deletions that are absent in more than 400 control chromosomes. Nine variations are located in the proteolytic domain, four in the AAA-domain and three substitutions are located in less conserved region, outside the functional domains.

Disease-causing mutations or rare benign variants? Baker's yeast has the answer.

Functional analysis in a yeast model allowed us to discriminate between disease-causing mutations and rare benign variants. Since the human wild-type *m*-AAA complexes are able to rescue the respiratory phenotype caused by the lack of the endogenous *m*-AAA protease, we tested the functionality of mutant *m*-AAA complexes investigating their ability to rescue the respiratory phenotype. We concluded that ten variations affect the functionality of human *m*-AAA complex demonstrating their pathogenic nature. By contrast, six substitutions do not compromise the activity of human *m*-AAA protease in yeast suggesting that they are likely rare benign variants. Interestingly, all these benign substitutions are located in less conserved regions: three in the N-teminal region, two in the AAA-domain and one in the very C-terminal part of the proteolytic domain. These results indicate the crucial importance of functional studies

to validate the pathogenic role of mutations especially when there are insufficient data about the segregation in the family. These studies expand the spectrum of AFG3Le mutations establishing an overall frequency of ~1,8%.

Haploinsufficiency or negative dominance?

Although AFG3L2 and paraplegin have a high sequence homology, share a common domain structure and co-assemble in an ubiquitous mitochondrial protease, mutations in these two proteins cause two neurodegenerative diseases that differ in patterns of inheritance, molecular mechanisms and degeneration of specific types of neurons. The different phenotypes caused by mutations in AFG3L2 and paraplegin demonstrate that these proteins have at least partially distinct functions. In fact, *SPG7* mutations are distributed on the whole gene and mutated alleles clearly cause loss of function. Thus, the pathogenesis of the hereditary spastic paraparesis SPG7 can be ascribed to the lack of the heterocomplex (paraplegin/AFG3L2). On the contrary, *AFG3L2* mutations hit conserved residues in the AAA and proteolytic domain, suggesting a dominant-negative effect. We therefore investigated whether haploinsufficiency or negative dominance was the mechanism underlying the effects of the identified mutations by coexpressing wild-type AFG3L2 with each mutant in our yeast model. Most of the mutations are fully rescued by the coexpression of $AFG3L2^{WT}$ subunits, suggesting a haploinsufficiency or weak dominant negative mechanism. By contrast, some mutations (3/10 identified in our lab and 2/5 identified in Cagnoli et al., 2010) are not rescued by wild-type subunits, clearly demonstrating a dominant-negative effect. Interestingly, these mutations exert a negative dominance also in the heterocomplex: we classified them as "non-paraplegin-responsive" because paraplegin coexpression does not complement their defective phenotype. On the contrary, the haploinsufficient or weakly dominant mutations are at least partially rescued by paraplegin coexpression indicating their "paraplegin-responsive" nature.

To each mutation its own molecular mechanism

These results suggest that AFG3L2 mutations could act through different molecular mechanisms. In order to verify this hypothesis, we investigated the molecular mechanism analysing the effect of each mutations on different aspect of *m*-AAA activity. In fact, it was proposed that *m*-AAA complexes could combine its proteolytic and ATPase activity in different way according to the requirement (Tatsuta et al., 2007). On one hand, MrpL32 is efficiently cleaved also by *m*-AAA protease variants with low ATPase activities, indicating that MrpL32 maturation requires proteolytic rather than ATPase activity. On the other hand, the maturation of Ccp1 depends on the ability of *m*-AAA complex to dislocate it from the inner mitochondrial membrane making a processing site accessible to the rhomboid protease. This pull-out activity imposes additional ATP requirements. We therefore used the conversion of MrpL32 from its precursor (pMrpL32) to its mature form (mMrpL32) as an indicator of the overall proteolytic competence and the maturation of Ccp1 as a detector of the ATP-dependent dislocase activity of *m*-AAA complex.

Notably, we observed that the defect of MrpL32 processing does not always correlates with the defect of Ccp1 maturation indicating that different mutations can affects differently proteolytic and dislocase activities. In particular, all the variants that show a respiratory phenotype present also a defect of MrpL32 processing even if at variable extent. On the contrary, not all the mutations present also a defect in Ccp1 processing. Moreover only two mutations, R468C and M666R, completely affect the maturation of Ccp1 which therefore exists only in the precursor form. Although the strains carrying the other mutations show a significant accumulation of the precursor form, they accumulate Ccp1 mostly as mature form. Thus, we can classify the mutations according to their effect on the dislocase activity as:

1. Mutations that retain dislocase activity
2. Mutations that partially affect dislocase activity
3. Mutations that abolish dislocase activity

These findings indicate that distinct mutations act with different molecular mechanisms.

Recent evidences demonstrated that in mammals Afg3l2 undergoes autocatalytic processing and mediates paraplegin maturation, thus indicating that proteolytic activity is necessary for the formation of active *m*-AAA complexes. Given that some mutations completely abolish the *m*-AAA protease activities, we verified the hypothesis that they compromise the assembly and the autocatalytic maturation of the complex. We demonstrated by co-immunoprecipitation experiments that both processed and unprocessed AFG3L2 and paraplegin subunits are able to interact. Moreover, all AFG3L2 mutants co-immunoprecipitate with paraplegin indicating that they are able to assembly with the cognate subunit protein. However, the two most severe mutations (R468C and M666R) drastically impair autocatalytic processing and paraplegin maturation. Thus, they are able to assemble in complexes that nevertheless result completely non-functional. These data can explain why these two mutations completely abolish both protease and ATPase activities. Interestingly, the severity of these two mutations seems to correlate with the age of onset of the disease: the patients carrying these mutations present an age of onset under 10 years and severe phenotypes associated with extrapyramidal signs. On the contrary, the other identified mutations may disrupt specialized AFG3L2 function. For example molecular modelling of mutants into the crystal structure of the eubacterial FtsH metalloprotease indicate that E691K drastically changes the electrostatic potential and the chemical characteristics of the pore in both the homo- and heterohexameric complexes. We might speculate that this hamper release of processed substrate or impair substrate recognition.

A new piece of the puzzle

Although several groups investigated the role of this protease in physiological and pathological conditions using different approaches and several animal and cellular models, the molecular basis leading to the SCA28 and the SPG7 pathogenesis are largely unknown.

In order to delve into the pathogenic mechanism, we investigated the consequence of human *m*-AAA alterations in patient-derived cells. Impaired mitochondrial protein synthesis due to aberrant processing of

MrpL32 was proposed to be the cause of *m*-AAA related neurodegeneration (Nolden et al., 2005). However, western blot analysis of human MrpL32 in patient's lymphoblast and fibroblasts did not reveal any differences in protein level and processing respect to control's cells, not even in condition that allowed precursor accumulation.

By contrast, we observed an altered pattern of OPA1, a dynamin-like GTPase necessary for the fusion of mitochondrial inner membrane, in patient-derived cells. In human cells, OPA1 exists in at least five forms generated by alternative splicing and proteolytic processing events: two long forms, L1 and L2, and three short forms, S3, S4 and S5 (Ishihara et al., 2006). Both long and short forms are required for mitochondrial fusion (Song et al., 2007). Although the regulation of OPA1 processing is largely unknown, the *m*-AAA protease seems to be involved in physiologic OPA1 processing in mice (Duvezin-Caubet et al., 2007; Ehses et al., 2009). Western blot analysis reveals the loss of L2 and S4 OPA1 forms in lymphoblasts and fibroblasts of the patient with the most severe clinical presentation characterized by an early onset optic atrophy (Magri et al., submitted). Notably, mutations in OPA1 gene are associated to a dominant form of optic atrophy. Consistently with OPA1 functions, analysis of mitochondrial morphology in patient's fibroblasts revealed an important fragmentation of the mitochondrial network compared to control cells. This fragmentation is presumably due to the impairment of fusion events caused by an unbalance between long and short OPA1 forms.

The fact that only one patient presents this defect of OPA1 in non-neuronal tissue could be ascribed to the crucial function of the residue mutated in AFG3L2 and/or the concurrent heterozygous mutation in SPG7 that may act as a disease modifier. Even if only the more severely affected individuals show a phenotype in non-neuronal-tissue, spinocerebellar neurodegeneration should be traced back to the same pathogenic mechanism in all the SCA28 patients. The aberrant OPA1 processing observed in patient's cells is a step forward into the comprehension of *m*-AAA-related neurodegenerative diseases.

However, important questions remain unsolved and new debates arise from recent findings. Is mitochondrial fragmentation a direct consequence

of the loss of *m*-AAA activity on OPA1, or a secondary effect caused by another mitochondrial injury? Which is the physiologic role of *m*-AAA complexes in humans? Why does the lack of the ubiquitous mitochondrial *m*-AAA protease lead to neuron-specific degeneration? Which is the specific role of homo- and heterocomplex? Do they differ in substrate specificity?

Future perspectives

The identification of additional and possibly neuronal-specific substrates of *m*-AAA will be crucial to enlighten the relative contribution of AFG3L2 and paraplegin in neurodegeneration. Furthermore, patient-derived cell lines are an invaluable resource to investigate the early consequences of *m*-AAA impairment and to test novel therapeutic strategies. As first, we will focus on the potential use of rapamycin. This pharmacological compound is a US Food and Drug Administration-approved antibiotic and immunosuppressant drug that has been used for several years to prevent rejection in organ transplantation and is currently approved for treatment of cardiovascular diseases (Bovè et al., 2011). Rapamycin inhibits the activity of mTOR (mammalian target of rapamycin), an intracellular serine/threonine protein kinase that has a central role in various cellular processes, including cell growth and proliferation, protein synthesis and autophagy. Because of these properties, rapamycin provides therapeutic benefit in experimental models of several age-dependent neurodegenerative diseases, including Alzheimer's disease, Parkinson's disease and Huntington's disease (recently reviewed in Bovè et al., 2011). In particular, we are interested in the role of rapamycin in promoting autophagy and mitophagy. Induction of autophagy with rapamycin may prevent and attenuate accumulation of aberrant and misfolded proteins due to an impaired mitochondrial quality control system. Moreover, the increase of mitophagy, a selective mitochondrial degradation process through autophagy, may improve the elimination of damaged organelles that can negatively influence cellular homeostasis. In the near future, we will investigate the effect of rapamycin on the mitochondrial fragmentation observed in patient's cell lines. If successful, this line of investigation will

be of crucial importance to plan a therapeutic strategy for *m*-AAA-related neurodegenerative diseases.

References

- Bové, J.; Martínez-Vicente, M. & Vila, M. (2011), 'Fighting neurodegeneration with rapamycin: mechanistic insights.', *Nat Rev Neurosci* **12**(8), 437--452.

- Cagnoli, C.; Stevanin, G.; Brussino, A.; Barberis, M.; Mancini, C.; Margolis, R. L.; Holmes, S. E.; Nobili, M.; Forlani, S.; Padovan, S.; Pappi, P.; Zaros, C.; Leber, I.; Ribai, P.; Pugliese, L.; Assalto, C.; Brice, A.; Migone, N.; Dürr, A. & Brusco, A. (2010), 'Missense mutations in the AFG3L2 proteolytic domain account for ?1.5% of European autosomal dominant cerebellar ataxias.', *Hum Mutat* **31**(10), 1117--1124.

- Casari, G.; Fusco, M. D.; Ciarmatori, S.; Zeviani, M.; Mora, M.; Fernandez, P.; Michele, G. D.; Filla, A.; Cocozza, S.; Marconi, R.; Dürr, A.; Fontaine, B. & Ballabio, A. (1998), 'Spastic paraplegia and OXPHOS impairment caused by mutations in paraplegin, a nuclear-encoded mitochondrial metalloprotease.', *Cell* **93**(6), 973--983.

- DiBella, D.; Lazzaro, F.; Brusco, A.; Plumari, M.; Battaglia, G.; Pastore, A.; Finardi, A.; Cagnoli, C.; Tempia, F.; Frontali, M.; Veneziano, L.; Sacco, T.; Boda, E.; Brussino, A.; Bonn, F.; Castellotti, B.; Baratta, S.; Mariotti, C.; Gellera, C.; Fracasso, V.; Magri, S.; Langer, T.; Plevani, P.; Donato, S. D.; Muz*i*-Falconi, M. & Taroni, F. (2010), 'Mutations in the mitochondrial protease gene AFG3L2 cause dominant hereditary ataxia SCA28.', *Nat Genet* **42**(4), 313--321.

- Duvezin-Caubet, S.; Koppen, M.; Wagener, J.; Zick, M.; Israel, L.; Bernacchia, A.; Jagasia, R.; Rugarli, E. I.; Imhof, A.; Neupert, W.; Langer, T. & Reichert, A. S. (2007), 'OPA1 processing reconstituted in yeast depends on the subunit composition of the *m*-AAA protease in mitochondria.', *Mol Biol Cell* **18**(9), 3582--3590.

- Ehses, S.; Raschke, I.; Mancuso, G.; Bernacchia, A.; Geimer, S.; Tondera, D.; Martinou, J.-C.; Westermann, B.; Rugarli, E. I. & Langer, T. (2009), 'Regulation of OPA1 processing and mitochondrial fusion by *m*-AAA protease isoenzymes and OMA1.', *J Cell Biol* **187**(7), 1023--1036.

- Fracasso; Magri; Plumari; Giunti; Boesch; Muz*i*-Falconi, M.; Lazzaro; Bella, D. & Taroni (submitted), 'Spinocerebellar ataxia type 28: identification and functional analysis of novel AFG3L2 mutations', .

- Ishihara, N.; Fujita, Y.; Oka, T. & Mihara, K. (2006), 'Regulation of mitochondrial morphology through proteolytic cleavage of OPA1.', *EMBO J* **25**(13), 2966--2977.

- Magri; Fracasso; Plumari; Rusmini; Gellera; Pantaleoni; Biasi, D.; Poletti; Plevani; Lazzaro; Muz*i*-Falconi; DiBella & Taroni (submitted), 'Concurrent mutations in AFG3L2 and paraplegin cause mitochondrial dysfunction in patients with spinocerebellar degeneration', .

- Nolden, M.; Ehses, S.; Koppen, M.; Bernacchia, A.; Rugarli, E. I. & Langer, T. (2005), 'The *m*-AAA protease defective in hereditary spastic paraplegia controls ribosome assembly in mitochondria.', *Cell* **123**(2), 277--289.

- Song, Z.; Chen, H.; Fiket, M.; Alexander, C. & Chan, D. C. (2007), 'OPA1 processing controls mitochondrial fusion and is regulated by mRNA splicing, membrane potential, and Yme1L.', *J Cell Biol* **178**(5), 749--755.

- Tatsuta, T.; Augustin, S.; Nolden, M.; Friedrichs, B. & Langer, T. (2007), '*m*-AAA protease-driven membrane dislocation allows intramembrane cleavage by rhomboid in mitochondria.', *EMBO J* **26**(2), 325--335.

Publications

- DiBella, D.; Lazzaro, F.; Brusco, A.; Plumari, M.; Battaglia, G.; Pastore, A.; Finardi, A.; Cagnoli, C.; Tempia, F.; Frontali, M.; Veneziano, L.; Sacco, T.; Boda, E.; Brussino, A.; Bonn, F.; Castellotti, B.; Baratta, S.; Mariotti, C.; Gellera, C.; Fracasso, V.; Magri, S.; Langer, T.; Plevani, P.; Donato, S. D.; Muz*i*-Falconi, M. & Taroni, F. (2010), 'Mutations in the mitochondrial protease gene AFG3L2 cause dominant hereditary ataxia SCA28.', *Nat Genet* **42**(4), 313--321.

- Magri, S., F. V. R. M. &. T. F. (2010), 'Preparation of yeast mitochondria and in vitro assay of respiratory chain complex activities.', Technical report, Nat. Protoc. published online,.

- Fracasso; Magri; Plumari; Giunti; Boesch; Muz*i*-Falconi, M.; Lazzaro; Bella, D. & Taroni (submitted), 'Spinocerebellar ataxia type 28: identification and functional analysis of novel AFG3L2 mutations.

- Magri; Fracasso; Plumari; Rusmini; Gellera; Pantaleoni; Biasi, D.; Poletti; Plevani; Lazzaro; Muz*i*-Falconi; DiBella & Taroni (submitted), 'Concurrent mutations in AFG3L2 and paraplegin cause mitochondrial dysfunction in patients with spinocerebellar degeneration', .